179

GROUTED TENSION PILES UNDER MULTI-DIRECTIONAL LOADS GOVERNED BY GROUT/PILE INTERFACE

by

Fathi Aloulou
Ingenieur Diplome, M.Sc ., D.I.C.

February 1989

A thesis submitted for the degree of
Doctor of Philosophy
of the University of London

Department of Civil Engineering
Imperial college of Science and Technology
London S.W. 7

Title : **Grouted Tension Piles under Multi - Directional Loads Governed by Grout/Pile Interface.**

Author : **Fathi Aloulou**

ABSTRACT

The development of buoyant offshore structures has created the need for more careful considerations for their foundation systems. For rock bed locations, such foundation usually consists of grouted tension piles. As soon as the upper structure is in place, these piles are subjected to a permanent tensile force, with an additional lateral loading generated by waves, water currents, and wind action on the floating structure. Consequently the grouted pile is subjected to a combination of axial tensile force and alternating lateral loads.

The purpose of the described study was to investigate the behaviour of grouted tension piles under combined vertical tensile and lateral loading in the particular circumstances when failure is controlled by the grout/pile interface. The principal result obtained is that even small horizontal loads have a significant effect in reducing the holding down capacity of the tension piles.

The load transfer to the embedding media is first developed between the pile and the surrounding cementitious grout. Bond strength and frictional resistance between the pile and the grout are prime factors governing the strength and behaviour of grouted piles. A new test is described to determine the shear bond strength at the interface between the pile and the grout. This involves twisting specially produced segmented pile specimens which have been grouted into a concrete block. The local pile surface/grout behaviour is assessed in this way under pure shear, although stresses normal to the interface are being developed as a result of dilation phenomena in the grout.

An idealized pile/grout interface spring model has been introduced to analyse the performance of a pile under an axial pull out force. The pile failure mechanism has been found to be influenced by interface bond behaviour, the pile dimensions, and the relative stiffness of the pile to the surrounding media. This analysis also provided a demonstration and explanation for the size effects on the pile behaviour.

In tests, grouted piles under axial pull out load have shown a failure mode similar to that of the local interface bond breakdown. However an application of a lateral force, either simultaneously with, or independently of, the vertical force, reduces considerably the axial capacity of the grouted pile to a residual value which can be related to the local interface frictional resistance. The pile residual resistance is also conditioned by the lateral load, relative to the vertical extracting force. Five proportional loading paths for different combinations of vertical and horizontal loads have provided an interaction diagram corresponding to the maximum pile resistances. It is clearly evident that the uplift resistance and behaviour of a grouted pile is conditioned by the application of the lateral loading prior to its extraction.

A grouted pile, under repeated axial or non axial loading, has shown a progressive failure. On each cycle additional pile end movement is accumulated, causing an irreversible pile end displacement. Recommendations are given for the procedures to be adopted when designing such tension piles. Consideration of the effects of horizontal loading should be included in the design process.

ACKNOWLEDGEMENTS

My interest in the present subject has been inspired from Professor J. W. Dougill, to whom I am deeply grateful for his supervision, frequent guidance, and the critical reading of the thesis. I am particularly indebted to Dr. C. J. Burgoyne for the support he gave me during the past year and for his very useful comments and criticisms.

I am grateful to the British Council for a scholarship which has enabled me to undertake the work described. The particular project was part of the continuum programme on Grout and Grouting for Offshore Structure managed by the London Center for Marine Technology. I am grateful for the opportunity to contribute to the programme.

I wish to thank the technical staff in the Concrete Laboratory for their assistance and their help in carrying the heavy work in this project, particularly L. Clark, T. Boxell, P. Jellis, K. Mitchell, J. Turner, B. Bobinski, R. Baxter, and their colleagues. The success of the experiments would not have been possible without their technical skills. Thanks are due to R. Packer, and A. Chipling for their photographic work, and to Mrs K. Crooks and Miss J. Underhill for their assistance in the library.

CONTENTS

Page Number

ABSTRACT ii
ACKNOWLEDGEMENTS iii
CONTENTS iv
NOTATIONS ix
LIST OF FIGURES xii
LIST OF TABLES xvii
ABBREVIATIONS xviii

CHAPTER 1 : INTRODUCTION 1

1.1 BACKGROUND 1

1.2 APPLIED LOADS ON GROUTED PILES 2

1.3 GROUTED CONNECTIONS BETWEEN TUBULAR MEMBERS 2

1.4 GROUTED PILES 4

1.5 GROUTED LENGTH L 5

1.6 INFLUENCE OF SURFACE CONDITION 6

1.7 COMMENTS 7

1.8 ESTABLISHMENT OF A THEORETICAL MODEL TO DETERMINE THE KEY PARAMETERS FOR GROUTED PILE 8

1.9 OVERALL OBJECTIVES 9

CHAPTER 2 : NUMERICAL MODEL 17

2.1 INTRODUCTION 17

2.2 INTERFACE MATERIAL MODEL 18

2.3 PILE IDEALISATION 19

2.4 FORMULATION OF THE GENERAL EQUATION 19

2.4.1 GENERAL EQUATION 19
2.4.2 BOUNDARY CONDITION 21
2.4.3 EIASTIC SOLUTION 21
2.4.4 PARAMETERS AFFECTING THE PILE BEHAVIOUR 22

2.5 NUMERICAL SOLUTION 22
2.5.1 COMPUTATION OF THE GENERAL EQUATION 23
2.5.2 RESULTS 24
2.5.3 OTHER NUMERICAL ALTERNATIVE 25

2.6 PILE LENGTH EFFECTS 26
2.6.1 PILE LENGTH FOR CRITICAL UNSTABLE BEHAVIOUR AND ITS RELATION TO SLIP SOFTENING RATE 26
2.6.2 AVERAGE SHEAR STRESS 27

2.7 DILATANCY MODELLING 27

2.8 CONCLUSION 28

CHAPTER 3 : OBJECTIVES OF THE EXPERIMENTAL INVESTIGATION

3.1 BACKGROUND 38

3.2 OBJECTIVES 38

3.3 SCOPE OF THE INVESTIGATION 39

CHAPTER 4 : GROUT INVESTIGATION 40

4.1 INTRODUCTION 40

4.2 BLEEDING 40

4.3 SHRINKAGE AND VOLUME CHANGE 41

4.4 GROUT QUALITY IMPROVEMENT 41
4.4.1 ADMIXTURE 41
4.4.2 PULVERIZED FUEL ASH 42
4.4.3 SILICA FUME 42
4.4.4 CEMEN T TYPE 43

4.5 OBJECTIVE OF THE INVESTIGATION 43

4.6 TEST PROCEDURE 43

4.7 TEST ARRANGEMENT 43

4.8 MIXING METHODS 44

4.9 EXPERIMENT 44

4.10 RESULTS AND GROUT SELECTION 45

4.11 MECHANICAL PROPERTIES OF THE CHOSEN MIX 46
4.11.1 COMPRESSIVE STRENGTH 46
4.11.2 ELASTIC MODULUS 46

CHAPTER 5 : MAIN RIG DESIGN 57

5.1 REQUIREMENTS 57

5.2 RIG GENERAL DESCRIPTION 57
5.2.1 STEEL FRAME 57
5.2.2 GENERAL RIG 58

5.3 RIG SAFETY TESTS 58
5.3.1 TEST CASE A 59
5.3.2 TEST CASE B 59

5.4 CONCRETE BLOCK 59

5.5 CONCRETE MATERIAL 59

5.6 CONCRETE POCKETS 60

CHAPTER 6 : PULL-OUT TESTS ON GROUTED TENSION PILES 71

6.1 INTRODUCTION 71

6.2 OBJECTIVES 72

6.3 TEST PROGRAMME DESCRIPTION 72

6.4 TESTS ARRANGEMENT 73

6.5 PILE LOCATION 74

6.6 GROUTING OPERATION 74

6.7 LOAD APPLICATION 74

6.8 PILE HEAD CONNECTORS 75
6.8.1 VERTICAL LOADING 75
6.8.2 HORIZONTAL LOADING 75

6.9 INSTRUMENTATION 75

6.10 RESULTS 76
6.10.1 PULL-OUT TESTS 76
6.10.2 PROPORTIONAL LOADING 78
6.10.3 PATH DEPENDENCY 80

6.11 DISCUSSION AND TEST IMPLEMENTATION 81

CHAPTER 7 : DESIGN OF NEW TORSION TEST 108

7.1 INTRODUCTION 108

7.2 REVIEW OF BOND TEST METHODS 108

7.3 TORSION TEST DESIGN 110
7.3.1 PILE ELEMENT 111
7.3.2 TWISTING TOOL 112
7.3.3 LOAD APPLICATION 112
7.3.4 SPECIMEN PREPARATION 113
7.3.5 CONCRETE POCKET 114
7.3.6 TWISTING TOOL INSTALLATION 114
7.3.7 TEST PROCEDURE 115

7.4 INSTRUMENTATION AND FORM OF THE OUTPUT 115
7.4.1 TWISTING KEY 115
7.4.1.1 Analysis of the Strain Gauges Outputs 117
7.4.1.2 Interface Shear Stress. 118
7.4.2 SLIP MEASUREMENT 119
7.4.3 NORMAL STRESS DILATANCY MEASUREMENT 121

CHAPTER 8 : TORSION TEST RESULTS 140

8.1 INTRODUCTION 140

8.2 SLIP DISPLACEMENT - SHEAR STRESS 142
8.2.1 GENERAL BEHAVIOUR 142
8.2.2 BOND FAILURE 143
8.2.3 ADHESION OF CEMENTITIOUS MATRIX TO OTHER MATERIALS 144
8.2.4 BOND STRENGTH AND FRICTION RESISTANCE 145
8.2.5 FRICTIONAL BEHAVIOUR FOR LARGE DISPLACEMENT 147
8.2.6 STRESS CYCLING 147

8.3 DILATANCY 149

8.3.1 SLIP - CIRCUMFERENTIAL STRAIN RELATIONSHIP 150
8.3.2 DILATANCY AND SHEAR STRESS 150
8.3.3 GROUTED INTERFACE BEHAVIOUR MODELING 151

8.4 SUMMARY 152

CHAPTER 9 : CONCLUSIONS AND RECOMMENDATIONS 177

9.1 NUMERICAL STUDY 177

9.2 GROUT SELECTION 177

9.3 LOAD COMBINATIONS : VERTICAL AND HORIZONTAL LOADS 178

9.4 INTERFACE PROPERTIES 179

9.5 PRACTICAL APPLICATIONS 180

9.6 FURTHER WORK 180

9.7 SUMMARY OF PRINCIPAL CONCLUSIONS 181

APPENDIX 1 182

APPENDIX 2 207

REFERENCES AND BIBLIOGRAPHY 211

NOTATION

The following notation is used for the variables used in the text unless it is specified differently.

A_{bond}	bonded area at the interface pile/grout
[A(U)]	stiffness matrix
[B(U)]	a load vector
A_p	pile cross section
a	radius of the interface pile/grout
b	radius of the interface grout/concrete
C_l	pile length parameter
C_s	surface condition parameter
D	diameter
D_{int}	slip softening rate of the spring interface model
E	elastic modulus
E_g	grout elastic modulus (Young's modulus)
E_s	steel elastic modulus
E_{int}	elastic stiffness of the spring interface model
E_p	elastic modulus of the pile steel
F	end pile force
F_{max}	maximum pile resistance
F_{bu}	ultimate bond strength parameter
f_{bu}	ultimate bond strength
f_{cu}	grout ultimate cube compressive strength
f(x)	tension force in the pile at a depth x (force distribution)
$G([u_m^{j-1}])$	function of the slip displacement at the node m obtained from the iteration j-1
G_{steel}	shear modulus of the steel
H	horizontal (lateral) force
h	shear key height
i	a node index
j	iteration index
K	grouted connection stiffness parameter
K_e	constant
k_p	pile stiffness factor
K_p^i	stiffness factor at the node i

$K_p^{i,j-1}$	stiffness factor at the node i during the iteration j-1
k_f	slip fracturing rateof the interface pile/grout
k_{normal}	an equivalent stiffness factor relating the normal stress at the interface pile/grout and the circumferential (hoop) strain at the interface grout/concrete
k_{rig}	an equivalent stiffness for the rig during the torsion test
k_{surr}	an equivalent stiffness for the grout and the concrete surrounding the pile ring during the torsion test
k_{sys}	an equivalent stiffness of the rig, twisting tool, surrounding media during the the torsion test for the assessment of the interface pile/grout
k_{tool}	an equivalent stiffness of the twisting tool and its head under a torque load
L	length
L_{bond}	length (height) of the bonded zone at the interface pile/grout
L_c	critical grouted pile length for the pile transition behaviour
L_p	pile length (grouted length)
N	number of pile sub-division
P_p	perimeter of the pile
P_i	radial pressure at the inner radius
P_o	radial pressure at the outer radius
PVV1	paste volume variation parameter
PVV2	paste volume variation parameter
R_{pile}	radius of the pile ring element used for the torsion test
S_i	load factor
s	shear key spacing
T	torque applied on the pile ring element
t	thickness
[U]	slip displacement vector
U	tip pile displacement
u	local slip at the pile/grout interface
u_i	slip displacement at the node i
u_{max}	spring model slip corresponding for the maximum shear stress (τ_{max})
u_{res}	spring model slip corresponding for the beginning of the residual behaviour
V	vertical tension force
W_f	energy dissipation during slip occurrence at the interface pile/grout
W_{sys}	stored energy in the experimental system around the interface pile/grout

X	non-dimensional pile depth
x	pile depth
δX	non dimensional pile interval length

α	factor from the numerical model
β	factor for pile stable behaviour
γ	factor fom the differential equation (chapter 2)
δ	slip displacement (or deformation) at the interface pile/grout.
ε_{pile}	pile axial deformation
ε_{axial}	axial strain of the cylinder in compression (elastic modulus determination)
ε_{trans}	transversal strain (hoop strain) of the cylinder in compression (elastic modulus determination)
ε_{SG}	pocket circumferential (hoop) strain
ε_1, ε_2, and ε_3	strain output from the gauges placed on the twisting tool tubular part
ε_{11}, ε_{22}	principal strains on the twisting tool tubular body
Φ	a notation for diameter
σ_{axial}	axial stress on cylinder specimen in compression (elastic modulus determination)
$\sigma_{c/g}$	normal stress at the interface concrete grout
σ_n	normal stress at the pile/grout interface
σ_r	radial stress
σ_{trans}	transverse stress (hoop stress) of cylinder specimen in compression (elastic modulus determination)
σ_θ	circumferential stress
σ_{11}, σ_{22}	principal stresses on the twisting tool tubular body
ν_g, ν_c	Poisson's ratio for grout and concrete
τ	local shear stress at the interface pile/grout
$\tau_{interface}$	shear stress resistance at the interface pile/grout
τ_{max}	maximum shear stress of the interface pile/grout
τ_{res}	residual shear stress of the interface pile/grout
λ	radius ratio (b by a)

LIST OF FIGURES

Page number

Chapter 1

1.1a : typical modern offshore structure in deep waters 10

1.1b : tethered tension leg platform with distributed piles around the structure base 10

1.2 : structural arrangement of grouted piles compared with the grouted connection system 11

1.3 : lateral forces action on the TLP legs and foundation 11

1.4a : tubular grouted connection (from Department of Energy (UK) (1982)) 12

1.4b : bond strength variation with the grout compressive strength (from Department of Energy (UK) (1982)) 12

1.4c : bond strength parameter variation with the connection stiffness factor (from Department of Energy (UK) (1982)) 13

1.4d : bond strength parameter variation with the grouted length (from Department of Energy (UK) (1982)) 13

1.5a : grouted pile behaviour (from Cox and Reeses (1976)) 14

1.5b : shear stress variation along the length of the grouted connection (from Loset (1981)) 14

1.6 : observation on the pile steel surface before and after sand shot blasting 15

1.7 : interfacial failure mode with and without shear key 15

Chapter 2

2.1a : interface bond-friction model 29

2.1b : grouted tension pile model 29

2.2a : equilibrium of a pile element 30

2.2b : pile element deformation 30

2.3a : finite difference description of the pile model 30

2.4a : local slip stress distribution along the pile model grouted length, with the corresponding tip force - tip displacement relationship for each step of the pile extraction (steps 1 and 2) 31

2.4b : local slip stress distribution along the pile model grouted length, with the corresponding tip force - tip displacement relationship for each step of the pile extraction (steps 3 and 4) 32

2.4c : local slip stress distribution along the pile model grouted length, with the corresponding tip force - tip displacement relationship for each step of the pile extraction (steps 5 and 6) 33

2.5 : alternative solution of the pile/grout model 34

2.6 : different pile behaviours under a pull-out forces 35

2.7 : slip softening modulus - pile length relationship for the critical unstable pile behaviour 36

2.8 : pile length parameter effect on the average interface resistance 37

2.9 : interface dilatancy and surrounding stiffness effects 37

Chapter 4

4.1 : grout degradation during the plastic stage 51

4.2 : measurement of early volumetric change of plastic cementitious mixtures (ASTM C827-75T) 51

4.3 : adopted test arrangement for measuring the early volumetric change of cementitious grout 52

4.4 : grout investigation - plastic shrinkage test results - 53

4.5 : standard gauged cylinder for the elastic modulus determination (BS 1881 Part 121 1983) 54

4.6a &b : grout behaviour in compression 55

Chapter 5

5.1 : concept for the testing rig 61

5.2a : rig main frame (rig front view) 62

5.2b : rig side view 63

5.2c : rig top view 64

5.3 : constructed experimental rig 65

5.4 : safety tests carried out on the constructed rig 66

5.5a : concrete block used during the main investigation 67

5.5b : general view of the rig with the concrete block 68

5.6 : failed concrete specimen under compression 69

5.7a & b : concrete block material behaviour in compression 70

Chapter 6

6.1 : test programme on grouted tension piles 84

6.2a : typical pile specimen 85

6.2b : grout pumping for the pile casting operation 85

6.3a : details of the pile head for vertical load application 86

6.3b : details of the pile head for lateral load application and connector head/pulling steel bar 87

6.3c : details of the top pile end 88

6.4a : view of the manufactured pile head for vertical load 89

6.4b : view of the manufactured pile head and head/pulling bar connector for the lateral load application 89

6.5a : grouted pile and vertical loading coupler prior to the pull-out test 90

6.5b : pile before complete extraction 90

6.5c : pile specimen under combined vertical and lateral load 91

6.5d : instrumentation of the pile top end for a combined loading test 91

6.6a : displacement at the pile head during cycles of horizontal load (PPLT 2 test) 92

6.6b : vertical pile end behaviour for preliminary tests 92

6.7a : axial grouted pile pull-out behaviour (length effect on the pile axial behaviour) 93
6.7b : axial grouted pile pull-out behaviour (curing time effect on the pile axial behaviour) 93
6.8a : axial grouted pile pull-out behaviour (surface treatment effect) 94
6.8b : grouted piles pull-out behaviour 94
6.9a : failure mode of grouted pile from test PLT 2 95
6.9b : tested piles under vertical pull-out load 95
6.10a : grouted pile vertical behaviour under combined proportional loads (comparison between tests PLT 2 and PLT 3) 96
6.10b : grouted pile vertical behaviour under combined proportional loads (comparison between tests PLT 2 and PLT 5) 96
6.10c : grouted pile vertical behaviour under combined proportional loads (comparison between tests PLT 2 and PLT 6) 97
6.10d : grouted pile vertical behaviour under combined proportional loads (comparison between tests PLT 2 and PLT 8) 97
6.10e : grouted pile vertical behaviour under combined proportional loads (comparison between tests PLT 3 and PLT 8) 98
6.10f : grouted pile vertical behaviour under combined proportional loads (comparison between tests PLT 5 and PLT 6) 98
6.11a : grouted pile horizontal behaviour under combined proportional loads (test PLT 3) 99
6.11b : grouted pile horizontal behaviour under combined proportional loads (test PLT 5) 99
6.11c : grouted pile horizontal behaviour under combined proportional loads (test PLT 6) 100
6.11d : grouted pile horizontal behaviour under combined proportional loads (test PLT 8) 100
6.12a : extracted pile specimen of test PLT 7 101
6.12b : extracted pile specimen of test PLT 8 101
6.12c : tested piles under combined loads 102
6.12d : failure view of the pile specimen of test PLT 5 (where V/H = 1) 102
6.12e : failure mode of the grouted piles submitted to horizontal and vertical loads 103
6.13 : lateral - vertical interface forces interaction diagram for grouted pile under combined proportional loads 104
6.14a : applied loads sequences for path dependency tests 105
6.14b : grouted pile behaviour for different combined loads paths 105
6.15a : lateral grouted pile behaviour for different combined paths 106
6.15b : pile end displacement for different combined loads paths 106
6.16a &b: loads cycling effect on grouted pile behaviour (test PLT 4) 107

Chapter 7

7.1a : conventional bond test method 125
7.1b : Tassios and Koroneos (1979) bond test method 125
7.1c : Jiang et al (1982) bond test method 125

7.1d : Stroeven and De Wind (1982) bond test method 125
7.1e : Chen et al (1987) concrete/soil interface test method 125
7.2a : local bond, slip curves at several areas along the embedded length(from Tassios and Koroneos (1979)) 126
7.2b : bond stress, slip and steel strain distribution for various loading levels (from Tassios and Koroneos (1979)) 126
7.2c : bond tests results on steel roughness effect (Stroeven and De Wind (1982)) 127
7.2d : Review of tests results on steel/concrete bond strength 128
7.3a : description of the pile rings arrangement designed for torsion test 129
7.3b : cross section of a grouted pile ring in the concrete block during the torsion test 129
7.4a : pile rings unit used during the preliminary investigation of the torsion test 130
7.4b : pile rings unit used during the main investigation of the torsion test 130
7.5 : assembly of the pile ring with the twisting key for the torsion test 131
7.6a : description of the twisting tool 132
7.6b : views of the manufactured twisting tool with the cross head 133
7.6c : description of the twisting key cross-head 134
7.7a : pile rings elements arrangement 135
7.7b : over break of the pocket due to miss-alignment of the pile elements 135
7.7c : casting operation of the pile rings unit 135
7.7d : concrete pocket instrumentation 135
7.8 : cross-head/pulling bars connection 136
7.9 : stiffening key arrangement 137
7.10 : torsion test arrangement 137
7.11a : view of the torsion test with the LVDTs for slip measurement 138
7.11a : view of the torsion test with the hydraulic equipment during the preliminary investigation 138
7.12 : view of the rig with the concrete block during the preliminary investigation 139

Chapter 8

8.1a : shear stress - slip (from preliminary test - ring 1 -) 154
8.1b : shear stress - slip (from preliminary test - ring 2 -) 155
8.1c : shear stress - slip (from preliminary test - ring 3 -) 156
8.2a : shear stress - slip (from main test - ring 1 -) 157
8.2b : shear stress - slip (from main test - ring 2 -) 158
8.2c : shear stress - slip (from main test - ring 3 -) 159
8.2d : shear stress - slip (from main test - ring 4 -) 160
8.3a : shear - slip relationship for initial stage of slip 161
8.3b : bond strength and frictional resistance with grout strength 162
8.3c : description of the nature of bond between steel surface and grout 163

8.4a : shear stress fluctuation (from main test - ring 1 -) 164
8.4b : shear stress fluctuation (from main test - ring 2 -) 164
8.4c : shear stress fluctuation (from main test - ring 3 -) 165
8.4d : shear stress fluctuation (from main test - ring 4 -) 165
8.5 : surface conditioning caused by large slip displacement 166
8.6 : effect of cyclic loading on shear stress - slip response (main test series - ring 2-) 167
8.7a : shear stress - slip cycling (ring 2 - stage A) 168
8.7b : shear stress - slip cycling (ring 2 - stage B) 168
8.8a : shear stress - slip cycling model (ring 2 - stage A) 169
8.8b : shear stress - slip cycling model (ring 2 - stage B) 169
8.9a : effect of dilation accompanying slip (test PTT 2) 170
8.9b : effect of dilation accompanying slip (test PTT 3) 170
8.9c : effect of dilation accompanying slip (test MTT 1) 171
8.9d : effect of dilation accompanying slip (test MTT 2) 171
8.9e : effect of dilation accompanying slip (test MTT 3) 172
8.9f : effect of dilation accompanying slip (test MTT 4) 172
8.10a : shear stress with effect of dilation (test PTT 2) 173
8.10b : shear stress with effect of dilation (test PTT 3) 173
8.10c : shear stress with effect of dilation (test MTT 1) 174
8.10d : shear stress with effect of dilation (test MTT 2) 174
8.10e : shear stress with effect of dilation (test MTT 3) 175
8.10f : shear stress with effect of dilation (test MTT 4) 175
8.11 : steel pile surface - cementitious grout interface model 176

Appendix 1

A1.1 : algorithm for solving the system of equations of the numerical model of a grouted pile 185
A1.2a : convergent numerical system of equations 186
A1.2b : non-convergence of the numerical system of equations 186
A1.3 : pile subdivisions effect on the output of the pile behaviour 187

Appendix 2

A2.1 : material and test equipment representation 210

LIST OF TABLES

Page number

Chapter 2

2.1 : interface and pile characteristics for both study cases (numerical model) 28

Chapter 4

4.1 : pulverized fuel ash chemical composition 47
4.2 : condensed silica fume chemical composition 47
4.3 : plastic shrinkage test results 48 - 49
4.4 : selected grout compressive strength 50
4.5 : selected grout mechanical properties 50

Chapter 6

6.1 : tests undertaken on grouted piles 83

Chapter 8

8.1 : summary of the bond strength and frictional resistance obtained from the torsion tests

ABBREVIATIONS

API	: American Petroleum Institute
ASCE	: American Society of Civil Engineering
ASTM	: American Society of Testing Material
BS	: British Standard
CEGB	: Central Electric Generating Board
FIP	: Federation Internationale de la Precontrainte
LVDT	: Linear Voltage Differential Transformer
PFA	: Pulverized Fuel Ash
TLP	: Tension Leg Platform
MTT	: Main Torsion Test (main investigation)
PTT	: Preliminary Torsion Test
PLT	: Pull out Test (main investigation
PPLT	: Preliminary Pull out Test

CHAPTER 1 : INTRODUCTION

1.1 BACKGROUND

The trend for offshore exploration is to move to deeper and deeper waters. As a result the conventional jacket is no longer the ideal and economic structural solution. New types of structures have been established and used in the deeper North Sea. Among these types of structures are the Tension Leg Platform (TLP), and the Catenary Anchored floater, which are shown in figure 1.1a. In many situations, tethered buoyant structures have emerged as the optimal solution. The basic idea behind these types of construction is to restrict the heave, pitch and the roll motions of a floating deck with tendons (cables or assembly of tubes) in tension and anchored to the sea bed.

The foundationsof tethered offshore structures consist of separate steel templates that are individually anchored to the sea bed by tubular steel piles. The piles themselves are either grouped around each leg of the structure or evenly distributed around the base of the structure forming skirting piles (figure 1.1b). If the sea bed is of sand or soft clay material and the water is not too deep, the foundation's piles are usually driven to the required depth in the sea strata, using traditional hammering techniques. Alternative techniques are required when the sub-sea bed is hard rock. This can lead to the use of the drilled and grouted pile type of foundation. The latter piling method can also be used when the structures site is in deep water, whether the foundation's stratum is sand, clay or hard rock, since the present hammering techniques are difficult in deep sea water.

The installation of grouted pile foundations requires the drilling of a pocket to a given depth into the sea bed rock. A steel pile is then inserted, and cementitious grout is later pumped in the space between the pile and its surrounding media. In some cases, a large diameter casing is first driven into the sea bed and the material from within and below is removed. Later, the pile is placed and grouted. In an alternative structural arrangement, the casing may be withdrawn at the time of grouting so that the grout is in intimate contact with the surrounding soil or rock. More details, about the selection and the installation of piled foundations for sea bed structures, can be found in the report by Tebbett et al (non dated internal report). The various structural arrangements are shown diagrammatically in figure 1.2, and compared with a typical grouted connection between tubular members.

1.2 APPLIED LOADS ON GROUTED PILES

The cables connecting a TLP structure to its foundations are usually vertical. The cables themselves are prestressed, so the foundation is subject at all times to a tensile force. In addition, the waves, the current and the wind generate an additional combination of lateral loading causing the structure to move sideways. Consequently the foundation is continuously subjected to a combination of axial tension and an alternating lateral loading. In design, a cable inclination of 10° is assumed to occur at the connection with the foundation as a result of the lateral load (St John et al 1983). Figure 1.3 summarizes the loading forces applied on one leg of the TLP.

If the cables are designed to be inclined, such as in the Catenary Anchored Floater and Guyed Tower, the introduction of lateral load is an inevitable part of the design and must be taken into account.

The resistance of the grouted pile to uplift is provided by the interaction between the pile and the grout, and also between the grout and the surrounding media. The result is that the pile/grout interface carries a complex combination of shear and normal stresses which must be transferred to the sea bed. Failure of the bond (or the interlock) between the pile and the grout directly affects the overall structural stability.

1.3 GROUTED CONNECTIONS BETWEEN TUBULAR MEMBERS

The grouted piled anchorage has many similarities to the connection used to link a conventional platform leg to its foundation. In the latter, sleeves are attached to the lower end of the main structural leg and grouted to the pile providing the load transfer from the structure to its foundation.

Recent experimental research by Billington et al (1978, 1980), has been directed to the formulation of a basic design procedure for grouted connections between tubular members. Shear keys or weld beads, placed on both the pile and its sleeve, have been found to increase the strength of the connection significantly. However, since the present work is aimed at the bond between the steel surface and the grout, only the results from the plain connections are of immediate interest.

Billington and Lewis (1978) established the range of parameters that are thought to influence the joint strength. These factors include the grout properties

(strength, elastic modulus, shrinkage expansion, etc.), the tube size and geometry, the length of the connection, imperfections and the pipe steel surface condition. They also described the strength of an axially loaded grouted connection in terms of an equivalent bond strength, obtained by dividing the ultimate capacity of the connection by the total surface area of the pile/grout interface. The shear bond strength f_{bu} is expressed in the form :

$$f_{bu} = B.\sqrt{f_{cu}} \; . \; K \tag{1.1}$$

where B is a constant, f_{cu} is the grout cube compression strength and where the stiffness parameter K is given by :

$$K = \frac{E_g}{E_s} \cdot \left(\frac{t}{D}\right)_g + \left[\left(\frac{D}{t}\right)_s + \left(\frac{D}{t}\right)_p \right]^{-1} \tag{1.2}$$

The indices s p, and g refer respectively to the sleeve, pile, and grout; t and D refer to the thickness and diameter. E_g and E_s are the elastic modulus of the grout and steel. The arrangement of the pile connection is shown in figure 1.4a. The constant B reflects the surface condition and the influence of the length/diameter ratio. The test specimens used a grouted length/diameter ratio in the range 1-8. For all results used, failure occurred along the interface between the grout and one of the tubular elements. The authors concluded that the bond strength is related to the square root of the grout compressive strength, although this relationship between f_{cu} and f_{bu} is not immediately apparent. These results are presented in figure 1.4b.

Billington and Tebbit (1980) continued the investigation on grouted connections by studying in more detail the influence of each influencing factor already described. More tests were carried out on grouted connections, particularly with different grout strengths, grouted lengths and sleeve stiffnesses. From these and the previous results, a design formula was developed. Results showing the effect of grouted pile length are shown in figure 1.4d, in terms of a non-dimensional shear stress bond factor :

$$F_{bu} = \frac{f_{bu}}{1.105} \cdot \sqrt{\frac{50}{f_{cu}}} \tag{1.3}$$

Here, the value 1.105 is the bond strength recommended by the API RP2A (1979) in

N/mm^2 multiplied by a safety factor of 6. The choice of this safety factor is discussed by Billington and Tebbett (1980) in terms of the partial factors covering the uncertainties met in the design and construction of grouted connections (i.e. loads, material characteristics, cycling load during grouting and curing time, lack of complete data, site conditions effects, load distribution). The partial factors were assigned using different experiences from offshore construction [API (1979), Department of Energy (1977), Federation International de la Precontrainte (1977), and Wimpey Laboratories Limited (1977, and 1979)]. The combination of these factors, which were regarded as independent, provided a global factor between 4.6 and 7.4. The intermediate value of 6 was adopted by Billington and Tebbett. More details can be found in Billington and Tebbett (1980).

During the previous investigations, connection sleeves of different stiffnesses were used. It was found that the bond strength depends on both pile and sleeve stiffnesses. The stiffness factor described in 1.2 quantifies the effect of the different stiffening arrangements. As a result the bond strength parameter F_{bu} is related to the stiffness factor by the following equation, given in the Department of Energy (UK) report (1983) :

$$F_{bu} = 76 \, . \, K \, . \, C_l \, . \, C_s \qquad (1.4)$$

In this expression, a factor C_l has been introduced to describe the effect of the grouted length whilst the second factor C_s is included to account for surface condition. C_s is given a value of unity where the surfaces are shot blasted, with lower values generally being used for different surface conditions. The value C_l is linked directly to the ratio of grouted length to diameter. Typical results showing the influence of different surface conditions are shown in figure 1.4c.

1.4 GROUTED PILES

Few experimental investigations have been conducted on grouted piles. These are reported by Abbs and Needham (1985), Fragio et al (1985) and Cox and Reese (1976). However, all of these investigations were aimed at failure due to breakdown at the grout/rock interface. Indeed the pile surface was reinforced by weld beads, so that the failure could only occur by breakdown along the grout rock interface.

When shear keys were not used (Cox and Reese 1976) one of the tested specimensdeveloped its failure along the interface between the pile and the grout. In this

case, the pile extraction was accompanied by a reduction of the pull out force, which would suggest a brittle mode of failure dependent on softening. When failure was caused by breakdown at the grout/rock interface, no dramatic fall off in the applied load occurred.

The tested piles had a 406 mm diameter, grouted inside a pre-drilled pocket of 610 mm diameter and 8.5 meters long. The behaviour of the pile with pile/grout failure mode is presented in figure 1.5a. It is this mode of failure which is the focus of the work presented in this thesis.

1.5 GROUTED LENGTH L

Figure 1.4d shows the variation of the bond strength factor with the grouted length (L) of the connection as given by results summarized by the Department of Energy UK (1982). A reduction on the bond strength is observed for long grouted piles. In reality the local bond strength is constant and independent of the grouted length, but a reduction has to be considered to take account of the shear stress distribution along the connection length. Since the majority of the tests, done on plain piles, had a pile length/diameter ratio of two, the Department of Energy (UK) recommends that C_1 can be considered as 1 for $(L/D)_p = 2$, and less than 1 for longer grouted connections.

Evidence for the variation in interfacial stress along a pile during slip is afforded by results obtained by Loset (1981), who measured strain on the steel tubes in attempt to determine the local bond stress. Results for axial strains in the steel tubes are shown in figure 1.5b.

For bond stress to be the same everywhere along the grouted length, the strain would need to vary linearly. The pronounced variation from linearity indicates a variation of the local bond stress and a difference between the maximum value and the average.

Billington and Tebbett (1980) suggested the following pile length factors for use in design of grouted connections :

$(L/D)_p$	C_l
2 - 4	1.0
4 - 8	0.9
8 - 12	0.8
12 - 20	0.7
> 20	0.6

The numerical study, presented in the following chapter, provides an explanation of the average shear strength variation and demonstrates the effects of the pile length on both behaviour and average shear resistance of the pile/grout interface.

1.6 INFLUENCE OF SURFACE CONDITION

The factor C_s in equation 1.4, reflects the influence of the steel surface condition. Only small amounts of data are available on the effect of steel surface roughness on bond strength.

Studies on the effect of surface roughness are limited to the work by Stroeven and De Wind (1982), which is applied to plain reinforcing bars for concrete. The surface was characterized using a steel roughness index deduced from the steel bar profile obtained using the Taylor-Hobson apparatus. The tests showed that the degree of steel roughness has significant influence on the bond characteristics. Further details of these tests are given in chapter 7 and figure 7.2c

BS 4232 defines the surface quality by its cleanliness and roughness. At present, there is no simple means of measuring the surface condition; and no completely satisfactory method of measuring surface roughness is available for use in the field. Cleanliness can be estimated from the appearance of the surface. Roughness is controlled by the treatment method of the surface, which is usually the shot blast-cleaning operation. The type of the abrasive used (sand, steel) is the prime factor that determines the surface condition. In addition, the surface roughness achieved for each quality, proposed by BS 4232, depends upon the steel type, and its condition before the blast-cleaning.

From the early studies on grouted connections, conservative values have been adopted on the effect of steel pipe surface condition. The Department of Energy UK (1982), recommends the following values for C_s according to which pile surface treatment is used :

- shot blasted surface : $C_s = 1$
- epoxy-resin/sand coating : $C_s = 0.86$
- new pipe with small scale : $C_s = 0.46$ ← mill scale?
- epoxy-resin coating : $C_s = 0.20$

During the present investigation the steel surface was sand blasted. To see the effect of this blasting treatment, the pile surface was examined using a scanning electron microscope before and after the steel sand blasting operation (figure 1.6). The treated surface apparently presents a more uniform texture. However, significant surface irregularities are still maintained.

The surface condition of the pile can be very critical. It governs the interaction between the pile surface and the grout, both the peak stress achieved and also during slip. The interface morphology dominates the mechanism of debonding and slip, and conditions the dilatancy phenomenon which occurs when the interface is submitted to shearing stress. The situation is complicated further as it appears that the grout itself has a different structure close to the steel from that elsewhere. For instance, there is strong evidence from the work by Barnes et al (1978) and Carles-Gribergues (1982), that the cementitious grout elements (Hydrated Silicates, and Calcium Hydroxide $Ca(OH)_2$) are developed in a particular manner along the steel/grout interface.

1.7 COMMENTS

The application of grouted connection formulae to a grouted pile involves major assumptions, which can be appreciated only by engineers who are sufficiently experienced in their field. The major difficulty is the choice of the equivalent rock mass in order to compute an equivalent pile sleeve stiffness (equation 1.2). Further difficulties follow from uncertainties in assessing the properties of the sea bed strata, which have a direct effect on the radial stiffness of the pile surrounding media. It must be recognized that the basic formulae approved by the Department of Energy UK, (1982) are valid only within a certain range of connection geometries, which are covered by the tests undertaken.

The suggested formulae by Billington for weld beaded connections, which form the basis for the recommended design rule given by the Department of Energy UK (1982), presents a point of view which is itself controversial. The equation giving the bond factor F_{bu} for connection with shear keys is :

$$F_{bu} = C_l \,.\, K \,.\, (76 \,.\, C_s + 9468. \frac{h}{s}) \qquad (1.6)$$

where h is the height or the thickness of the welded key, and s is the spacing between the keys.

In equation 1.6, the roughness factor is regarded as having a separate influence from that of the shear key factor. This might be thought to be surprising as the surface condition is not likely to be influential with closely spaced keys, but would be most important when the pipe surface is plain. Figure 1.7 shows the most likely failure mode for both plain and weld beaded tube. It is clear that the failure of a connection with weld keys would be developed in the grout matrix rather than along the interface between the grout and the tube.

The design formulae provided for grouted connections do not take account of the applied lateral loading. Consideration of such loading may not be critical for a grouted connection, but is more likely to be necessary in dealing with the axial tension capacity and behaviour of a grouted pile. Part of the purpose of the work reported in this thesis is to establish the importance of lateral loading in assessing axial load capacity.

1.8 ESTABLISHMENT OF A THEORETICAL MODEL TO DETERMINE THE KEY PARAMETERS FOR GROUTED PILES

The behaviour of grouted tension piles is complicated and varies when the pile is subjected to different load conditions. Grouted pile design can not be based on previous experience of driven piles or similar structural elements. It is clearly important to establish the principal parameters involved so that these can be studied in detail.

Any mathematical model designed to describe the complete behaviour would be complicated and unwieldy. On the other hand, there is a need to focus attention on the prime governing factors. In the following chapter a simple mathematical model will be presented to provide a demonstration of the effect of quantities such as grouted length, pile stiffness etc. on axial load capacity. The results of this study confirm the trends described in the introduction and have been used as the basis for an experimental programme to determine particularly the local interface behaviour of the pile/grout system, and the effect of lateral load on pile resistance.

1.9 RECENT RESEARCH ON TUBULAR CONNECTION AND OBJECTIVES OF THE PRESENT WORK

In section 1.3, attention was focused on the design recommendations that follow from Billington's work on tubular connection. More recently, there has been a significant body of work undertaken to determine more precisely the mechanisms involved and to model connections under axial pull-push regimes using finite element methods. The scope of this work will be appreciated from the addendum to the bibliography which is given in page 227.

In some circumstances, the analytical tools developed (Elnashai (1984), Elnashai and Dowling (1984), (1986), (1989), and Chilvers (1984)) will allow the behaviour of grouted tension pile to be analysed using the model for grouted connection with appropriate choice of stiffness for the outer cylinder. Tests on small and large scale grouted connections (Carroll (1984)), had proved the validity and the performance the finite element approach proposed in representing the behaviour of grouted connections under axial loading. In this reference, a friction equation was derived and shown to yield results in very good agreement with the exprements.

In the present work the focus of attention is on the behaviour of grouted tension piles under combined loading and examining the local shear - slip relationship during failure at the pile/grout interface.

For this work, it was felt appropriate to adopt directly the grout pile arrangement in devising tests, rather than to adopt the test procedure for tubular connection.

Failure of grouted pile, either along the grout/rock, or the pile/grout interface can lead to catastrophic instability particularly in the TLP type of structures. The study of the interfacial strength and behaviour is of paramount importance.

During this investigation, tests were carried out to analyse the interface pile/grout behaviour and the effect of lateral loads on the axial pile capacity.

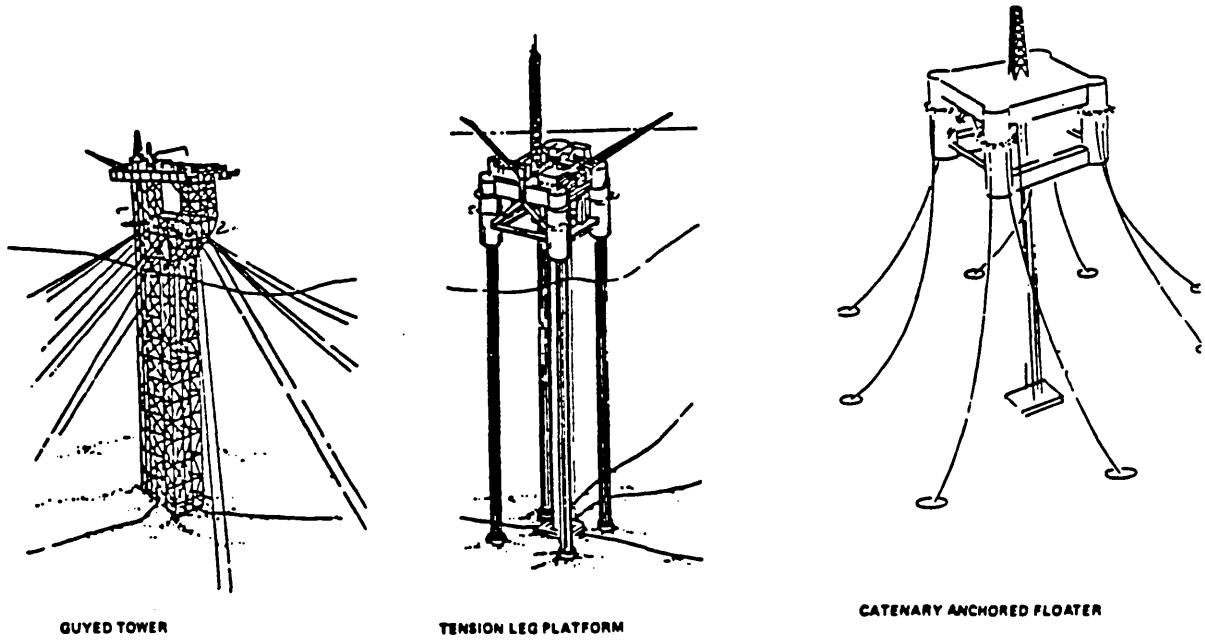


Figure 1.1a : TYPICAL MODERN OFFSHORE STRUCTURE IN DEEP WATERS

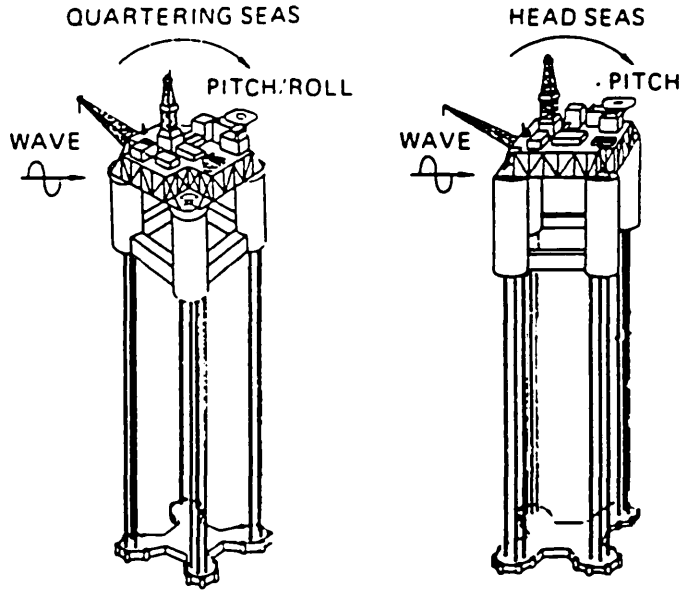


Figure 1.1b : TETHERED TENSION LEG PLATFORM WITH DISTRIBUTED PILES AROUND THE STRUCTURE BASE

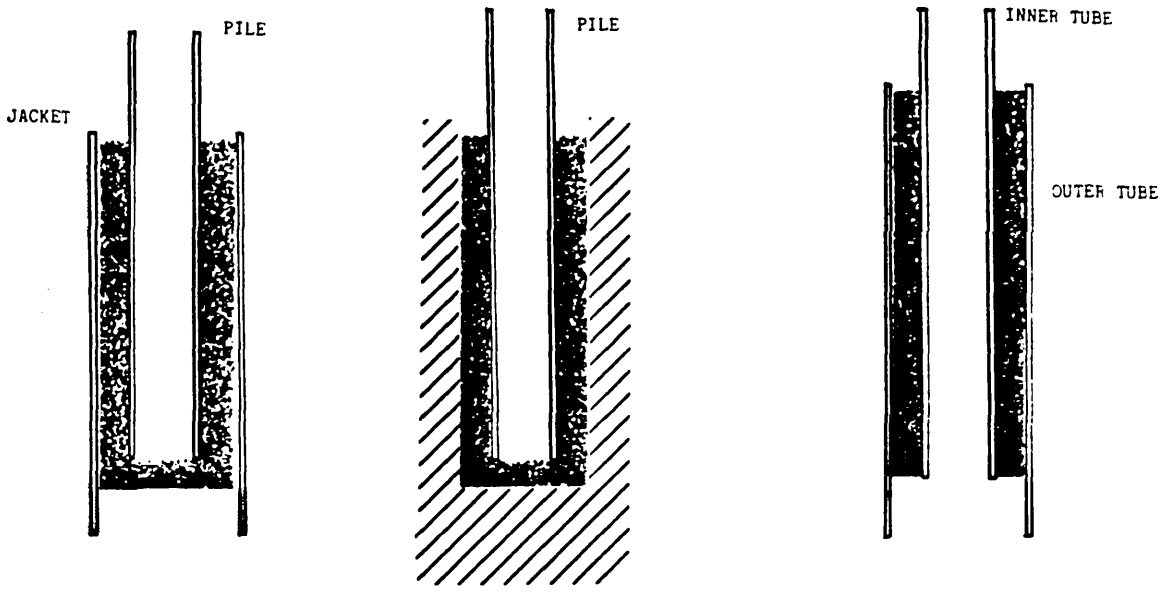


Figure 1.2 : STRUCTURAL ARRANGEMENT OF GROUTED PILES COMPARED WITH THE GROUTED CONNECTION SYSTEM

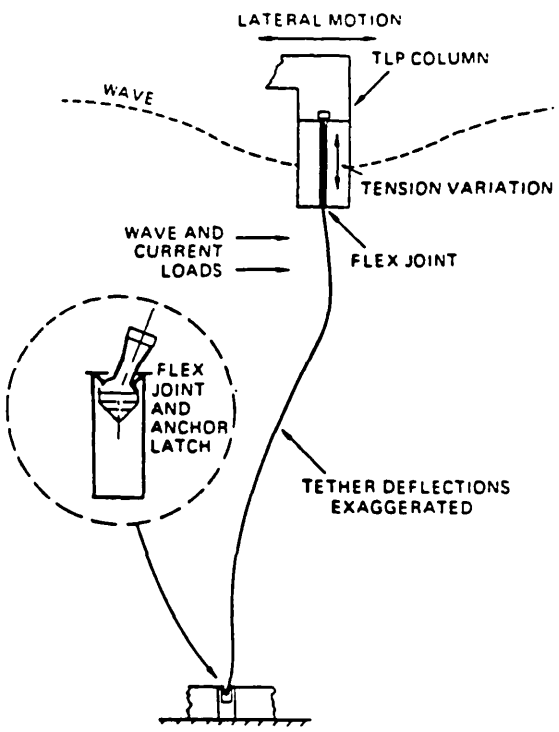


Figure 1.3 : LATERAL FORCES ACTION ON THE TLP LEGS AND FOUNDATION

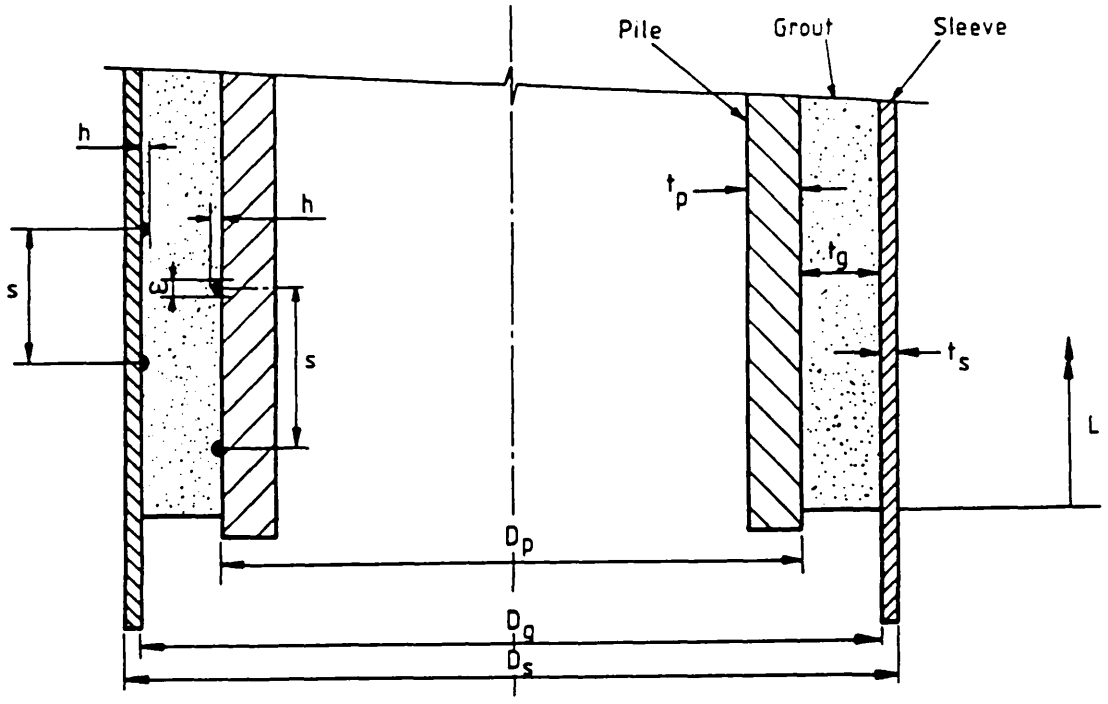


Figure 1.4a : TUBULAR GROUTED CONNECTION
(from Department of Energy (UK) (1982))

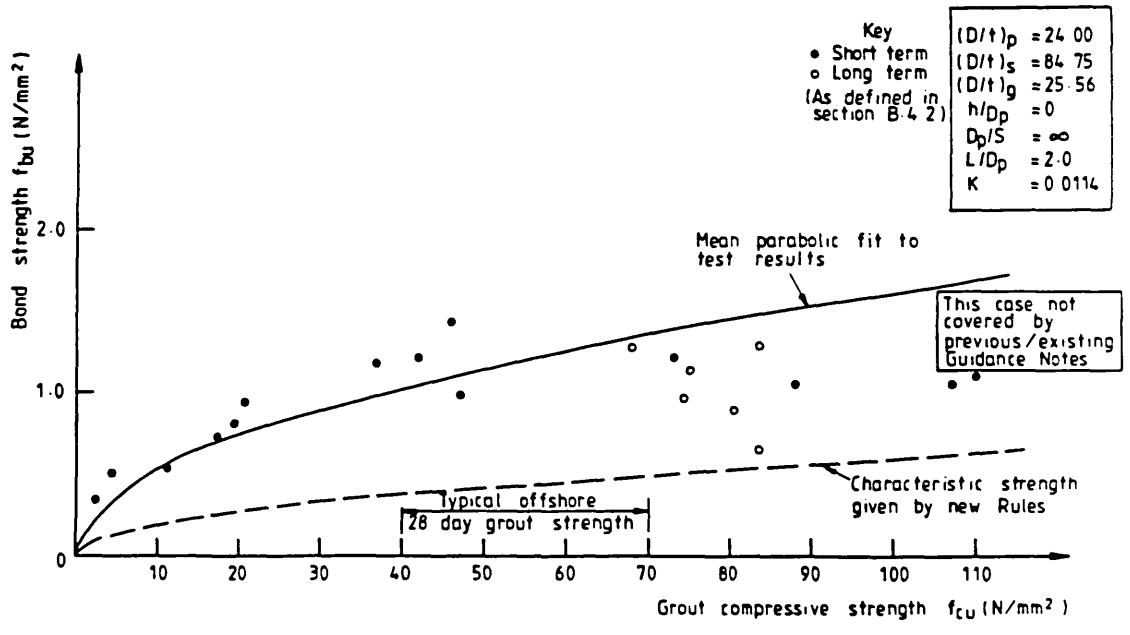


Figure 1.4b : BOND STRENGTH VARIATION WITH THE GROUT COMPRESSIVE STRENGTH
from Department of Energy (UK) (1982)

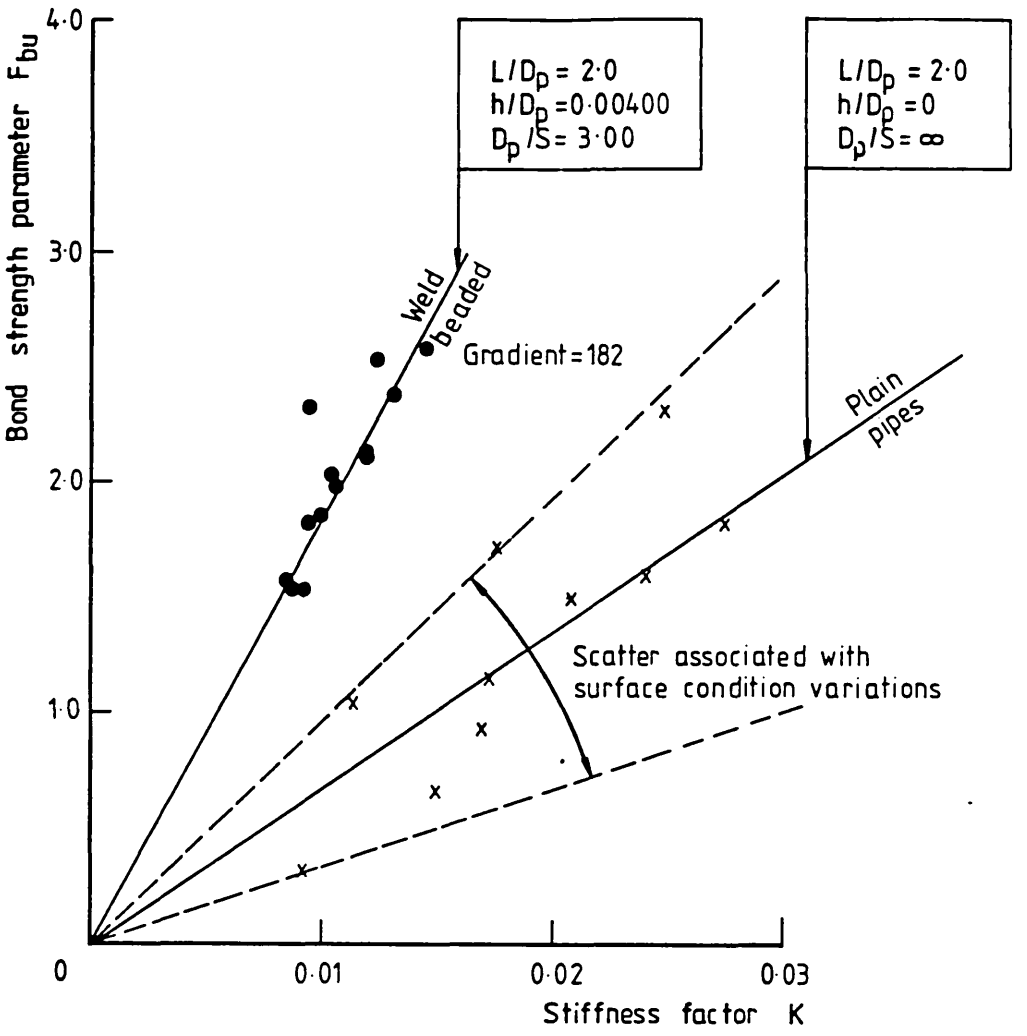


Figure 1.4c : BOND STRENGTH VARIATION WITH THE CONNECTION STIFFNESS FACTOR
from Department of Energy (UK) (1982)

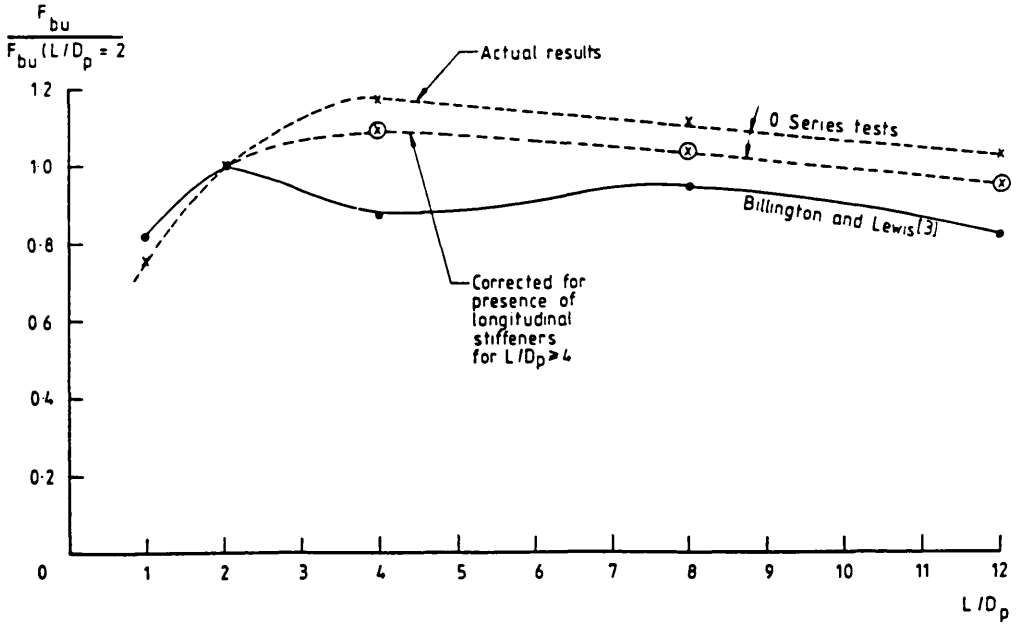


Figure 1.4d : BOND STRENGTH PARAMETER VARIATION WITH THE GROUTED LENGTH
from Department of Energy (UK) (1982)

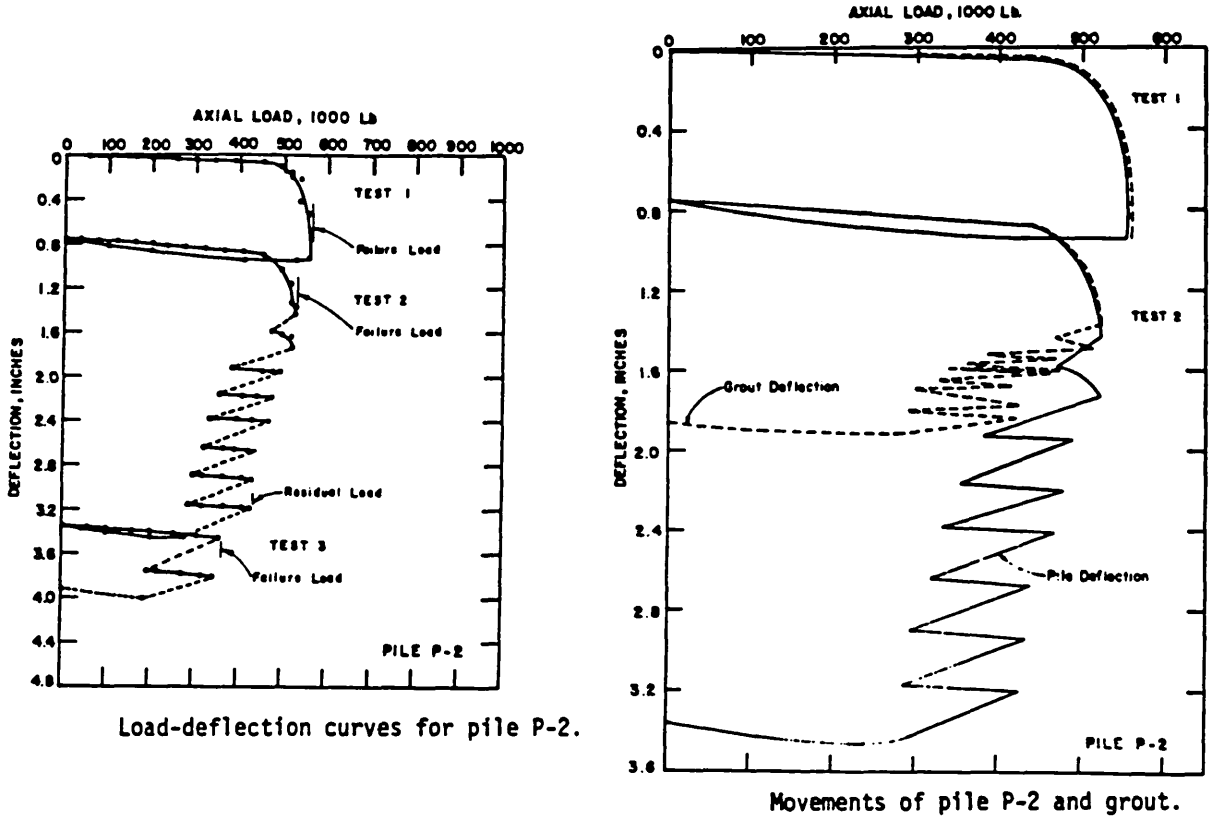


Figure 1.5a : GROUTED PILE BEHAVIOUR (from Cox and Reeses (1976))

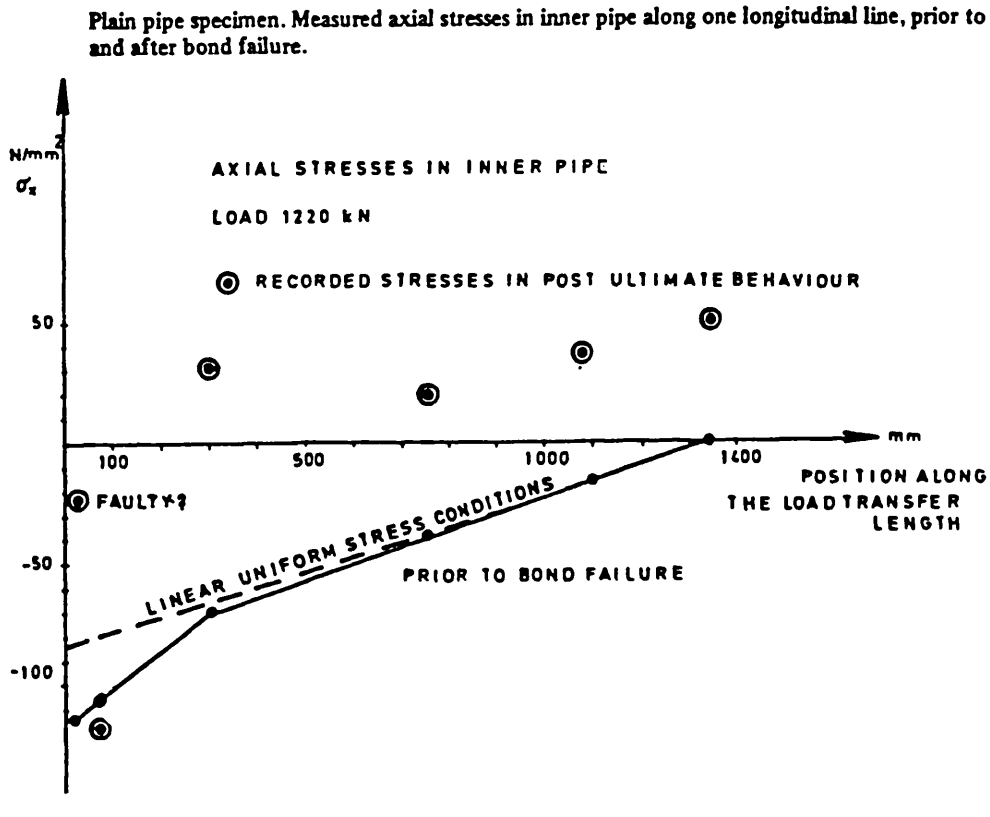


Figure 1.5b : SHEAR STRESS VARIATION ALONG THE LENGTH OF THE GROUTED CONNECTION (from Loset (1981))

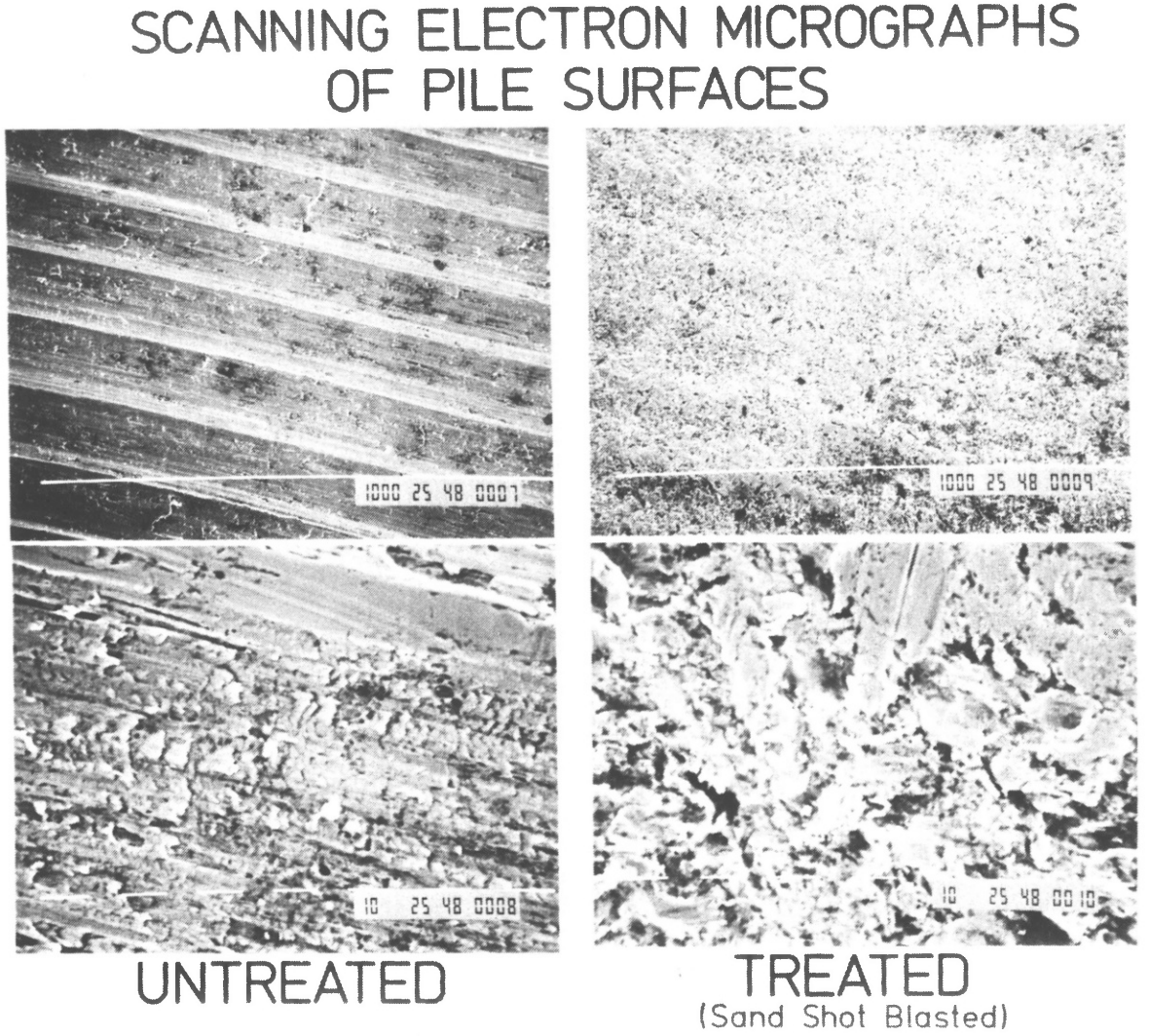


Figure 1.6 : OBSERVATION ON THE PILE STEEL SURFACE BEFORE AND AFTER SAND SHOT BLASTING

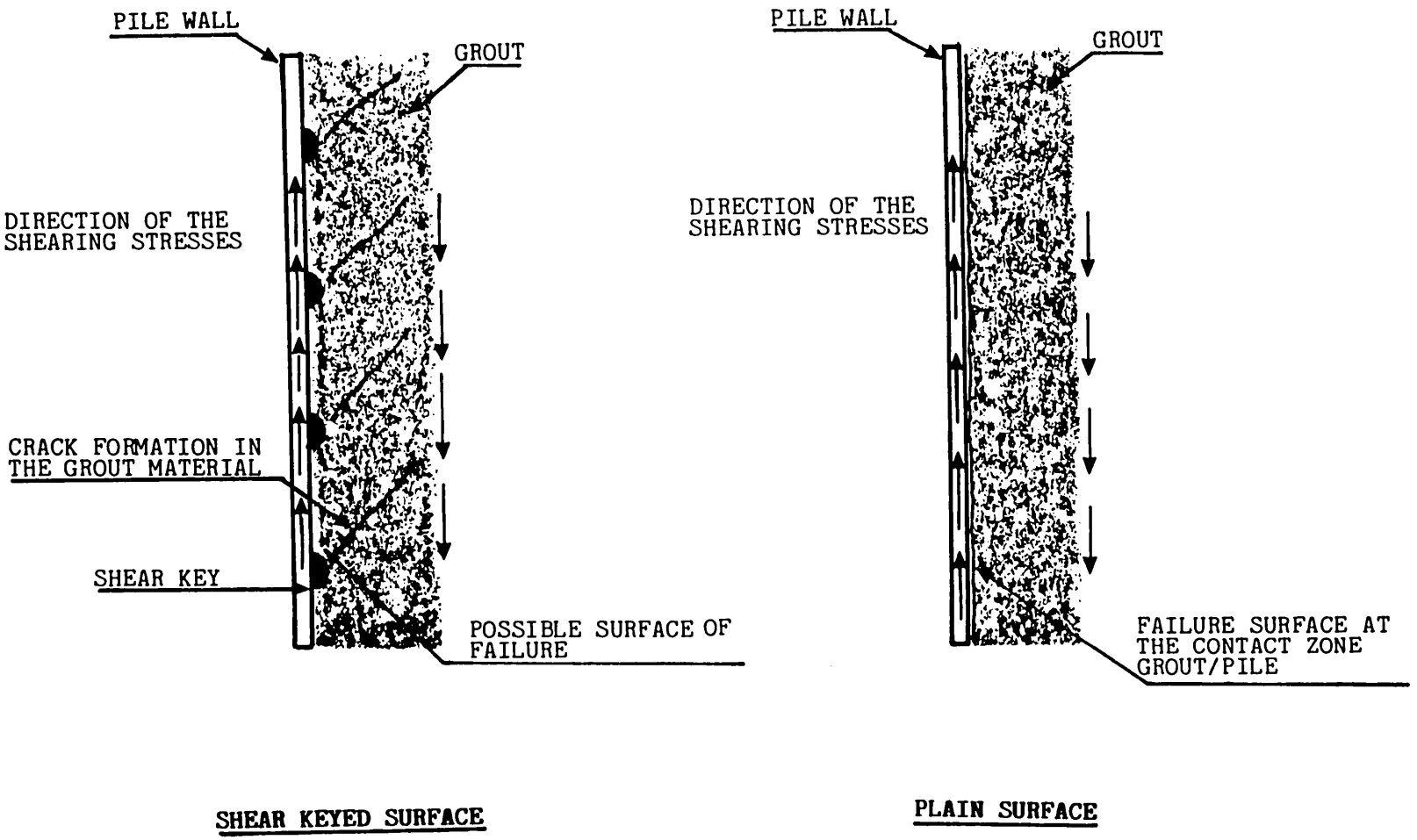


Figure 1.7 : INTERFACIAL FAILURE MODE WITH AND WITHOUT SHEAR KEY

CHAPTER 2 : NUMERICAL MODEL

2.1 INTRODUCTION

The behaviour of a complete system compromising the pile, its interface and the surrounding medium is complicated. In approaching this situation, it seemed useful to study the behaviour of a simpler system in which interaction with the surrounding medium is defined by a single shear/slip relationship unaffected by dilatancy and restraint effects from the surrounding medium. Accordingly, a model system was investigated involving a straight elastic pile with its load capacity being developed by interfacial shear with the surrounding medium. A one-dimensional model is used and the analysis confined to pile extraction under tensile loading or prescribed displacement. In this way, an initial view is developed of the effects of softening in the shear stress/slip relationship describing interface behaviour and on the factors influencing the overall load capacity of the pile and its mode of failure.

A previous analytical investigation by Morrison et al (1988) was carried out to determine the crack propagation along a straight steel circular fibre embedded in cement paste, with the fibre submitted to an extraction force. Their analysis was based solely on the behaviour of the tip of the fibre, and aimed to deduce the local shear stress : slip relationship along the interface, as well as the length of the debonded fibre length with relation to the applied force at the fibre tip. According to these authors, there are two principal approaches to the analysis of an interface debonding process. The first one is based on shear stress distribution, where the debonding occurs when the shear stress exceeds the interface strength. The second approach is built on a fracture mechanics basis, where debonding is associated with the energy release along the interface. The authors considered that the latter approach is more convenient since it permits the avoidance of the problems that accompany stress concentrations.

The present work, adopts the alternative procedure and derives the global pile behaviour from the interface local shear/slip characteristics by means of a one-dimensional model. The relationship between interface softening and global pile response softening is thereby established.

2.2 INTERFACE MATERIAL MODEL

The actual behaviour of the pile/grout interface is complex, and varies according to many parameters (surface condition, stiffness of both bonded media). Consequently considerable simplification is essential in order to develop a practical mathematical model to demonstrate the main aspects of pile behaviour.

The relative shear : displacement behaviour involves slip softening. For simplicity, the constitutive relation for the pile/grout interface is considered to be linear. The slope of the loading and the softening (stress relief) regions are respectively E_{int} and D_{int}. Figure 2.1a shows the assumed shear stress-slip relationship of the spring model. For large slip values the shear stress is assumed to be constant, reflecting the frictional behaviour at the interface. The viewpoint adopted here is that the drop of the shear stress with slip is based on the fracturing behaviour of the interface, and the change of the interface nature from bonded state to frictional contact surface.

The interface model is characterised by four variables that can be defined by the maximum and residual shear stresses (τ_{max}, τ_{res}) and their corresponding slip displacement values (u_{max}, u_{res}). The use of the slopes of stress variation E_{int} and D_{int}, instead of two other parameters can be an alternative for the model representation.

From a mechanical point of view, the interface fracturing behaviour can be regarded as the result of a progressive damage caused by the applied stress history. The pile/grout interface experiments, under pure shear stress, the results of which will be presented in chapter 8 of this thesis, supports such an approach to interface modelling. The shear stress : slip displacement relationship can be defined by :

$$\begin{bmatrix} \tau(u) = - E_{int}\, u & \text{if } |u| \le u_{max} \\ \tau(u) = D_{int}\, u - (E_{int} + D_{int})\, u_{max} & \text{if } u_{max} \le |u| \le u_{res} \\ \tau(u) = D_{int}\, u_{res} - (E_{int} + D_{int})\, u_{max} & \text{if } u_{res} \le |u| \end{bmatrix} \qquad (2.1)$$

(Note : the negative sign (-) is being introduced, since the shear stress acts in the opposite direction to the slip displacement)

2.3 PILE IDEALISATION

The pile is assumed to be under an axial tensile force. Consequently a one-dimensional presentation would be sufficient. The pile is modelled by a simple steel rod linked to a rigid foundation by an interface with the properties described by equations 2.1. Figure 2.1b presents the structural model with the pile and the interface represented by springs.

2.4 FORMULATION OF THE GENERAL EQUATION

2.4.1 GENERAL EQUATION

Static equilibrium, on a pile element with a finite length dx, is given by equation 2.2 :

$$\frac{df(x)}{dx} + P_p \tau(u) = 0 \qquad (2.2)$$

where P_p is the pile perimeter, f is the axial force in the pile at the location x, and $\tau(u)$ is the interface resistance along the element length, which depends on the slip displacement u of the element (figure 2.2a), which is the same as slip with respect to the rigid foundation.

The strain in the element (figure 2.2b) is given in terms of pile deformation by :

$$\varepsilon_{pile} = \frac{du(x)}{dx} \qquad (2.3)$$

where ε_{pile} is the pile strain, which is assumed to be uniform across the section. The pile is taken to behave elastically for all magnitudes of stress so that the pile strength is not considered in the analysis. The study focuses on the implication of the interface behaviour, but in practice the pile strength will be an additional parameter to be taken into account. The pile strain deformation can then be expressed as a function of f through

$$\varepsilon_{pile} = \frac{\sigma}{E_p} = \frac{f(x)}{E_p A_p} \qquad (2.4)$$

where E_p is the elastic modulus of the pile, and A_p the pile cross section. The general equation is obtained by the combination of (2.2) and (2.4) as :

$$\frac{d^2u(x)}{dx^2} + \frac{P_p}{A_p} \cdot \frac{1}{E_p} \cdot \tau(u) = 0 \qquad (2.5)$$

To normalise the depth coordinate, a non-dimensional $X = x/L_p$ is introduced. The general equation (2.5) will take the following form :

$$\frac{d^2u(X)}{dX^2} + \frac{P_p}{A_p} .L_p^2 \cdot \frac{1}{E_p} \cdot \tau(u) = 0 \qquad (2.6)$$

During the pile loading the interfacial spring model can undergo different states of stress along the pile length :

- elastic state (before reaching τ_{max})
- fracturing state (decreasing stress with increasing slip)
- residual state (constant residual stress)

The set of general equations, covering all three regions, is non linear, and the derivation of a single analytical solution is very complicated, so it has been ruled out for the present work. For each given load, the partial pile length for every stress state would have to be defined. Accordingly, several trials of stress state distributions, along the pile length, would be needed for each pile load and a procedure for iterating to complete the boundary position would be required. The solution procedure would be laborious, so an alternative numerical procedure has been carried out.

The use of force and stress variables to resolve the general equation induces unsystematic procedures and leads to numerical difficulties during the programming of the problem. In addition it can cause the non-uniqueness of the solution (Casey and Naghdi (1984)). The difficulties arise particularly when the shear stress reaches its maximum value τ_{max}. Then the reduction of the stress might follow either an unloading path or a strain softening path. An additional procedure must be provided to describe the interfacial stress history, and to guide the stress path of the element in terms of the slip displacement u. The definition of the general equation in terms of slip displacement is

imperative.

2.4.2 BOUNDARY CONDITIONS

The boundary conditions can be expressed alternatively in terms of forces f (i.e. stress variables), or displacement u i.e. :

$$f(x=0) = -F \quad \text{and,} \quad f(x=L) = 0 \tag{2.7a}$$

or

$$u(x=0) = -U \text{ and,} \quad \frac{du}{dx}(x=L_p) = 0 \tag{2.7b}$$

(note : the negative sign (-) is being introduced because F, and U are taken to be absolute values)

2.4.3 ELASTIC SOLUTION

When the interface shear stress along the total pile length does not experience any fracturing stress load history, the shear stress can be expressed in terms of the local slip displacement as :

$$\tau(u) = -E_{int}\, u \tag{2.8}$$

The general solution for the displacement is then found by solving the general equation (2.5) with the application of the boundary conditions. It follows that for elastic behaviour the slip displacement along the embedded length is given by :

$$u(x) = u_{max}\left[\frac{(e^{\alpha(L_p - x)} + e^{-\alpha(L_p - x)})}{(e^{\alpha L_p} + e^{-\alpha L_p})}\right] \tag{2.9}$$

where

$$\alpha^2 = \frac{P_p}{A_p} \cdot \frac{E_{int}}{E_p}$$

The maximum force that could be applied to the pile without causing any fracturing stress along the interface can then be expressed as :

$$F_{max} = \sqrt{\frac{E_p}{E_{int}} \cdot P_p \cdot A_p}\ \tau_{max} \tag{2.10}$$

2.4.4 Parameters Affecting the Pile Behaviour

In the region where softening occurs at the interface ($u_{max} \leq u \leq u_{res}$), the general equation (2.6) and (2.1) can be written :

$$\frac{d^2u(X)}{dX^2} + \beta u = \gamma \qquad (2.11)$$

where $$\beta = \frac{P_p}{A_p} . L_p^2 . \frac{D_{int}}{E_p} \text{ and, } \gamma = (\beta + L_p^2 \alpha^2) u_{max}$$

It will be seen later that the non-dimensional parameter β characterises the mode of behaviour of the pile, the influence of the pile length and the interfacial stiffness on the mode of failure.

2.5 NUMERICAL SOLUTION

Computational procedures containing softening plasticity are rarely used, because of their complexity and the numerical instability caused by strain softening. The loading of the pile results in local interface slip softening along a partial pile length. Consequently, the pile experiences irreversible displacement. As in hardening plasticity, incremental analysis is required to follow the loading process of the pile model. This is described by the relation between the pile end force and the pile tip displacement.

After initial hardening behaviour, overall pile behaviour during extraction with controlled displacement will show pile end displacement softening followed by a constant residual resistance. This will be caused by the propagation of the local interface slip softening and the development of a residual constant stress state along the pile length. The final residual constant pile resistance will be the summation of the residual stress applied on the total pile surface.

The boundary conditions have to be expressed in terms of pile tip slip displacement and not pile end force parameters, to avoid the numerical difficulties discussed above (general equation). If the boundary condition at the pile top end is given in terms of a given loading force, the solution of the pile post-peak behaviour cannot be determined. In fact at this stage, while the pile resistance is decreasing (softening), the

pile loading is being described in terms of additional force increment. Under these circumstances a solution does not exist. The adopted method has to incorporate the top pile displacement in order to obtain a full description of the global pile behaviour.

2.5.1 COMPUTATION OF THE GENERAL EQUATION

The finite difference method has been adopted to solve equation 2.5 under incrementally increasing pile end displacement. The pile is divided into N elements, with N+1 nodes (figure 2.3). Equation 2.5 is then written in finite difference terms for each node i.e. :

$$u_{i-1} - 2u_i + u_{i+1} + k_p \delta X^2 \tau(u) = 0 \qquad (i = 2,3,4.....N) \qquad (2.12)$$

where,

$k_p = \frac{P_p L_p^2}{E_p A_p}$ (pile stiffness factor) $\delta X = \frac{1}{N}$, and u_i is the displacement at the i^{th} node

This set of equations must be solved for the boundary conditions :

$$u_1 = -U \qquad \text{and,} \quad u_{N+1} - u_N = 0 \qquad (2.13)$$

and the shear stress/slip relation given by equation 2.1. (since U had been chosen to be an absolute value, a sign (-) had to be introduced).

For each increment of prescribed displacement at the pile tip, an iterative procedure is needed to take account of the nonlinear local interface behaviour. Starting with the elastic solution, an increment of end displacement is added to the previous tip displacement condition. The global equation forms a nonlinear system. The matrix elements depend on the state of interface behaviour at each pile node. The method adopted is to create index vectors for two successive iterations, which indicate the state of the interface material at each of the nodes (i.e elastic (+1), fracturing (-1), and residual (0)). The iterations will stop when two successive index vectors are identical. Then the slip distribution is obtained as well as the corresponding stress distribution and the corresponding resisting force. Additional details about the equation system and its resolution are presented in Appendix 1. A listing of the Fortran program is also given.

2.5.2 RESULTS

Two pile study cases, with different lengths, are analysed using the finite difference program. The results are shown for both cases in figures 2.4. The details of the piles and the interface characteristics are given in table 2.1.

Distribution of the shear stress and pile displacement along the length of the pile are shown at two stages during extraction in figures 2.4a. With these results is given the graph of end force to a base of end displacement as would be obtained by external instrumentation. For the study case No 2, the embedded pile length is ten times greater than that of the first study case.

At stage 1 in the extraction history, the interface is purely elastic. The end slip/end force is linear and the shear stress along the pile is limited to the maximum shear stress τ_{max}.

By the time of achieving stage 2, there is an influence of softening over a part of the pile length. The total force-end slip relationship is now non-linear.

Figure 2.4b shows subsequent stages in the extraction process. Stage 3 coincides with the maximum load necessary to extract the pile. Any further pile tip displacement increment causes the reduction of the pile end force. This stage of the pile loading might correspond to the fracture region reaching the bottom of the pile. This depends on the interface resistances τ_{max}, τ_{res}, the parameters E_{int}, D_{int} as well as the pile length. In other terms, there is a strong possibility that the factor β dictates the shear stress and slip distribution at this stage.

By stage 4 the continued effects of extraction and the consequences of slip softening on the load required can be observed whilst stages 5 and 6 (figure 2.4b) show the load required for further extraction being dependent solely on the residual strength τ_{res}.

Although the increase of the embedded length provides a greater resistance to pile extraction, there is an important difference in behaviour between the two cases once the maximum load has been reached. The behaviour of a short stiff pile (case 1) follows that of the local shear bond model, with a stable progressive failure, whereas longer piles can fail in a brittle unstable manner. This is shown by the achievement of the residual

pile strength only after a dramatic snap through type instability.

This mode of failure is not governed by the pile length only. For certain combinations of the interface properties, pile stiffness and geometry, the pile extraction would never follow the actual end pile force/end pile displacement curve. Once the pile maximum resistance has been reached, any pile end force or displacement increment will result in a snap-down of the resisting force accompanied by a brittle and sudden end pile large displacement. This failure mode would be brittle and sudden. In practice such a brittle failure mode would be undesirable. A reduction of the pile length would avoid unstable failure, but at the expense of load capacity.

2.5.3 OTHER NUMERICAL ALTERNATIVE

The distribution of the shear slip and stress along the pile length depends on the extent of the pile extraction. A combination of elastic, fracturing, and frictional behaviours can be established along the pile length. An alternative approach can be used to define the pile global behaviour under a monotonic extraction. The pile can be divided into three regions, elastic, fracturing and frictional. The governing differential equations can be solved within each region and, by imposing conditions of compatibility and equilibrium at each interface (figure 2.5), the behaviour of the whole pile can be determined. However, since it has been shown above that the pile behaviour, when expressed in terms of the force or displacement at the top of the pile, presents a fracturing behaviour, an alternative independent variable must be chosen. When part of the pile/grout behaviour is elastic, this can most conveniently be done by relating the pile behaviour to the position of the elastic zone - fracturing zone interface. When none of the pile/grout interface is responding elastically, an adequate parameter is the displacement of the bottom of the pile. It is reasonable to suppose that both of these variables behave monotonically during pile extraction, even if the pile top displacement does not.

The pile tip force can be found easily at any stage from the sum of the shear stresses along the interface. The pile tip displacement is obtained directly as an unknown parameter of the system of equations.

This latter method is simple and convenient for the establishment of the pile global behaviour during a simple extraction. However, once the pile is submitted to a cycling load, this procedure would be much more complicated, since the unloading behaviour would necessitate dividing the pile length into many sub-regions to account for the variety of history-dependent behaviours which could result. For this reason the

solution of the problem is established by the finite difference method described here, which permits the imposition of any pile tip loading pattern, and the adoption of more general shear/slip relationships than those of equation 2.1.

2.6 PILE LENGTH EFFECTS

2.6.1 PILE LENGTH FOR THE CRITICAL UNSTABLE BEHAVIOUR AND ITS RELATION TO THE SLIP SOFTENING RATE

The critical pile length L_c can be defined by the value for which there is a transition from unstable to stable failure. In other words, once the maximum pile resistance has been reached, any incremental pile tip displacement will cause a drop of the pile resistance to its residual value without any change of the pile end displacement (figure 2.6).

A detailed investigation has been carried out to establish numerically the relation between the interface softening modulus Dint and the critical pile length L_c. Such a relation is presented in figure 2.7. There is a linear relationship between the softening modulus and the critical pile length, defined by the following equation:

$$D_{int} \cdot L_c^2 = K_e \qquad (2.14)$$

(For values used in the present study, K_e has been found to be $5.6142\ 10^9$ N/m)

We can deduce that the transition from stable to unstable behaviour will occur at a critical value of β, which is in agreement with the study shown in figure 2.7, and discussed above, in which $D_{int}\ L_c^2$ was a constant when all the other parameters were invariant. The substitution of the actual values used for P_p, A_p, E_p, and the observed value of $D_{int}\ L_c^2$, leads to the conclusion that $\beta < 2.69$ is needed for stable behaviour to result.

For large pile diameter with a thickness considerably smaller with respect to the pile radius ($t << R_{pile}$) the expression of β can be written as:

$$\beta = \frac{L_p^2}{t_p\ R_{pile}} \cdot \frac{D_{int}}{E_p} \qquad (2.15)$$

The term β could be relatively important for a designer to provide safer construction for grouted tension piles. A limiting value has been established, so that, for a given pile steel surface and grout material (D_{int}), with a selected pile diameter and thickness, a critical pile embedded length can be imposed.

However, it seems that more studies are required so that the effects of the parameter γ (equation 2.11) could be analysed. The non-linearity of the present problem, and the fact that equation 2.11 only applies over a part of the pile length could be an additional consideration to be taken into account. As a result, one can deduce the effects of the interface resistance τ_{max}, τ_{res}, with their corresponding slip displacement u_{max}, u_{res}, and the variable E_{int}.

2.6.2 AVERAGE SHEAR STRESS

The average shear stress, corresponding to the maximum pile resistance, is computed by assuming that the shear resistance is uniform along the embedded length, then plotted on the base of pile length. This is shown in figure 2.8. Here, for long piles the average shear stress tends to the residual shear stress value of the local spring model, emphasising the importance of the residual (frictional) rather than the peak (bond) shear stress in the design of long pile.

2.7 DILATANCY MODELLING

The tests results carried out on the interface between the pile and grout under shear stress condition , presented in chapter 8 of this thesis, indicate the existence of a dilatancy phenomenon. The dilatancy of the interface during the breakdown can be introduced by reducing the slip softening modulus D_{int}. In this way, failure would be more stable and will be developed in a more progressive stable manner. Dilatancy would also increase the maximum and residual interface shear stress. This would be observed more frequently when the pile is confined in stiff surrounding. However the variations of the latter parameters have to be established. They include the grout and the surrounding media properties, as well as the pile surface roughness. Figure 2.9 summarises the practical approach to include the dilatancy of the pile/grout interface and the stiffness of the pile surrounding media. The experimental results, which will be presented in chapter 6 and 8, can be regarded as a fundamental basis to the suggested approach.

2.8 CONCLUSION

The form of the results obtained using the model show good qualitative agreement with results in chapter 6 from tests on model piles. This suggests that with more information available on dilatancy and the effect of normal stress on the interface shear/slip relationship the model could be extended to provide a useful practical tool for the behaviour of grouted pile under axial loading. At present however, the main value of the model has been in demonstrating the possible occurrence of instability and brittle snap-through modes of failure for long piles and the influence of the pile length on the average shear strength and load capacity.

No attempt has been made to devise a simple model which would deal with the combined effects of the longitudinal and lateral loading as required in evaluating the effects of path dependence. Clearly the problem is no longer axis-symmetric once horizontal loading is applied, and a more complete treatment would be needed.

Table 2.1 : Interface and Pile Characteristics for both Study Case

	Case 1	Case 2
Outer pile diameter (mm)	112	112
Inner pile diameter (mm)	90	90
Pile length (mm)	600	6000
Number of pile subdivisions	300	300
Interface maximum strength (N/mm^2)	3.5	3.5
Interface residual resistance (N/mm^2)	0.8	0.8
Slip for maximum stress u_{max} (mm)	0.06	0.06
Slip for residual stress u_{res} (mm)	0.5	0.5

Note : The values of the interface characteristics are selected from the test data on bond from Stroeven and De Wind (1982).

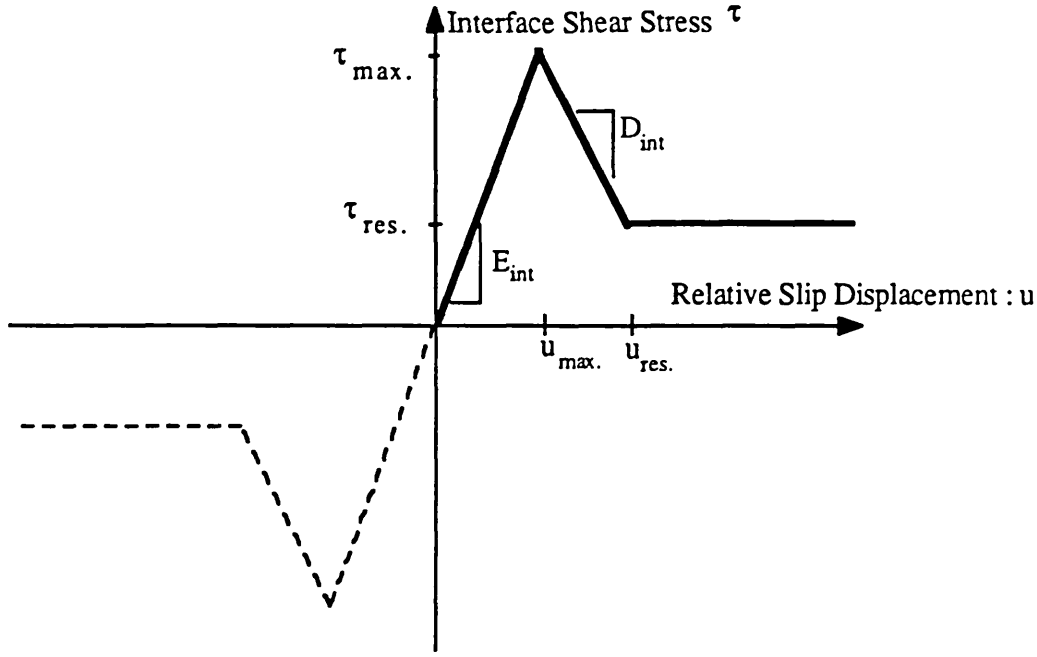


Figure 2.1a : INTERFACE BOND - FRICTION MODEL

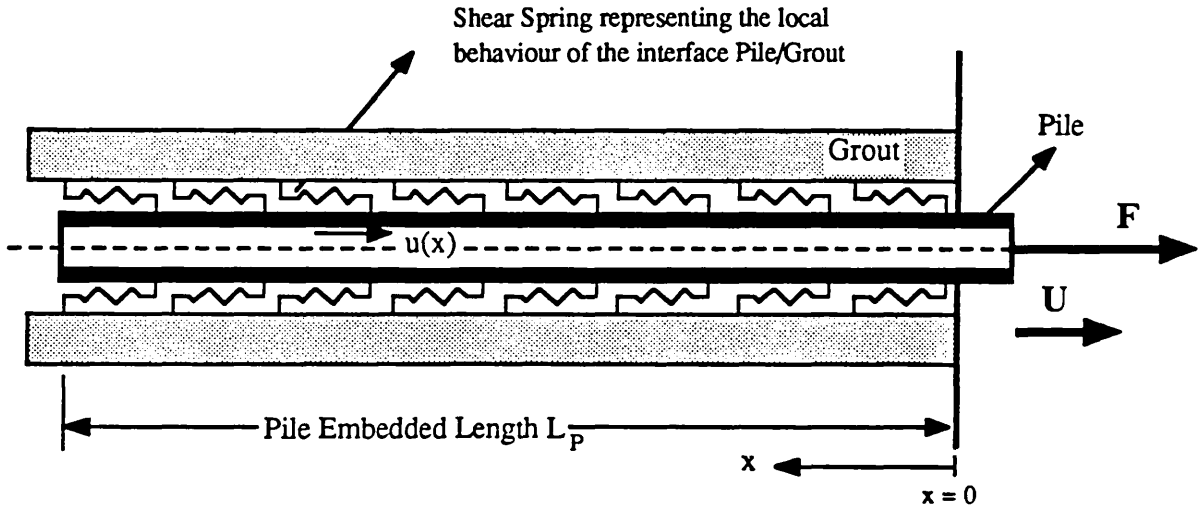
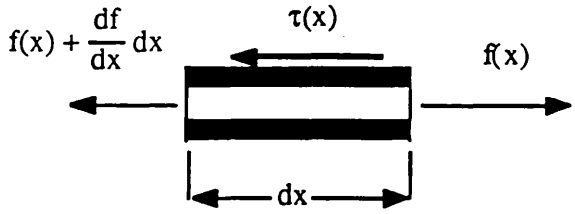
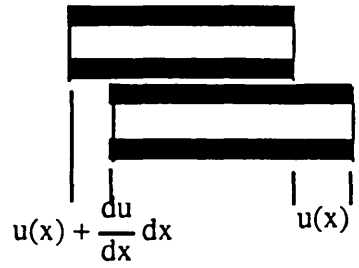


Figure 2.1b : GROUTED TENSION PILE MODEL



2.2a : Equilibruim of a Pile Element



2.2b : Pile Element Deformation

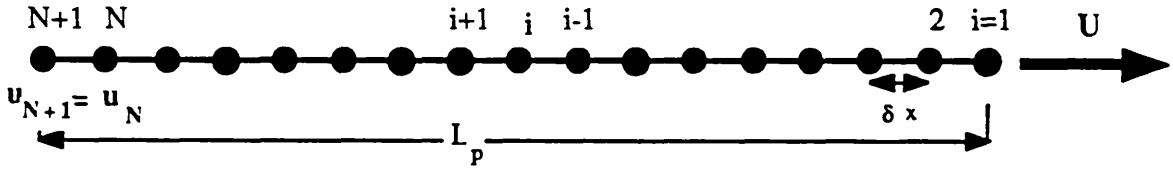


Figure 2.3 : FINITE DIFFERENCE DESCRIPTION OF THE PILE MODEL

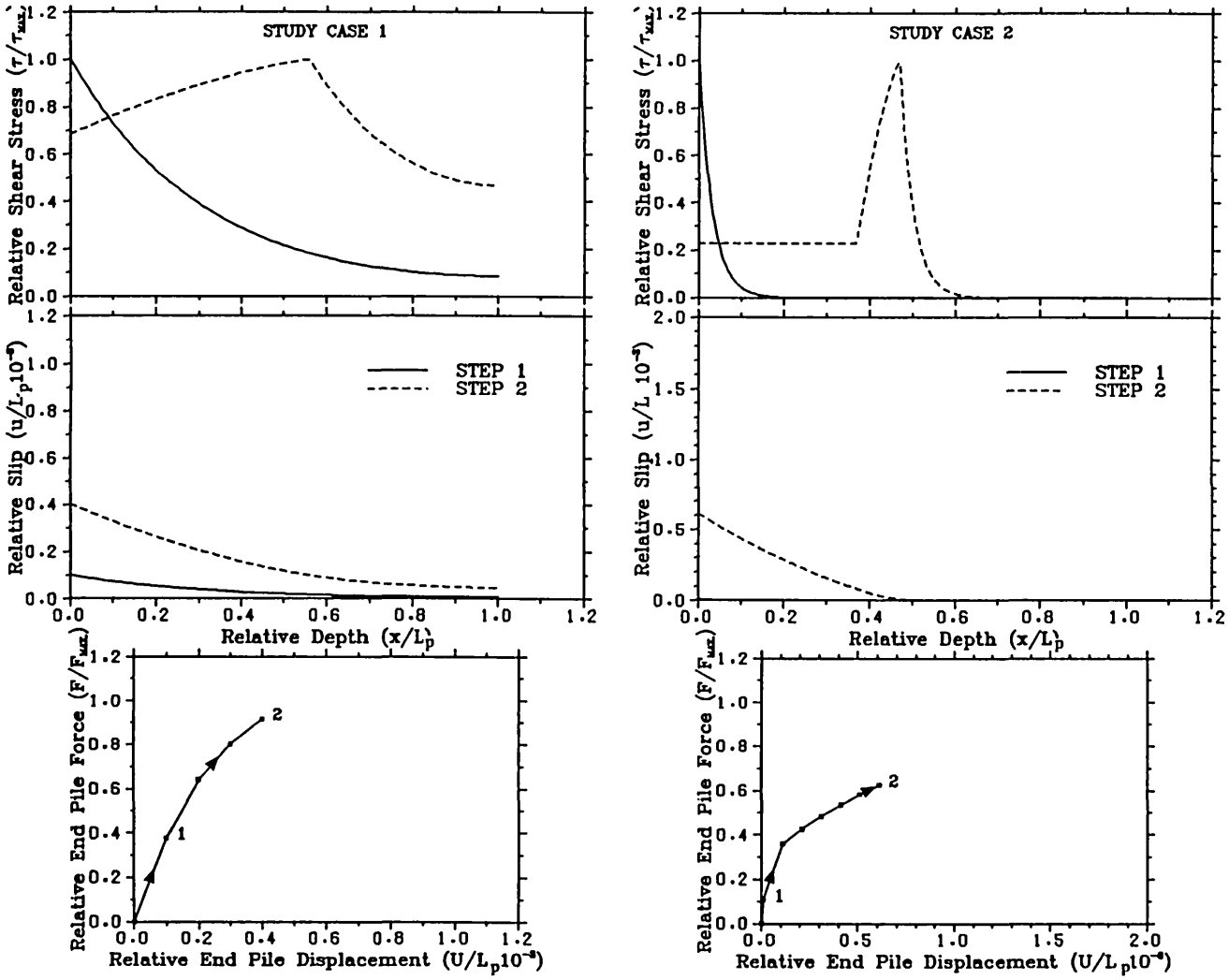


Figure 2.4a : SLIP AND STRESS DISTRIBUTION ALONG THE PILE LENGTH WITH THE CORRESPONDING END PILE FORCE – END PILE DISPLACEMENT RELATIONSHIP (Stages 1 & 2)

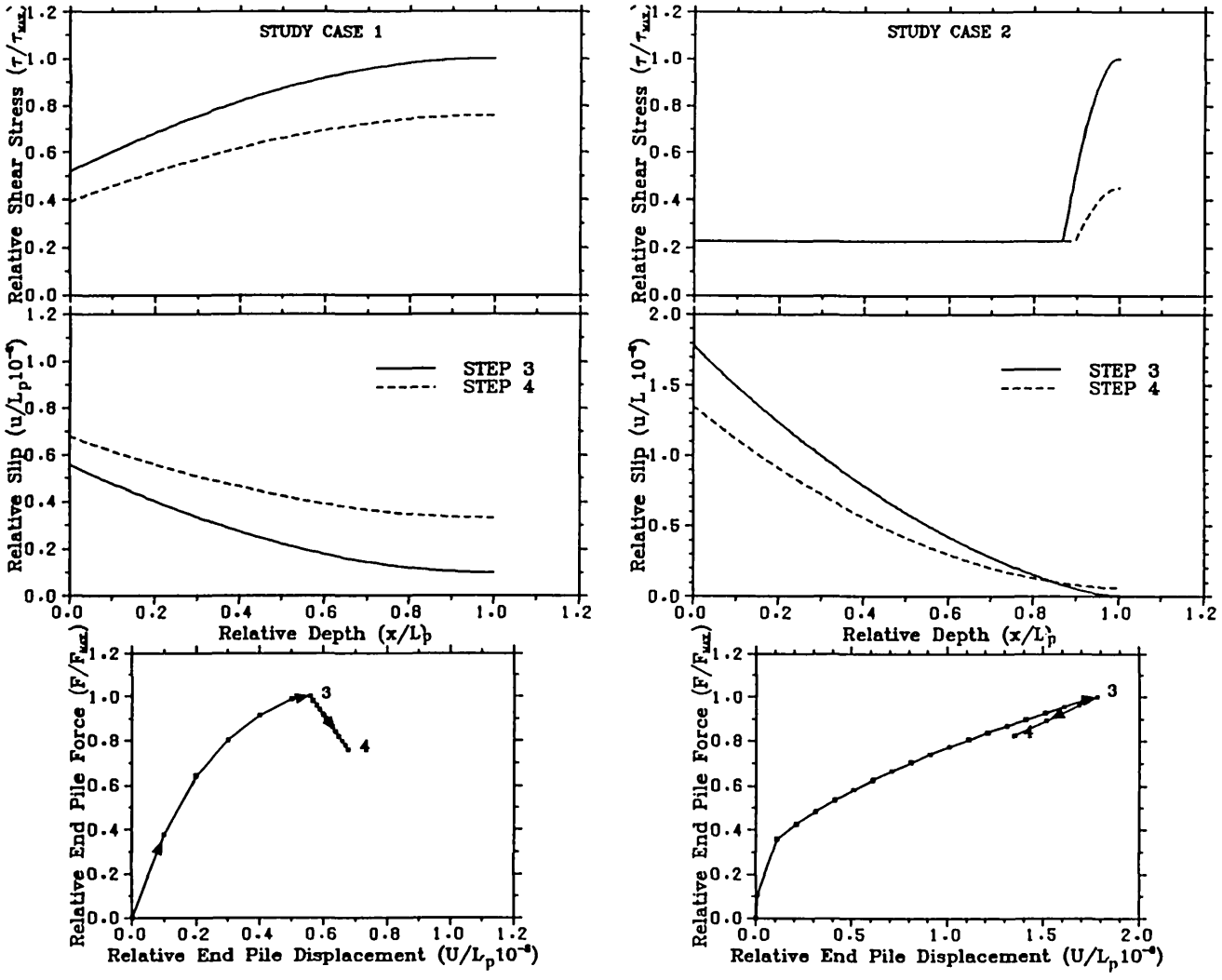


Figure 2.4b : SLIP AND STRESS DISTRIBUTION ALONG THE PILE LENGTH WITH THE CORRESPONDING END PILE FORCE – END PILE DISPLACEMENT RELATIONSHIP (Stages 3 & 4)

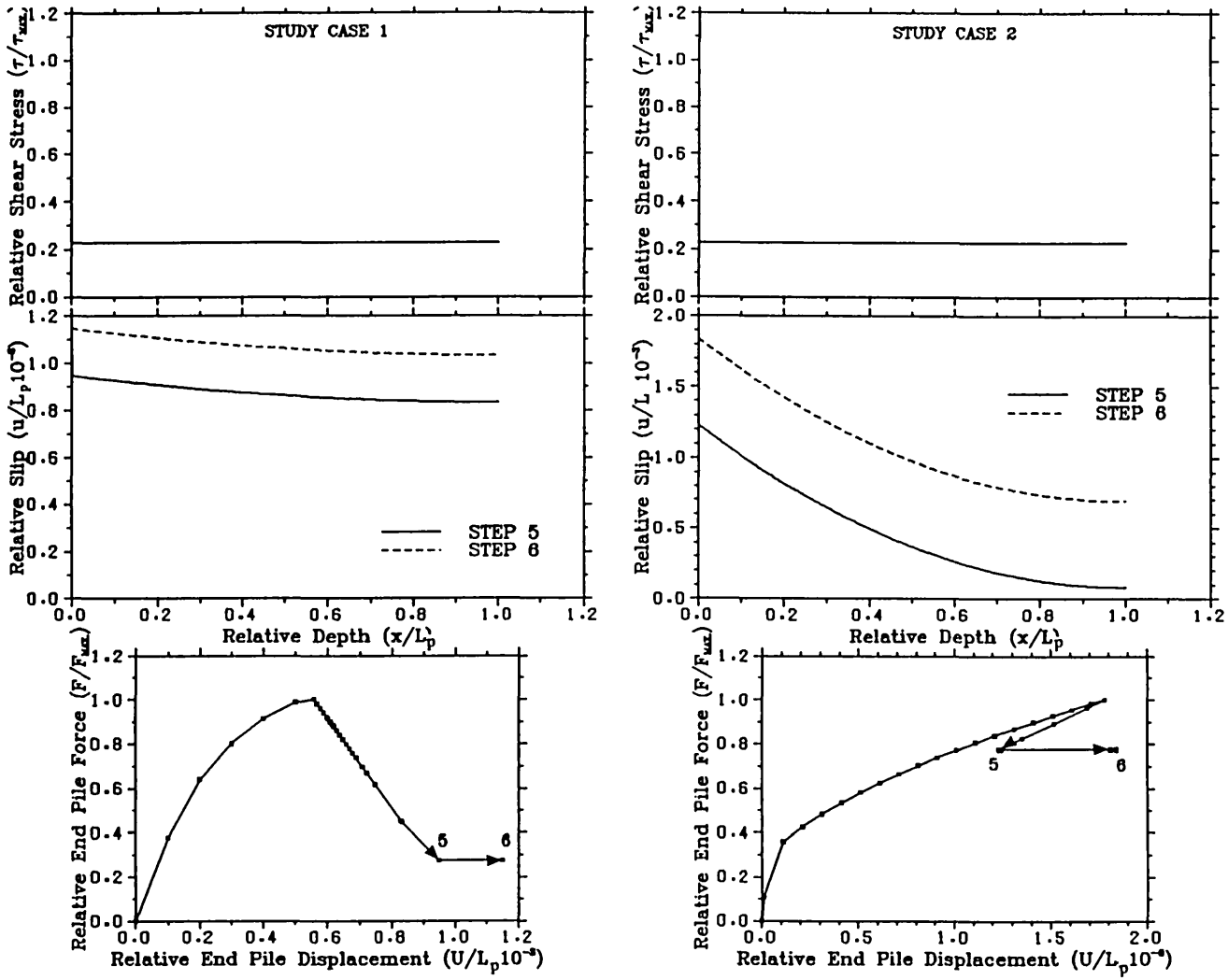


Figure 2.4c : SLIP AND STRESS DISTRIBUTION ALONG THE PILE LENGTH WITH THE CORRESPONDING END PILE FORCE – END PILE DISPLACEMENT RELATIONSHIP (Stages 5 & 6)

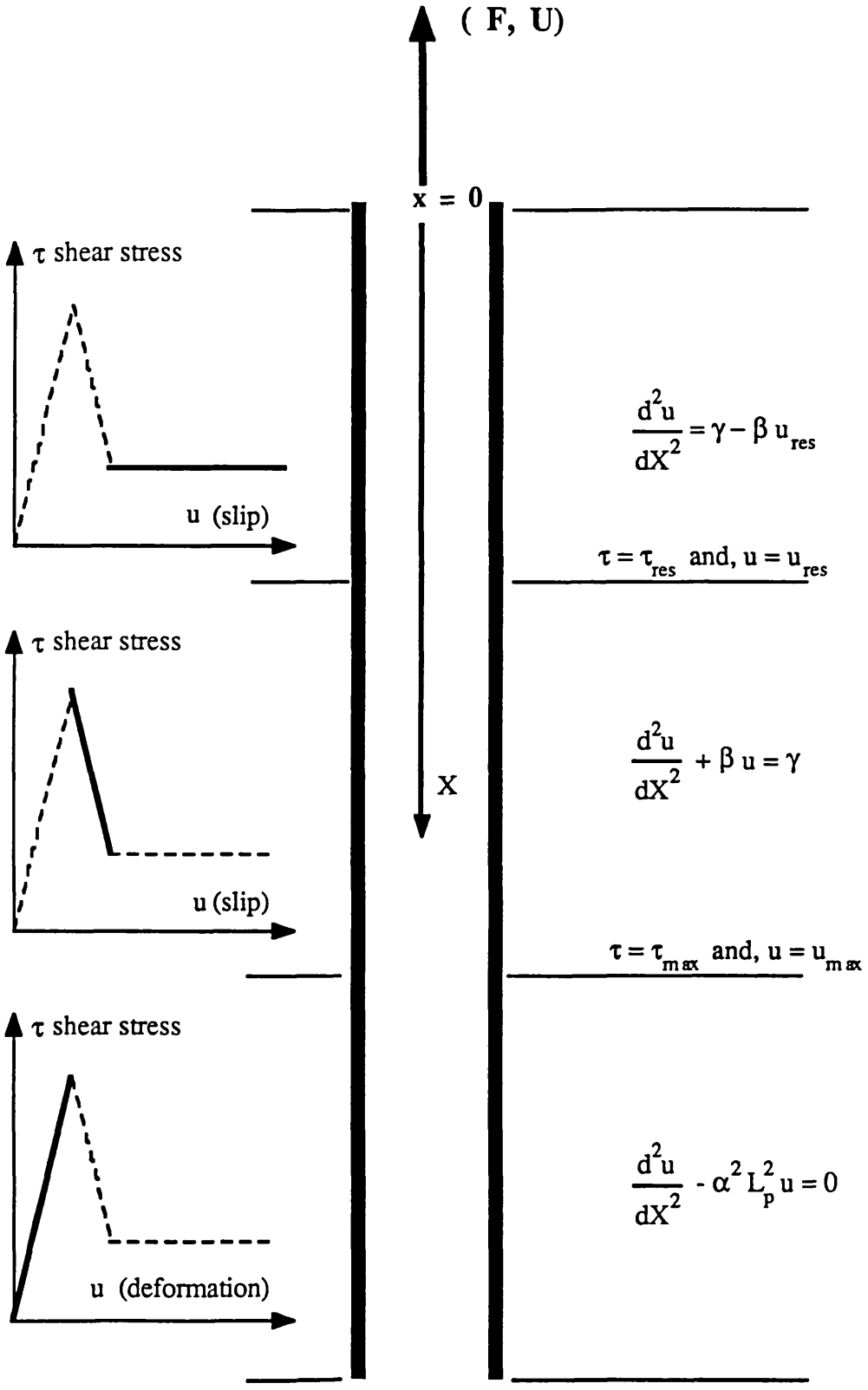


Figure 2.5 : ALTERNATIVE SOLUTION OF THE NUMERICAL MODEL

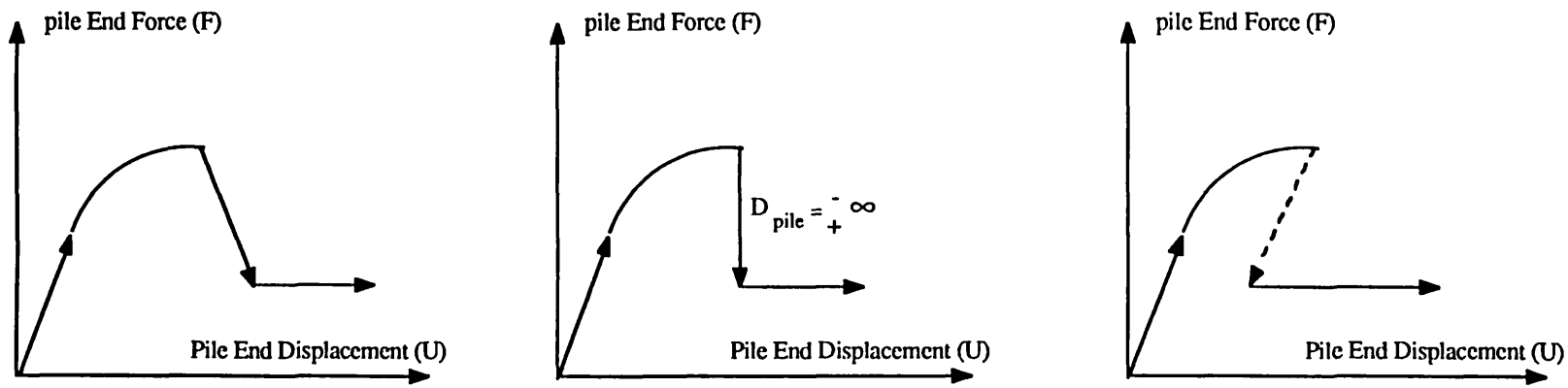


Figure 2.6 : DIFFERENT PILE BEHAVIOUR UNDER A PULL-OUT FORCE

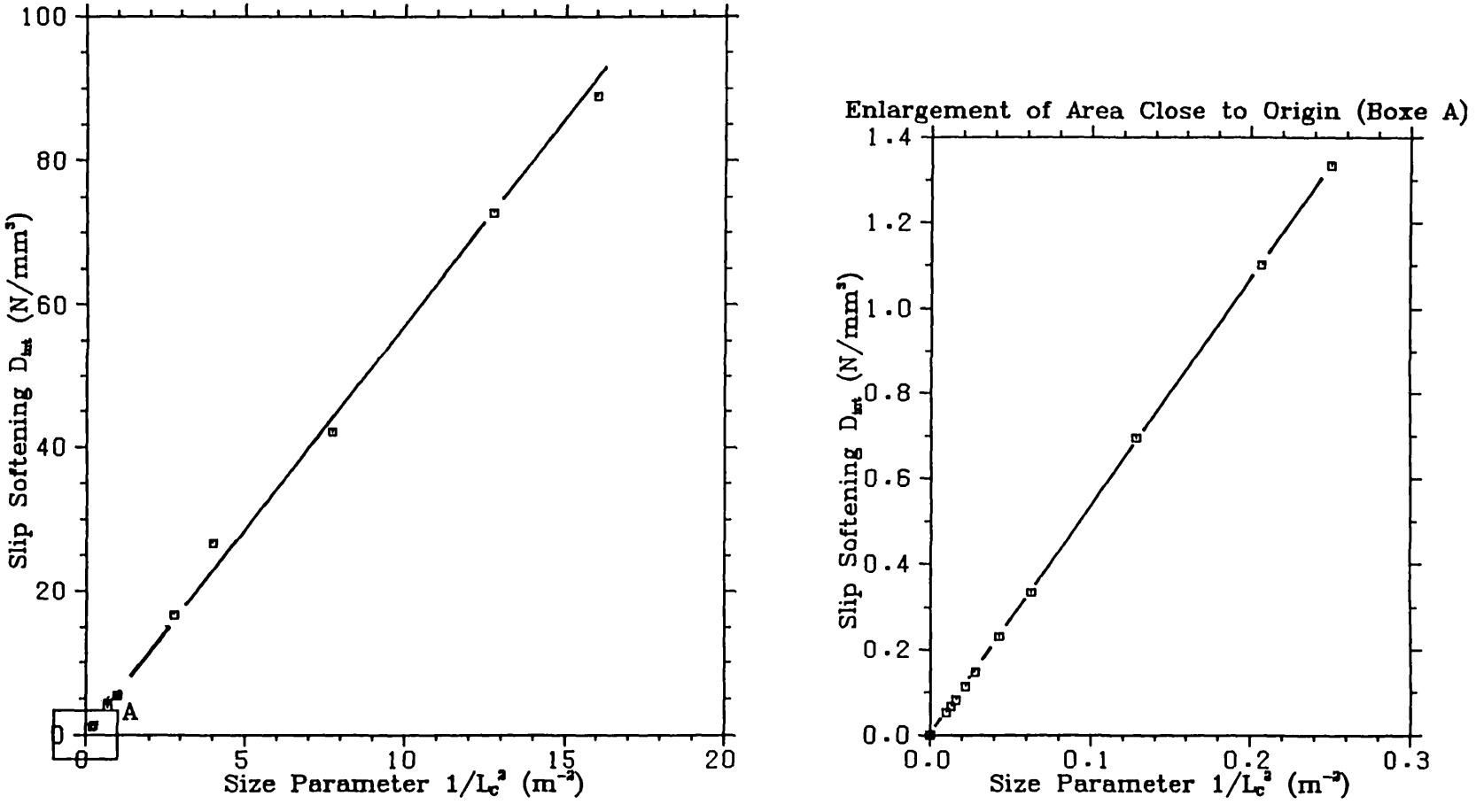


Figure 2.7 : STRESS SOFTENING MODULUS – PILE LENGTH RELATIONSHIP FOR THE CRITICAL UNSTABLE PILE FAILURE TYPE

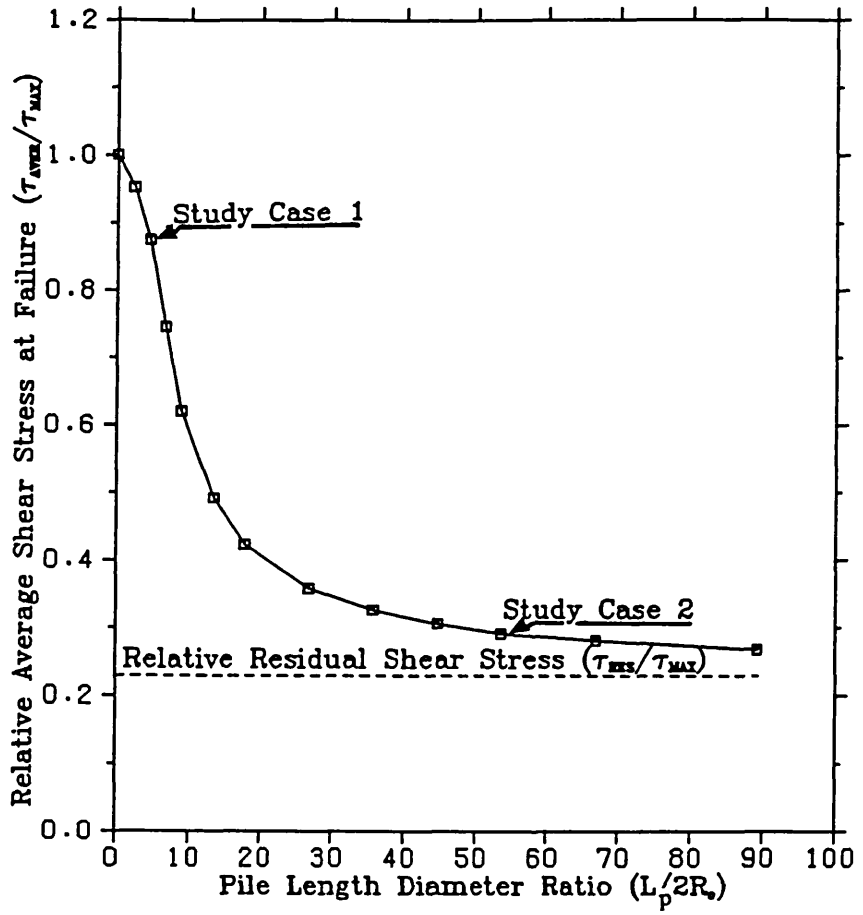


Figure 2.8 : PILE LENGTH EFFECT ON THE AVERAGE INTERFACE RESISTANCE (at Pile Failure)

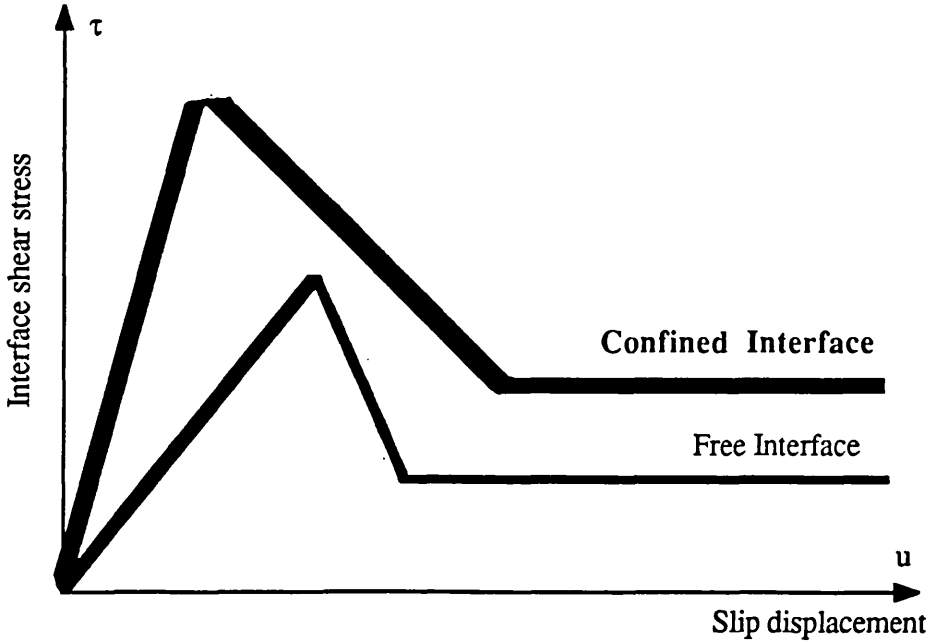


Figure 2.9 : INTERFACE DILATANCY AND SURROUNDING STIFFNESS EFFECTS

CHAPTER 3 :
OBJECTIVES OF THE EXPERIMENTAL INVESTIGATION

3.1 BACKGROUND

No specific design method has hitherto been established for grouted tension piles, and present knowledge on the properties and behaviour of grouted tension piles is very limited. The design of grouted tension piles has been achieved using data from other situations, such as grouted connections, using a large factor of safety. The penalty of a high safety factor (factor of "ignorance") is the high cost of foundation construction. Better knowledge of behaviour leading to a more realistic factor of safety is desirable, and should lead to economic savings.

3.2 OBJECTIVES OF PRESENT WORK

The present work is aimed at the grouted tension pile with the following broad objectives :

1- to investigate the influence of lateral load on the axial pull-out capacity of grouted piles.

2- to investigate the influence of the pattern or order of loading of various combinations of axial and bending loads.

3- to attempt to understand the behaviour of the pile/grout and pile/foundation assembly in greater detail and particularly the behaviour involving breakdown of bond or bond slip at the pile/grout interface.

In some circumstances, failure of a grouted pile can lead to catastrophic instability. Study of pile behaviour is therefore of paramount concern. In fact there is more than one parameter to deal with and the adhesion of the pile to the grout and, more generally, a cementitious matrix to a steel surface is one of the most important factors. The numerical model, presented in the previous chapter, indicates that the local interface characteristics affect the strength and the global behaviour of the pile. This behaviour includes the maximum shear stress, the residual shear strength, the rate of slip softening, and whether failure is gradual or sudden.

3.3 SCOPE OF INVESTIGATION

The results from the numerical model suggest that it would be useful to study the behaviour of pile/grout and pile/foundation assembly in greater detail and particularly the behaviour involving breakdown of bond or bond slip at the grout/pile interface. An experimental investigation of local interface behaviour was planned and carried out. Details of the testing procedure are described in chapter 7. The test results obtained are presented and analysed in chapter 8.

The numerical study indicated that determination of the local bond strength is not sufficient on its own to describe the overall behaviour of a grouted pile behaviour. In addition, the one dimensional model gives no indication of the possible effects of lateral load in combination with an axial pull. Consequently, experiments on test piles have to be carried out. Tests, with the introduction of lateral loading applied simultaneously and independently, are needed to establish the effect of such loading on the axial pile resistance. Chapter 6 describes the tests carried out on grouted piles, and presents the results obtained from the tests.

To minimize the effect of shrinkage and non-homogeneity in the grout, trials were undertaken to select a suitable grout mix design. Chapter 4 deals with the grout selection based on results of simple tests. Results of the plastic settlement of different trial mixes are also given.

Chapter 5 provides a description of the test rig specially built to perform tests on model piles under combined axial and lateral loading.

CHAPTER 4 : GROUT INVESTIGATION

4.1 INTRODUCTION

Cementitious grouts are widely used in prestressed concrete elements for steel protection, and in geotechnical applications for soil stabilisation and weak ground anchors. The principal requirement for a grout is the fluidity of the mix in order that the material can be put into place by pumping.

Particular care is necessary in choosing the mix design, when the placed material has a load bearing or structural role in a concrete member. In grouted tension piles, the grout must be designed so that it enables the pile to resist uplift forces, by the development of bond at the pile/grout and grout/soil interface.

Cementitious grout normally consists of cement and water, with an admixture being used to improve bleeding and shrinkage. The need for grout fluidity, in practical operations, requires the use of a high cement/water ratio (W/C = 0.35 - 0.45, up to 0.6 for long pumping distance). Because of this, bleeding and shrinkage during both plastic and hardened stages, are very real dangers that can affect the physical and the mechanical properties of the hardened grout, and consequently the performance and behaviour of the final structure. Both bleeding and plastic shrinkage will result in poor quality, non uniform grout, with large air pockets which affect both strength and effectiveness as a barrier. The water cement ratio is the main parameter affecting the grout properties. Most specifications for grout use the degree of bleeding, and the compressive strength as the controlling parameters.

4.2 BLEEDING

Most of the material structure, due to the cement hardening reaction, usually develops within the first two hours from the time of adding water. During this stage, the cement particles and the water form a suspension. With excess water, the suspension is unstable, and the cement particles tend to settle forcing the excess water out of the mixture. The water appears at the surface as bleeding. This can affect the final grout matrix in three ways :

1 - production of voids where water has accumulated, and which form a subsequent danger in freezing condition.
2 - formation of channels caused by the water circulation.
3 - segregation along the column due to the settlement of cement grains and consequent water movement.

Reports on grouting vertical ducts, for anchorages, and prestressed strand in nuclear power stations, noted the formation of large voids at the top of the grout columns, due to bleeding (Long (1976)). The amount of bleeding depends on the water content, time, setting time and the height of the grout column. Figure 4.1 illustrates these effects for grouted pile systems. With a long vertical grouted length, there is a high potential for the development of poorly grouted zones, due to the bleeding and water accumulation at different places along the embedded length.

4.3 SHRINKAGE AND VOLUME CHANGE

Shrinkage is caused by loss of water, by evaporation, bleeding and water suction by the surrounding media. Shrinkage may occur with grout in both the plastic and hardened conditions. Such shrinkage will result in tensile stresses in the grout matrix which can produce cracking and loss of performance. The effect of grout shrinkage has been assessed by Billington et al (1980), where it has been found that grout shrinkage can reduce the bond strength by as much as 42%.

4.4 GROUT QUALITY IMPROVEMENT

4.4.1 ADMIXTURE

Additives can be provided either in plasticiser form, or as an expanding agent (hydrogen gas generation in the grout matrix). Admixtures as plasticisers, can be used in order to reduce the water/cement ratio, so reducing bleeding, and providing a stronger grout. Alternatively, an expanding agent can be used to counteract shrinkage and reduce cracking.

During this investigation a plasticiser "FebAdmix" was used which enabled the water cement ratio (or water solid ratio) to be reduced to around 0.35. According to the manufacturer's data sheet (FEB (1985)), this product is air-entraining plasticiser, that dissolves the lime in the mix, and provides a "quick set" of the grout (Hewlett (1980)).

The use of the admixture eliminates bleeding, and reduces shrinkage. The expanding "FebGrout" was also being tried, but this had little effect on bleeding, even though shrinkage was reduced.

4.4.2 PULVERIZED FUEL ASH (PFA)

Pulverized Fuel Ash (PFA) is also widely used in grout as a cement replacement. Material costs are reduced which can be important with large quantity operations. The use of fly ash as a filler also reduces the evolution of heat and bleeding. PFA consists of glassy material, with a fine powder of silica, alumina, iron and calcium. The powder comprises spherical grains (20μ) which might allow a water content reduction. PFA is a pozzolanic product that is not cementitious by itself, but reacts with the free lime in the presence of water to form a cementitious compound. Mehta (1983) showed that PFA addition in grout reduces the shrinkage, and provides a more workable mix.

The PFA used during the present work was provided by Central Electricity Generating Board (CEGB), with chemical composition presented in table 4.1.

4.4.3 SILICA FUME

Burges (1982), has found that 5% cement replacement by silica fume increases the bond between the grout and steel. Besides acting as a filler, the silica fume participates directly in the formation of cement gel, and so leads to a very dense matrix, decreases the porosity by 15% at 28 curing days. Research work on the effect of silica fume on cementitious grout is reported by Grutzek et al (1983), Meland (1983), Sellevold et al (1983), Carette et al (1983), and Regourd et al (1983). The use of 10% - 20% silica fume to replace cement will raise the water demand, increase the cement reaction speed, and provide a stronger concrete at an early cement age. Accordingly bleeding and matrix shrinkage will be reduced. The optimal silica fume quantity is also related to its particle grain size.

Preliminary tests undertaken as part of the present investigation, showed that the use of silica fume reduced the grout workability and provided a very rapid set. Accordingly silica fume was not used in the main programme. The composition of the silica fume used is presented in table 4.2.

4.4.4 CEMENT TYPE (ASTM description)

Different types of cement can be used in grout. In practice, the cement selection depends on the site requirement. Ordinary Portland Cement, OPC (type 1) is the type most frequently used. Occasionally either Rapid Hardening Portland cement (type 3), Low heat Portland cement (type 4), or Sulfate Resistance Cement (type 5) are specified according to the location and the condition where grout has to be placed. Bleeding and shrinkage are also a function of the cement particles size. A smaller cement particle provides a faster reaction, which reduces bleeding, but increases the grout shrinkage (Neville (1983)).

4.5 OBJECTIVES OF THE INVESTIGATION

The present work has been undertaken to provide a reliable mix design for use during the tests on pile assemblies, and determine the grout physical and mechanical behaviour. A series of grout mix designs were established and tested. Acceptable bleeding and early volume change were the fundamental criteria for the final mix selection. By varying the grout composition, attempts were made to minimise bleeding and the plastic shrinkage.

4.6 TEST PROCEDURE

It is not practical to measure the effects of bleeding and plastic shrinkage separately, since both phenomena occur simultaneously, and are possibly related to each other. The test method used is designed to measure the early grout volumetric change and to observe the amount of bleeding water. The choice of the final mix is established on a comparative basis between all mixes tested during this investigation. The values for bleeding and shrinkage are related to the test situation. Different amounts would occur in a very long duct, and different test procedure might provide different measures of the bleeding and shrinkage.

4.7 TEST ARRANGEMENT

The American Society of Testing Material -in its tentative standard C 827-75T suggests a method of measuring the early volume changes of a cement paste using optical equipment to assess the change of the specimen level. Figure 4.2 shows such a method.

In the present work a similar arrangement was adopted but with a modification previously used by Jefferis (1988) of King's College (figure 4.3), in which a series of three transducers measure the vertical grout movement placed in rigid mould. The cylindrical mould used complies with the specification of ASTM C 827-75T, where it is required to be rigid, water-tight and to have a smooth interior surface. The mould has 300 mm height and 150 mm diameter.

4.8 MIXING METHODS

Initially, the mixing method used was similar to that specified in ASTM C 305-65. The mixer consisted of rotating paddles within a grout container. The results obtained were satisfactory with the grout having a good consistency. However, by using a roller mixer instead of the paddle one, the grout mix was improved considerably. The same mix prepared with the roller mixer proved to have more workability than when it was prepared with the paddle one. Consequently, further trials were carried out, using the roller mixer, to set up the final grout mix design.

During mixing, the following procedure was used :

1 - the water was placed in the bowl
2 - cement was added for 30 seconds while the mixer was at low speed.
3 - the mixer was run at its maximum speed and left for 1 minute.
4 - mixing was stopped and the bowl was scraped.
5 - mixing continued for another 1 minute at high speed.

By using the roller mixer, all the mixing steps were carried out at the same speed, since the mixer had only one speed option. The rotation speed of the rolling cylinder was about 1400 rotations per minute.

4.9 EXPERIMENT

After casting the grout in the mould, a perspex plate was placed on the top of the specimen. The two transducers were placed on top of the plate and data collection started. ASTM. C 827-75T specifies timing intervals for readings as follow:

- a reading every 5 minutes during the first hour.
- a reading every 10 minutes during the following two hours.
- a reading every 20 minutes until the paste was hardened.

4.10 RESULTS AND GROUT SELECTION

Several mixtures of cement and cement replacement materials with and without admixtures were tested. The results are listed in Table 4.3, where the different mix proportions with their corresponding maximum plastic settlements are presented. The grout paste volume variation (PVV1 = Percentage of Volume Variation by grout total volume) is defined by the ratio of perspex plate movement to the height of the specimen (300 mm)

$$PVV1 = 100 \cdot \frac{\text{Settlement } (\Delta)}{\text{Original Height of Specimen}} \qquad (4.1)$$

The grout plastic shrinkage can be related to the amount of cement in the mix. In this case the grout volume variation (PVV2) will be defined as the ratio of the paste volume variation to the volume of cement in mix :

$$PVV2 = 100 \cdot \frac{\text{Settlement } (\Delta) \cdot \text{Specimen Cross Section}}{\text{Total Cement Volume in the Specimen}} \qquad (4.2)$$

The paste volume variation as described above is given in table 4.3 in brackets. The time of its occurrence is related to time from when there is little change of the specimen height. This can be interpreted as the paste setting time. In addition, the settlement variation during the tests is plotted in figures 4.4. Figures 4.4a and 4.4b show the results of the mixes without and with cement replacement respectively, when the grout was prepared using the paddle mixer. Figure 4.4c represents the trial mixes tests results, with the grout prepared with the roller mixer.

Following these tests the grout chosen for the tests piles was number 9 with the following composition :

- 65% Ordinary Portland Cement
- 35% Pulverized Fuel Ash
- 0.5 water cement ratio (water solid ratio 0.325)
- 5 cc Feb Admix (non bleed) admixture per kilogramme of cement

This mix showed no bleeding either during the plastic shrinkage test or during the pile tests grouting. The mechanical properties of this mix will be presented later in this chapter. It is evident that cement replacement by the PFA has considerably improved the cement paste properties, and the grout compressive strength would be regarded as

acceptable for site practice.

Table 4.3 also gives values for the density and compressive strength measured from tests on 100 mm cubes. Tensile strengths were also determined using the standard Brazilian test (BS 1881 Part 117 1983) on mixes 1 to 8. The strength at 28 days was high and could have caused difficulties in the pile test. Accordingly, it was decided that the pile tests programme should be carried out at an early stage of the grout curing to ensure pile/grout interface failure, and to avoid the effects of the grout plastic shrinkage in the hardened paste.

4.11 MECHANICAL PROPERTIES OF THE CHOSEN MIX

4.11.1 COMPRESSIVE STRENGTH

The compressive strength of the selected mix was evaluated at different grout ages. The results are presented in table 4.4. The grout ages correspond to the age of the tests carried out during the piles tests investigation to analyse the effect of the compressive strength of the bond resistance.

4.11.2 ELASTIC MODULUS

To complete the description of the grout mix properties, the elastic modulus and the Poisson's Ratio were determined. The test consisted of placing a series of resistance strain gauges placed in the middle of a cylindrical specimen with, a height of 300 mm and a diameter of 100 mm, which is tested in compression (BS 1881 Part 121 1983, and BS 1881 Part 206 1986).

Two diametrically opposite strain gauges were placed in parallel to the axis of the cylinder, to measure the specimen axial deformation (ε_{axial}), providing the material elastic modulus with two additional strain gauges placed in the circumferential direction of the cylinder for the transversal strain measurement (ε_{trans}), for the determination of the Poisson' Ratio. Figure 4.5 shows a gauged cylinder used for the test.

Figure 4.6a shows the axial strain and stress variations obtained during the axial compressive test on grout cylinder specimens at the age of 2 and 8 days respectively. The transversal strain of the same specimens was plotted with the axial strain in figure 4.6b. The tests were repeated on three grout specimens at the age of 28 days. The results are summarized in table 4.5.

Table 4.1 : Pulverized Fuel Ash Chemical Composition

Mineral	Percentage (%)
Silica (as SiO_2)	50.0
Aluminium (as Al_2O_3)	31.1
Iron (as Fe_2O_3)	8.1
Calcium (as CaO)	1.9
Magnesium (as MgO)	1.6
Sodium (as Na_2O)	0.9
Potassium (as K_2O)	4.3
Titanium (as TiO_2)	1.1
Loss of Ignition	3.8
Total of Sulfate (as SO_3)	0.84

Table 4.2 : Condensed Silica Fume Chemical Composition
(Super Refractory Grade)

Mineral	Percentage (%)
SiO_2	94 - 98
SiC	0.1 - 1.0
C (total)	0.2 - 1.3
Fe_2O_3	0.02 - 0.15
Al_2O_3	0.1 - 1.4
CaO	0.08 - 0.3
MgO	0.2 - 0.9
Na_2O	0.1 - 0.4
K_2O	0.2 - 0.7
P	0.03 - 0.06
S	0.1 - 0.3
TiO_2	0.001 - 0.02
Mn	0.004 - 0.05
Pb	0.001 - 0.01
Zn	0.006 - 0.04
L.o.I	0.8 - 1.8
Material Specific Area	22 - 25 m^2/g

Table 4.3 : Plastic Shrinkage Test Results
(Grout prepared with paddle mixer)

Test	Grout Composition (% per weight)	Maximum Settlement Magnitude (%)	Maximum Settlement Time of occurrence	Density (kN/m^3)	Strength (N/mm^2) Tensile (at 28 days)	Strength (N/mm^2) Compressive (at 28 days)
1	OPC = 100 w/c = 0.35	0.98 (2.1)	4h00	21.0	3.27	69.2
2	RHPC = 100 w/c = 0.35	0.74 (1.59)	3h30	20.5	3.75	71.0
3	OPC = 100 w/c = 0.35 FA = 2.17	0.93 (1.95)	1h30	20.2	1.93	63.0
4	OPC = 65 PFA = 35 w/c = 0.45 w/s = 0.30 FA = 5.13	0.61 (1.95)	2h00	20.2	2.23	43.2
5	OPC = 66 PFA = 33 w/c = 0.45 w/s = 0.30 FA = 5 FG = 5	0.76 (2.39)	2h30	19.5	3.40	55.0
6	RHPC = 66 PFA = 33 w/c = 0.45 w/s = 0.30 FA = 5 FG = 5	0.93 (2.93)	3h00	18.5	2.32	55.0
7	OPC = 60 PFA = 40 w/c = 0.47 w/s = 0.28 FA = 5	0.39 (1.35)	1h30	20.2	3.71	82.0
8	OPC = 55 PFA = 36.7 CSF = 8.3 w/c = 0.57 w/s = 0.31 FA = 5.6	0.33 (1.32)	3h00	19.4	2.78	60

Table 4.3 (continued) : Plastic Shrinkage Test Results

(Grout prepared with roller mixer)

Test	Grout Composition (% per weight)	Maximum Settlement Magnitude (%)	Maximum Settlement Time of occurrence	Density (kN/m^3)	Compressive Strength (N/mm^2) (at 3 days)
9	OPC = 65 PFA = 35 w/c = 0.50 w/s = 0.32 FA = 5.	0.52 (1.75)	2h30	19.4	34.0
10	OPC = 65 PFA = 35 w/c = 0.51 w/s = 0.33	0.77 (2.59)	2h00	19.3	27.0
11	OPC = 60 PFA = 40 w/c = 0.56 w/s = 0.33 FA = 5.	0.77 (2.63)	2h00	18.5	28.0
12	OPC = 60 PFA = 40 w/c = 0.47 w/s = 0.32	0.65 (2.22)	3h00	19.3	31.0

GLOSSARY

CSF	- Condensed Silica Fume
OPC	- Ordinary Portland Cement
PFA	- Pulverized Fuel Ash
w/c	- Water/Cement ratio
w/s	- Water/Solids ratio
FA	- plasticiser and non-bleeding agent (FebAdmix)
FG	- expanding agent (Feb Grout)

Note : The admixture quantities are unit volume (cc) per kilogramme of cement.

Table 4.4 : Selected Grout Compressive Strength

Grout Age (Days)	Compressive Strength (N/mm^2)	Corresponding Test Description
1	18	Tests PLT 1 to PLT 8 and Test MTT 1
2	30	Test PLT 1
3	34	Test PTT 1
7	43	Tests PPT 2 and MTT 2
10	45	Test PTT 3
28	60	
37	62	Test MTT 3
45	66	Test MTT

Table 4.5 : Selected Grout Mechanical Properties

Grout Age (Days)	Elastic Modulus 10^3 N/mm^2	Poisson's Ratio
2	9.0	0.20
8	16.5	0.22
28	20.00	0.27

PTT	Preliminary Torsion Test
MTT	Main Torsion Test
PPLT	Preliminary Pull-out Test
PLT	Pull out Test

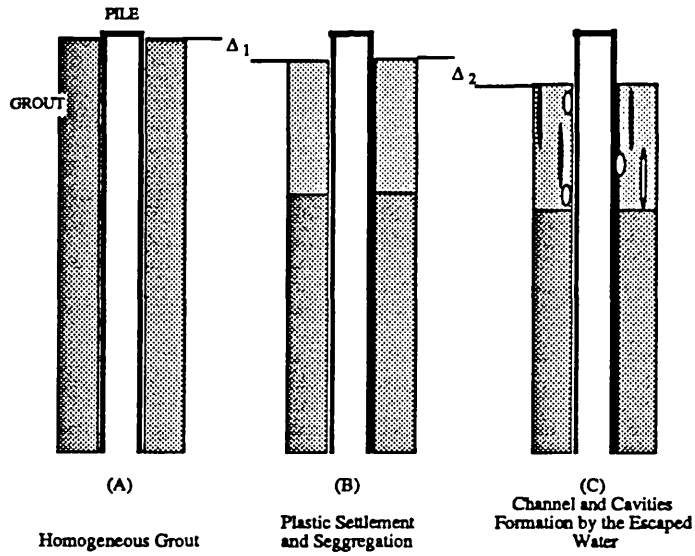


Figure 4.1 : GROUT DEGRADATION DURING THE PASTE PLASTIC STAGE

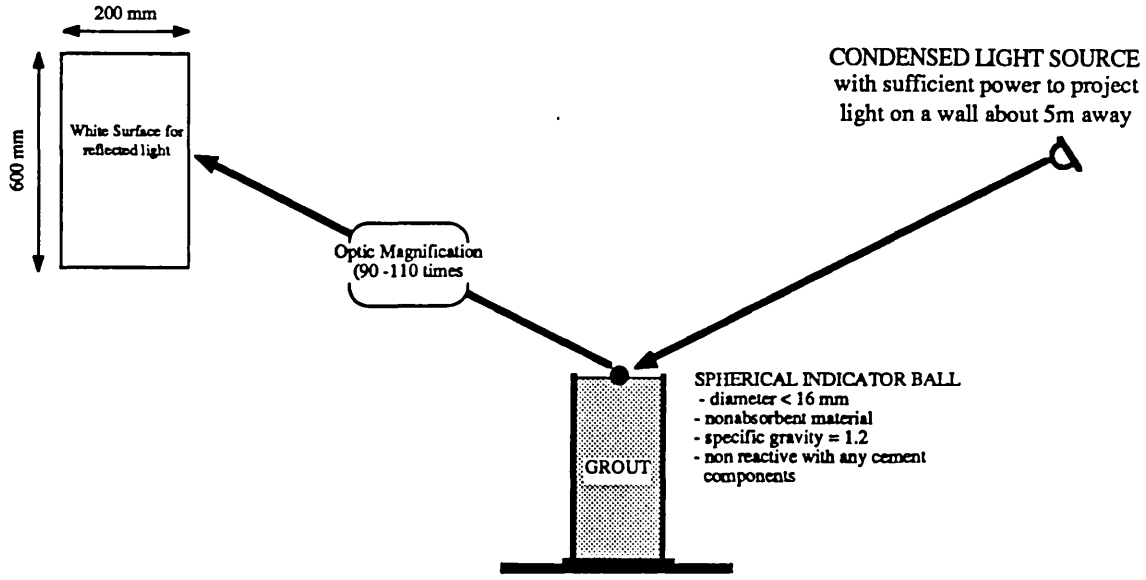


Figure 4.2 : MEASUREMENT OF EARLY VOLUMETRIC CHANGE OF PLASTIC CEMENTITIOUS MIXTURES (ASTM C827 75T)

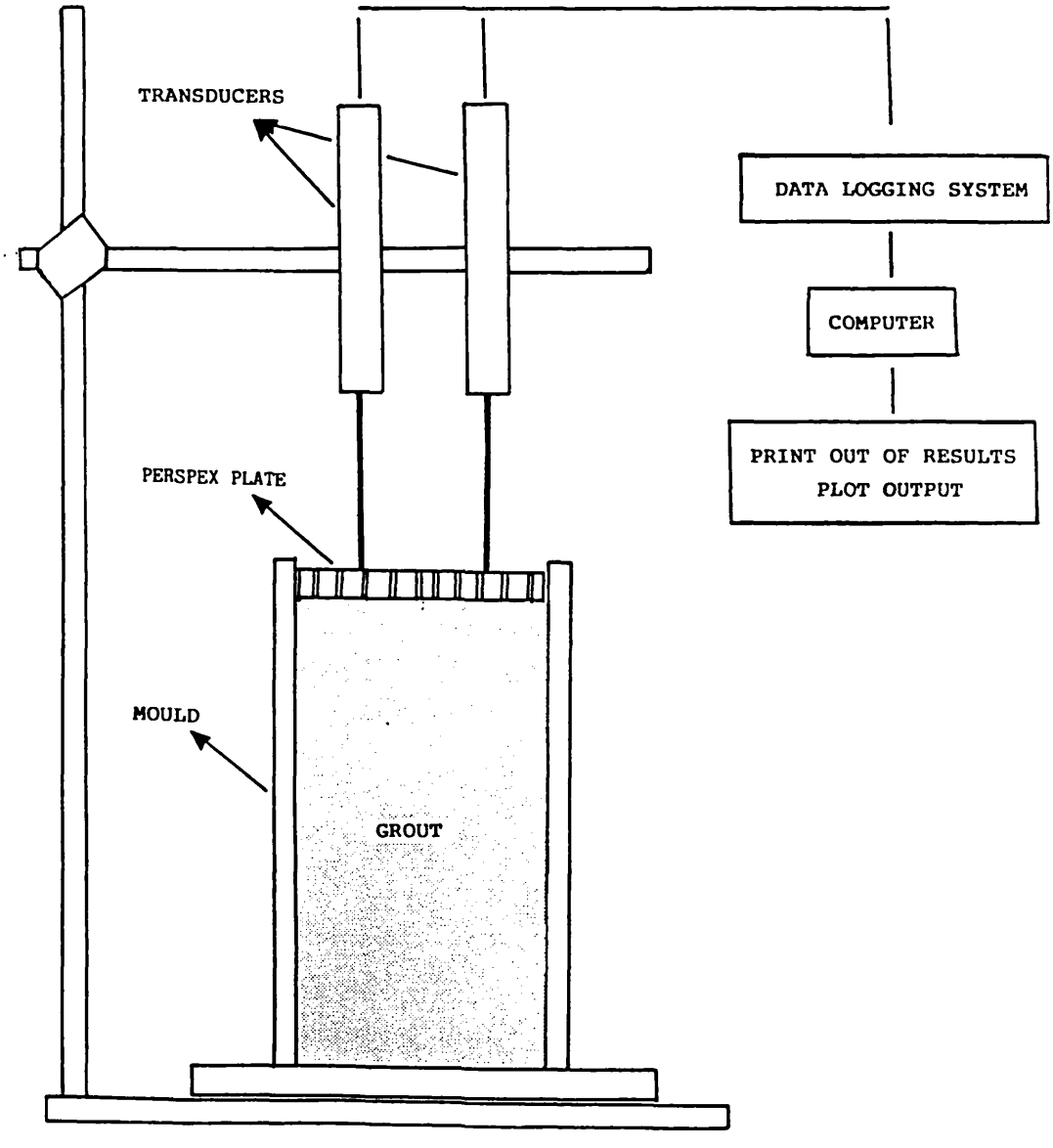


Figure 4.3 : ADOPTED TEST ARRANGEMENT FOR MEASURING THE EARLY VOLUMETRIC CHANGE OF CEMENTITIOUS GROUT

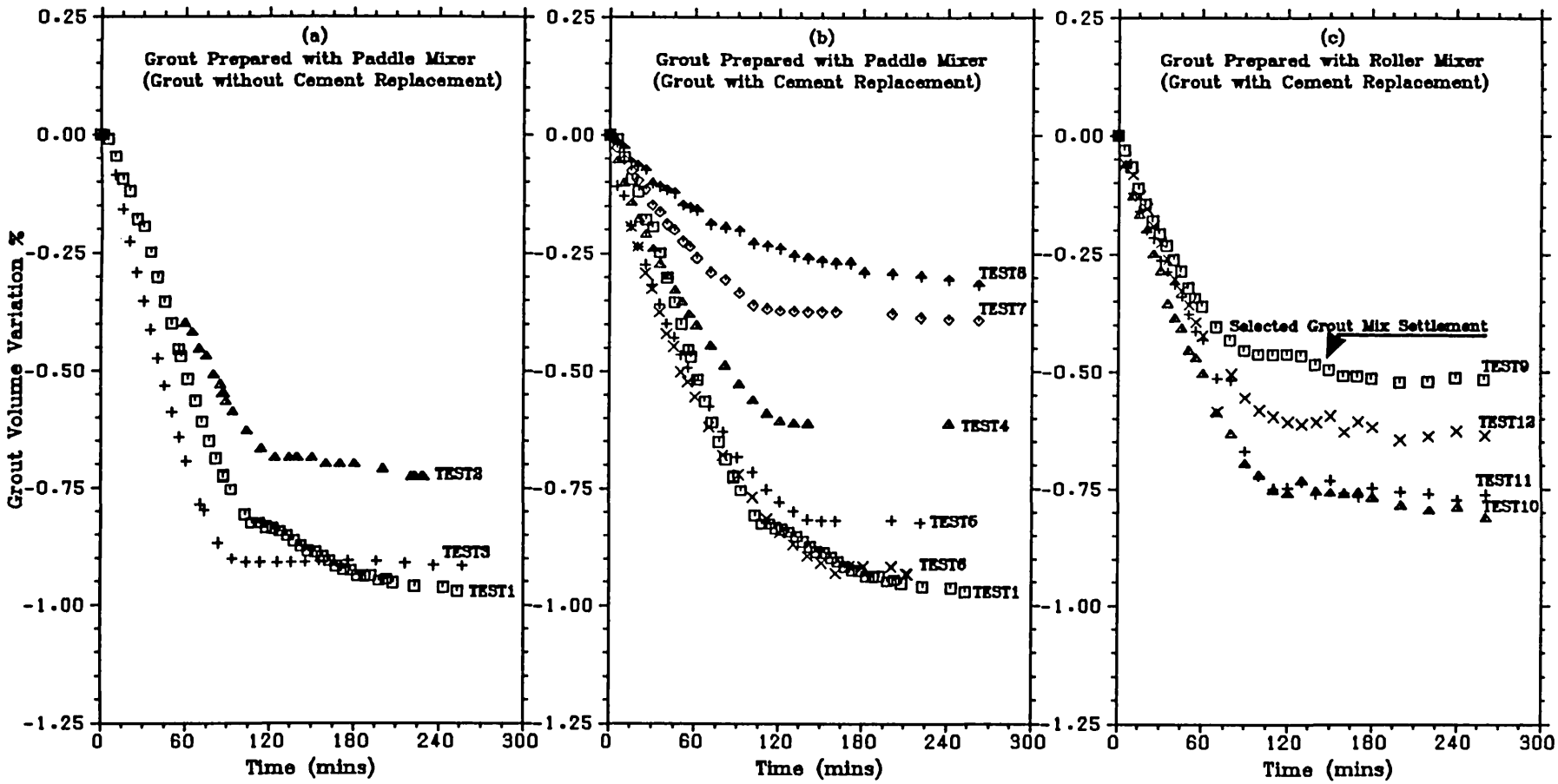


Figure 4.4 : GROUT INVESTIGATION – PLASTIC SHRINKAGE TEST RESULTS –

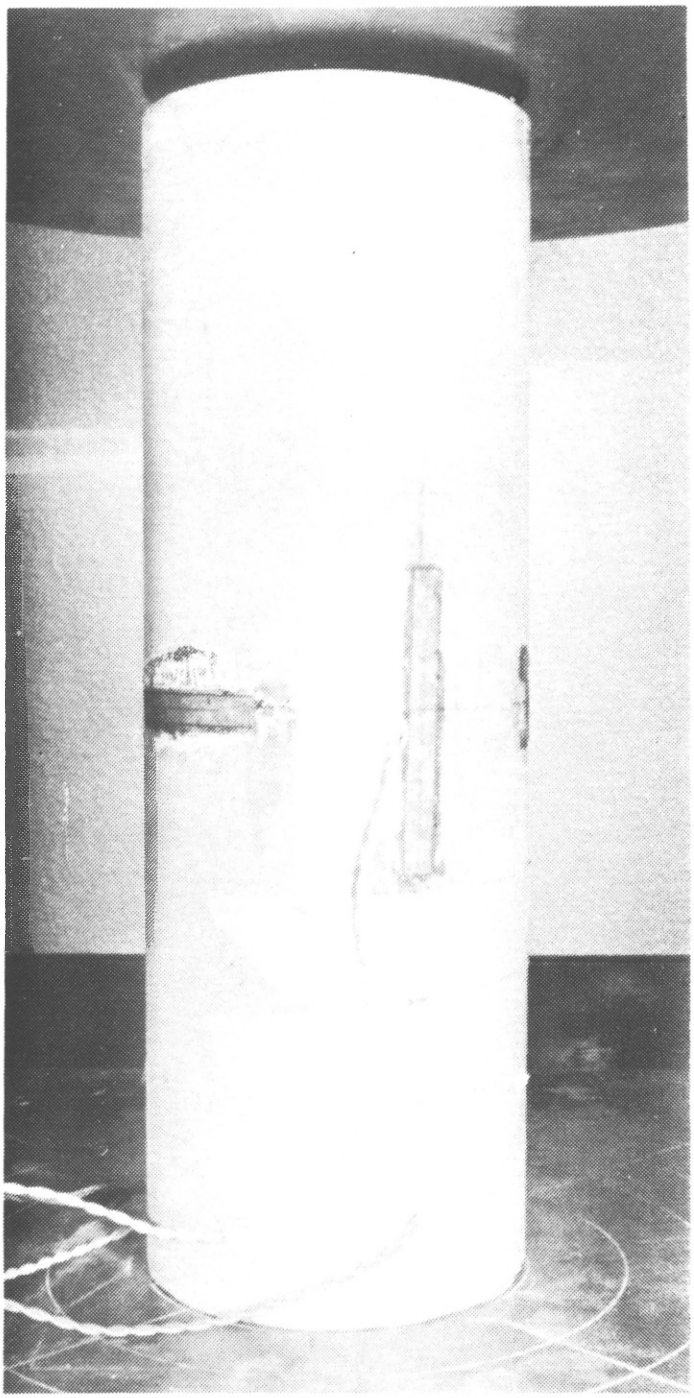
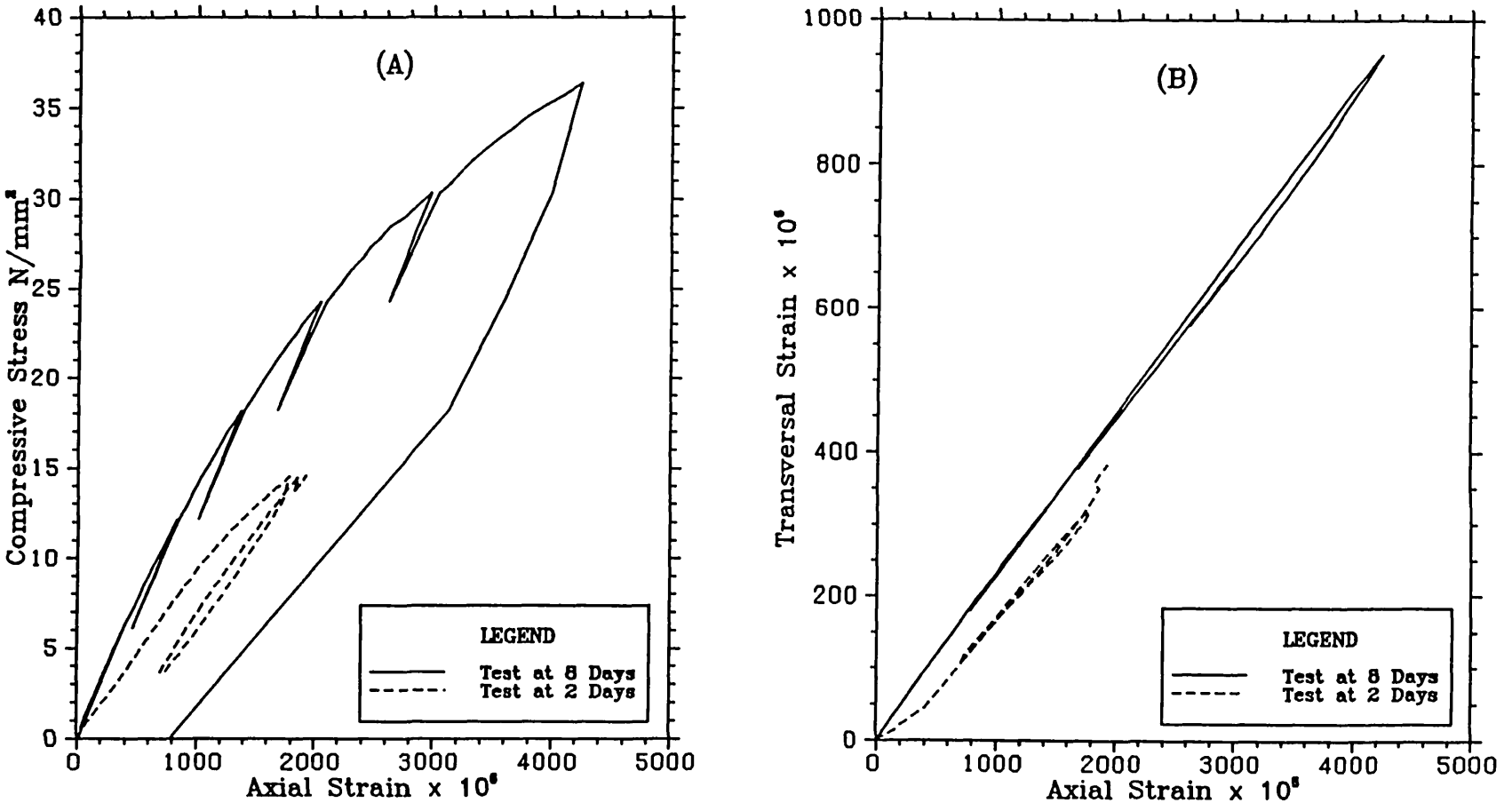


Figure 4.5 : STANDARD GAUGED CYLINDER FOR THE ELASTIC MODULUS DETERMINATION
(BS 1881 Part 121 1983)



Figures 4.6 : GROUT BEHAVIOUR IN COMPRESSION

(Grout Composition : OPC = 65%, PFA = 35%, W/C = 0.325, FA =5)

CHAPTER 5 : MAIN RIG DESIGN

5.1 REQUIREMENTS

The planned rig had to provide facilities for combinations of vertical and horizontal loads. The loads had to be applied either simultaneously or independently. The rig needed to be able to apply horizontal forces in two opposite directions, in order that either 'through-zero' forces, or pure torque applied about a vertical axis, could be generated.

The failure of the pile has to be generated between the pile and the grout. In practice, the pile extraction can be caused either by the grout/pile or the grout/surrounding media interfaces breaking down. The soil model has to be sufficiently strong with good grout/model strata interlock, to ensure a failure at the grout/pile interface.

Concrete can be regarded as a rock type material. The concrete stiffness can be selected to match the real site conditions, and the concrete strength and aggregate specified accordingly. Light weight aggregate concrete can model quite well weak rock sites. For hard rock condition, concrete with heavy aggregates and high cement content would be more appropriate.

5.2 RIG GENERAL DESCRIPTION

An experimental rig has been designed and constructed for the load application to the different pile specimen arrangements. The concept adopted, consists of a three-dimensional rig, with two principal frames. A general scheme of the rig concept is shown in figure 5.1. The rig is constituted by :

1- a concrete block, to represent rock with holes for piles location, which is bolted to the laboratory floor to prevent uplift movement.

2- frames surrounding the concrete block with moveable beams supporting jacks applying horizontal and vertical loads.

5.2.1 STEEL FRAMES

The geometry of the steel frames is shown in figure 5.2a. The frames consist of two steel box columns (400 x 200 x 12.5 mm), joined with a horizontal beam, which is composed of 2 'U' section steel elements (305 x 89 mm). The beam/column joint is provided by eighteen high tensile friction grip bolts.

An additional precaution was taken to reduce any rig movement relative to the concrete block. At the low level of the frame, a steel box element (200 x 200 x 12.5 mm) was fixed to the columns. This element provided an additional stiffness to the frame, and permitted the fixing of the concrete block to the rig. Two high tensile steel rods went through the concrete block, at 100 mm above the floor level. They were prestressed with a force of 150 kN each. In this way, the frame was fastened to the concrete block. Figures 5.2b and 5.2c scheme the side and plan shows of the general rig.

Each frame was fixed to the laboratory floor by two prestressed bolts at each side. They were each tensioned to 250 kN against the lower steel box element.

5.2.2 GENERAL RIG

At the top, two additional steel box elements (200 x 200 x 12.5 mm) linked the two frames, to form a rigid rig. Thus the frames were restrained against any out-of-plane deflection. The distance between the two frames can be adjusted for any required space. If a larger space was needed, the two frames would have to be shifted for the desired position, and longer elements would be required for the linking pieces.

There were three cross beams. The first one, supported by the frame beams, was used to support the hydraulic actuator for the vertical tension force. It was also used as a support for the twisting key, during the torsion tests (see chapter 7 below). The actuator can be placed at any position along the cross beam, while the cross beam itself can be fixed at any position on the frame beams.

Two horizontal cross beams were placed against the frame columns, on both sides of the rig; they can be positioned at any height. The hydraulic actuators, for the lateral load application, were supported by these two cross beams.

The freedom of positioning the jacks allowed the pile specimens to be placed anywhere within the rig space. Multiple tests can thus be carried out using a single concrete block. Only tensile vertical load can be provided, but reverse lateral load cycling can be generated. Figure 5.3 shows the completed experimental rig, before the concrete block was cast, with the vertical and the horizontal actuators supported by the cross beams.

5.3 RIG SAFETY TESTS

The rig was tested for safety considerations. This also provided a check of the rig under different design load cases. The deflections of the cross beams and the frame beams were also measured.

5.3.1 TEST CASE A

Horizontal forces were applied on the mid-span of the lateral cross beams. The applied force was restricted to a maximum of 250 kN, due to the hydraulic actuators limited capacity. At the maximum applied force, the lateral cross beams deflection/span ratio reached a value of 1/600. Figure 5.4a shows the arrangement of this rig test case.

5.3.2 TEST CASE B

The test of the rig under vertical forces is carried out by two loading force positions, used later for the pile pull out tests. Figures 5.4b and 5.4c illustrate the test arrangement. In both cases the load was increased to 350 kN. The maximum vertical deflection/span ratio of the vertical cross beam was less than 1/750; while that of the frame beams was less than 1/1000.

5.4 CONCRETE BLOCK

In the case of the present study, normal concrete (grade 40) was chosen to simulate a strata model for the pile. Simple calculation showed that, with grade 40, the failure should occur at the pile/grout interface. Concrete blocks with cylindrical pockets, prepared by using styrene foam, were cast in situ within the rig space. During the preliminary investigation, the block contained three pockets, where three torsion tests, and two pull-out tests were carried out. This square block had a width of 1200 mm and a height of 400 mm. However, a second concrete block was designed with nine pockets, (for four torsion tests and eight pull-out tests), for the main experimental programme. This block was 2048 mm long, 1300 mm wide and 620 mm high. Figure 5.5a shows the concrete block used during the main investigation.

After being placed within the rig space, the concrete block is anchored down the floor by four bolts. Each bolt is stressed to 150 kN. Figure 5.5b shows a general view of the constructed rig.

5.5 CONCRETE MATERIAL

The compressive strength attained for both blocks cast was 44 N/mm^2 at 28 days. The elastic modulus and the Poisson's ratio were measured using the same procedure adopted for the grout properties determination (chapter 4). The failed concrete cylinder, (100 mm diameter, and 300 mm length), used in these tests, is shown in figure 5.6. Figure 5.7 presents the axial and the transversal behaviour of the concrete block

material in compression. The initial elastic modulus and the Poisson's Ratio were found to be 28 10^3 MPa and 0.16 respectively.

5.6 CONCRETE POCKET

During the preliminary investigation, the pockets diameter was 170 mm; this was reduced to 145 mm for the second block to reflect more accurately the relative size of the grout annulus used in practice.

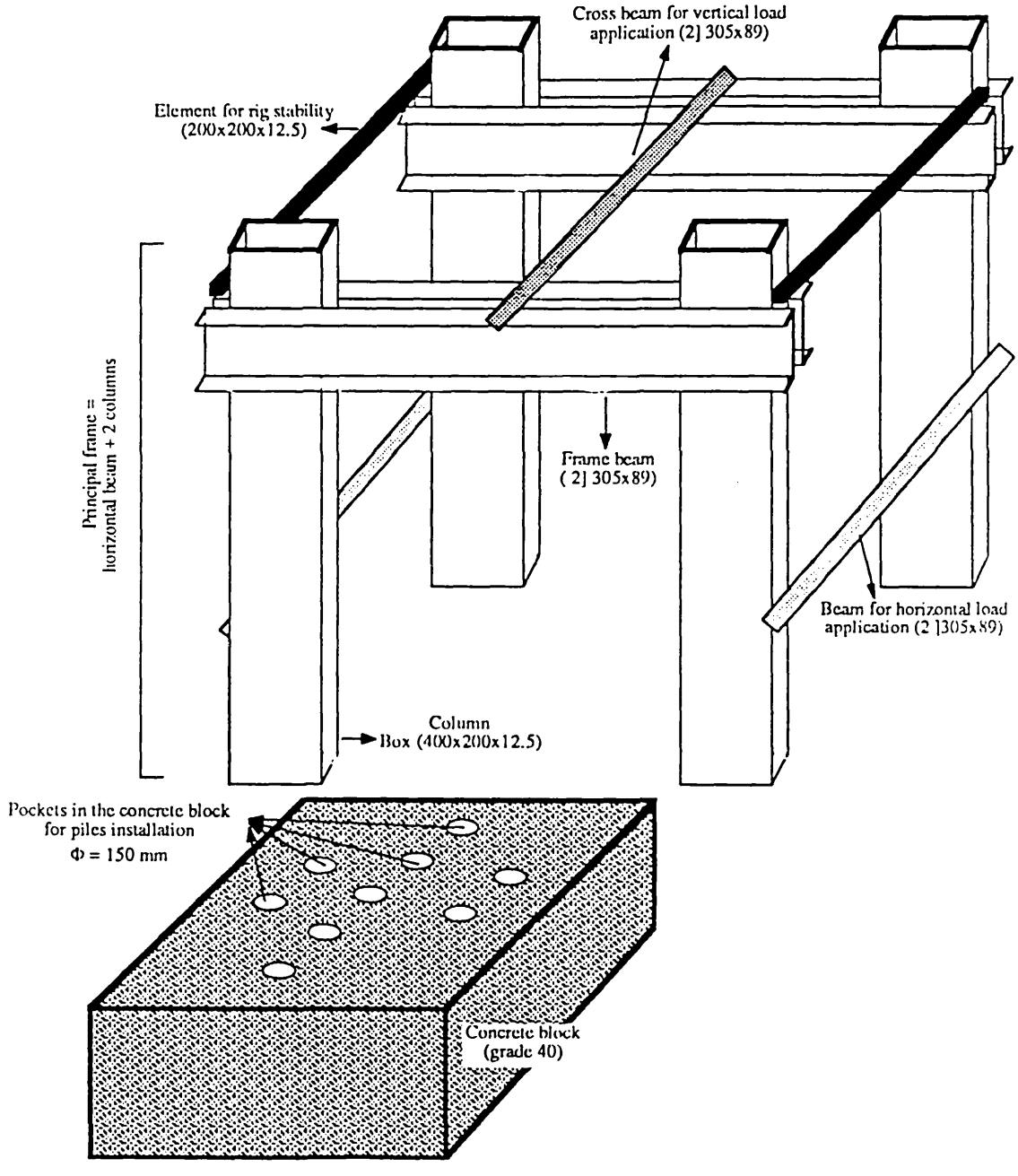


Figure 5.1 : CONCEPT FOR THE TESTING RIG

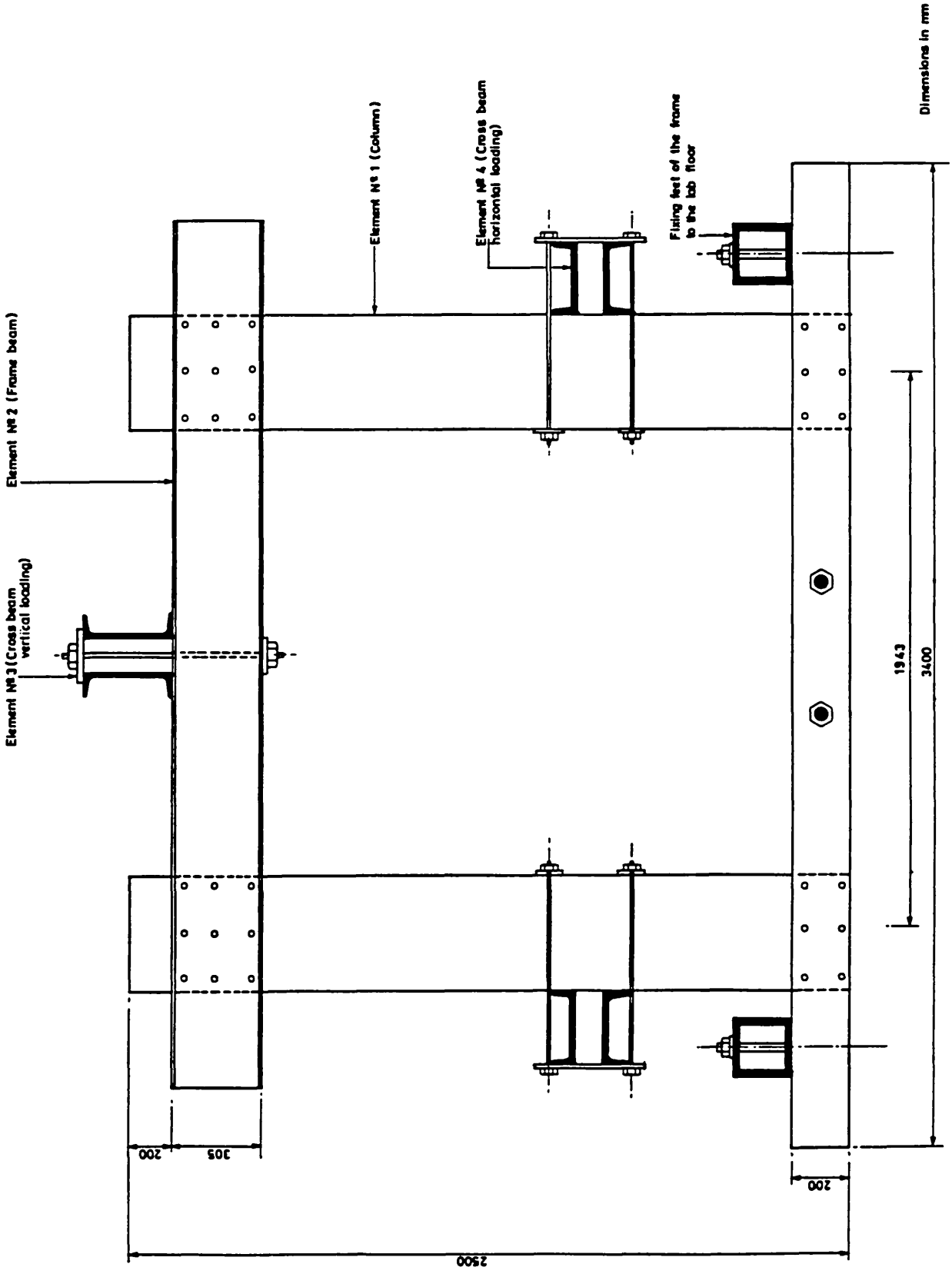


Figure 5.2a : RIG MAIN FRAME (RIG FRONT VIEW)

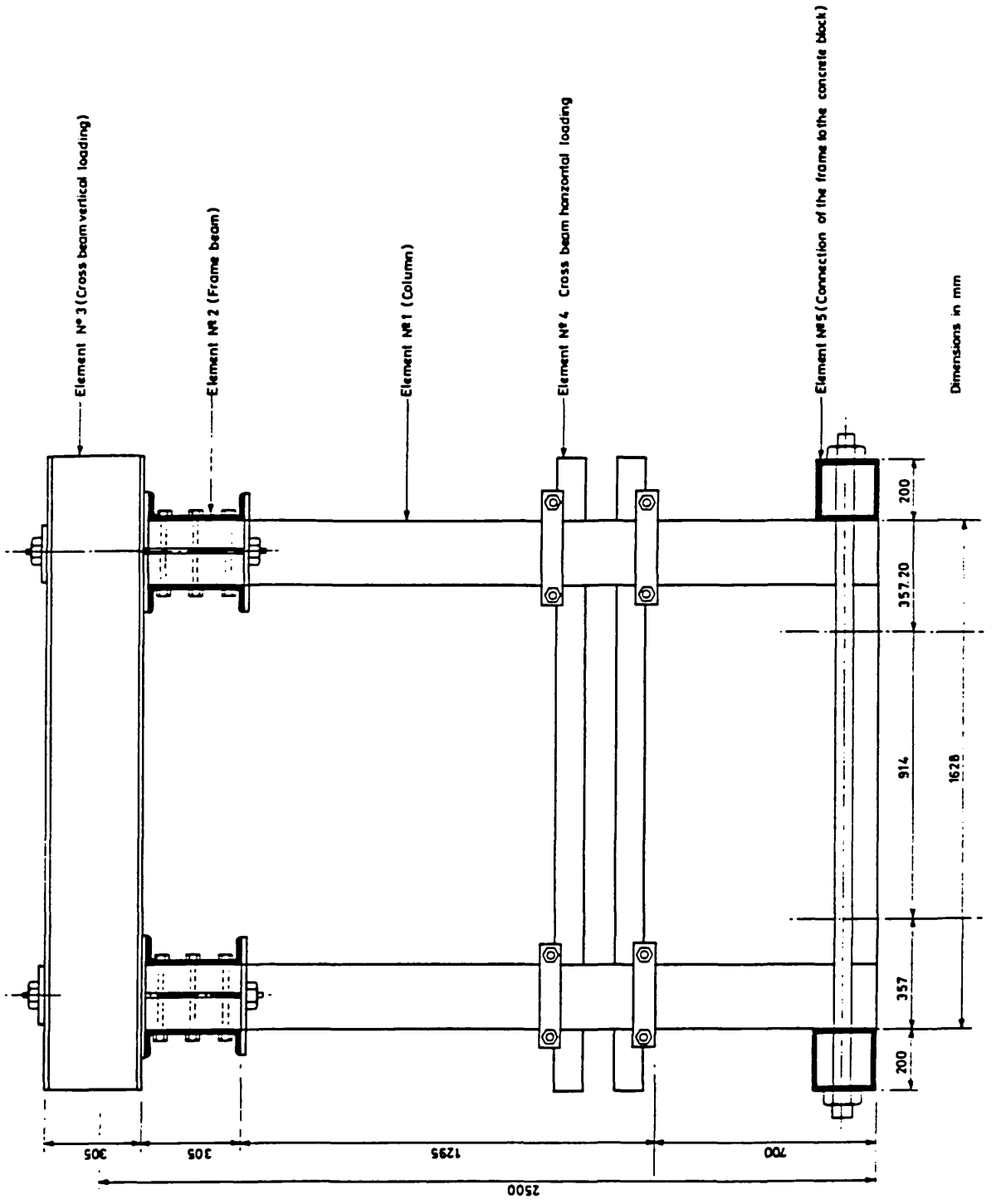


Figure 5.2b : RIG SIDE VIEW

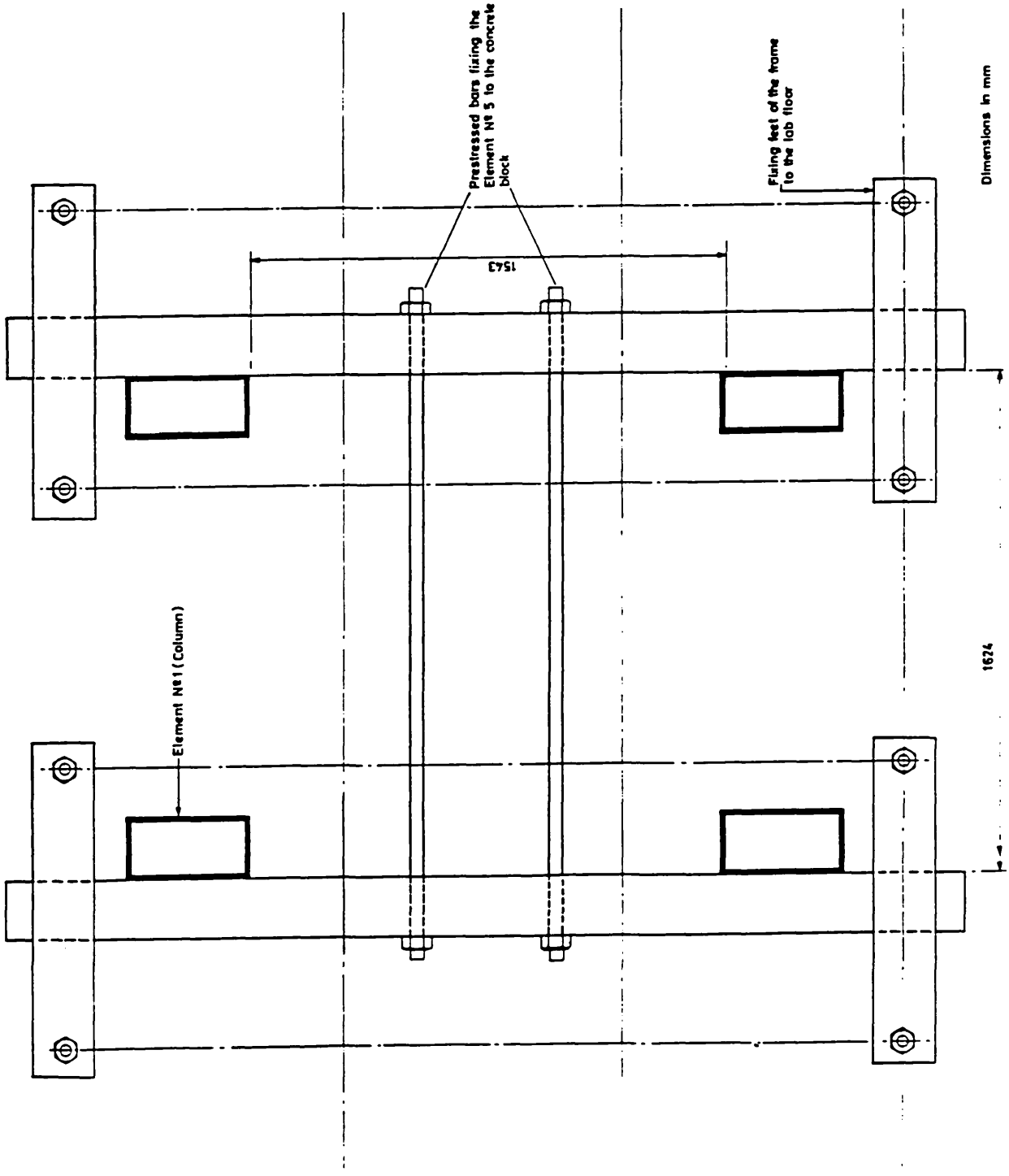


Figure 5.2c : RIG TOP VIEW

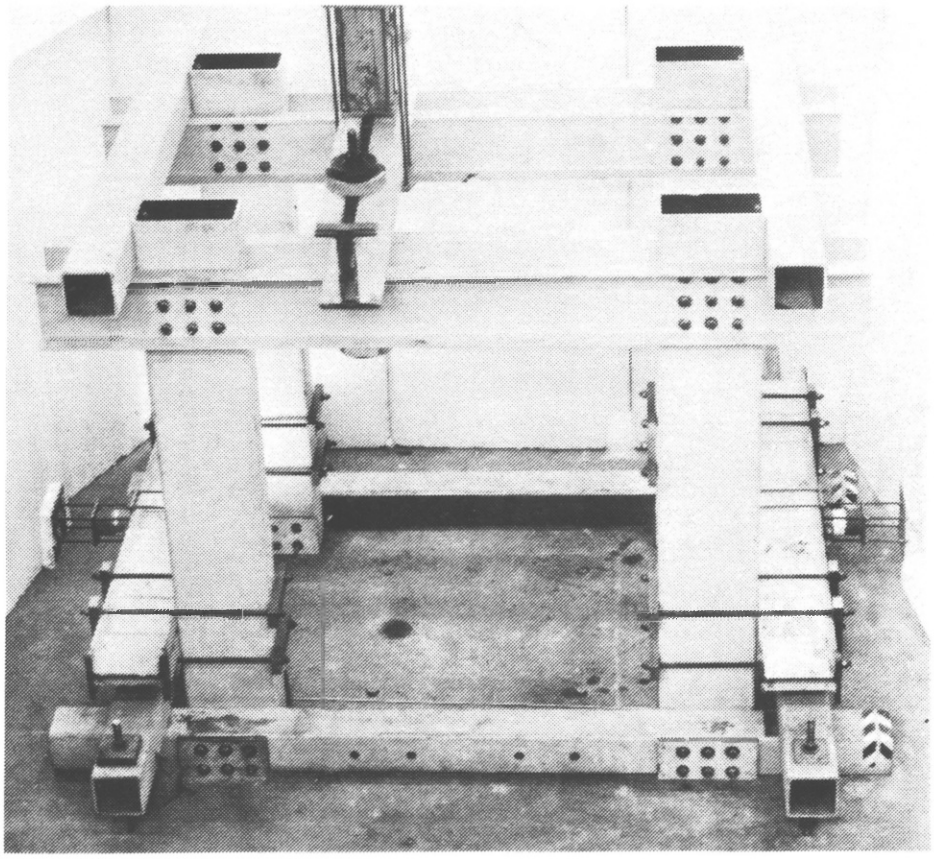
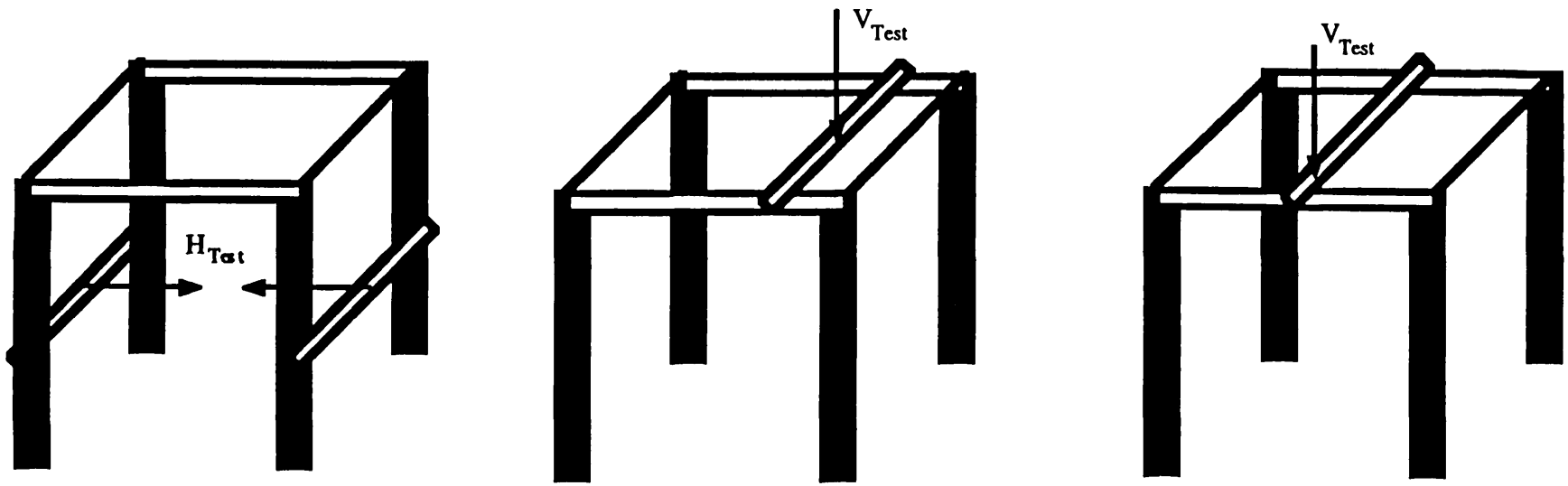


Figure 5.3 : CONSTRUCTED EXPERIMENTAL RIG



(a) Rig's Safety Test for Horizontal Loads
H_{Test} = 250 kN

(b) Rig's Safety Test for Vertical Loads
First Load Case V_{Test} = 350 kN

(c) Rig's Safety Test for Vertical Loads
Second Load Case V_{Test} = 350 kN

Figure 5.4 : **SAFETY TESTS CARRIED OUT ON THE CONSTRUCTED RIG**

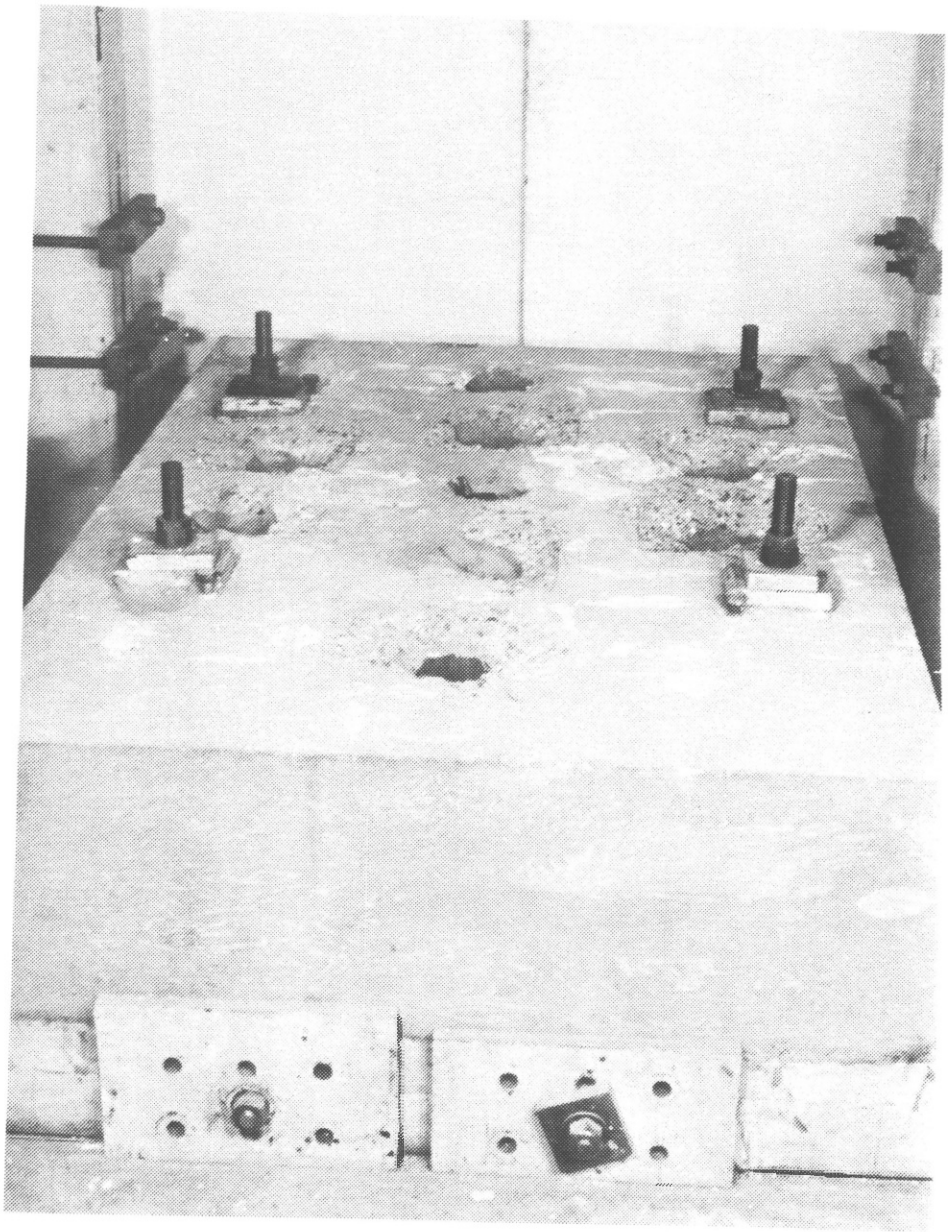


Figure 5.5a : CONCRETE BLOCK USED DURING THE MAIN INVESTIGATION

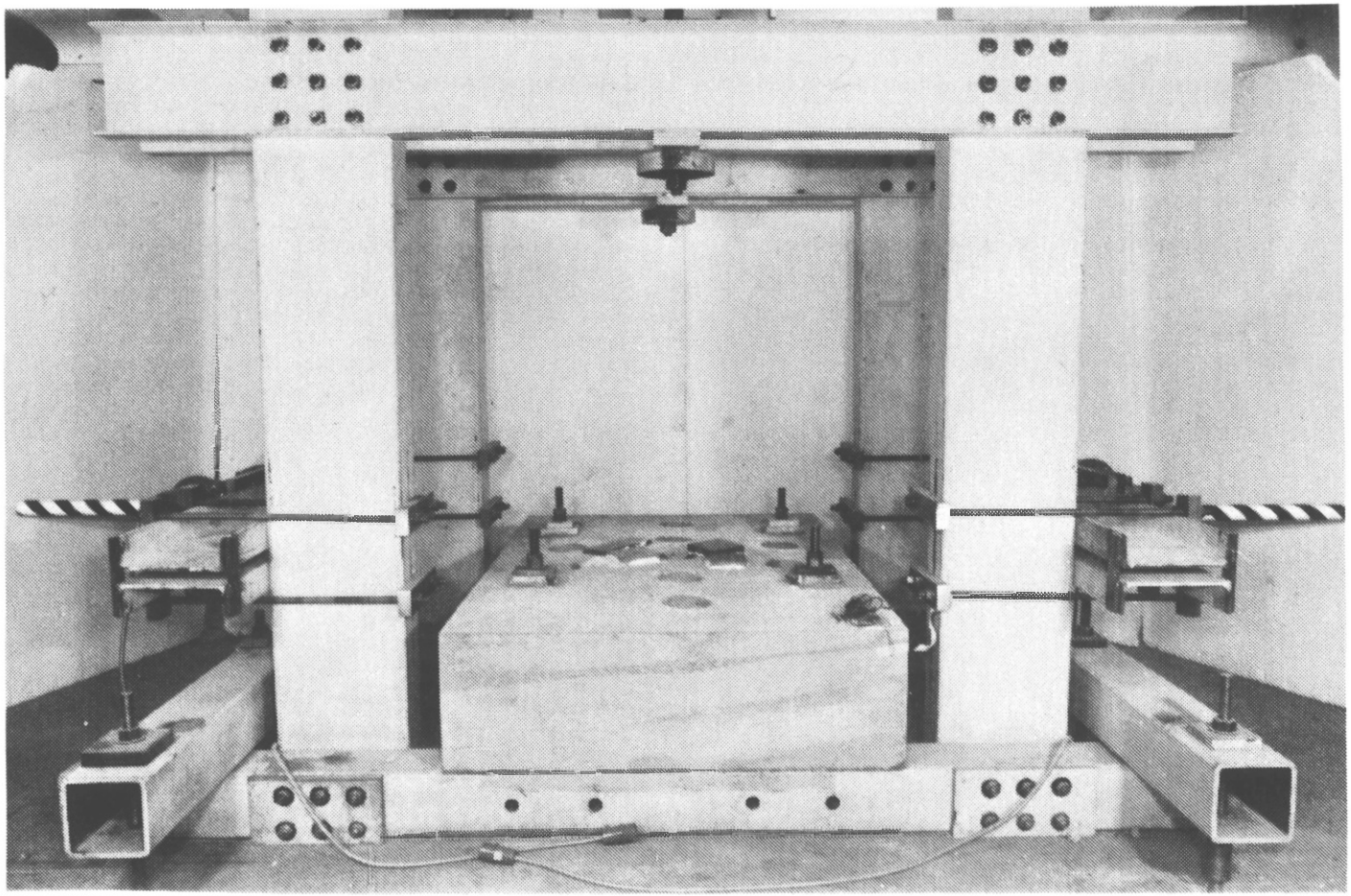


Figure 5.5b : GENERAL VIEW OF THE RIG WITH THE CONCRETE BLOCK

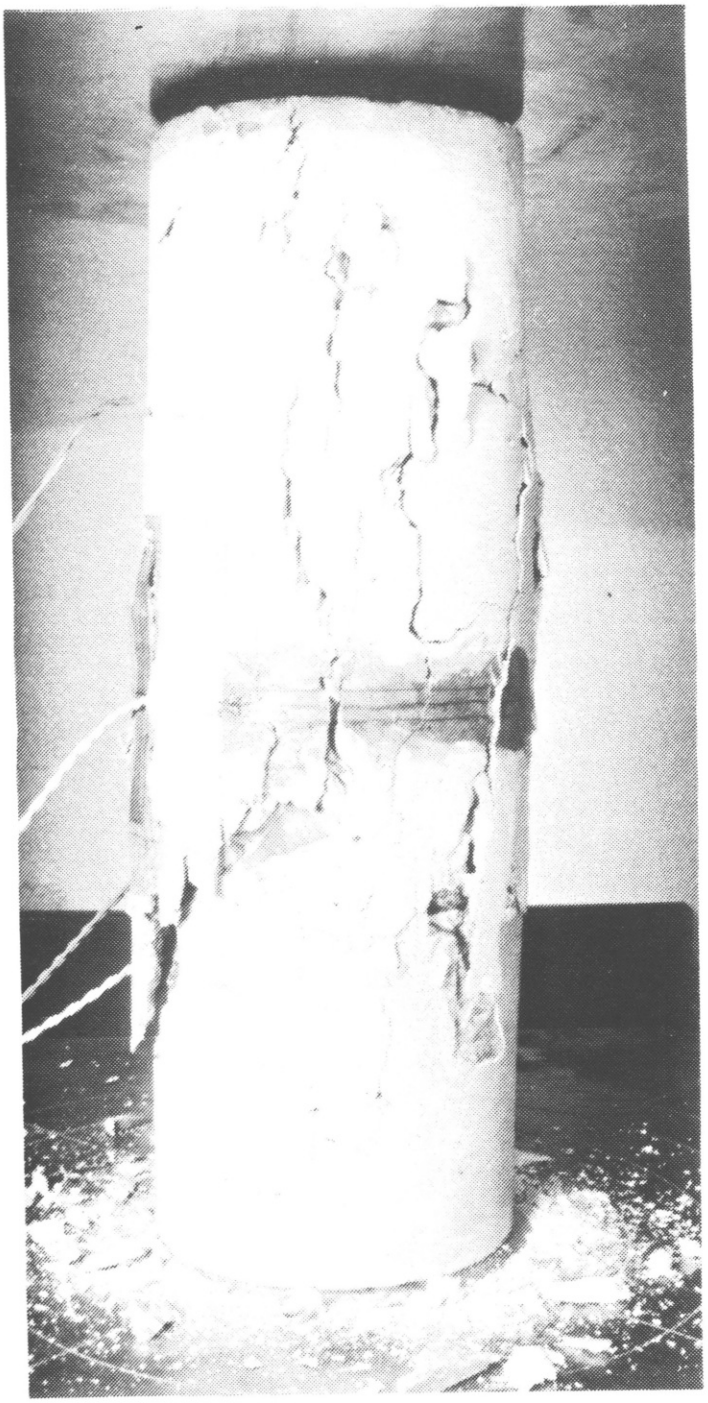


Figure 5.6 : FAILED CONCRETE CYLINDER UNDER COMPRESSION
(used for the measurement of the elastic modulus and Poisson's ratio)

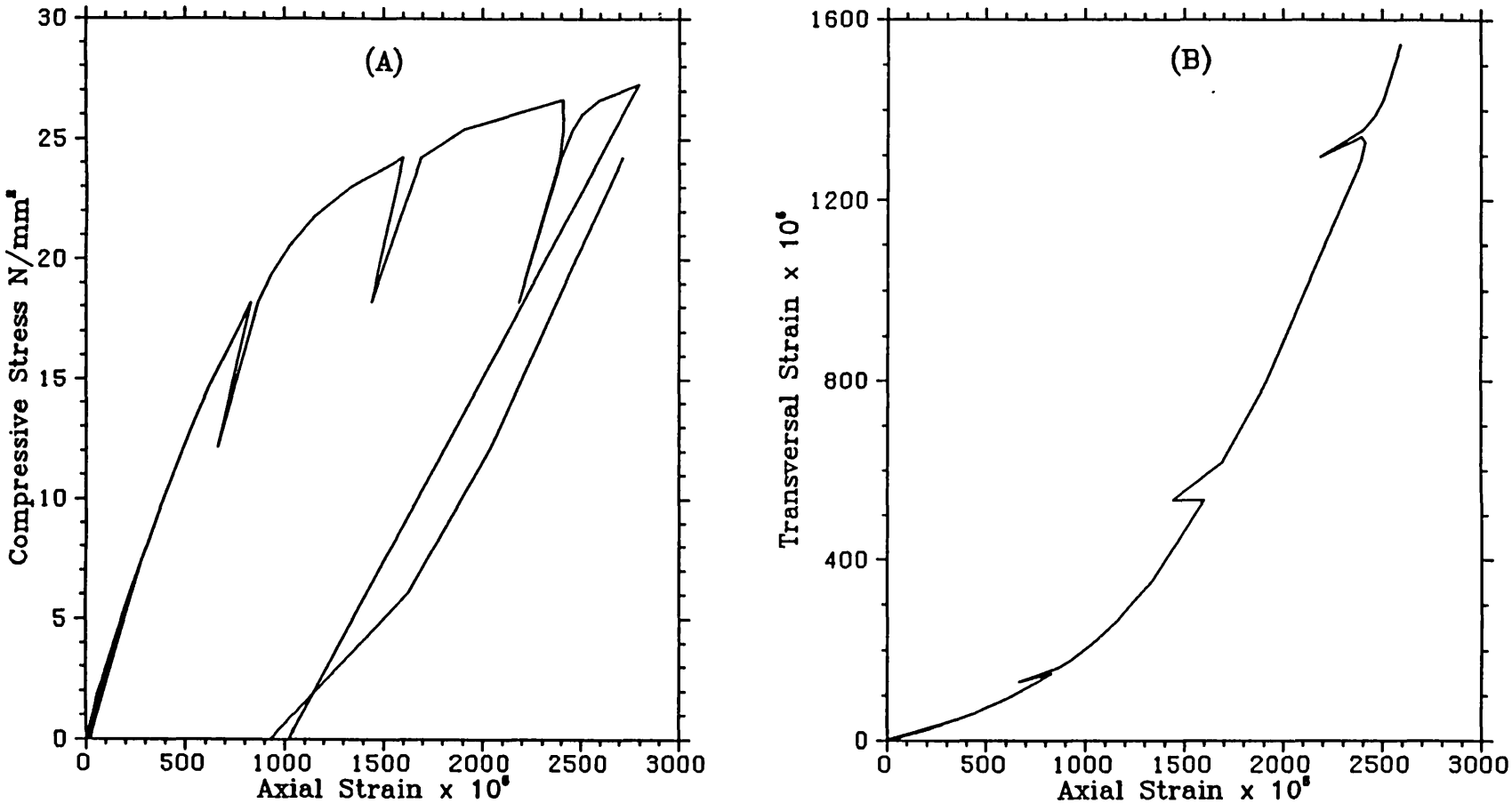


Figure 5.7 : CONCRETE BLOCK MATERIAL BEHAVIOUR IN COMPRESSION (Grade 40)

CHAPTER 6 : PULL-OUT TESTS ON GROUTED TENSION PILES

6.1 INTRODUCTION

Grouted tension piles are used in a range of foundations, but their main application is in offshore construction, particularly for floating structures. Such piles are usually adopted in rock strata or in difficult soil conditions such as chock, or stiff clay (Cox and Reese 1976) soils. St. John et al (1983) noted that even piles grouted in clay have a higher capacity in tension than driven piles. However, since the use of tension grouted pile foundations is a relatively new development, design rules have not yet been firmly established. As a result there is a considerable interest in investigating the behaviour of grouted piles in greater detail.

In offshore structures, tension pile foundations may be critical elements for the stability of the overall structure. Most design methods for grouted piles continue to rely on the formulae for the capacity of driven piles. The API code of practice (1986) and the Department of Energy (UK) (1982), drew attention to a possible failure mechanism of this type of foundation at the pile/grout interface. However, designers are referred to the rules for grouted joints between tubular members (which have been derived for grouted connections between piles and sleeves on the jacket legs) to calculate the limiting grouted pile load capacity. This latter approach is based on test results obtained by Billington et al (1978, 1980). The API recommendations (1986) specify that, the average bond strength along the grouted length has a value of 0.184 N/mm^2. This value of bond strength includes a safety factor in the range of 2.5 to 33.6 with an average of 11. The use of such a large safety factor is partly to cover uncertainties due to the limited knowledge of the subject, and the large difference in bond values between plain pipe and grout that had been already suggested from previous work on pipe connections.

There are basically three types of loading conditions which have to be considered either separately or in combination:

1 - static and dynamic tension loads
2 - cyclic tension loads
3 - lateral loads

So far in design the effects of lateral load acting in combination with either

tension or compression have not been considered in detail. However, with tensile loading in particular, it would seem very probable that lateral loads could influence the amount of debonding and significantly affect the axial load capacity. In addition, as was shown by results from the numerical model in chapter 2, the pile cannot be designed on the basis of average shaft friction, since the average shear stress at failure decreases with pile length (St John et al 1983). The pile length effect on the average shear stress was also reported by St John et al (1983), for driven piles under axial tension load.

The ultimate pile strength depends primarily on the bond between the pile and the grout as well as between the grout and the surrounding media. Kraft (1974) called attention to the bond between pile and grout, and suggested that it is mainly controlled by :

1- grout "wetting" of the pile surface.
2- roughness of the pile surface.
3 - grout mix design.

When grouted piles fail in tension, extraction of the pile is accompanied by one or a combination of the following mechanisms :

1- sliding failure at the pile/grout interface.
2- sliding failure at the grout/soil interface.
3- failure of the grout ring by over-stressing.
4- development of a slip surface in the surrounding soil.

6.2 OBJECTIVES

The principal aim of the present work has been to improve understanding of the grout/pile failure mode and resistance, when the pile is subjected to axial and non-axial loads.

6.3 TEST PROGRAMME DESCRIPTION

The loading conditions for the ten tests undertaken are outlined in table 6.1. The two preliminary tests PPLT 1 and PPLT 2 were carried out to test the equipment and loading rig and to demonstrate the influence of lateral loading. Test PPLt 1 was a simple axial tension pull-out test whilst in test PPLT 2, the pile was submitted to cyclic horizontal loading prior to the application of axial tension.

The second test series have been conducted with the pile submitted to proportional loads (PLT 3, 5, 6, 8). During this test series, the vertical load (V) and the lateral load (H) were increased keeping the ratio (V/H) constant. The results from this series are used to generate an interaction diagram corresponding to pile failure under proportional loads V and H.

The third test series (PLT 3, 4,and 7) is focused on the effect of the force sequence application on the pile behaviour. The load paths chosen have a number of common points corresponding to proportional loading with V/H = 20. Any pronounced difference between the amount of slip and force resistance obtained from the different applied force paths is an indication of path dependency.

Details and description of the tests are summarized in figure 6.1 and table 6.1.

6.4 TEST ARRANGEMENT

The piles used in this investigation had an outer diameter of 112 mm and a wall thickness of 11 mm; the pile steel was of grade TI 54. Before each test the pile was sand blasted to remove dust and to provide a uniform surface condition.

For the preliminary investigation (tests PPLT 1 and PPLT 2), the piles had an overall length of 560 mm, and were sand blasted using college facilities. Subsequently, the main test pile specimens were designed for a longer pile embedded length (560 mm) and so with an overall length of 910 mm could not be fitted inside the college sand blasting machine. For these tests, the pile surface treatment was performed outside the college in a "Decco Spray" machine which provided a considerable improvement to the steel surface finish. Because of this, conditions for the preliminary tests and the main test series were different and the results not directly comparable.

For the preliminary tests the embedded pile length was 300 mm. It had been planned to use a longer length for the main test series and test PLT 1 was undertaken with an embedded length of 560 mm. Because of the improved surface treatment the test pile required a high load for extraction which was uncomfortably near the rated capacity of the test frame. Because of this, the grouted length was reduced to 300 mm for the subsequent tests, as it had been during the pilot tests. A typical pile specimen is shown in Figure 6.2a.

6.5 PILE LOCATION

The piles were centralized in a pocket in the concrete block. The pocket diameters were 170 mm and 145 mm during the pilot and the main investigations respectively. To improve the surface condition between the grout and the concrete block, so that failure would be more likely to happen at the interface pile/grout rather than the grout/concrete interface, the concrete aggregates were left exposed. Before pile installation, the concrete surface was brushed and wetted to reduce the loss of the grout water by absorption in the concrete.

6.6 GROUTING OPERATION

Filling of the space between the pile and the concrete was carried out by using an air pressure grout pump. Figure 6.2b shows the pump in place with a pile specimen inside the concrete pocket. The pump hose was connected to a small diameter tube, which was passed inside the pile, so that the grout was applied directly to the bottom of the pocket. When the air pressure was released, the grout was pushed from the pump and forced to fill the gap from the bottom upward. The bottom of the pile specimen was closed by a steel plate, to stop the grout filling the inside of the pile.

The grout mix was that selected during the grout investigation described in chapter 4. All tests were conducted at a grout age of one day, except for test (PLT 1), where the final test was carried out two days after the grouting operation to permit modifications to the load application equipment.

The mean grout compressive strength at one day is 18 N/mm^2 with standard deviation of 1.5 N/mm^2, measured over 20 cube specimens. The grout compressive strength at the age of two days is 30 N/mm^2.

6.7 LOAD APPLICATION

The tension load was applied to the pile by means of a hydraulic jack (100 tones capacity, and 300 mm travel) fixed to the top frame cross beam. The lateral loading was generated by a smaller hydraulic jack (30 tones capacity and 150 mm travel) fixed to the lateral frame beam. The lateral load was provided by a tensile force applied 160 mm above the top level of the grout, which corresponded to the concrete block surface.

In the case of the laterally loaded pile tests, the horizontal force was disconnected after the vertical force reached a constant resistance. The pile extraction was then completed by the vertical axial force acting alone.

6.8 PILE HEAD CONNECTORS

Special connectors between the pile and the hydraulic jacks were designed to transmit the applied forces to the grouted piles. Figures 6.3 show the detailed dimensions of the vertical and lateral connections and the pile specimens.

6.8.1 VERTICAL LOADING

The pile head connector for vertical force consists of two parts. The first, which has to be inserted inside the top end of the pile, is fixed to the pile specimen by two high tensile steel pins. The second part is designed to connect a high tensile steel bar (40 mm diameter), which transmits load from the vertical jacks to the element already joined with the pile. by means of a pin allowing a rotational movement. This degree of freedom is needed when the pile is submitted to simultaneous vertical and horizontal forces.

6.8.2 HORIZONTAL LOADING

The link between the horizontal jack and the pile is provided by a second connector. It consists of two half steel blocks which are firmly fastened to the pile. The head permits the application of a lateral force in two opposite directions, so enabling through zero lateral force cyclic tests to be undertaken. An additional steel element connects the 25 mm diameter pulling bar and the lateral head. The steel element is joined to the lateral head by a pin which can move in a vertical slot, so the pile can undergo a large vertical displacement whilst subject to lateral loading.

General views of both vertical and horizontal pile head connectors are shown in Figures 6.4. Figures 6.5a and 6.5b show the connection of the pile to the vertical loading coupler both prior to an axial pull-out test, and with the pile just before complete extraction. A view of a pile specimen under combined load is presented in figure 6.5.c.

6.9 INSTRUMENTATION

The behaviour of the pile is described by the applied forces and the

displacement at the top of the pile. The deflections at the top of the pile were measured by Linear Voltage Differential Transformers (LVDTs), measuring to around 0.02 mm. The vertical pile displacement was taken as the average of two LVDTs, placed against the vertical pile connector. Two other LVDTs were placed 20 mm from the top level of the grout, in order to assess the horizontal displacement. An additional LVDT was placed horizontally at a higher level (320 mm from the concrete block surface). Figure 6.5d shows the LVDT arrangement just before a proportional combined force pull-out test.

6.10 RESULTS

6.10.1 PULL-OUT TESTS

Two preliminary tests were undertaken to prove the equipment and to identify the key factors to be taken into account in subsequent tests. The first of these (PPLT 1), was for vertical load only. The second (PPLT 2), involved cyclic horizontal loading followed by vertical pull-out. Figure 6.6a shows the horizontal displacement at the head of the pile during the sequence of horizontal loading in test PPLT 2.

The vertical behaviour of the pile in both pilot tests is shown in figure 6.6b. The axial load-deflection curve for the pile without any prior lateral loading is shown by a full line, while the behaviour of the second pile is shown by a dotted line. When lateral loading cycles have been applied prior to the pile extraction, the pile/grout bond might fail, leaving only the development of frictional resistance to restrain the pile during further extraction. This was certainly what had caused the change of the pile behaviour during the test PPLT 2. Both pile stiffness and strength were affected by the lateral loading history on the pile. Figure 6.6b shows the lateral load effects observed during the pilot investigation.

The results presented in figure 6.6a for behaviour of the pile under lateral loading, show that behaviour is far from elastic and that large irrecoverable deformations occurred. These appear to be due to the separation between the pile and the grout. This is evident from the large displacement occurring at zero load as the direction of loading is reversed after the first cycle. Clearly, lateral loading causes not only bond failure, but also a separation between pile and grout.

Two further axial pull-out tests (PLT 1 and PLT 2) were carried out during the main investigation. The pile embedded lengths were respectively 560 mm and 300 mm. Results of these tests are shown in figure 6.7a.

In all the axial pull-out tests carried out during this programme, the piles displayed a relatively small amount of pile end displacement before failure. After failure there was a progressive reduction in the pile resistance to vertical movement which eventually led to a relatively constant value. This suggests that pile failure was caused by a progressive pile/grout bond breakdown along the embedded pile length, followed by a constant post-failure resistance provided by the frictional stress at the pile/grout interface.

The effect of grout age (i.e. strength, and stiffness) is particularly significant for behaviour prior to the attainment of maximum load. Test PLT 1 was carried out over two days. Figure 6.7b shows the pile behaviour at the grout ages of 24 and 48 hours in dotted and full lines respectively. The pile stiffness was almost doubled when the grout was left for an additional 24 hours. The test does not reveal the effect of grout strength on the pile failure load, since the pile was not taken to failure on the first day.

Figure 6.8a compares the results obtained from the pilot test (PPLT 1) and the main investigation (PLT 2) for the same pile embedded length. This permits an assessment of the influence of the two types of sand blasting operations undertaken during this work. It is evident that there was a considerable improvement of the pile surface state for the main programme tests. The pile specimen in test (PLT 2) provided an increase of resistance of almost 70%.

During this test, the extracted pile came out with a grout ring bonded to the pile. The jointed grout had a height of 100 mm. This means that the failure along the corresponding section, occurred at the grout/pile interface. In addition, a horizontal crack of 10 mm, developed all around the grout section, at a pocket depth of 200 mm (2/3 of the embedded length). This was certainly caused by a tensile failure of the grout. Figure 6.9a describes the mode of failure obtained during this test. Accordingly, the pile extraction was developed by a combination of failure modes pile/grout, grout/concrete, and tensile failure of the grout.

These observations provide a clear indication that the surface condition of the pile has a significant effect upon the maximum load as well as the failure mode of a grouted pile.

Figure 6.8b compares the behaviour of all piles failing under uni-axial tensile loading. The conditions are different in each test, but in all cases the unloading sequence during the tests shows that pile extraction is accompanied by irreversible deformation.

Even at low tension forces, there was non-recoverable upward pile movement. This could be an important factor especially for floating offshore structures which may need to be addressed in design. The pile specimens tested for this section are presented in figure 6.9b.

6.10.2 PROPORTIONAL LOADING

As a part of the main series, pile tests under combined lateral load (H) and vertical load (V) were carried out. Both forces were applied and increased simultaneously. A proportional test with a ratio V/H = 20 (PLT 3) followed by three additional tests with V/H = 1, 5, 10 (PLT 5, 6, 8) were undertaken. The vertical pile responses are shown in figures 6.10; with the results of each test being compared with the pile behaviour under axial extraction (H = 0) obtained from test PLT 2. The horizontal displacement of the piles is shown in figures 6.11.

Application of a lateral force to the piles reduces considerably the axial load capacity and affects the mode of behaviour. Pile failure is defined by an excessive pile end displacement, which is usually developed with small variation of the resistance force. As a result, the bond along the total pile embedded length would have been broken, and the pile resistance would have only been provided by friction between the pile and the grout.

After pile failure, the lateral force was removed and the pile extraction was continued only under axial tension force. At this stage, elimination of the lateral load caused an additional reduction of the axial pile resistance. The vertical load/vertical displacement results for all proportional tests, before and after the horizontal force removal, are presented in figures 6.10e and 6.10f. The reduction in pile resistance force is easily observed.

Evidently, lateral loading has a double effect. On the one hand it reduces the pile axial capacity by inducing bond failure. On the other hand, it permits more pile resistance for additional pile upward movement by locking the pile in the socket, and so provides a more stable pile upward movement, and additional stiffness.

The effect of lateral loads on pile stiffness for vertical movement can be seen clearly from figures 6.10e, and by comparing the behaviour of grouted piles from tests PLT 3, and PLT 8. The pile stiffness during test PLT 8 (V/H = 10) is significantly

greater than that for test PLT 3 (V/H = 20). The same observation can be drawn, from figures 6.10a, 6.10b, 6.10c and 6.10d, where the pile deformation under pure axial tension pull-out is compared with those obtained in the presence of lateral forces.

Lateral loading caused some damage to the grout at the top surface. In all proportional tests carried out, a grout ring, with a maximum depth of 100 mm, was extracted with the pile. It seems that the lateral loading provides a bending moment in the pile and in the grout which produces tensile failure in the grout to a depth where separation has occurred. Figures 6.12a and 6.12b illustrate these modes of failure obtained from tests PLT 7 and PLT 8 respectively. Figure 6.12c shows all the specimens tested in the proportional combined loading programme.

For test PLT 5, the loading path initially adopted was with V/H = 1. However, it was observed that a significant part of the concrete block around the pile was crushed as shown in figure 6.12d. To avoid any excessive damage to the concrete pockets needed for the remaining tests, the pile was unloaded and the load path was replaced with higher force ratio (V/H = 10). Figure 6.12e shows the possible effects of lateral loading on the mode of failure of grouted piles under combined horizontal and vertical loads.

The pile lateral displacement is measured at 20 mm above the top of the grout. The lateral force / lateral displacement behaviour of the piles tested under proportional load is presented in figures 6.11. The zero unloading of the lateral load corresponds to the removal of the horizontal force.

For high V/H ratio (20), lateral pile displacement is recovered with removal of the lateral force (figure 6.11a). For lower ratio of V/H, the lateral pile movement is irreversible (figure 6.11c and 6.11d). In addition, evidence of overall softening behaviour is seen from the graphs of lateral load to a base of lateral displacement. Observation of the condition of the piles after extraction suggests that the irreversible deformations might be caused by crushing of the grout resisting to lateral displacement, as well as tensile failure of the grout ring around the pile.

Softening is evident from the results for vertical slip when the ratio of V/H is high. For low V/H ratios, vertical pile displacement softening is not so evident and slip occurs with an approximately constant pull-out force. The latter behaviour follows the pattern of the pile displacement observed in test PPLT 2, when the pile was submitted to through zero lateral rocking before application of vertical loading. In both cases, the

interface pile/grout bond is likely to be disturbed over a considerable pile depth, leaving only the frictional interlock pile/grout for the pile resistance to a pull-out force.

An interaction diagram of the pile load capacity under combined proportional loading is presented in figure 6.13. A vertical/lateral load ratio of 10, caused a 30% decrease in the pile axial capacity. The same proportional reduction was caused by the reverse lateral cyclic load, used in test PPLT 2 in comparison with test PPLT 1. This result focuses attention on the need for consideration of lateral loading in the design of grouted piles especially those with a short grouted length such as those tested here.

6.10.3 PATH DEPENDENCY

For some structures, factors such as stress path and type of loading, (static or cyclic), can be very important. In a grouted pile under axial and lateral loading, different elements of the pile/grout interface undergo different load, or stress, paths according to the sequence of the applied force. Accordingly it seemed probable that a grouted pile might exhibit different behaviour and strength under different load combination sequences.

A sequence of loads, which describes a particular path, is defined by the order of the forces to which the pile is submitted. A series of three tests were carried out to elaborate the path dependency factor. The path dependency effect can be obtained by the comparison of the pile behaviour (i.e. end pile force/displacement relationship) obtained from the different load paths exercised. The series consists of the following loading paths illustrated in figure 6.14a, which have a number of common points in V,H load space when V/H = 20 :

1 - proportional loading path (PLT 3, path 1) with V/H = 20.
2 - cycling loading loops (horizontal/vertical), where the horizontal force is applied prior to the vertical tensile force and then removed before unloading of the axial force (PLT 4, path 2).
3 - cycling loading loops (vertical/horizontal), where the vertical force is applied before the horizontal force, then removed with constant horizontal force before unloading in the horizontal direction (PLT 7, path 3).

The results were plotted in figures 6.14 for the vertical pile behaviour and in figures 6.15 for the lateral pile behaviour. The pile subjected to a proportional loading

path provided the lowest resistance. Howevernodefinite conclusion can be obtained since the results from test PLT 3 seems to be a low result when compared to the other tests results. Pile loading under path 2 and path 3 sequences, provided not only stronger pile resistance, but also an additional pile stiffness against an upward movement.

As a result of these observations, an application of a lateral force, prior to the vertical tension, will generate an additional pile stiffness; this may well be caused by a build up of normal stresses at the interface. On the other hand, when the pile has already been subjected to a tensile force, a lateral force causes an additional pile extracting movement.

These test results also provide additional information on the behaviour of grouted piles under cyclic loading. It is clear that the pile end movement undergoes an irreversible upward movement even at low tensile forces. Load cycling effects need more careful study. However detailed and final conclusions on such effects cannot be concluded from the present work. The vertical cyclic behaviour obtained from test PLT 4 (path 2) and PLT 7 (path 3) is shown in figures 6.16.

The results presented here are not conclusive due to the limited number of tests. The stiffening effect of lateral loading at high V/H ratio is demonstrated however. The effects of load path on pile load capacity are inconclusive because it appears that the result for proportional loading (test PLT 3) may be low.

6.11 DISCUSSION AND RESULTS IMPLEMENTATIONS

The conventional approach for assessing the effect of lateral loads on the pile, is to analyse the horizontal load/displacement relationship, which is the so called P-Y curve criterion; particularly when the pile is designed to resist compressive loads. This method is principally used in the case of driven pile placed in sand or clay strata. Frequently, the analysis of laterally loaded piles, mainly driven in the foundation strata and not pre-drilled and grouted in, is based on semi-empirical correlation, from the tests data on basic soil properties that have been established on a limited number of soil types (Kay et al 1983). Considerable engineering judgement and practical design pile experience are required when extrapolating these design criteria for specific soil sites. This approach clearly does not apply to situations where failure occurs at the grout pile interface.

The condition of the grouted pile location imposes a stiff surrounding (grout

and rock). Consequently, the lateral pile deformation could be far less than that of a driven pile. As a result lateral pile deformation could lead to a false assessment of the effect of lateral loads on grouted piles. Interface resistance could also be developed along the debonded depth, since the grout plastic deformations are only developed with large lateral loads.

The effect of lateral loading on a grouted pile depends on many factors:

1 - pile stiffness
2 - stiffness of the surrounding media
3 - combination of lateral force and bending moment
4 - pile head condition.

The pile design is usually done for vertical load and horizontal load taken separately. This might be admissible when the pile is essentially under compression loads, since the end pile bearing capacity could be considerable. The validity of such a design approach could no longer be admissible in the case of tension piles. An interaction diagram of vertical and lateral loads would be useful in design. This would permit a direct analysis of the strength of grouted piles under combined loads. In addition, when a lateral load causes material degradation around the pile, care must be taken in choosing the pile effective embedded length. Such considerations occur for low V/H ratios

The effect of a lateral load, on a grouted tension pile, is to change the mode of failure at the bonded pile/grout interface. Interface design strength should be based on the friction resistance along the pile surface/grout interface. This would be affected by the pile surface condition and the stiffness of the surrounding media including the grout.

Determination of the local interface grout/pile properties is necessary. It is essential to distinguish between the bond strength and the frictional resistance. The behaviour of grouted pile under axial tension load is governed by these parameters. Dilation along the interface will be shown in chapter 8, to affect the pile/grout sliding process. Dilation at the interface leads to an increase in interfacial shear and leads to stress hardening behaviour for large pile/grout slip.

Table 6.1 : Tests Undertaken on Grouted Piles

	V	H		L (embedded length)
Preliminary series				
PPLT 1	V	H = 0	Axial loading only	300 mm
PPLT 2	V	H	Horizontal loads applied and cycled before application of vertical load	300 mm
Main series : Proportional loading				
PLT 1	V	H = 0	Axial loading only	560 mm
PLT 2	V	H = 0	Axial loading only	300 mm
PLT 3	V/H = 20		Proportional loading	300 mm
PLT 5	V/H = 1, changed to V/H = 10, during test series			300 mm
PLT 6	V/H = 5		Proportional loading	300 mm
PLT 8	V/H = 10		Proportional loading	300 mm
Main series : pilot tests on path dependency				
PLT 3	V, H proportional loading, V/H = 20			300 mm
PLT 4	load path 2 (figure 6.1)			300 mm
PLT 7	load path 3 (figure 6.1)			300 mm

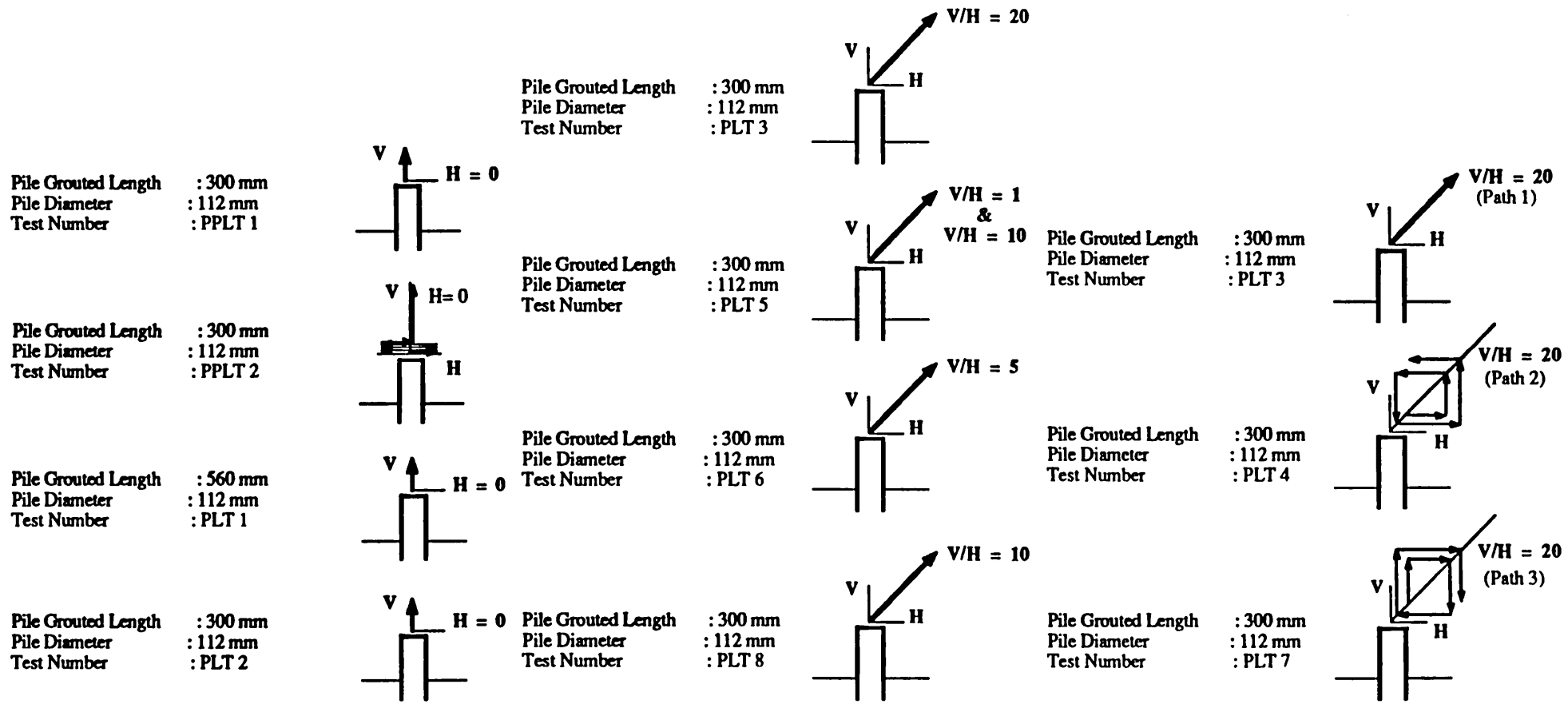


Figure 6.1 : **TEST PROGRAMME ON GROUTED TENSION PILES**

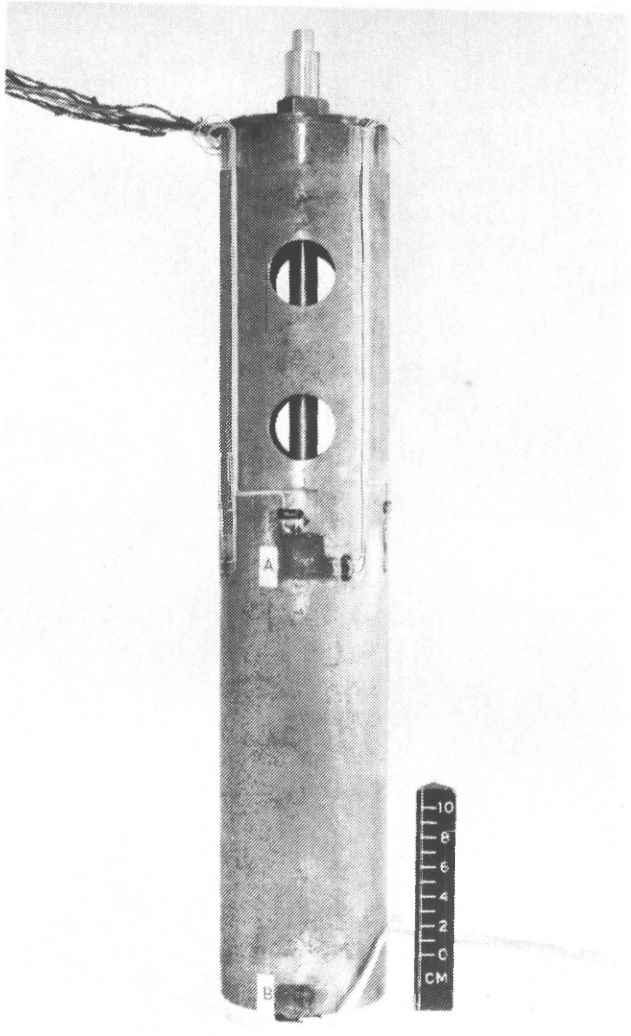


Figure 6.2a : TYPICAL PILE SPECIMEN

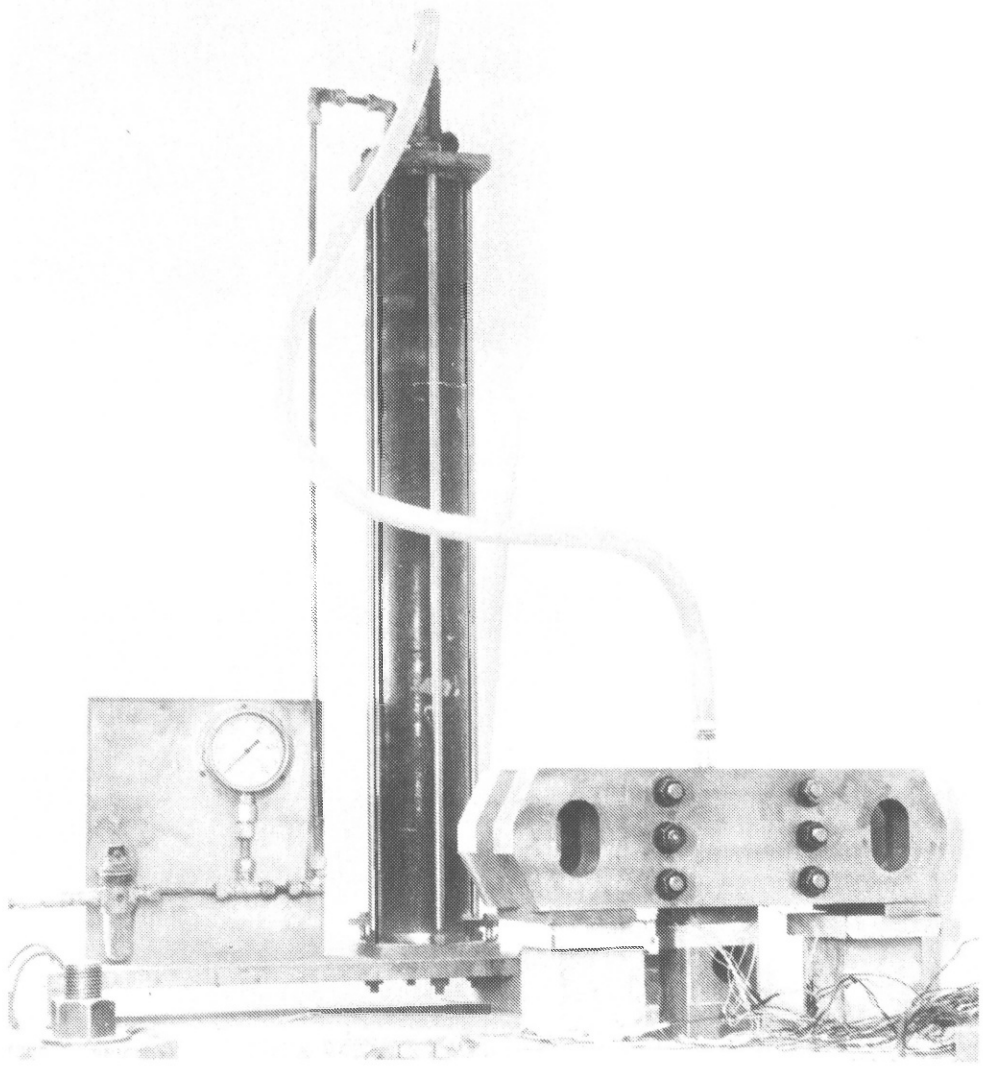


Figure 6.2b : GROUT PUMPING FOR THE PILE CASTING OPERATION

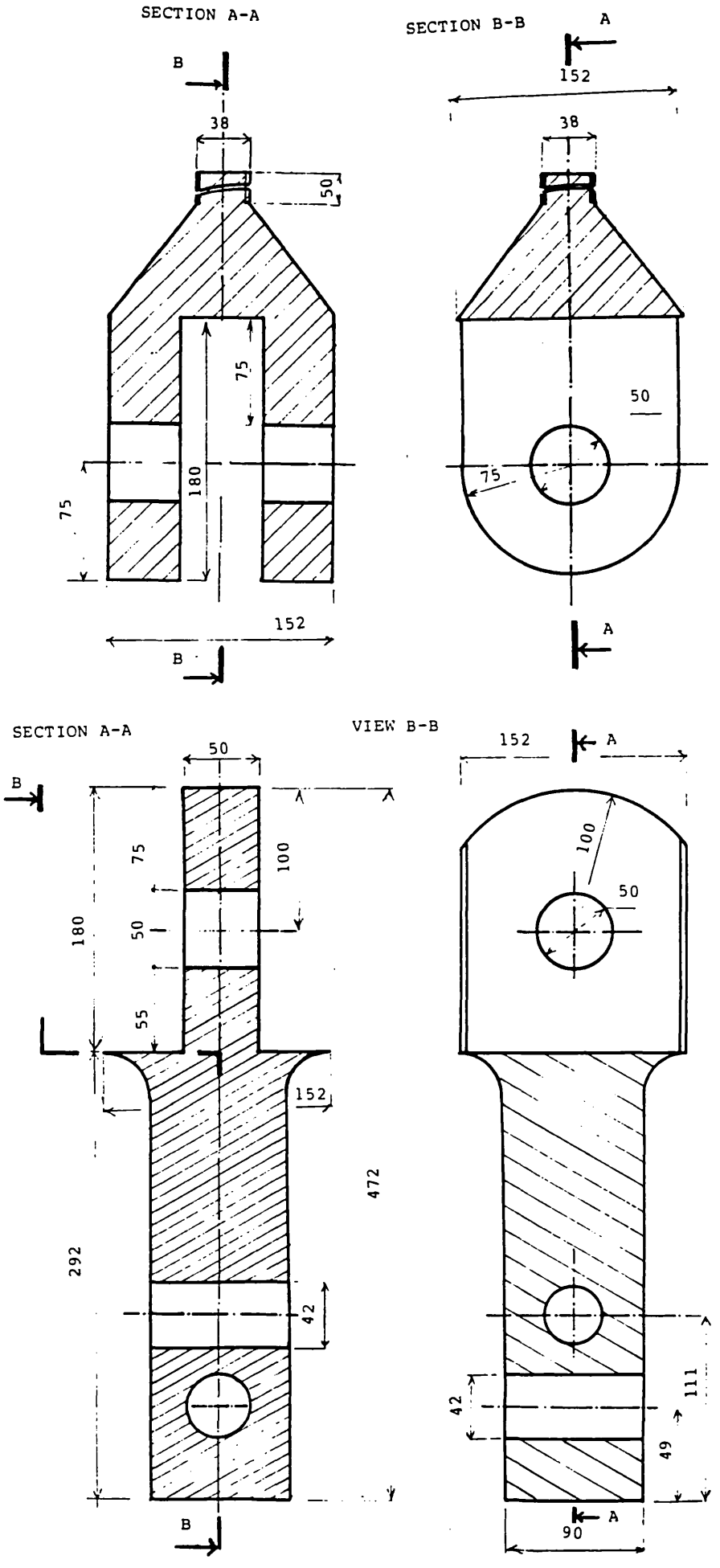


Figure 6.3a : DETAILS OF THE PILE HEAD FOR THE VERTICAL LOAD APPLICATION

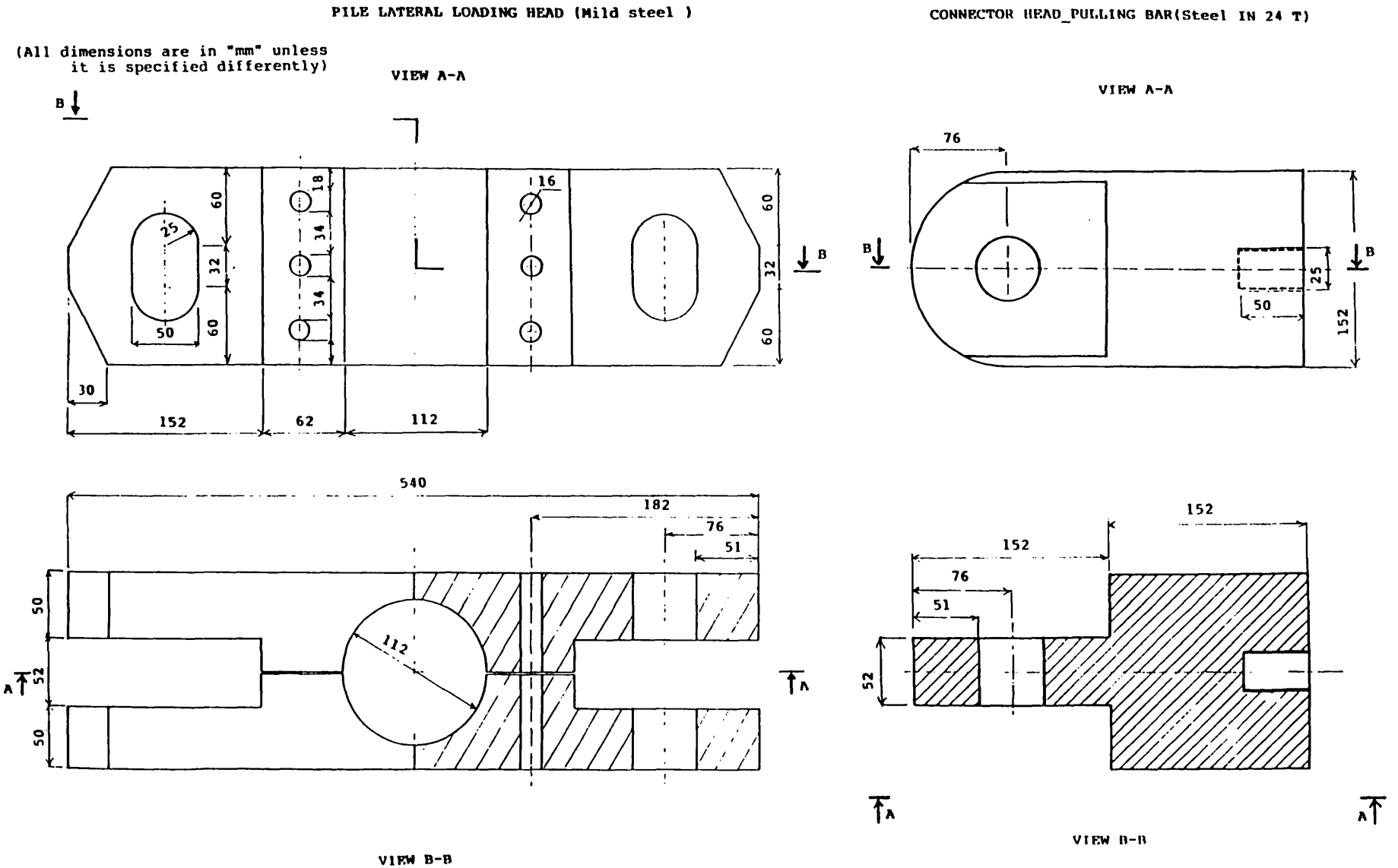


Figure 6.3b : DETAILS OF THE PILE HEAD FOR THE LATERAL LOAD APPLICATION AND CONNECTOR HEAD/PULLING STEEL BAR

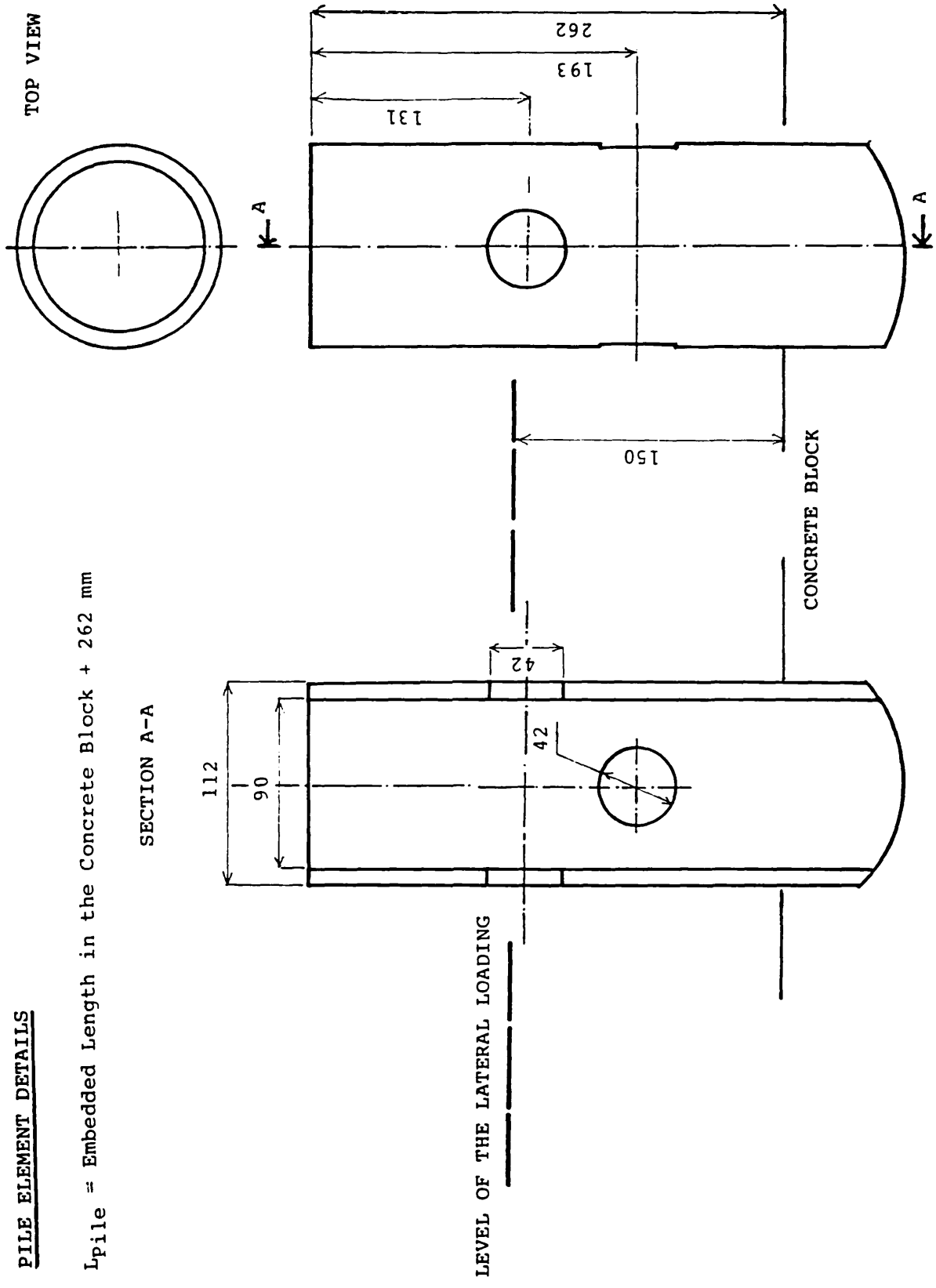


Figure 6.3c : DETAILS OF THE PILE TOP END

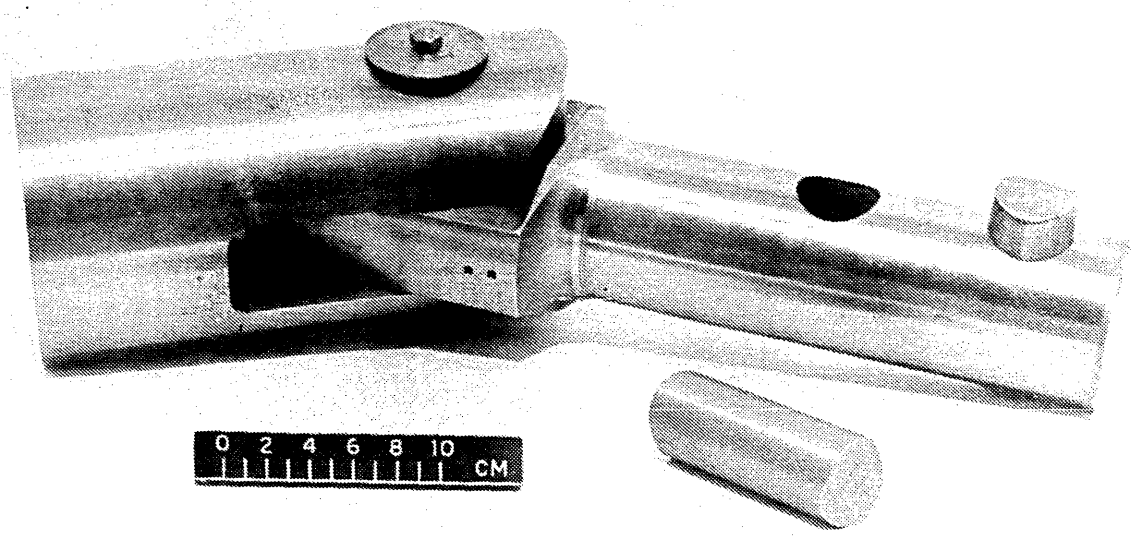


Figure 6.4a : VIEW OF THE MANUFACTURED PILE HEAD FOR VERTICAL LOAD

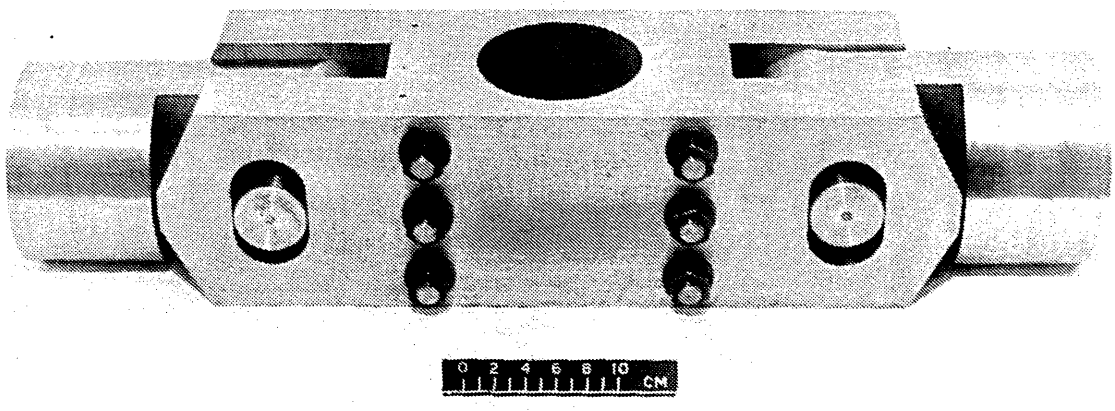


Figure 6.4b : VIEW OF THE MANUFACTURED PILE HEAD AND HEAD/PULLING BAR CONNECTOR FOR THE LATERAL LOAD APPLICATION

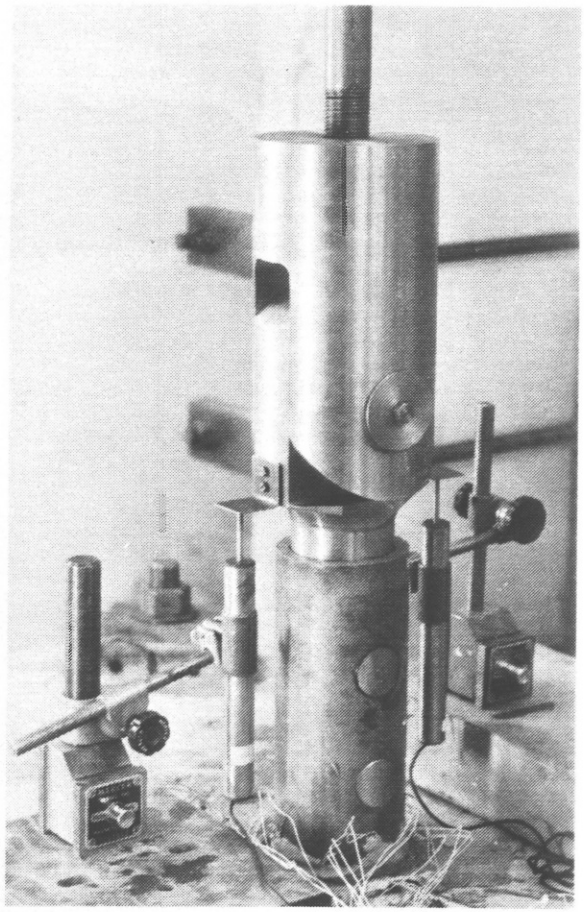


Figure 6.5a : GROUTED PILE AND VERTICAL LOADING COUPLER PRIOR TO THE PULL-OUT TEST

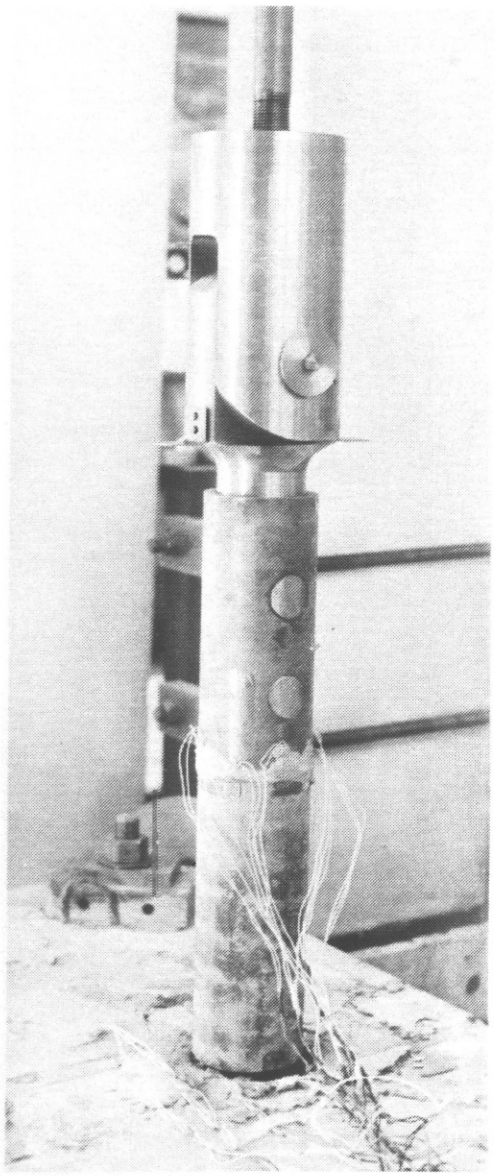


Figure 6.5b : PILE BEFORE COMPLETE EXTRACTION

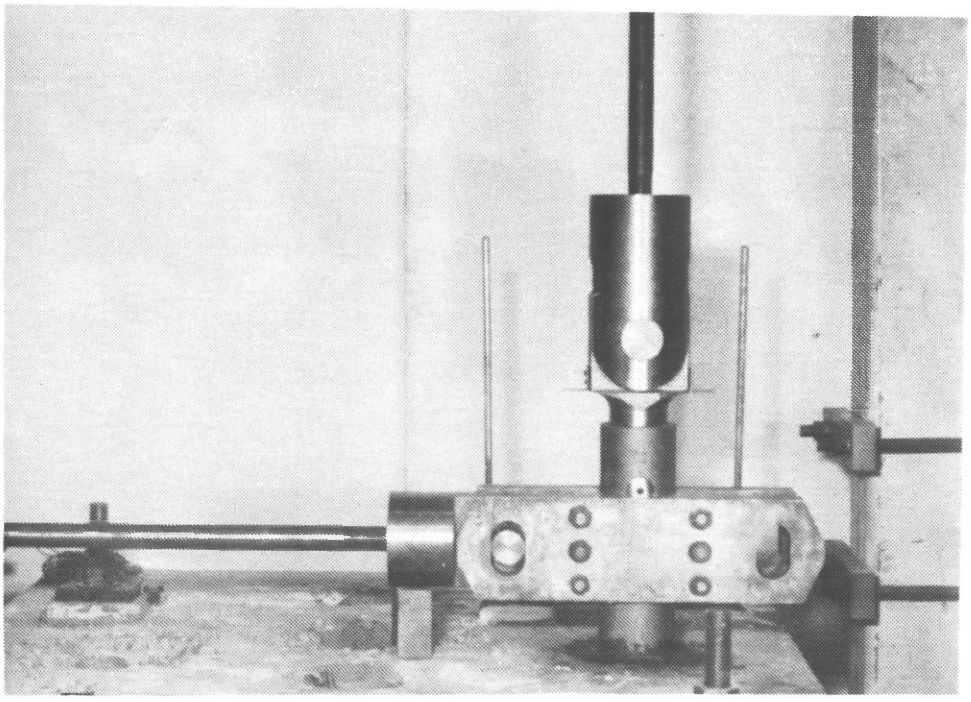


Figure 6.5c : PILE SPECIMEN UNDER COMBINED VERTICAL AND LATERAL LOAD

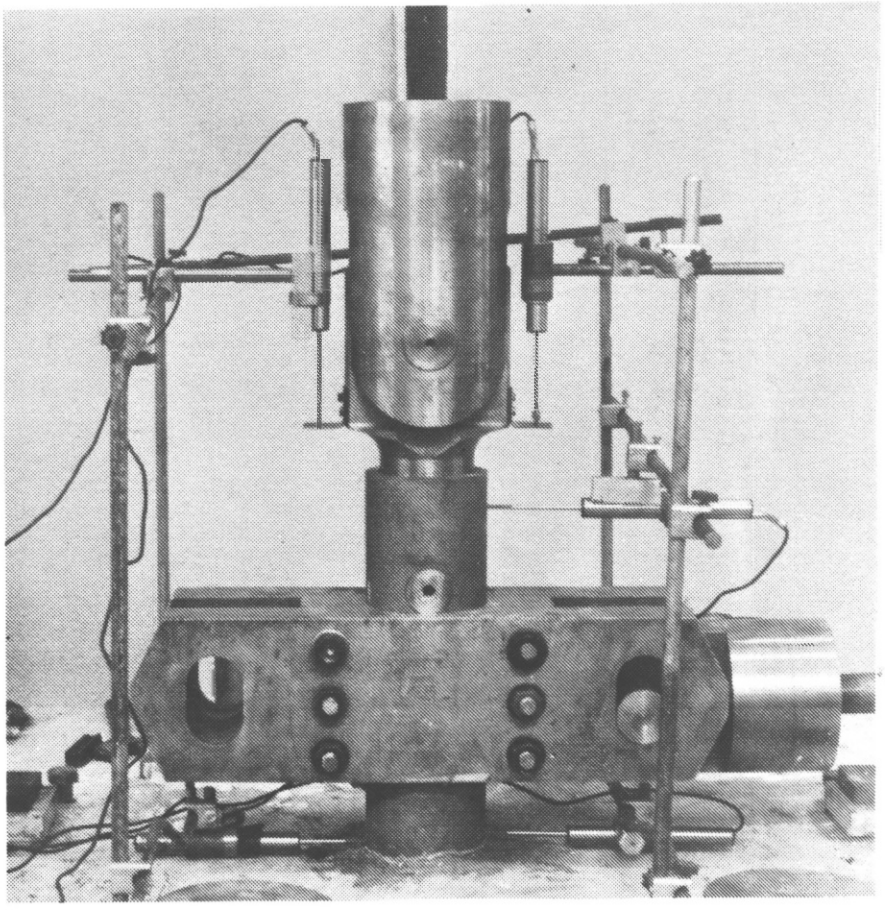


Figure 6.5d : INSTRUMENTATION OF THE PILE TOP END FOR A COMBINED LOAD TEST

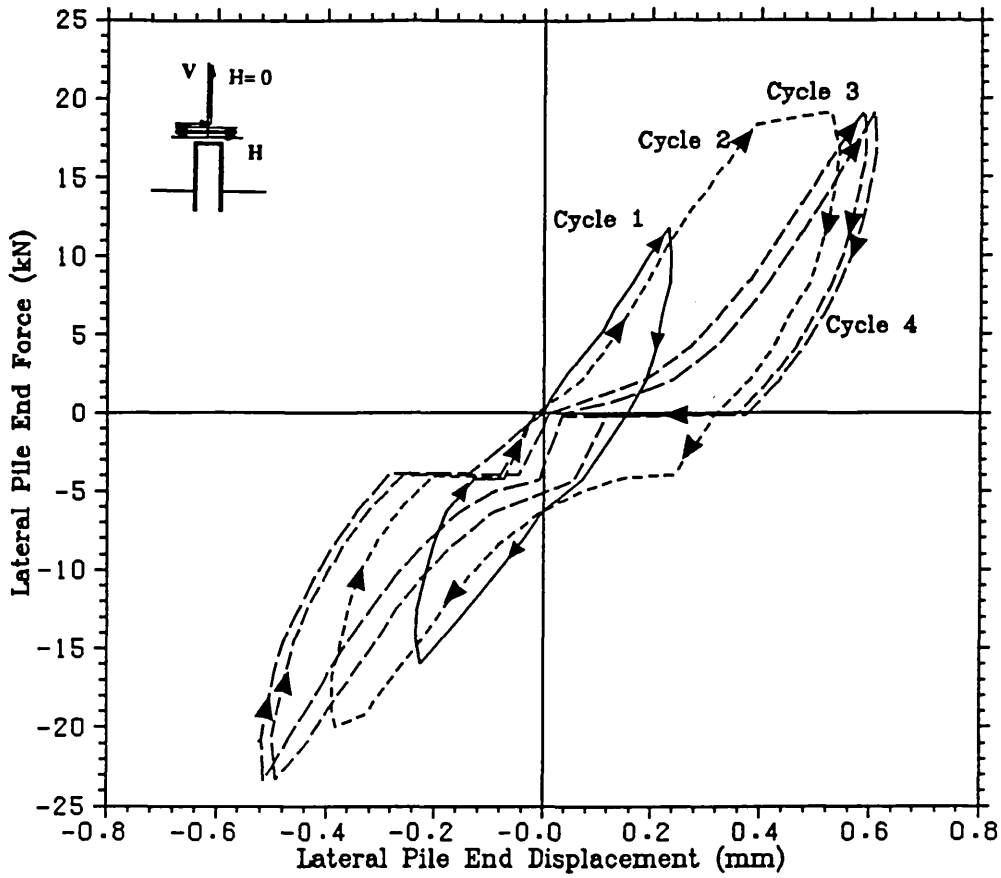


Figure 6.6a : DISPLACEMENT AT THE PILE HEAD DURING CYCLES OF HORIZONTAL LOAD (PPLT 2 Test)

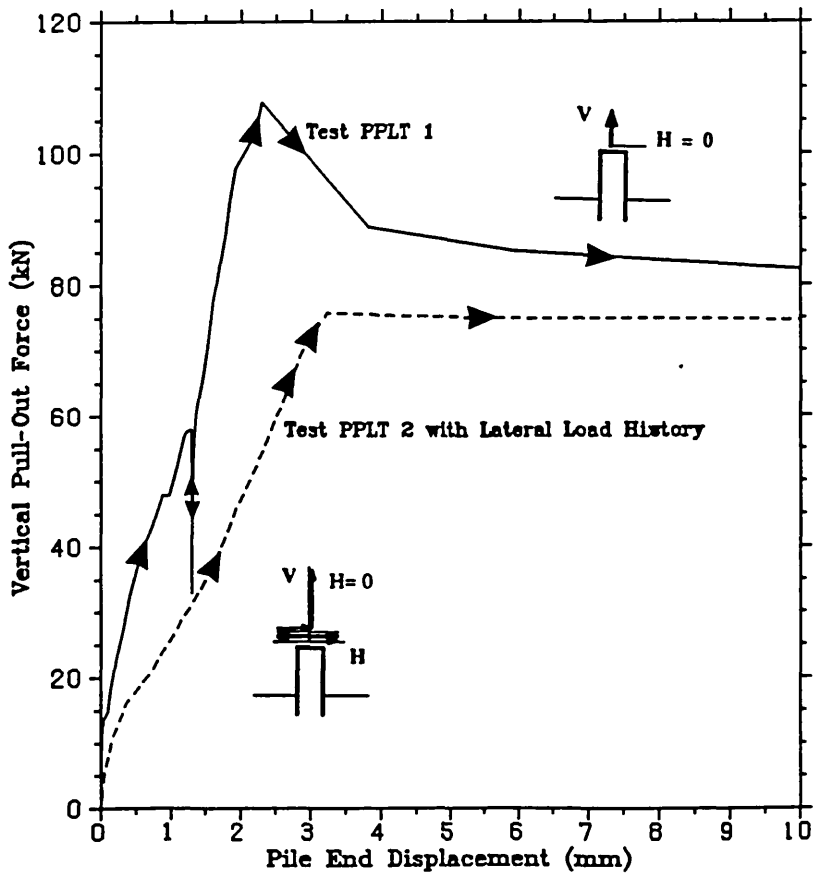
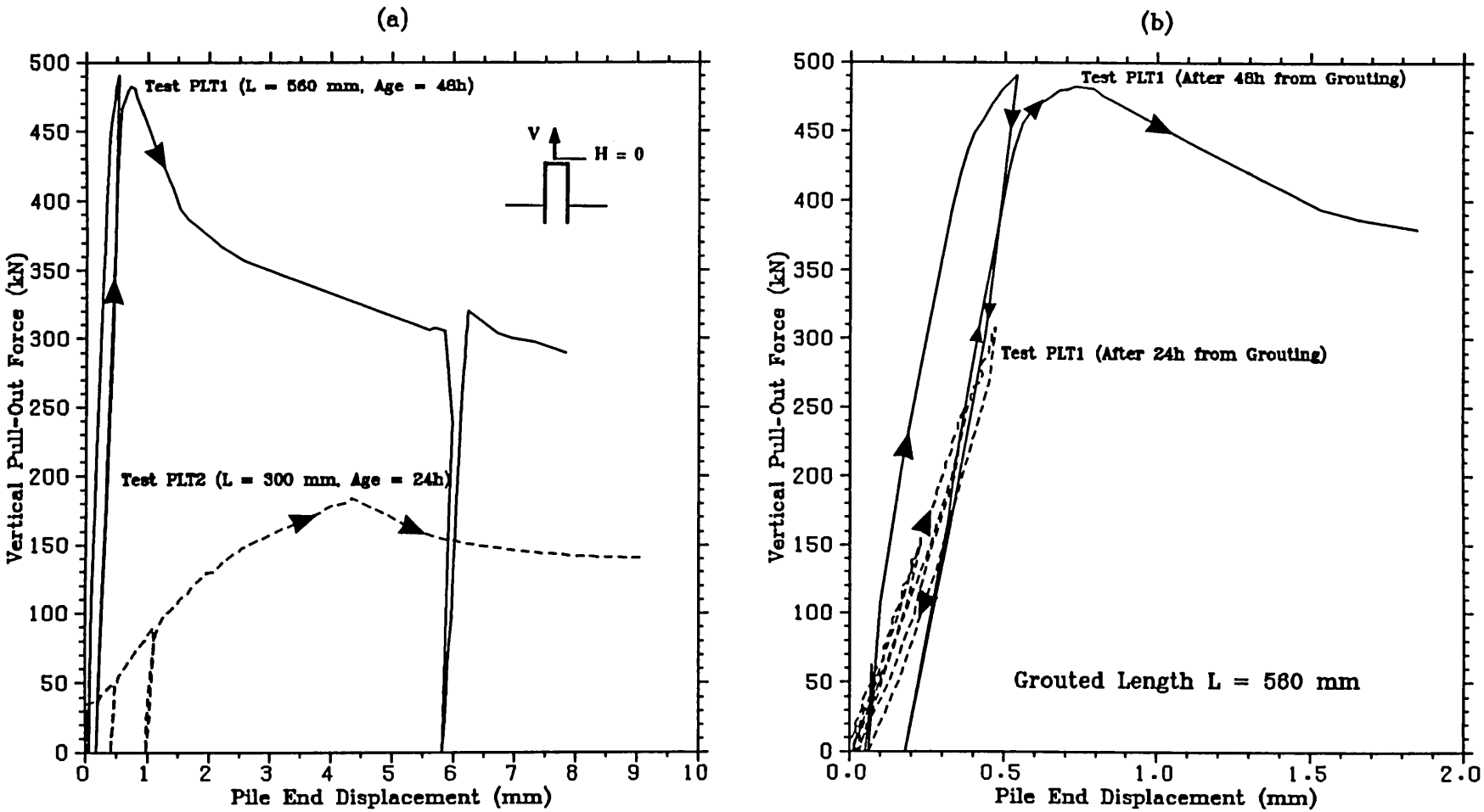


Figure 6.6b : VERTICAL PILE END BEHAVIOUR FOR PRELIMINARY TESTS



Figures 6.7a & b : AXIAL GROUTED PILE PULL-OUT BEHAVIOUR

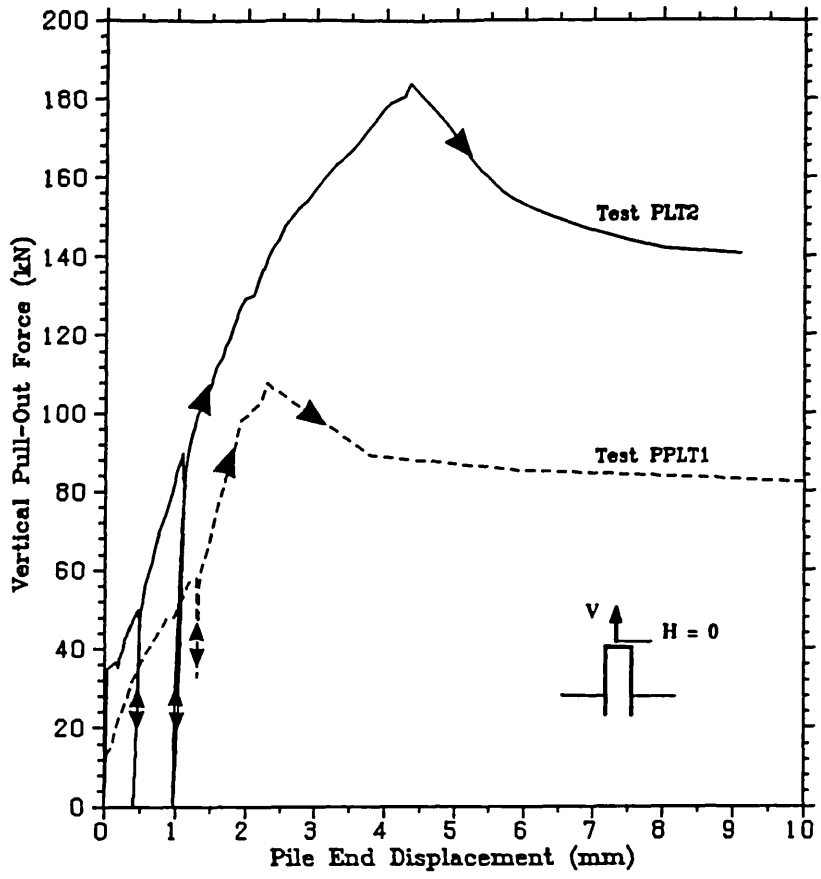


Figure 6.8a : AXIAL GROUTED PILE PULL-OUT BEHAVIOUR

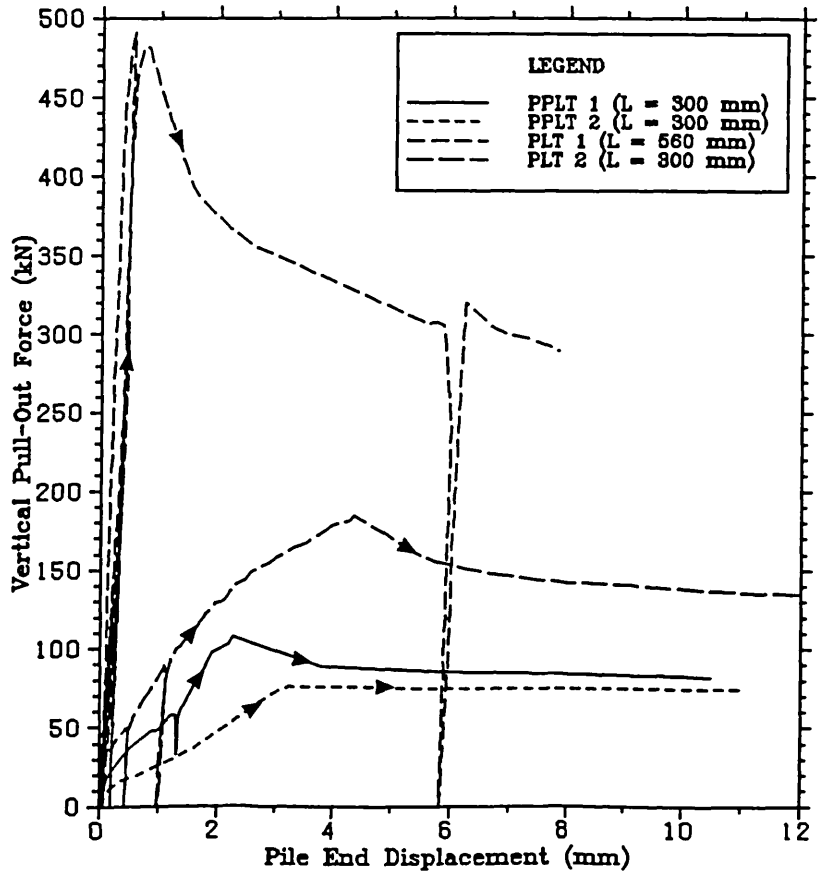


Figure 6.8b : GROUTED PILES PULL-OUT BEHAVIOUR

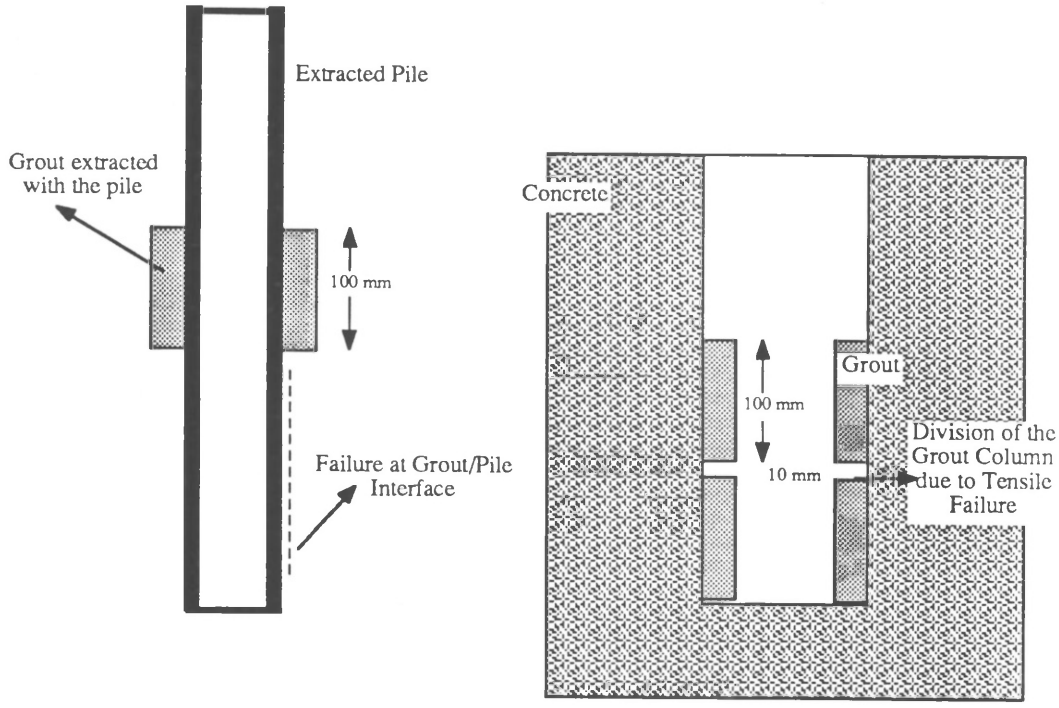


Figure 6.9 a : **FAILURE MODE OF GROUTED PILE FROM TEST PLT 2**

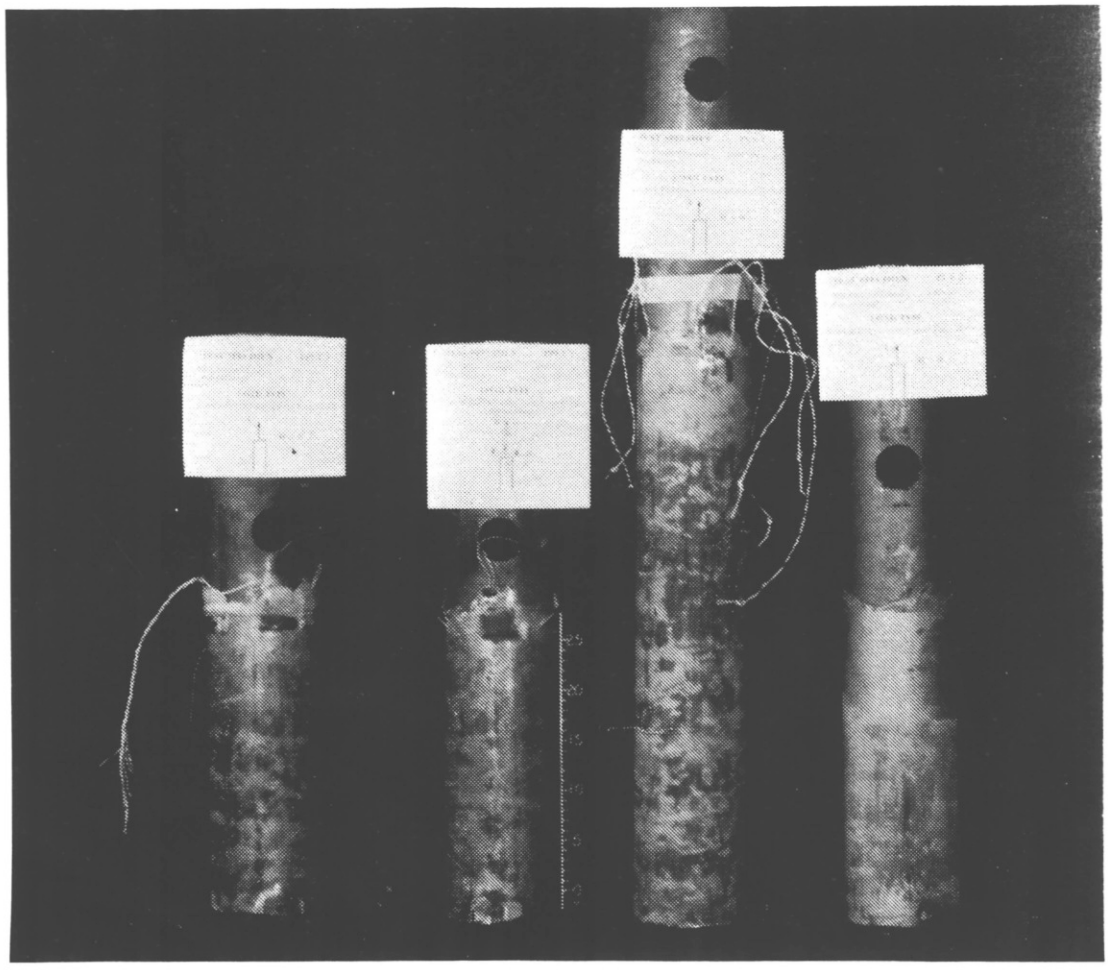
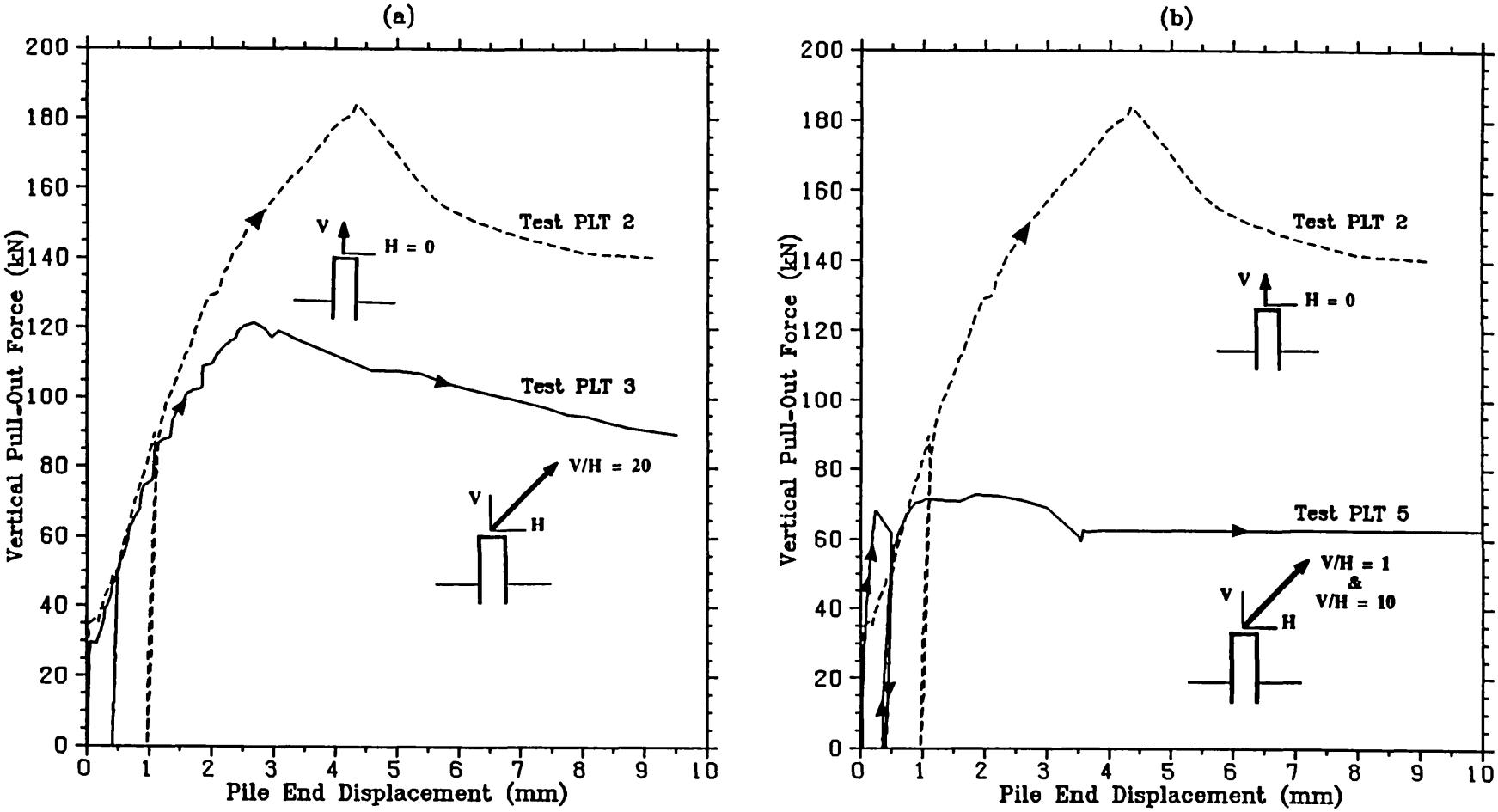
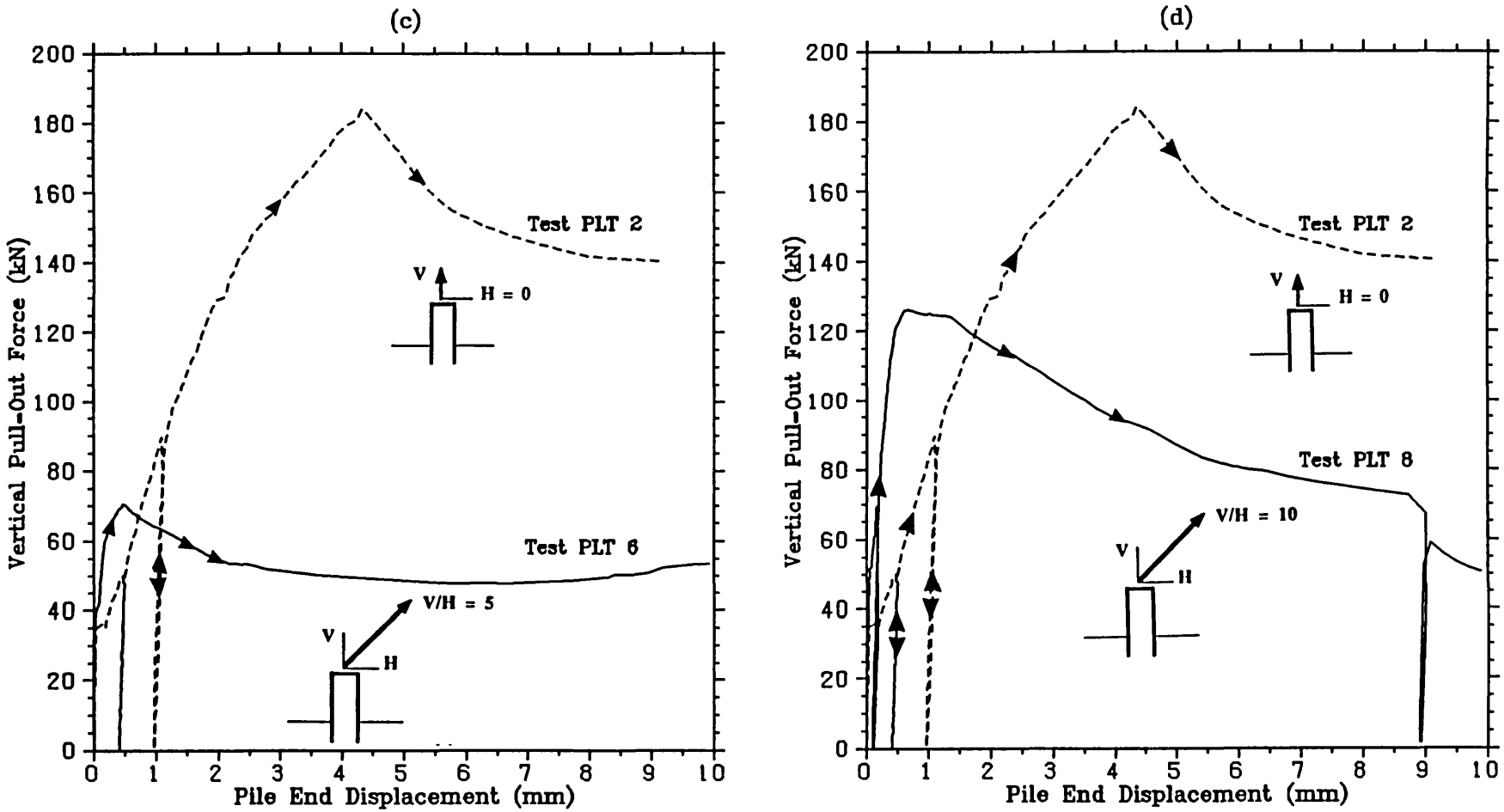


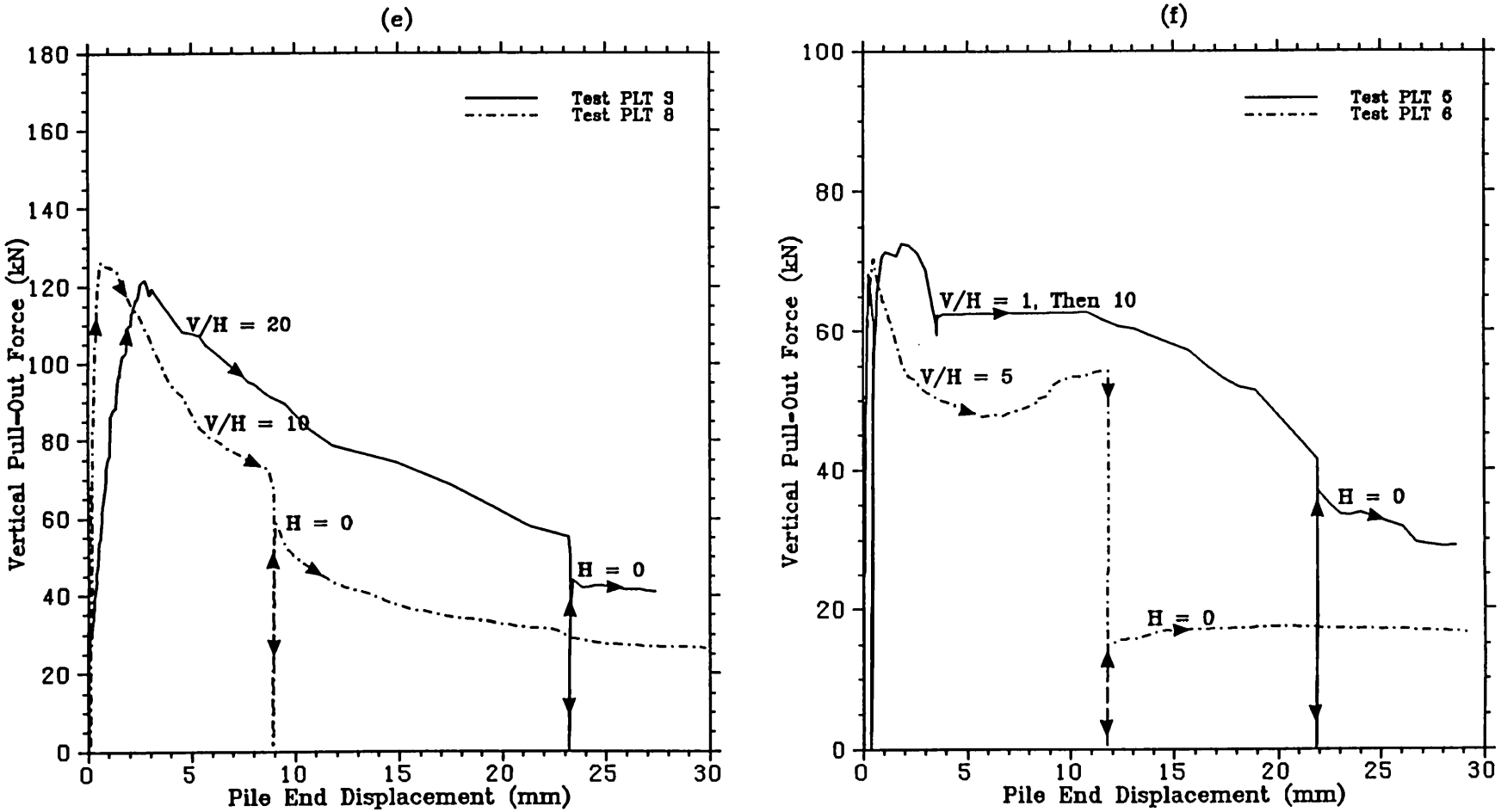
Figure 6.9b : TESTED PILES UNDER VERTICAL PULL-OUT LOAD



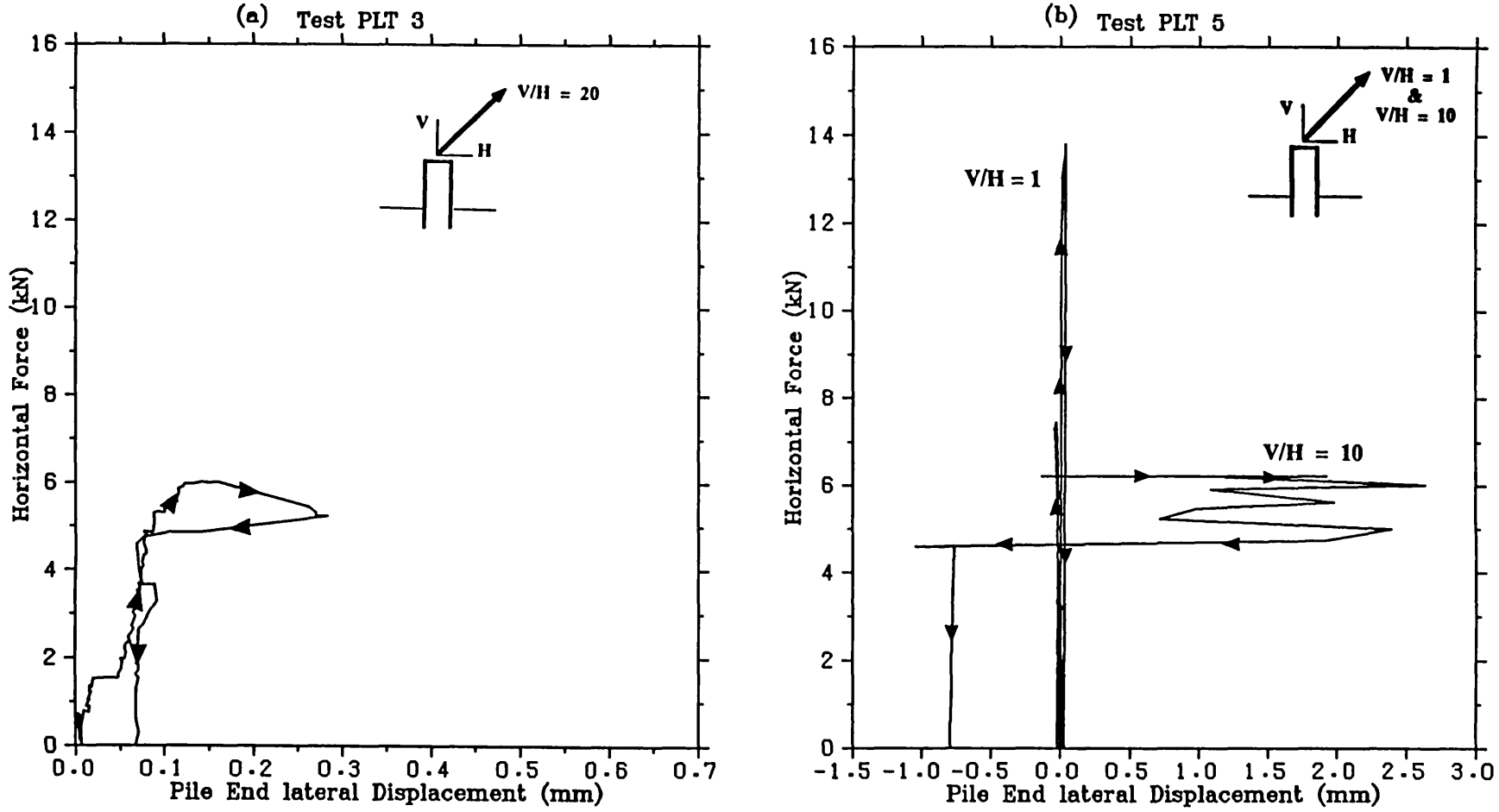
Figures 6.10a & b : GROUTED PILE VERTICAL BEHAVIOUR UNDER COMBINED PROPORTIONAL LOADS



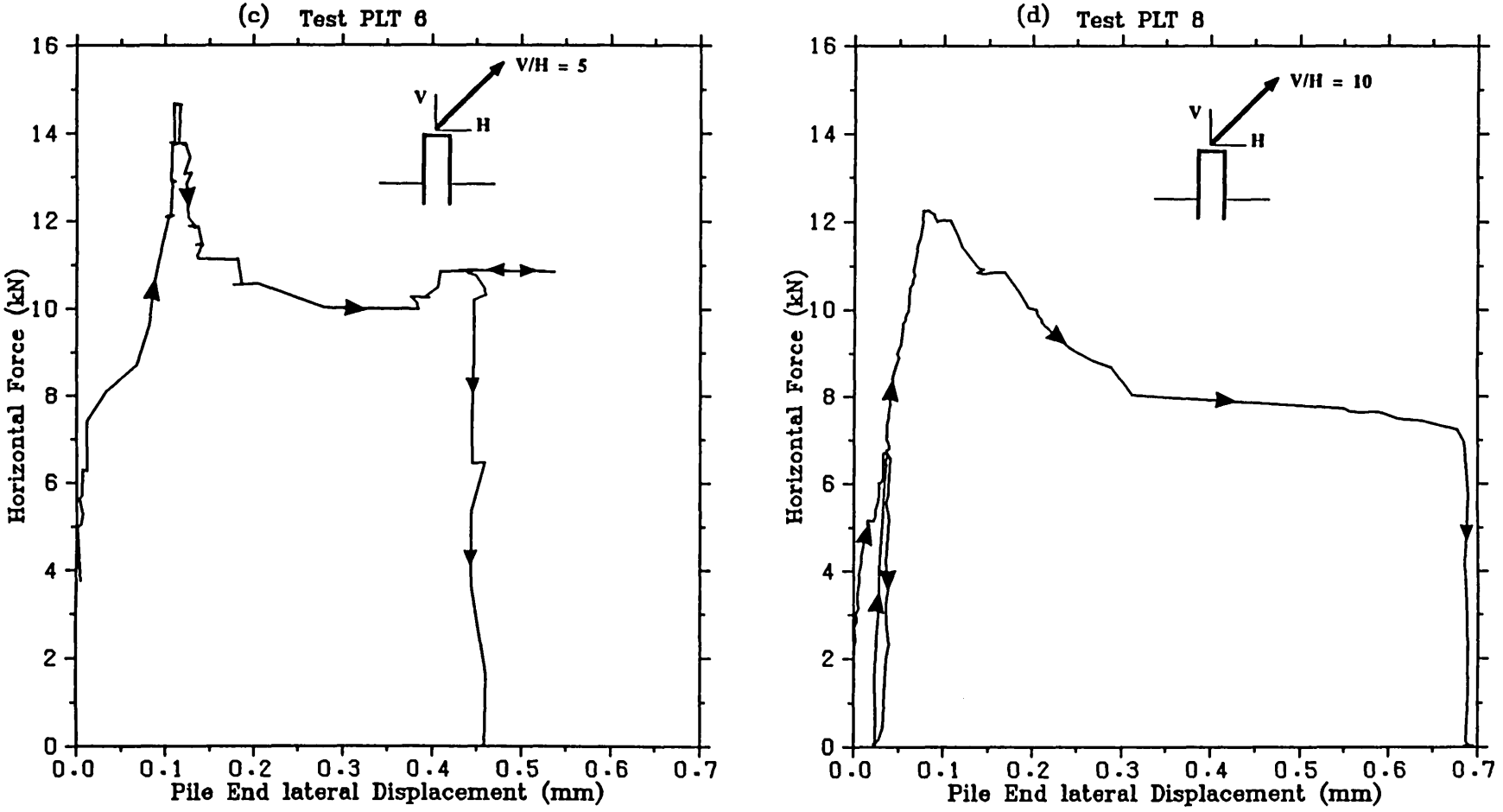
Figures 6.10c & d : GROUTED PILE VERTICAL BEHAVIOUR UNDER COMBINED PROPORTIONAL LOADS



Figures 6.10e & f : GROUTED PILE VERTICAL BEHAVIOUR UNDER COMBINED PROPORTIONAL LOADS



Figures 6.11a & b : GROUTED PILE HORIZONTAL BEHAVIOUR UNDER COMBINED PROPORTIONAL LOADS



Figures 6.11c & d : GROUTED PILE HORIZONTAL BEHAVIOUR UNDER COMBINED PROPORTIONAL LOADS

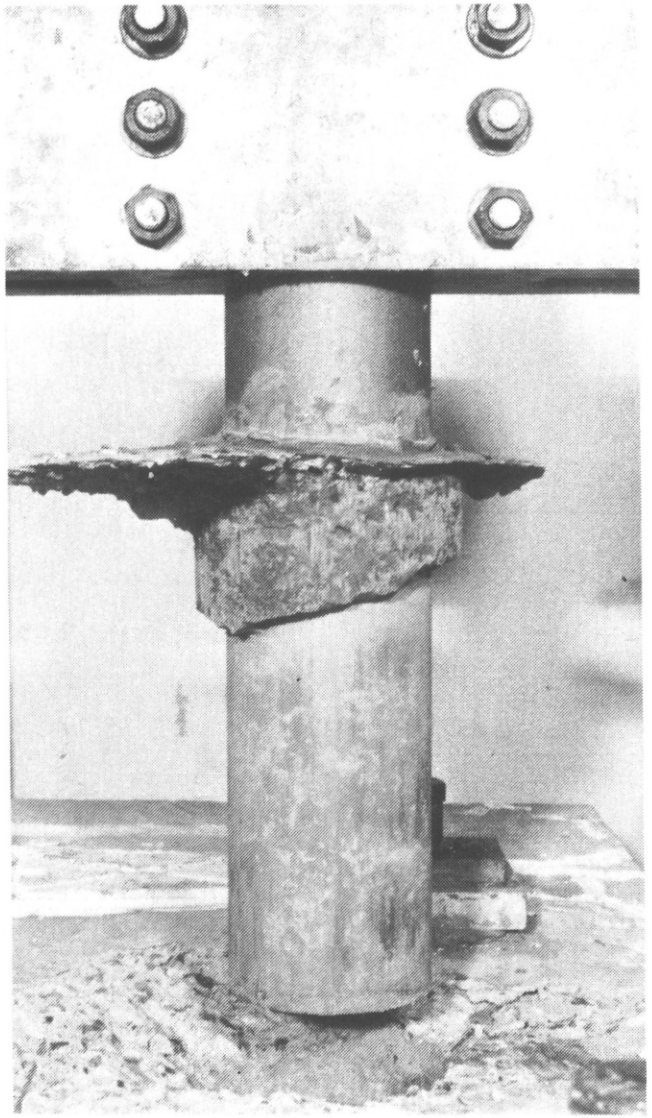


Figure 6.12a : EXTRACTED PILE SPECIMEN OF TEST PLT 7

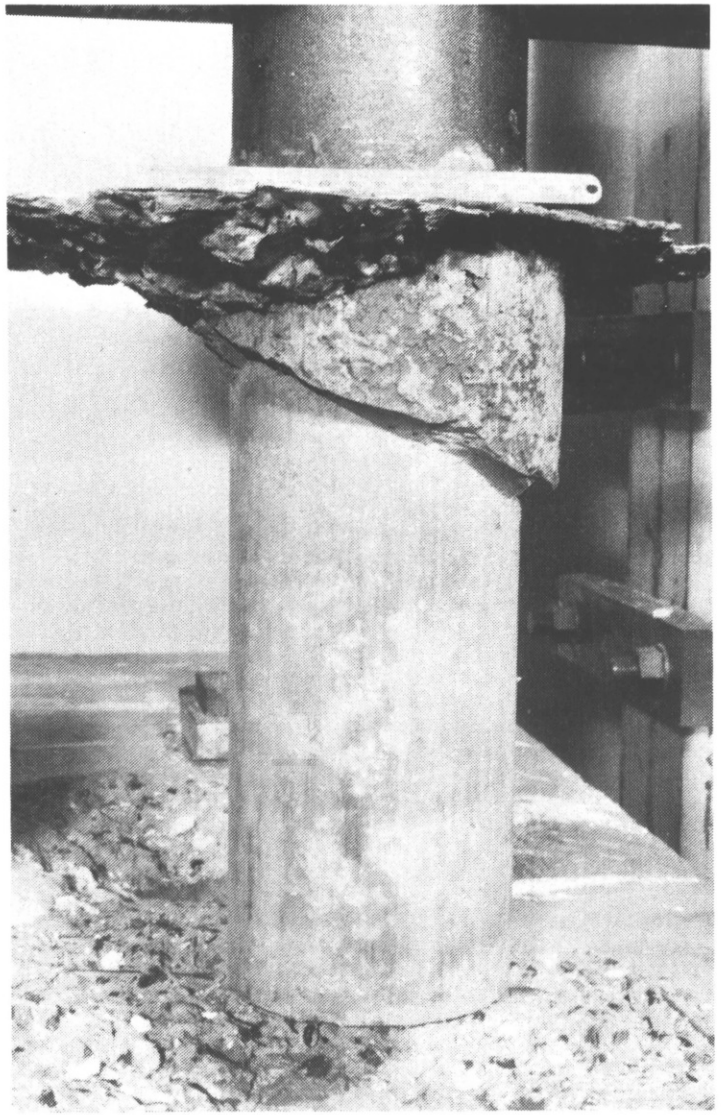


Figure 6.12b : EXTRACTED PILE SPECIMEN OF TEST PLT 8

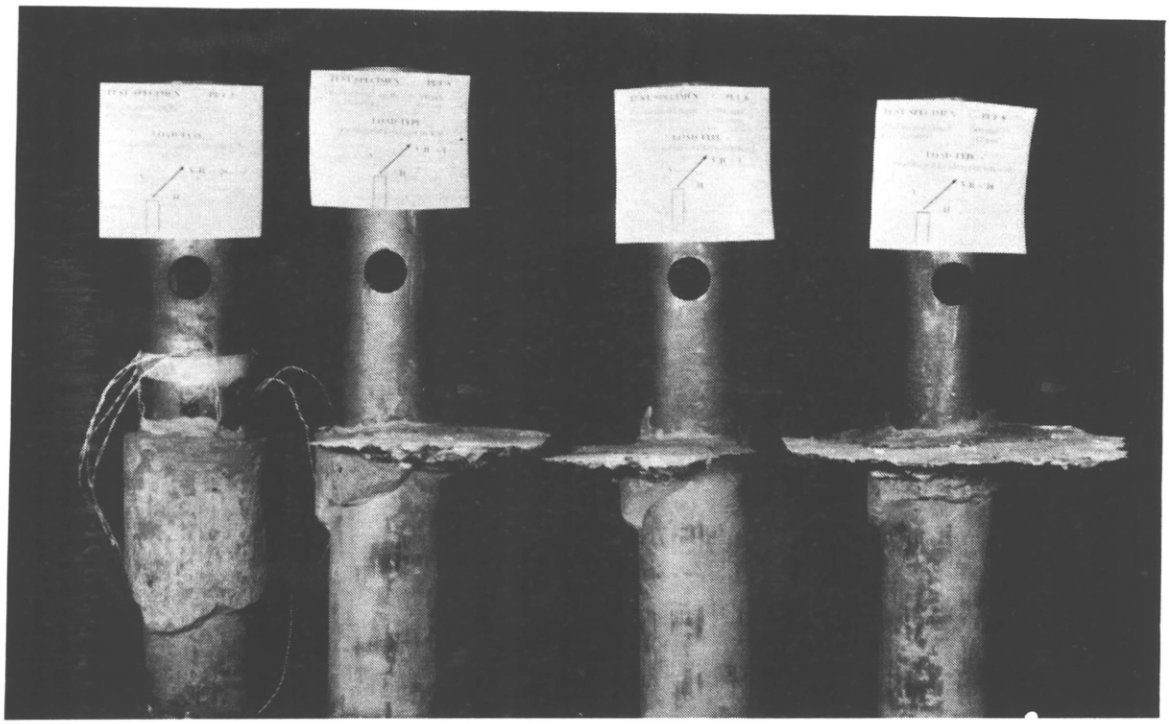


Figure 6.12c : TESTED PILES UNDER COMBINED LOADS

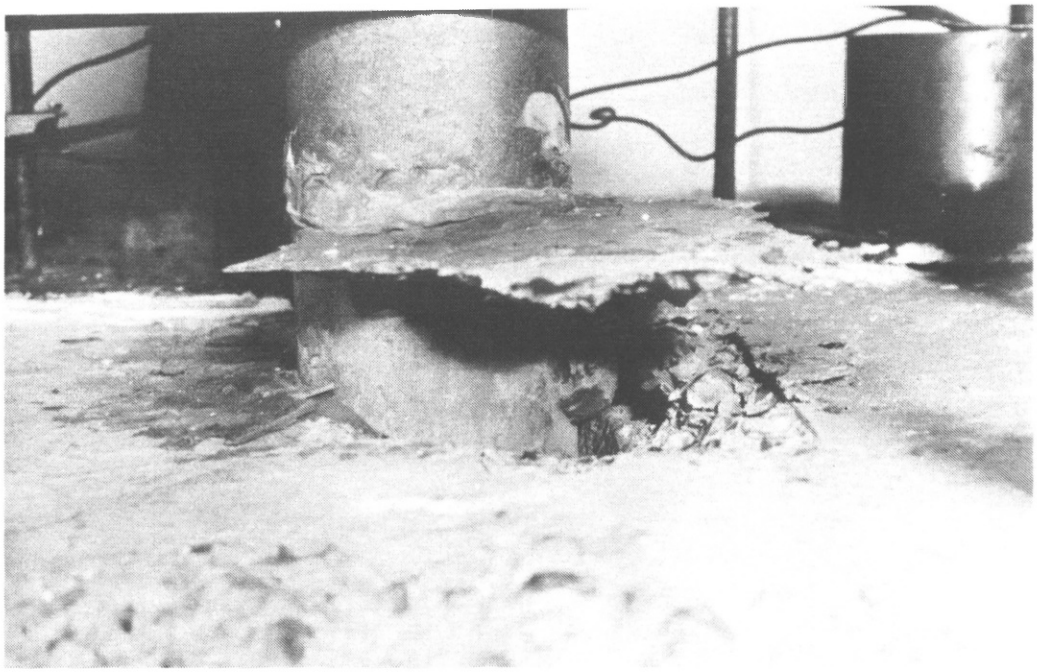


Figure 6.12d : FAILURE VIEW OF THE PILE SPECIMEN OF TEST PLT 5
(where V/H = 1)

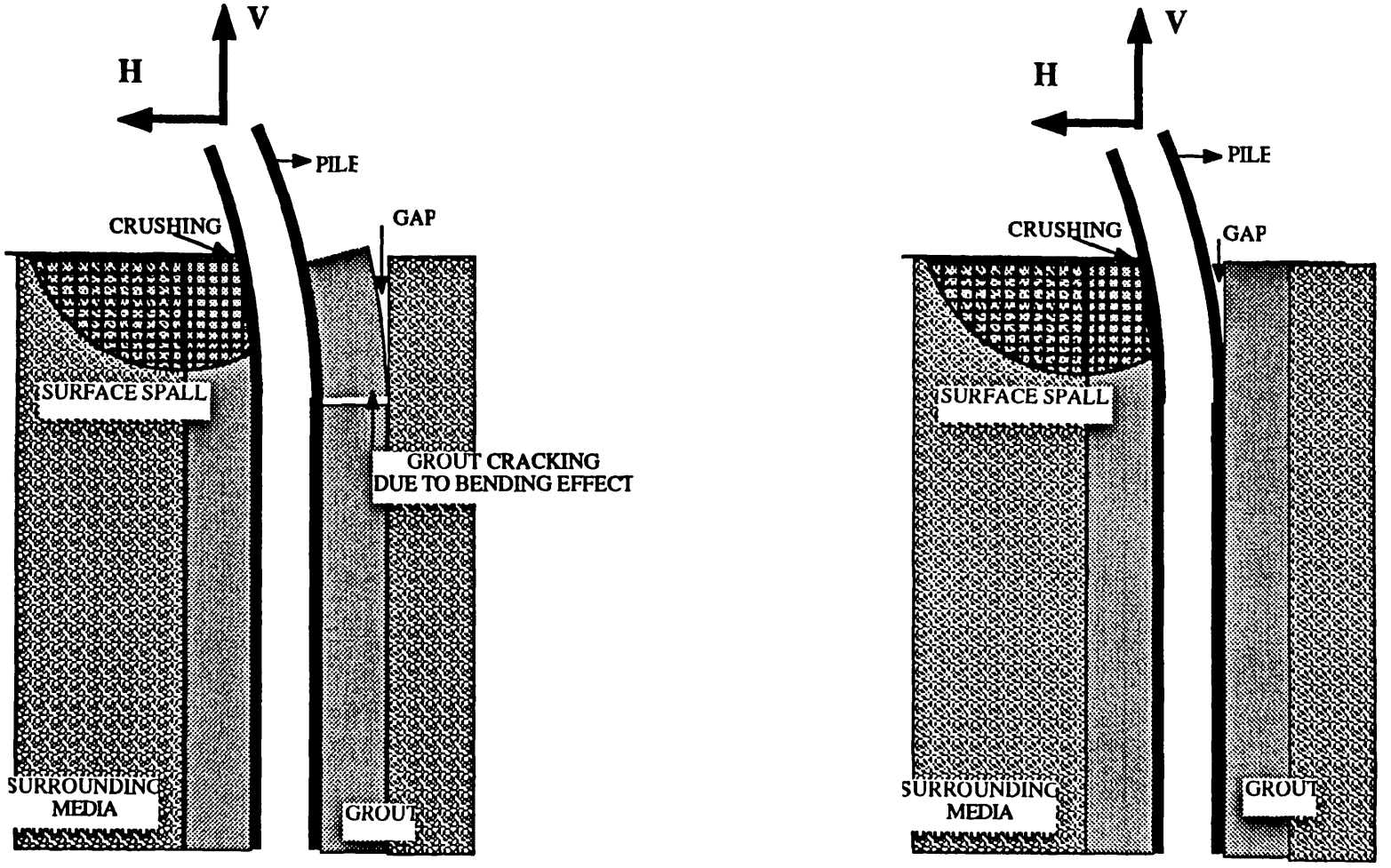


Figure 6.12e: **FAILURE MODE OF GROUTED PILE SUBMITTED TO HORIZONTAL AND VERTICAL LOADS**

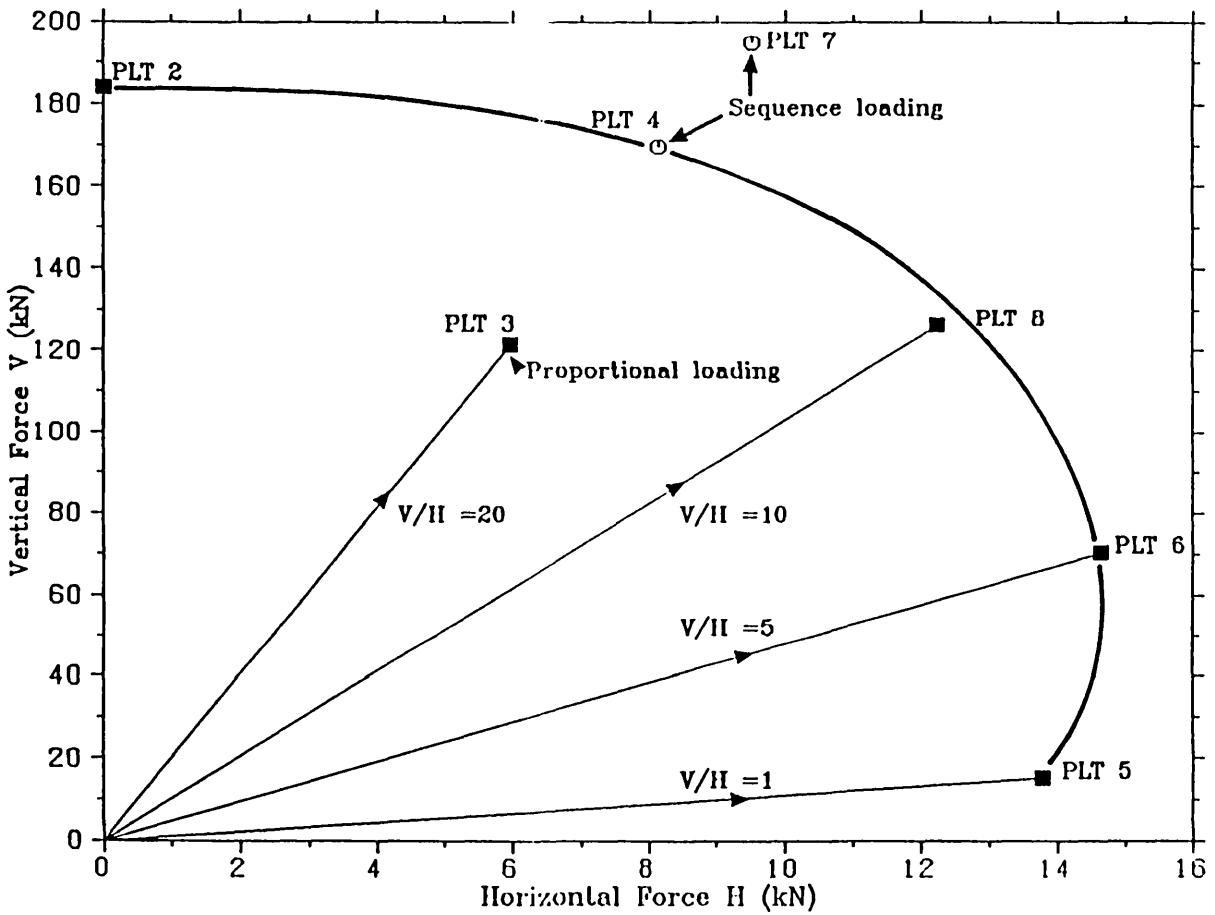


Figure 6.13 LATERAL – VERTICAL FORCES INTERACTION DIAGRAM FOR GROUTED PILE UNDER COMBINED PROPORTIONAL LOADS

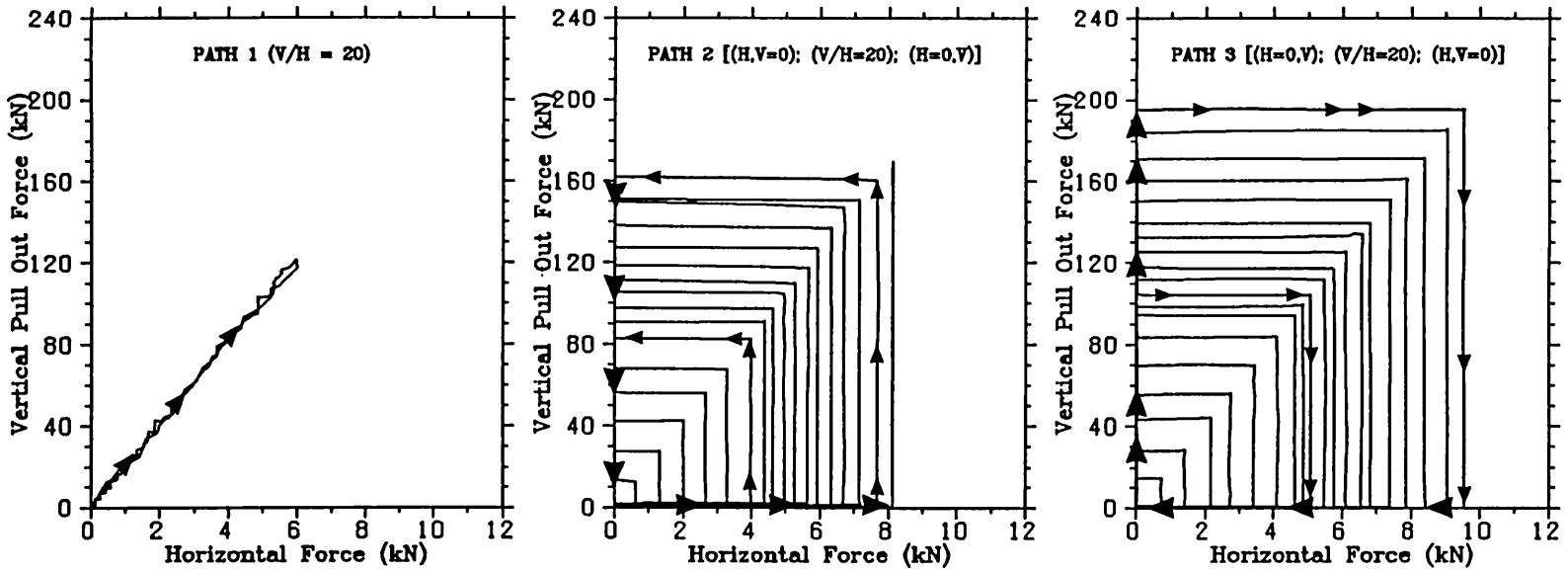


Figure 6.14a : APPLIED LOADS SEQUENCES FOR PATH DEPENDENCY TESTS

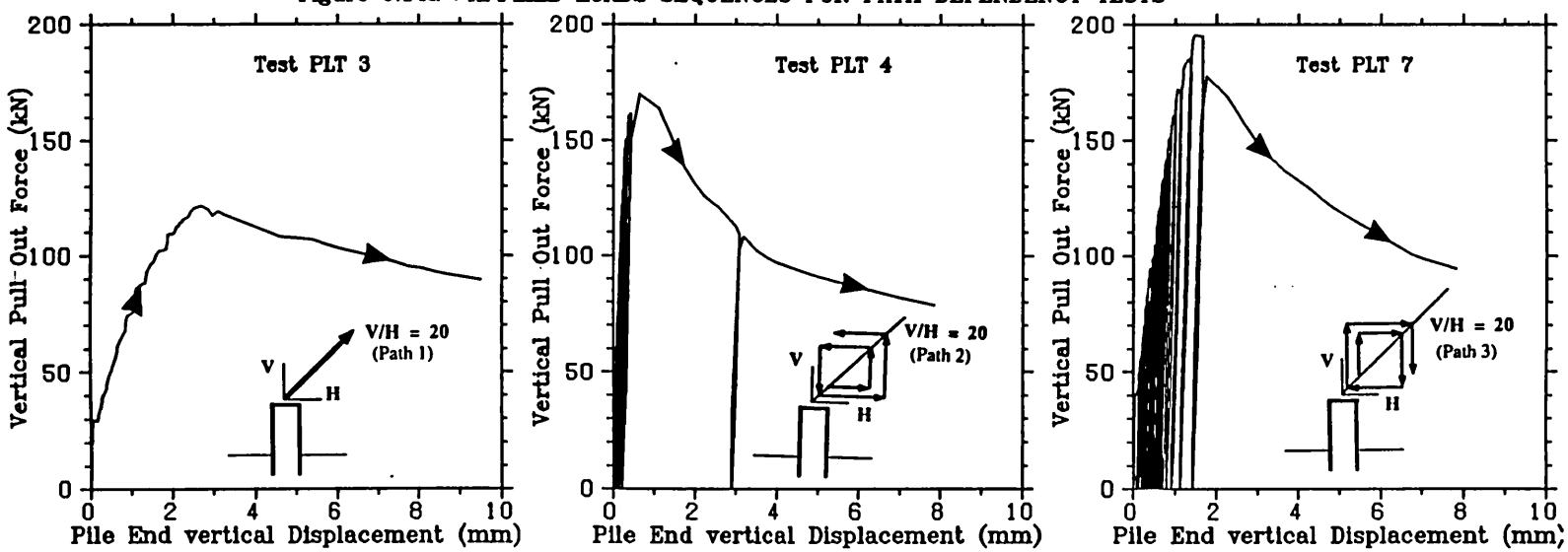


Figure 6.14b : GROUTED PILE BEHAVIOUR FOR DIFFERENT COMBINED LOADS PATHS

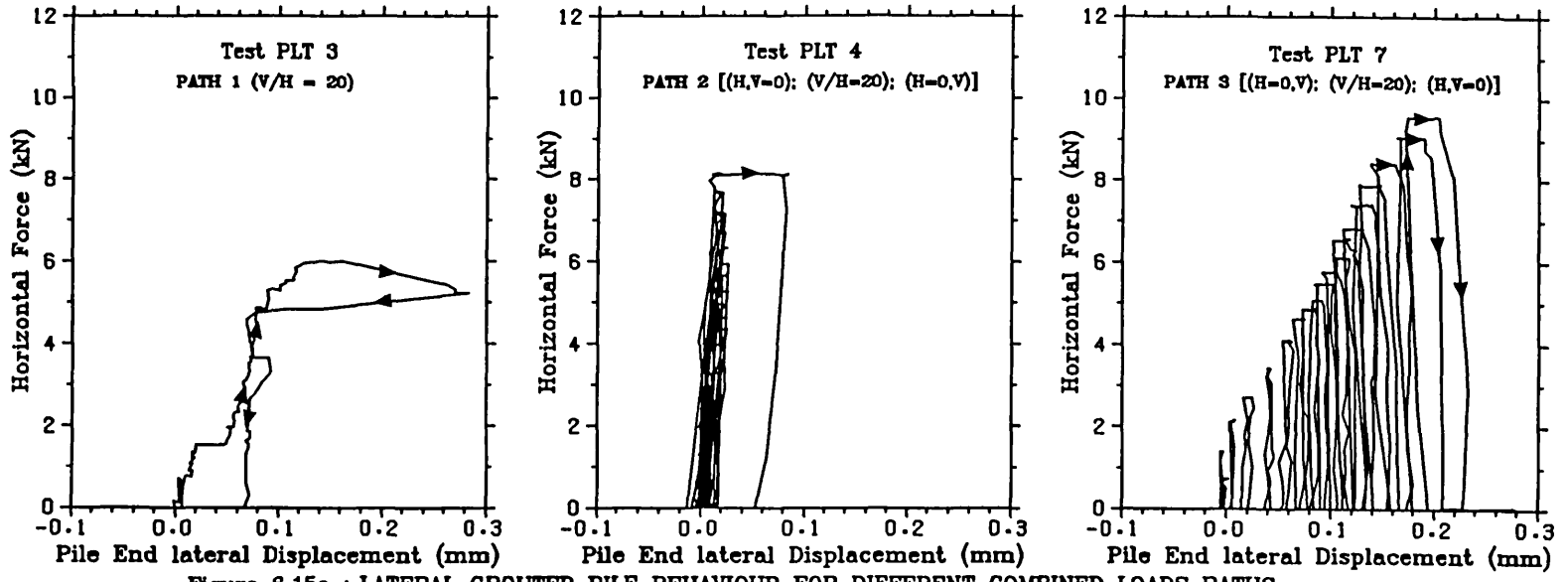


Figure 6.15a : LATERAL GROUTED PILE BEHAVIOUR FOR DIFFERENT COMBINED LOADS PATHS

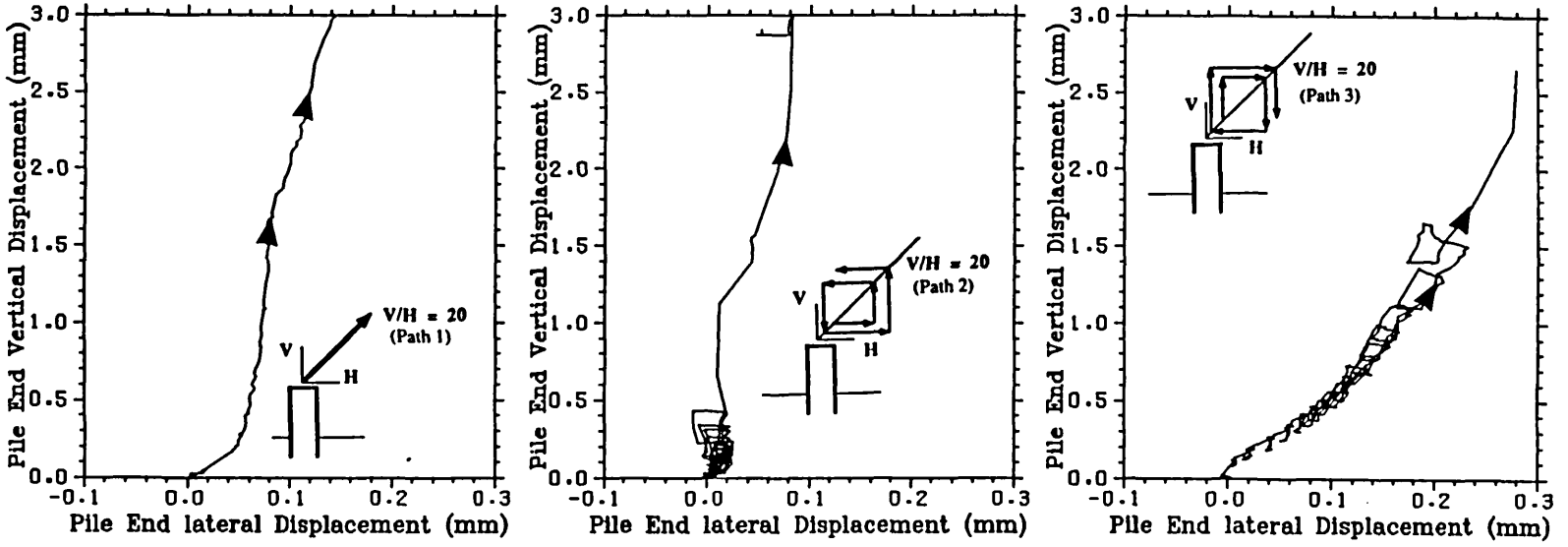
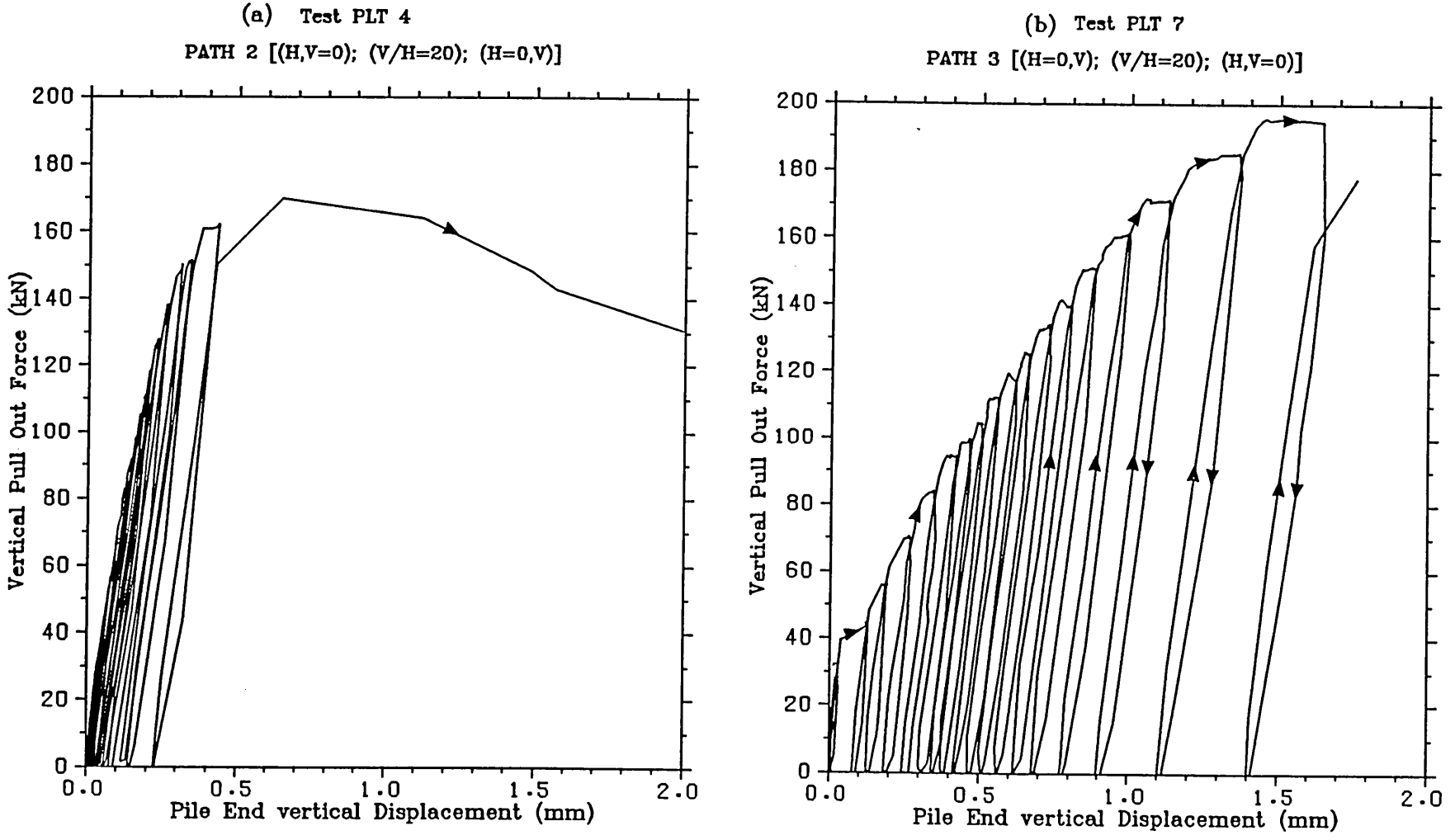


Figure 6.15b : PILE END DISPLACEMENT FOR DIFFERENT COMBINED LOADS PATHS



Figures 6.16a & b : LOADS CYCLING EFFECT ON GROUTED PILE BEHAVIOUR

CHAPTER 7 : DESIGN OF NEW TORSION TEST

7.1 INTRODUCTION

The experimental work reported here is concerned with the establishment of a new test to determine bond behaviour at a steel/grout interface. This chapter provides a detailed description of the test. The aims of the test are discussed as well as the design of the equipment, instrumentation, operational procedures, and the transformation of the output data to the desired form.

The mechanisms of pile/grout bond are not well understood. There are also no standard tests to measure the local bond strength. There have been attempts to determine such values, but these were restricted to reinforced concrete; such tests were carried out mainly on steel bars embedded in concrete, and the application of these test results to general cases is not necessarily acceptable, particularly bearing in mind the large differences in geometry.

In this part of the research programme, a new torsion test method has been developed to assess the bond between the steel pile surface and a cementitious grout. The method has been shown to work satisfactorily. The main objectives of the test are :

1- to provide values of the shear strength of the bond between a steel pile and cementitious grout.

2- to determine the behaviour of the interface zone for both small and large slippage.

3- to examine interaction between the pile and its surrounding medium during bond breakdown and large relative displacement.

Before describing the new test, a brief review of the test methods used to investigate bond for reinforced concrete structures and geotechnical applications will be introduced.

7.2 REVIEW OF BOND TEST METHODS

The conventional bond test (figure 7.1a) consists of embedding a steel bar in a concrete cube. Then, the steel bar is pulled out; the extracting force determines the degree of the bond between the steel bar and the reinforced concrete.

Tassios and Koroneos (1979) used a rectangular concrete specimen in which a steel plate was sandwiched (figure 7.1b). The strains as well as the local slip were measured by means of the Moire method. Lateral pressure was applied on the concrete (and so to the interface) to avoid premature separation of the concrete from the steel bar. The principal advantage of this method is that the interface is visible and can be examined directly. Their results provided a local slip - shear stress relationship particularly for small local slip values (<50 micro-strains). This relationship is shown in figure 7.2a. Tassios and Koroneos (1979) were also able to describe experimentally the shear stress distribution along the steel embedded length. Such stress variation is presented in figure 7.2b. However, the interface is submitted to a constant normal stress, providing a stress condition not reflecting either the stress distribution in a concrete structure or the interaction between the steel bar and the concrete media before and after bond failure.

Jiang et al (1982) developed another method, shown in figure 7.1c. Steel strain variations were recorded using strain gauges glued to the steel bar. The results show very important variations of the stresses and strains in the steel along the embedded length. The end slip was measured but there was no way of measuring local slip so that it was not possible to obtain a true local shear stress/slip relationship.

Stroeven and De Wind (1982) investigated the influence of steel roughness on the bond strength and behaviour. The specimen used was similar to the one used in the conventional test, with a major reduction of the bar embedded length (figure 7.1d). Two types of bond behaviour were observed for different steel bars roughness :

1- a smooth steel bar generates a brittle breakdown without any pre-failure slip. The bond strength hardly varies with the steel roughness.
2- a rough surface condition provides much stronger bond. Before the loss of the strength, slip was observed between the bar and the surrounding concrete.

Figures 7.2c present some of Stroeven and De Wind's test results.

The conventional test configuration was also used by Robins and Standish (1982) in order to investigate the effect of the lateral stress on the bond strength. Other works have been carried out on ribbed bars using the same procedure. More literature on this can be found in Bartos (1982).

Recently, a number of workers concerned with interfacial problems involving steel or concrete piles in granular soils, have also adopted a form of torsion test in order to obtain shear bond/slip relationships. Figure 7.1e shows the arrangement used by Chen et al (1987). The test has a number of advantages. Provided the steel cylinders are sufficiently stiff, each part of the interface is subject to the same amount of slip. Also, the contact area remains the same even at high values of relative displacement.

Chen's test focused on the interface between concrete and sand under uniform shear stress. The test arrangement (figure 7.1e) permitted a visual display of the field of deformation in the sand due to slippage between the inner cylinder and the surrounding sand. Krizek and Vipulanandan (1985) also used the torsion test concept to determine the adhesive strength of chemical grout to quartz rock (simulating sand) under conditions of pure shear stress.

A brief recapitulation of the tests results from different investigations on bond strength is presented in figure 7.2d. The results emphasize the variation of the bond strength due to the following parameters :

1- steel surface roughness.
2- curing time.
3- grout composition.
4- grout compressive strength.
5- stiffness of the surrounding media.

The variation of these results, under the different testing conditions emphasizes the importance of these parameters. For instance, the results of Stroeven and De Wind (figures 7.2c) provide a clear idea of the importance of the steel roughness parameter, which affects both the interfacial strength and behaviour. However, the disaccord between the tests results could also be related to the tests methods adopted by each investigator.

7.3 TORSION TEST DESIGN

The torsion test was developed in order to investigate the local behaviour of the bond between the pile surface and cementitious grout under shear. The torsional loading was considered to be the most suitable method to generate such a loading condition, having the advantages discussed above (section 7.1).

The same diameter specimen was used as for the pull-out tests so that the

results could be applied directly without any concern for the size effects.

The test arrangement is shown in figure 7.3a. The grouted steel pile is made up of a number of separate short stiff ring elements. Each element can be rotated independently using a special key and actuators. Shear bond stress/slip relationships could then be found for each ring from measurements of the torque and rotation.

The test equipments consist of :

1- a series of stiff pile elements with internal key ways as shown in figure 7.3b.

2- a key for inserting into the elements to enable them to be twisted, and its associated cross head (figure 7.6a)

3- actuators and tie bars to transmit forces from the test frame to the cross head attached to the pile element.

7.3.1 PILE ELEMENT

Using a standard steel (grade TI 52) pile, elements of 90 mm length were prepared. The outside diameter of the pile is 112 mm, and the inner diameter is 90 mm (wall thickness 11mm). In the inner side of the pile element, three slots at 120° to each other were cut along the pile length. The depth of the slot is 5.5 mm (half of the pile wall thickness). Figure 7.3b shows a cross section of the pile element grouted inside the concrete pocket.

The use of a deep concrete block gave the opportunity for multiple independent tests within the same pocket. Several pile elements are aligned and grouted in one pocket. During the testing operation, the top pile element is twisted first, then extracted from the pocket so allowing testing of the second pile element. Later, the second element itself is extracted, and so the test can be carried out on the third pile element.

To avoid shear stress transfer from the tested element to its neighbour, a debonded zone is provided by using either bees wax or polythene sheet for a height of 30mm on the boundaries of two adjacent elements. This left a bonded length in the middle of the pile elements of 60 mm. During the preliminary tests, three pile elements were used (figure 7.4a). Later, four pile elements were used during the final test series (figure 7.4b). The number of the pile elements that can be used depends on the depth of the concrete pocket as well as the length of the twisting key.

7.3.2 TWISTING TOOL

To generate the shear stresses at the pile surface/grout interface, a twisting key is inserted with a sliding fit inside the pile element (figure 7.5). Consequently the twisting is locked within the pile element by lowering the tool inside the pile ring.

At the top, outside the pile, the cross head (figure 7.6c) is placed on the key to enable a torque to be generated by means of forces applied by two separate actuators. The key itself is formed by welding two solid steel ends to a cylindrical tube of the required length. The bottom solid part is designed to fit the pile element and contains three outstanding splines (figure 7.6a).

In order to measure rotation of the ring, three stiff steel bars are fixed to the lower solid section of the key. These bars extend upward to the level of the cross head so that they project outside the pile and can be used to measure the rotation using external displacement transducers. More details of this are given in section 7.4.2.

The connection between the key and the cross head is obtained through six pins uniformly distributed in the top solid part. Detailed pictures of the cross head are given in figures 7.6b and, 7.6c.

During the test, the key is supported by a steel bar from a cross beam at the top of the test frame

7.3.3 LOAD APPLICATION

Two actuators were placed on the lateral cross beams of the frame built around the concrete block, which forms the test bed (figure 7.12). The actuators were operated simultaneously in order to provide two equal tension forces, to provide a torque on the cross head.

During the preliminary tests, hydraulic jacks were used. Due to the sudden post-peak drop in shear stress with continued slip, the test could not be fully controlled. The major point of concern, in using the hydraulic equipment, was the difficulty of observing the amount of slip in the initial stage of the loading, where the behaviour was momentarily unstable. This can be an important region in assessing the behaviour of stiff

piles. However, the loading system was not rigid enough to permit a stable progressive failure of the bond. The breakdown was brittle, showing a snap rotation of the pile element, allowing only the observation of the frictional residual resistance of the pile/grout interface. In effect, the use of hydraulic jacks and small tie bars gave a system which was not sufficiently stiff to provide a stable and controlled fond failure. A note on the test stability will be given in appendix 2.

The objective of the test is to obtain the behaviour of the interface resistance in the post failure stage, as well as up to the maximum stress. For this reason the hydraulic actuators were replaced by screw jacks. The thickness of the tie rods was also increased. Thus, the cross head rotation is controlled rather than the torque. The rotation can be maintained at any time to a given slip, regardless of the resisting force. The movement of the head, and so the slip at the interface, can be maintained during the data logging.

Each of the jacks is connected to an electric motor. The speed of the motors, and so the rate of the slip, can be varied; the motors can be run either separately or in a synchronized manner.

7.3.4 SPECIMEN PREPARATION

After the pile elements had been sand blasted, a tube of 20 mm diameter was used to assemble the desired number of elements in one column unit. The elements have to be aligned and stressed together to be maintained in place during grouting. It was convenient to use the grout tube itself to stress the elements and hold them in position (figure 7.7a). The top cover plate and the grouting tube were later removed, allowing the key to be inserted and locked inside the pile element. The alignment of the pile element is of great importance, since it permits the easy extraction of the element once it is tested. As shown in figure 7.7b, extraction of a non-aligned pile element requires a considerable pull-out force, and may cause damage or over-break to the grout in the upper part of the concrete pocket and possibly the concrete block itself.

Once the pile rings are assembled, the debonded zone is prepared for each element, and the unit is placed inside the concrete pocket. Grouting of the space between the pile elements and the concrete block then follows as shown in figure 7.7c. Using this technique, the grout moves in an upward direction, as in practice.

7.3.5 CONCRETE POCKET

The lateral dilation of the grout is affected by the radial stiffness of the surrounding medium. If confined, dilation induces radial stresses in the grout along the steel/grout interface, in addition to the shearing stress component. The resulting stress state is a combination of compressive shear stress and normal stress on the interface region.

To investigate these effects, four strain gauges have been placed in the circumferential direction on the pocket wall at each level of the pile elements (figure 7.7d). The gauge outputs represent the local hoop strains in the concrete at the surface of the pocket. Since the pocket was narrow and deep, the direct installation of the gauges on the concrete wall was not possible. For this reason, the gauges were glued on a steel shim of 0.06 mm thickness (10 mm x 50 mm), which was placed on the surface of the concrete pocket. The purpose of placing such strain gauges was not to measure the exact amount of dilation, but to find out the existence of such phenomenon; and how it interacts with the development of grout deformation and excessive slip between the pile ring and the grout.

7.3.6 TWISTING TOOL INSTALLATION

After the tool has been locked inside the grouted pile, the two rods are inserted in the slots through the cross head. Two roller bearings are threaded on the ties to connect them to the cross head as shown in figure 7.8. These bearings can slide along the cross head sides. As shown in the figure, the bearings are constrained, so that the tie rods are equidistant from the axis of rotation. Thus, the lever arm of the applied forces remains constant while the head is rotating. The bearings are at all times placed symmetrically to the axis of rotation so that only a pure torque is generated. To do this, the two bearings are fixed to each other by a steel plate placed on the head and pivoted on the axis of rotation. These details are shown in figure 7.6c, together with the key and the head of the twisting tool.

To prevent any lateral movement of the key, and so bending in the pile, a ring is placed around the top solid part of the key. Four steel bars of 16 mm diameter are attached to the ring and fixed to a supporting frame. By doing this, the key is fixed to a position where it can only rotate, and any lateral movement -in a horizontal direction- due to eccentric forces will by prevented. Any eccentric forces will be carried to the frame

through the four steel bars. This arrangement is shown in figures 7.9 and 7.10.

7.3.7 TEST PROCEDURE

Once the pile element has rotated, and the bond has failed, a sequence of loading and unloading is undertaken with increasing values of slip. The frictional behaviour is then obtained under large pile element rotation and pile/grout slippage (pile element rotation of 60°). At the end of this sequence, the pile element is rotated in a reverse direction to its original position by changing the direction of the forces acting on the cross head. More details will be presented for each case in the next chapter dealing with the test results.

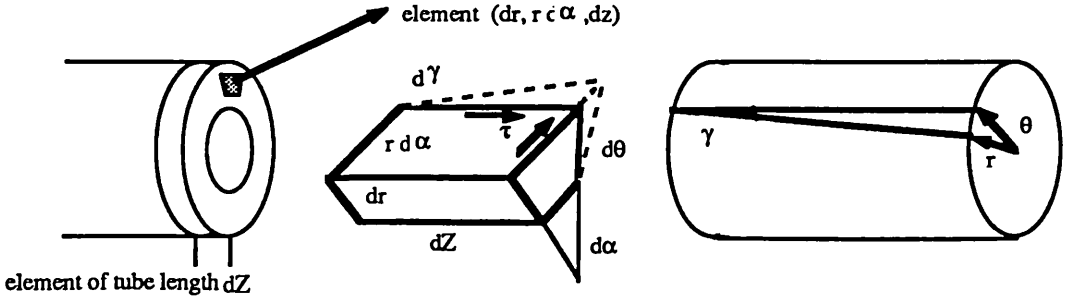
The extraction of the pile follows using the twisting key. Three pins are placed on the slot-fitting side of the key, backed up by spring (figure 7.6c). These are locked in between two adjacent elements into a groove, allowing the extraction of the pile element by pulling out the locked key.

7.4 INSTRUMENTATION AND FORM OF THE OUTPUT

7.4.1 TWISTING KEY

Strain gauges were mounted on the cylindrical tube of the twisting key in order to obtain a direct measurement of the torque, independent of the variation in the lever arm at the cross head.

Six rosette gauges were used on the cylinder with each gauge giving reading of strains in three directions. The following analysis outlines how the strain measurements were used to determine the applied torque.



Consider the deformation shown in the above figure, the condition for

compatibility :

$$d\gamma\, dZ = d\theta\, dr$$
$$d\gamma = dr\,(d\theta/dZ) \qquad (7.1)$$

Since the tube is under pure torsion, $d\theta/dZ$ remains constant. Integration of (7.1) leads to

$$\gamma = r\,(d\theta/dZ) = r\,\theta_u \qquad (7.2)$$

where θ_u is the tube rotation per unit length. Assuming that the steel behaves elastically with G_{steel} as shear modulus,

$$\tau_{steel} = G_{steel}\,\gamma$$
$$\tau_{steel} = G_{steel}\,\theta_u \cdot r \qquad (7.3)$$

From equation 7.3, one can deduce that the shear stress is linearly distributed along the radius of the tube. The equilibrium equation of the tube submitted to a torque T can be written ,

$$T = \int_A \tau\, r\, dA$$ where A is the tube cross section

Performing the integration of this equation, and using equations (7.3),and (7.4), it follows that

$$T = G_{steel}\,\theta_u\,\frac{\pi}{2}\,(R_{out}^4 - R_{in}^4) \qquad (7.5)$$

where R_{out}, and R_{in} are the outer and the inner radii of the twisted tube.

Equation (7.2) can be written as :

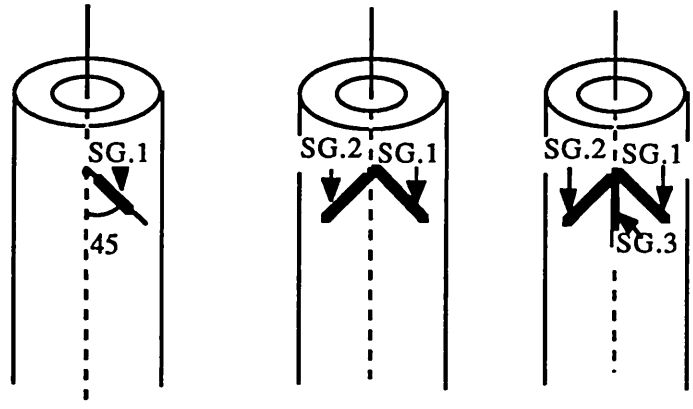
$$\theta_u = \frac{\gamma}{r} = \frac{\gamma_{out}}{R_{out}}$$

where γ_{out} is the shear deformation along the outer surface of the key tube. The torque can then be expressed as:

$$T = G_{steel}\,\gamma_{out}\,\frac{\pi}{2}\left(\frac{R_{out}^4 - R_{in}^4}{R_{out}}\right)$$

where $G_{steel}\,\gamma = \tau_{max}$ the maximum shear stress applied on the outer radius of the tube, thus,

$$T = \frac{\pi}{2}\left(\frac{R_{out}^4 - R_{in}^4}{R_{out}}\right)\tau_{max} \qquad (7.6)$$



case 1 case 2 case 3

SG = Strain Gauge

Since a pure torsion is applied to the tube, a state of pure shear stress will be developed within the tube. Ideally, one resistance strain gauge - placed at 45° to the main axis of the cylinder- would be enough to obtain the maximum shear deformation (case 1). For practical reasons, this would not be possible, since it is difficult to set up the gauge in the right direction. Even a system of two gauges (case 2) can not be relied upon to obtain the exact shear stress at the tube surface. To avoid any doubt due to the gauges installation a three element rosette gauge is used.

7.4.1 1 Analysis of the Strain Gauges Outputs

On the twisting key, six rosettes strain gauges were used. Three rosettes were uniformly distributed around the key cylindrical tube at 120° to each other at two different levels on the key. The gauges were placed so that the middle element were nearly vertical. (case 3). From the output of these strain gauges the principal state of strains can be obtained from equations 7.7

$$\varepsilon_{11} = \frac{1}{2}\left[(\varepsilon_1 + \varepsilon_2) + \sqrt{(\varepsilon_1 - \varepsilon_2)^2 + (2\varepsilon_3 - \varepsilon_1 - \varepsilon_2)^2}\right] \qquad (7.7a)$$

and

$$\varepsilon_{22} = \frac{1}{2}\left[(\varepsilon_1 + \varepsilon_2) - \sqrt{(\varepsilon_1 - \varepsilon_2)^2 + (2\varepsilon_3 - \varepsilon_1 - \varepsilon_2)^2}\right] \qquad (7.7b)$$

where ε_1, ε_2, and ε_3 are the strain readings given by gauges 1, 2, and 3 respectively.

The principal stresses can be computed from the principle strain :

$$\sigma_{11} = \frac{E}{1-\nu^2} (\varepsilon_{11} + \nu \varepsilon_{22})$$

$$\sigma_{22} = \frac{E}{1-\nu^2} (\varepsilon_{22} + \nu \varepsilon_{11})$$

so that the shear stress can then be found from

$$\tau = \frac{\sigma_{11} - \sigma_{22}}{2}$$

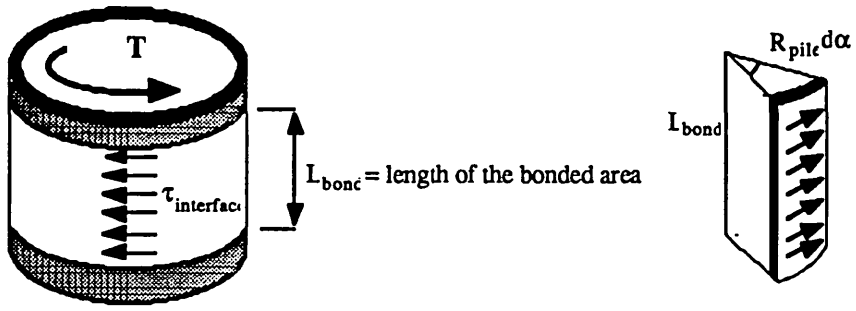
The torque then follows from equation 7.6 i.e.

$$T = \frac{\pi E (R_{out}^4 - R_{in}^4)}{4 (1+\nu) R_{out}} \cdot \sqrt{(\varepsilon_1 - \varepsilon_2)^2 + (2\varepsilon_3 - \varepsilon_1 - \varepsilon_2)^2} \qquad (7.8)$$

From each rosette gauge, a torque value can be computed. The average value from the six rosettes is used.

7.4.1.2 Interface Shear Stress.

When the pile element is forced to rotate, it is assumed that a uniform shear stress will be induced at its surface due to the bond and friction resistance.



The equilibrium condition can be written as :

$$T = L_{bond} \int_0^{2\pi} (\tau_{interface} \cdot R_{pile} \cdot d\alpha) R_{pile} = 2\pi R_{pile}^2 L_{bond} \tau_{interface} \qquad (7.9)$$

so that using equation 7.8 the interface shear stress :

$$\tau_{interface} = \frac{1}{8} \cdot \frac{1}{R_{pile}^2 \cdot L_{bond}} \cdot \frac{E_{steel}(R_{out}^4 - R_{in}^4)}{(1+\nu) \cdot R_{out}} \cdot \sqrt{(\varepsilon_1 - \varepsilon_2)^2 + (2\varepsilon_3 - \varepsilon_1 - \varepsilon_2)^2}$$

now defining

$$K = \frac{1}{8} \cdot \frac{1}{R_{pile}^2 \cdot L_{bond}} \cdot \frac{E_{steel}(R_{out}^4 - R_{in}^4)}{(1+\nu) \cdot R_{out}}$$

$$\tau_{interface} = K \sqrt{(\varepsilon_1 - \varepsilon_2)^2 + (2\varepsilon_3 - \varepsilon_1 - \varepsilon_2)^2} \qquad (7.10)$$

For the test as undertaken, K is equal to 3.086 10^{-3} N/mm^2/με

7.4.2 SLIP MEASUREMENT

As soon as load is applied, the pile element will undergo a rotational movement generating circumferential deformation of the surrounding grout at low loading and a frictional slip once the bond at the pile grout interface has broken down. The interfacial slip between the ring pile element and the grout is defined by the circumferential movement of one point at the ring surface from its original position. Since the pile is placed inside the concrete pocket, it is not practical to fit displacement measuring devices in direct contact with the pile. However, assuming that the pile element and the lower solid part of the tool, which are locked together, form a rigid body, the slip occurring at the interface will be the same as the rotation at the bottom of twisting key. The ring pile elements are assumed to be rigid (the stiffness of the steel is at least 15 times higher than that of the grout). Consequently three bars are fixed on the solid base of the key and brought out from the concrete pocket to enable the base rotation to be measured.

Against each one of these bars, a linear voltage differential transformer (LVDT, or transducer) is placed, so that the bars' circumferential movement can be measured. These LVDT's have a range of 100mm and an accuracy of 0.01 mm, and were mounted using magnetic bases onto steel plates fixed to the concrete block. The LVDT outputs represent the tangential movement of an 89mm diameter circle at three points corresponding to each one of the steel bar position. However, this measurement of slip is reliable only for a small movement of the steel bar. For a larger movement, the LVDT position is no longer tangential to the bars' rotation.

If the bars rotate with an angle of 10° which is equivalent to 8 mm slip, the

error between the real slip and the LVDT output hardly exceeds 1% .This error is limited to 0.01% for 1mm slip.The use of these transducers is designed to assess the small movement of the pile elements, providing the early deformation of the bond in its pre-failure stage, which includes the grout deformation around the pile ring element. For subsequent loadings, the positions of these transducers are adjusted after every sequence of loading and unloading, minimizing the error on the slip readings.

At the top, the three steel bars are welded to a steel ring -with 110mm outside diameter, to increase their rigidity. The assembly of bars and rings is shown in figure 7.6c. The rotation of the bar ring assembly is independent of the key movement, and is only related to the key base and pile element rotation. In this way there is no need to consider the twist of the key itself under the torque moment. A plastic wire -1mm thick- is placed around the ring and kept taut by heavy steel masses at its ends, where two transducers are placed. The output of these two transducers gives the total rotation of the pile element. These two transducers do not need readjustment even for large rotation. Figure 7.11 shows the transducers placed against the three steel bars.

To summarize, the rotation of the pile is determined by two independent sets of transducers :

1 - three transducers to measure small pile rotation occurring early in the test. The circumferential slip will be given as

$$\delta_1 = \frac{\phi_{pile}}{\phi_{LVDT}} \cdot \quad \text{Average of the three LVDT's ouputs} \qquad (7.11a)$$

2 - two transducers measuring the total rotation of the pile element and giving the slip as :

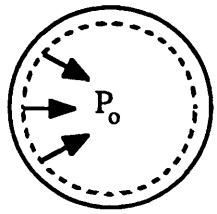
$$\delta_2 = \frac{\phi_{pile}}{\phi_{ring}} \cdot \text{ Avearge of the two LVDT's outputs} \qquad (7.11b)$$

where ϕ_{pile}, ϕ_{ring}, and ϕ_{LVDT}, are respectively the outside diameters of the pile element, the ring, and the circumferential position of the first three transducers; δ is the interface slip displacement.

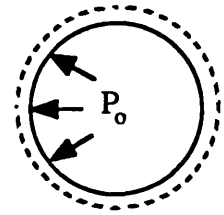
The output result δ represents the sum of the grout deformation and the elastic interface movement during the pre-failure stage, and the relative movement of the pile ring to the grout when failure occurs at the pile/grout interface.

7.4.3 NORMAL STRESS AND DILATANCY MEASUREMENT

The application of shearing stresses on the pile/grout interface causes radial (normal) strains and stresses due to interaction between the pile and its surrounding. By installing strain gauges on the concrete pocket in the circumferential direction, this effect can be detected. It could occur by either compressive (due to dilatancy) or tension (due to contraction) stresses normal to the pile surface as shown below :



Pocket deformation under uniform tensile radial stress (contraction)



Pocket deformation under uniform compressive radial stress (dilatancy)

It can be expected that the shear and normal stresses developed, are dependant on each other. The dilatancy phenomenon, due to shear in grout, will be affected by the radial stiffness of the surrounding concrete. Therefore, the normal stresses acting on the pile surface will increase with dilation. This increase in normal stress will increase the shear stress necessary for further slip and confirm the influence of radial stiffness on bond strength and frictional resistance noted in chapter 2. When compressive normal stresses are generated, the circumferential strain gauges indicate extension.

By studying the hoop strains, the normal stress at the interface can be deduced. The installation of a limited number of strain gauges on the concrete pocket surface will not provide full information on the distribution of normal stresses around the pile element. However, limited readings are enough to indicate the existence and behaviour of the phenomenon .

In the case of the present study, the concrete pocket is built in a large concrete block. Theoretically, the latter can be represented as an infinitely large block, as the ratio of the concrete pocket diameter to the concrete block dimension is about 1/10. Since the radial stress distribution decreases as of the square of the distance to the pocket, the error will be within 1%.

The transformation of the strain gauges outputs ε_{SG} to the equivalent normal stresses σ_n at the interface is based on results given in Timoshenko and Goodier (1982). Both the grout and the concrete are considered to be linearly elastic with Young's modulus and Poisson's ratio E_g , ν_g, and E_c, ν_c respectively. Both the grout and the concrete media are assumed to be under a plain stress condition, and the deformation to dilation is assumed to be axis-symmetric.

The elastic analysis of an annulus under uniform internal radial pressure P_i, and uniform external radial pressure P_o provides the expression for the radial stress σ_n, and the circumferential stress σ_θ as :

$$\sigma_r = \frac{R_i^2 R_o^2}{R_o^2 - R_i^2}(P_o - P_i)\frac{1}{r^2} + \frac{P_i R_i^2 - P_o R_o^2}{R_o^2 - R_i^2} \qquad (7.12a)$$

$$\sigma_\theta = -\frac{R_i^2 R_o^2}{R_o^2 - R_i^2}(P_o - P_i)\frac{1}{r^2} + \frac{P_i R_i^2 - P_o R_o^2}{R_o^2 - R_i^2} \qquad (7.12b)$$

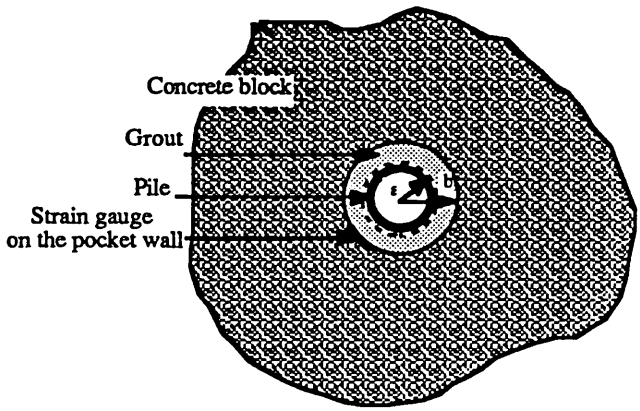
where R_i and R_o are the inner and the outer radii of the annulus. The radial and circumferential deformations in the annulus are :

$$\varepsilon_r = \frac{1}{E}(\sigma_r - \nu\,\sigma_\theta) \qquad (7.13a)$$

$$\varepsilon_\theta = \frac{1}{E}(\sigma_\theta - \nu\,\sigma_r) \qquad (7.13b)$$

where E and ν are the Young's modulus and the Poisson's ratio of the annulus material.

The pile element, grout and surrounding concrete media are shown in the figure below :



The radial stress at the pile/grout interface due to the lateral effect is σ_n and the radial stress at the interface grout/concrete is $\sigma_{c/g}$

a is outer radius of the pile element = R_{pile}

b is the radius of the concrete pocket = R_{pocke}

By applying equations (7.12) and (7.13), to the surrounding concrete, and putting the outer radius R_o as infinite, P_o zero, and $P_i = \sigma_{c/g}$:

$$\sigma_r = -\sigma_{c/g}\frac{b^2}{r^2} \quad \text{and} \quad \varepsilon_r = -\frac{(1+\nu_c)}{E_c}\sigma_{c/g}\frac{b^2}{r^2} \tag{7.14a}$$

$$\sigma_\theta = \sigma_{c/g}\frac{b^2}{r^2} \quad \text{and} \quad \varepsilon_\theta = \frac{(1+\nu_c)}{E_c}\sigma_{c/g}\frac{b^2}{r^2} \tag{7.14b}$$

At the interface between the grout and the concrete block media (r=b) these expressions become :

$$\sigma_r = -\sigma_{c/g} \quad \text{and} \quad \varepsilon_r = -\frac{(1+\nu_c)}{E_c}\sigma_{c/g} \tag{7.15a}$$

$$\sigma_\theta = \sigma_{c/g} \quad \text{and} \quad \varepsilon_\theta = \frac{(1+\nu_c)}{E_c}\sigma_{c/g} \tag{7.15b}$$

On the other hand equations (7.12) applied to the grout provide the stresses at the grout concrete interface and concrete at r = b as :

$$\sigma_r = -\sigma_{c/g} \tag{7.16a}$$

$$\sigma_\theta = \frac{1}{\lambda - 1}\left[\, 2\,\sigma_n - (1+\lambda)\,\sigma_{c/g}\right] \text{ where } \lambda = \frac{b^2}{a^2} \tag{7.16b}$$

$\sigma_{c/g}$ is still indeterminate. However a further assumption has to be made to obtain an expression of $\sigma_{c/g}$. This can be expressed by assuming the continuity of the radial

deformation at the grout/concrete interface. The radial deformation in the grout matrix at the level of the grout/concrete interface is :

$$\varepsilon_r = -\frac{1}{E_g}\left[\left(1 - \nu_g \frac{\lambda+1}{\lambda-1}\right)\sigma_{c/g} + \frac{2\nu_g}{\lambda-1}\sigma_n\right] \qquad (7.17)$$

By matching the radial deformation in the concrete (7.14a) and that of the grout matrix (7.17), $\sigma_{c/g}$ can be expressed as function of σ_n as :

$$\sigma_{c/g} = \frac{2\nu_g E_c}{E_g(1+\nu_c)(\lambda-1) + \nu_g E_g(\lambda+1) - E_g}\sigma_n \qquad (7.18)$$

Since the gauges were placed on the concrete pocket wall, their outputs are the circumferential deformation of the concrete at the interface between the grout and concrete. This can be written as :

$$\varepsilon_{SG} = \frac{2(1+\nu_c)\nu_g}{E_g(1+\nu_c)(\lambda-1) + \nu_g E_c(\lambda+1) - E_c(\lambda-1)}\sigma_n \qquad (7.19)$$

Consequently the normal stress along the interface pile element/grout σ_n can be expressed as function of the strain gauges output ε_{SG} as :

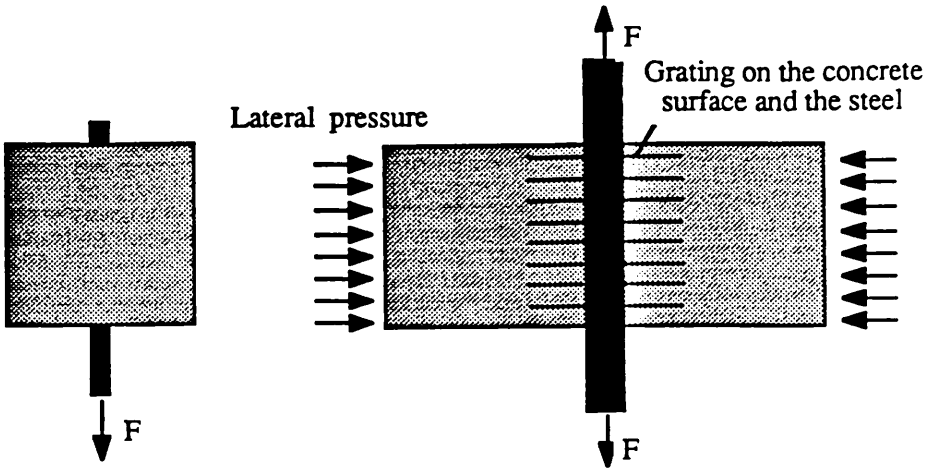
$$\sigma_n = \frac{E_g(1+\nu_c)(\lambda-1) + \nu_g E_c(\lambda+1) - E_c(\lambda-1)}{2(1+\nu_c)\nu_g}\varepsilon_{SG}$$

$$\text{or} \qquad \sigma_n = K_{normal}\,\varepsilon_{SG} \qquad \text{with} \quad K_{normal} = \frac{E_g(1+\nu_c)(\lambda-1) + \nu_g E_c(\lambda+1) - E_c(\lambda-1)}{2(1+\nu_c)\nu_g}$$

The concrete used during this investigation had the following characteristics :

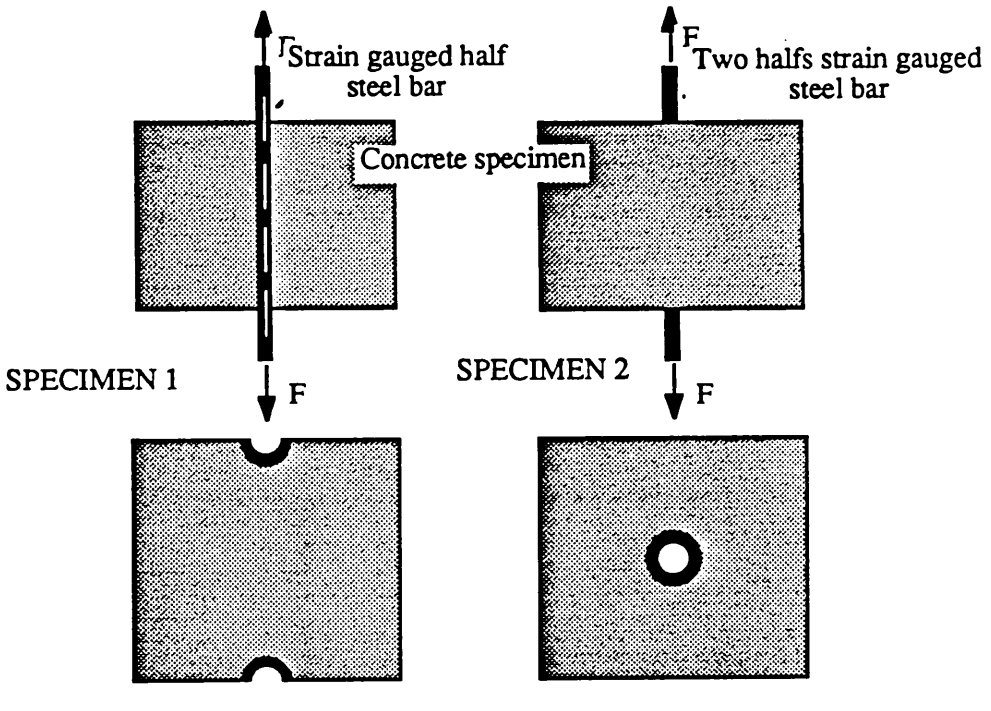
$$E_c = 30\ 10^3\ \text{N mm}^{-2}, \text{ and } \nu_c = 0.15.$$

During the preliminary investigation the pocket diameter was 80 mm (λ = 2.041), which was reduced to 75 mm (λ =1.676) for the subsequent tests. The grout characteristics vary with the curing times. However, their variation after three days is considered to be small enough to assume a constant value E_g of 20 10^3 N mm^{-2}, and ν_g = 0.25. At the age of one day, E_g, ν_g were measured to be 9 10^3 N mm^{-2} and 0.3 respectively. In these cases K_{normal} varies from 10 to 27 10^{-3} N mm^{-2}, when ε_{SG} is expressed in micro strain.

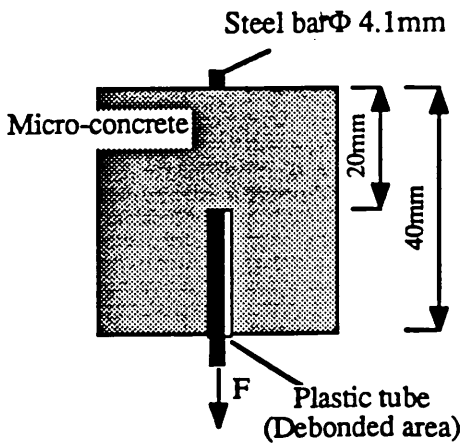


7.1.a - Conventional Test Method

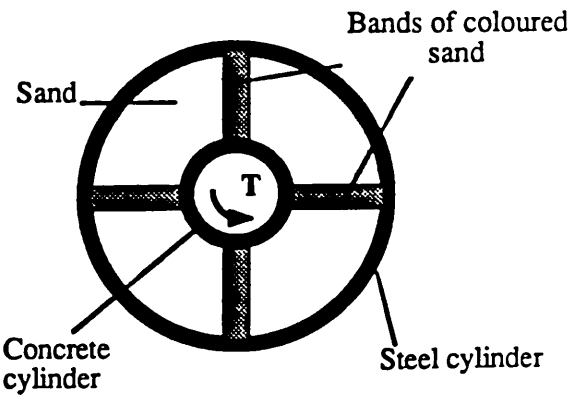
7.1.b - Tassios and Koroneos (1979)



7.1.c - Jiang et al (1982)



7.1.d - Stroeven and De Wind (1982)



7.1.e - Chen et al (1987)

Figures 7.1

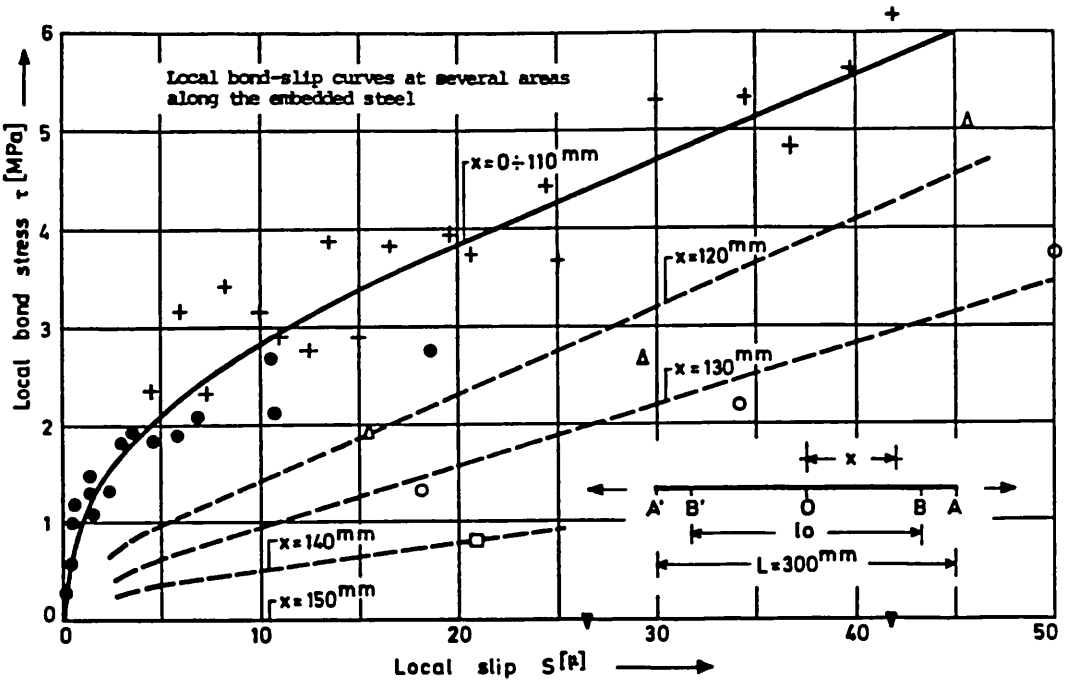


Figure 7.2a : LOCAL BOND - SLIP CURVES AT SEVERAL AREAS ALONG THE EMBEDDED LENGTH (From Tassios and Koroneos (1979))

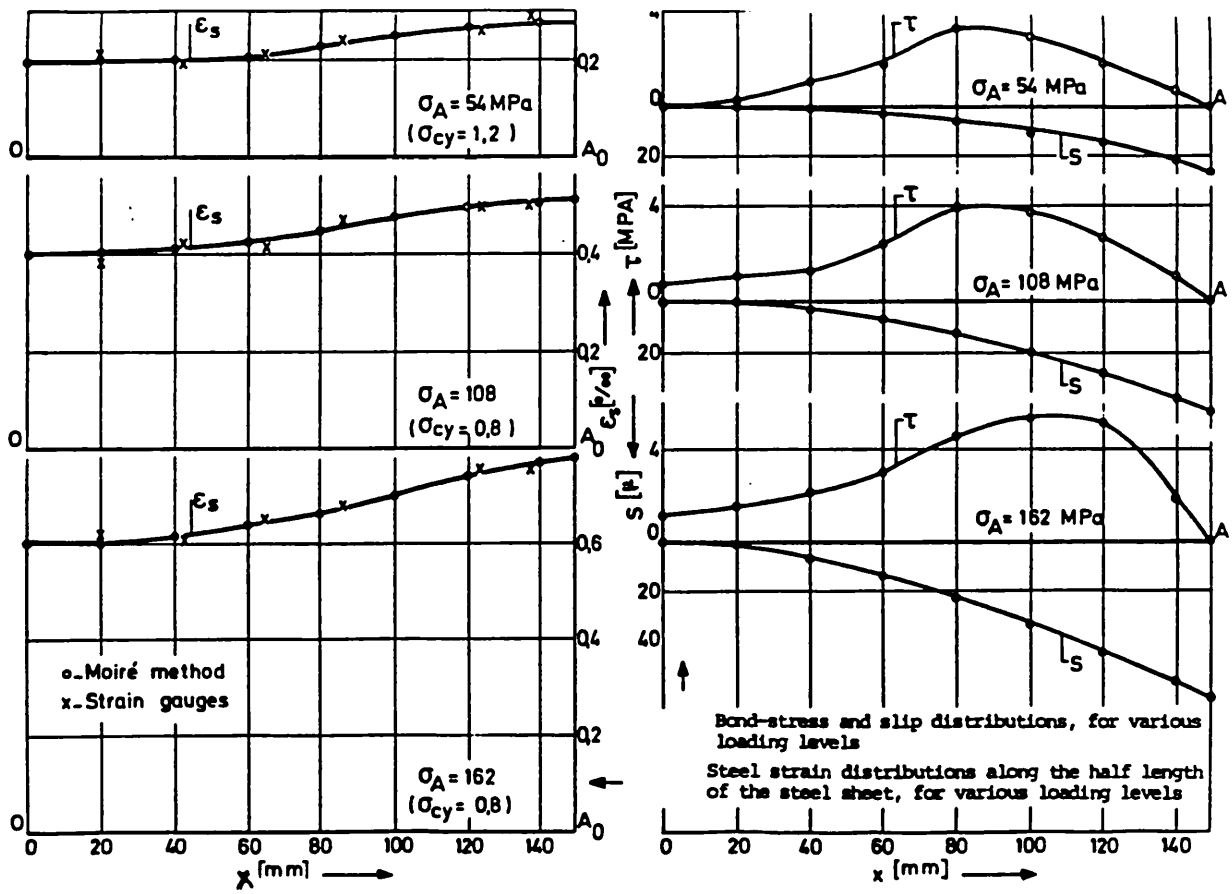
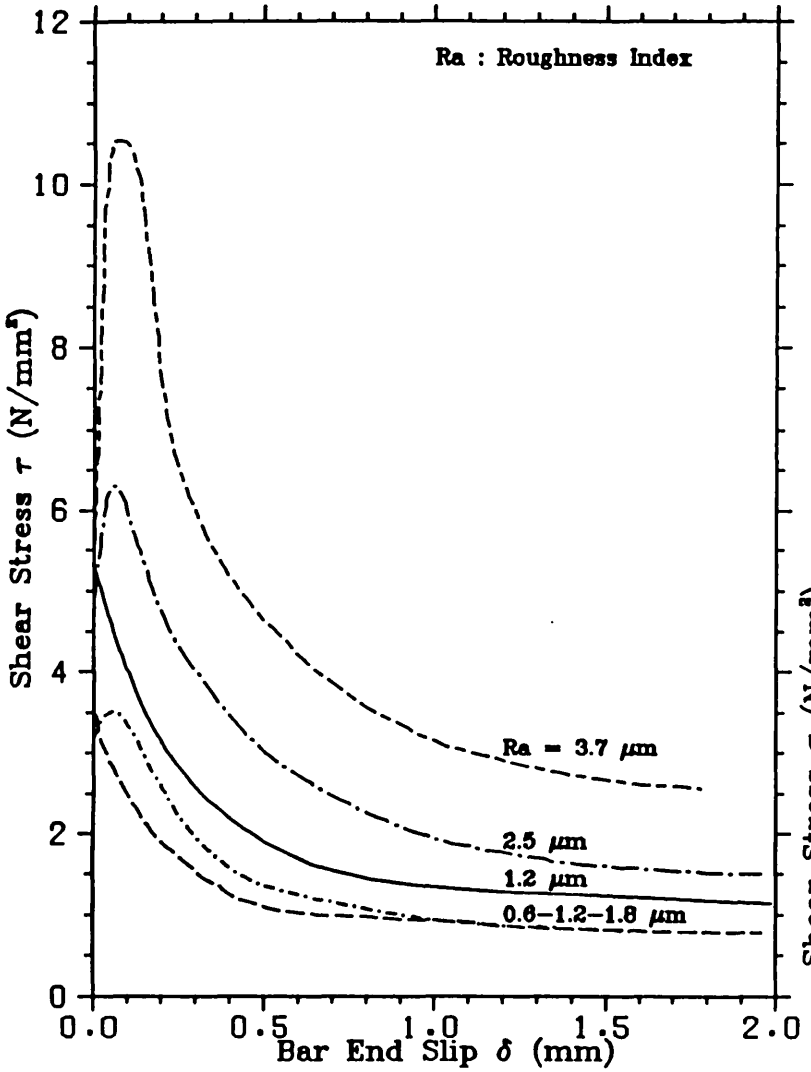
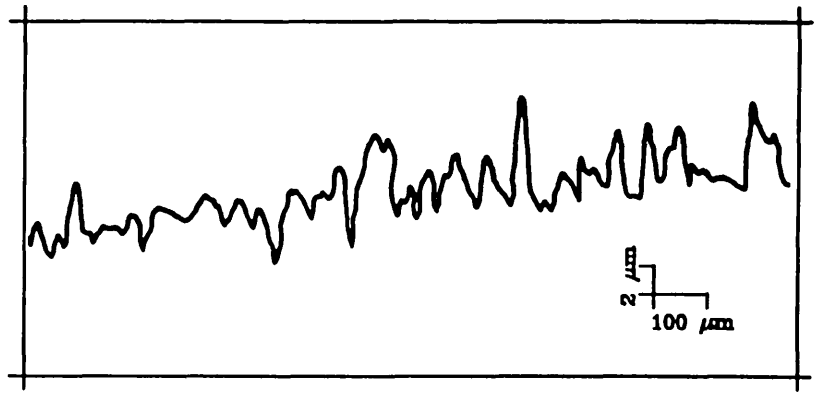


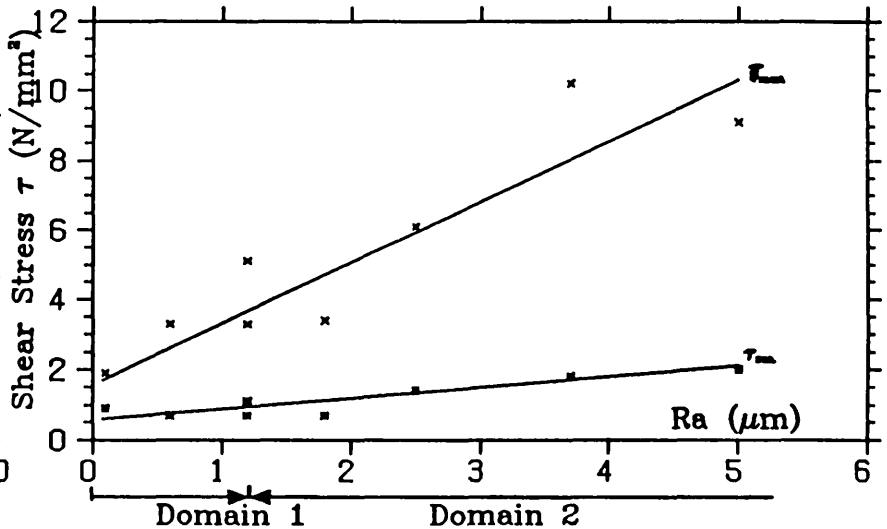
Figure 7.2b : BOND, SLIP, AND STEEL STRAIN DISTRIBUTIONS FOR VARIOUS LOADING LEVELS (From Tassios and Koroneos (1979))



Pull-out characteristics of steel bar embedded in concrete
(Stroeven and De Wind 1982)



Longitudinal roughness profile of steel wire detremined with Taylor – Hobson apparatus
(Stroeven and De Wind 1982)



Maximum shear stress and friction resistance from the pull-out tests
(Stroeven and De Wind 1982)

Figures 7.2c

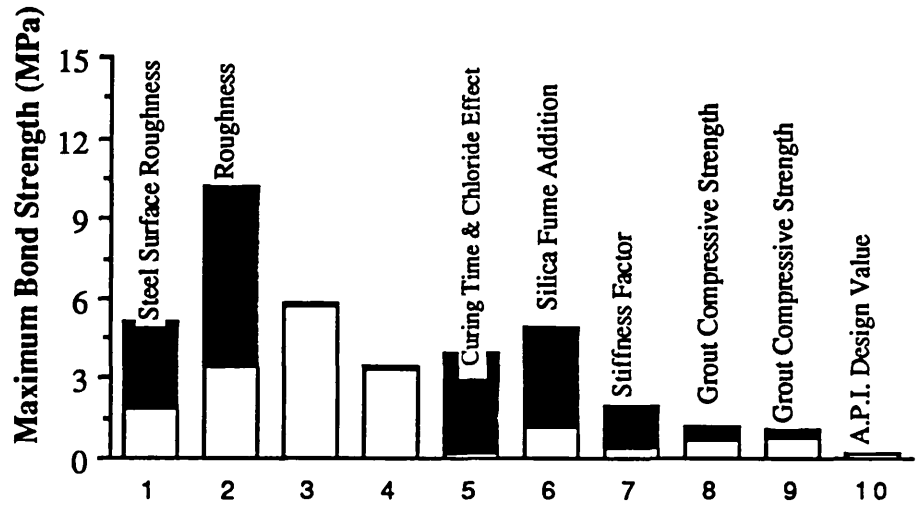


Figure 7.2d : **REVIEW OF TESTS RESULTS ON BOND STRENGTH**

1- Stroeven and De Wind (1982) : smooth steel surfaces
2- Stroeven and De Wind (1982) : rough steel surfaces
3- Jiang et al (1982)
4- Brandt (1982)
5- Sakamoto and Iwasaki (1982)
6- Theodor (1982)
7- Billington et al (1979-1980)
8- Woodward (1982)
9- Loset (1981)
10 Recommended design value given by the A.P.I.(1986)

the bond strength is given within a certain range according to the parameter indicated in the corresponding graph.

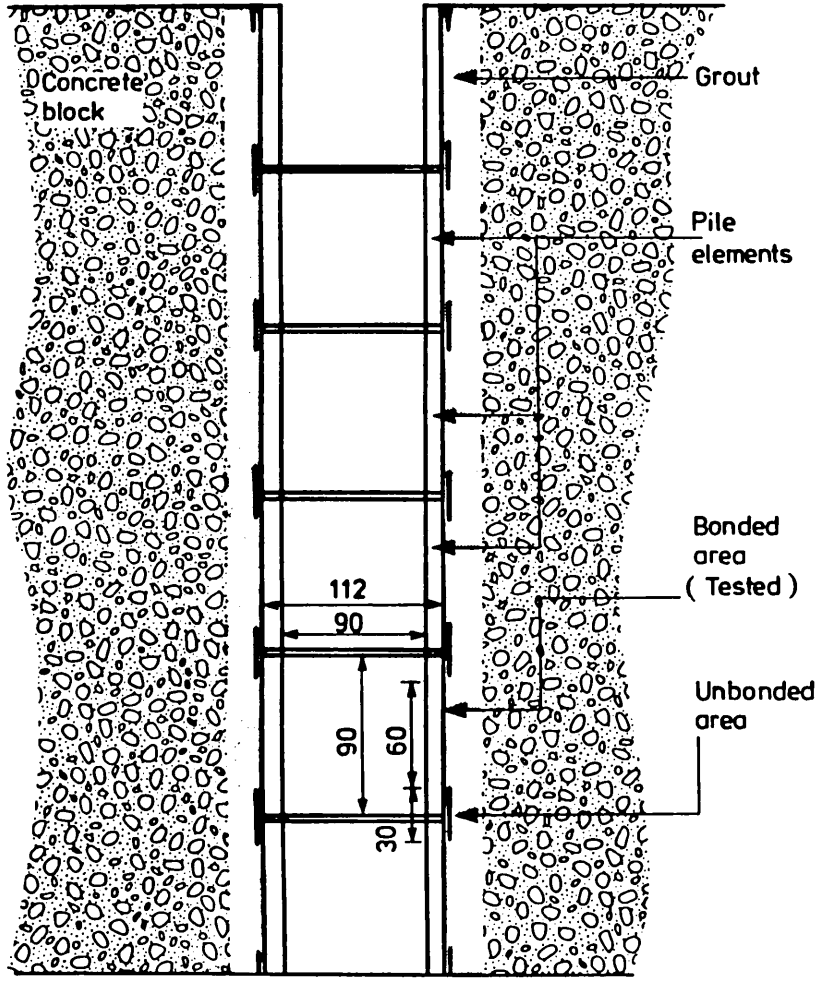


Figure 7.3a : DESCRIPTION OF THE PILE RINGS ARRANGEMENT FOR THE DESIGNED TORSION TEST

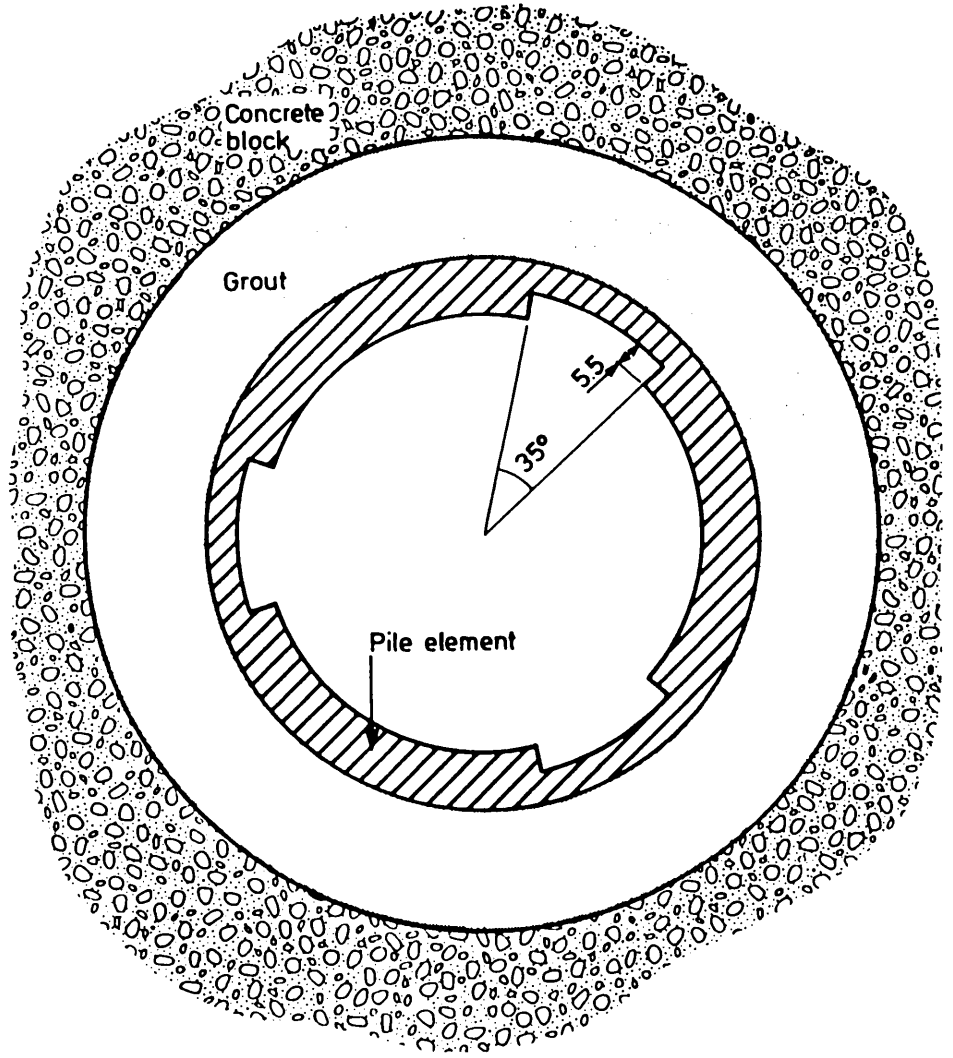


Figure 7.3b : CROSS SECTION OF A GROUTED PILE RING IN THE CONCRETE BLOCK DURING THE TORSION TEST

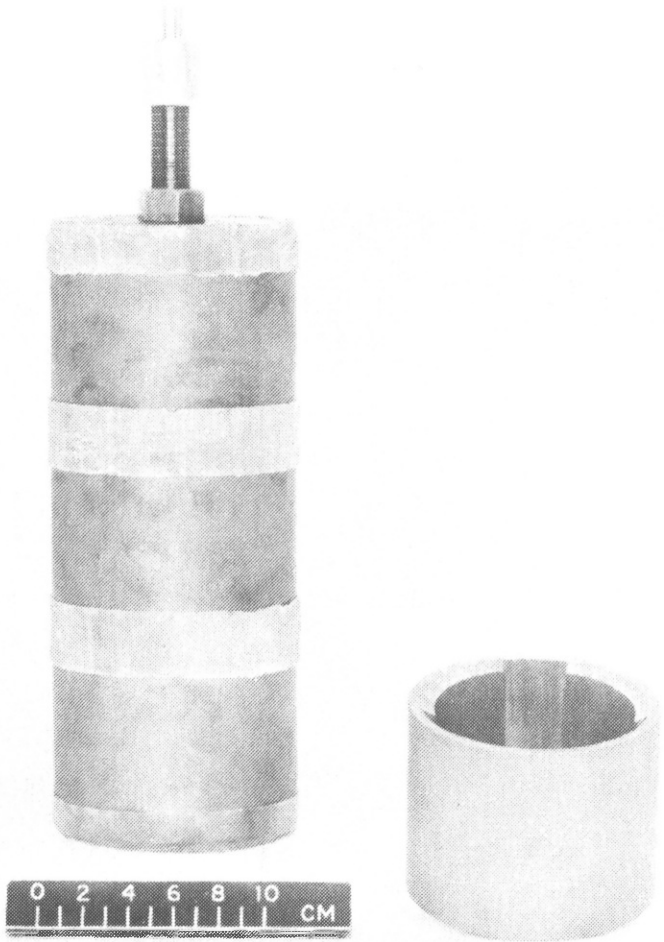


Figure 7.4a : PILE RINGS UNIT USED DURING THE PRELIMINARY INVESTIGATION OF THE TORSION TEST

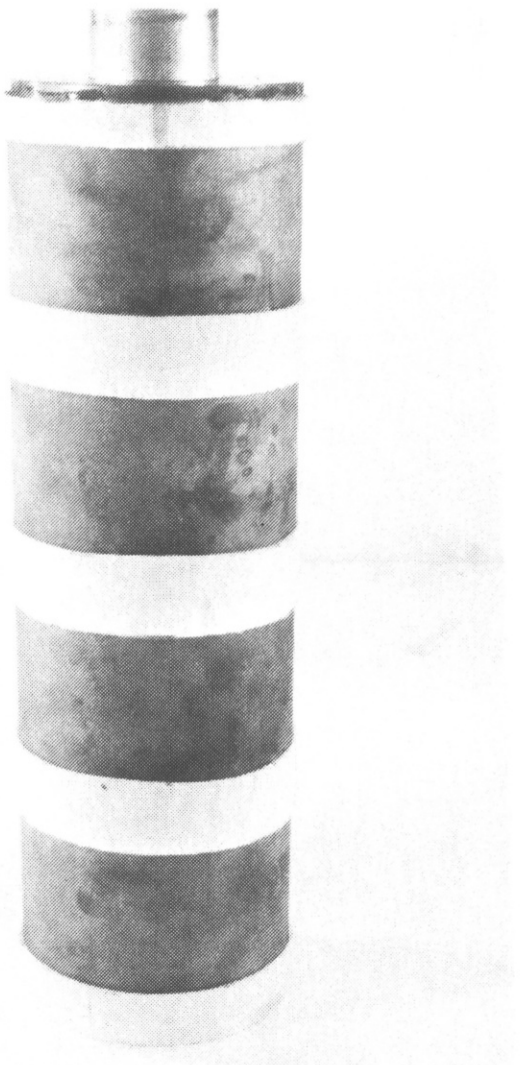


Figure 7.4 : PILE RINGS UNIT USED DURING THE MAIN INVESTIGATION OF THE TORSION TEST

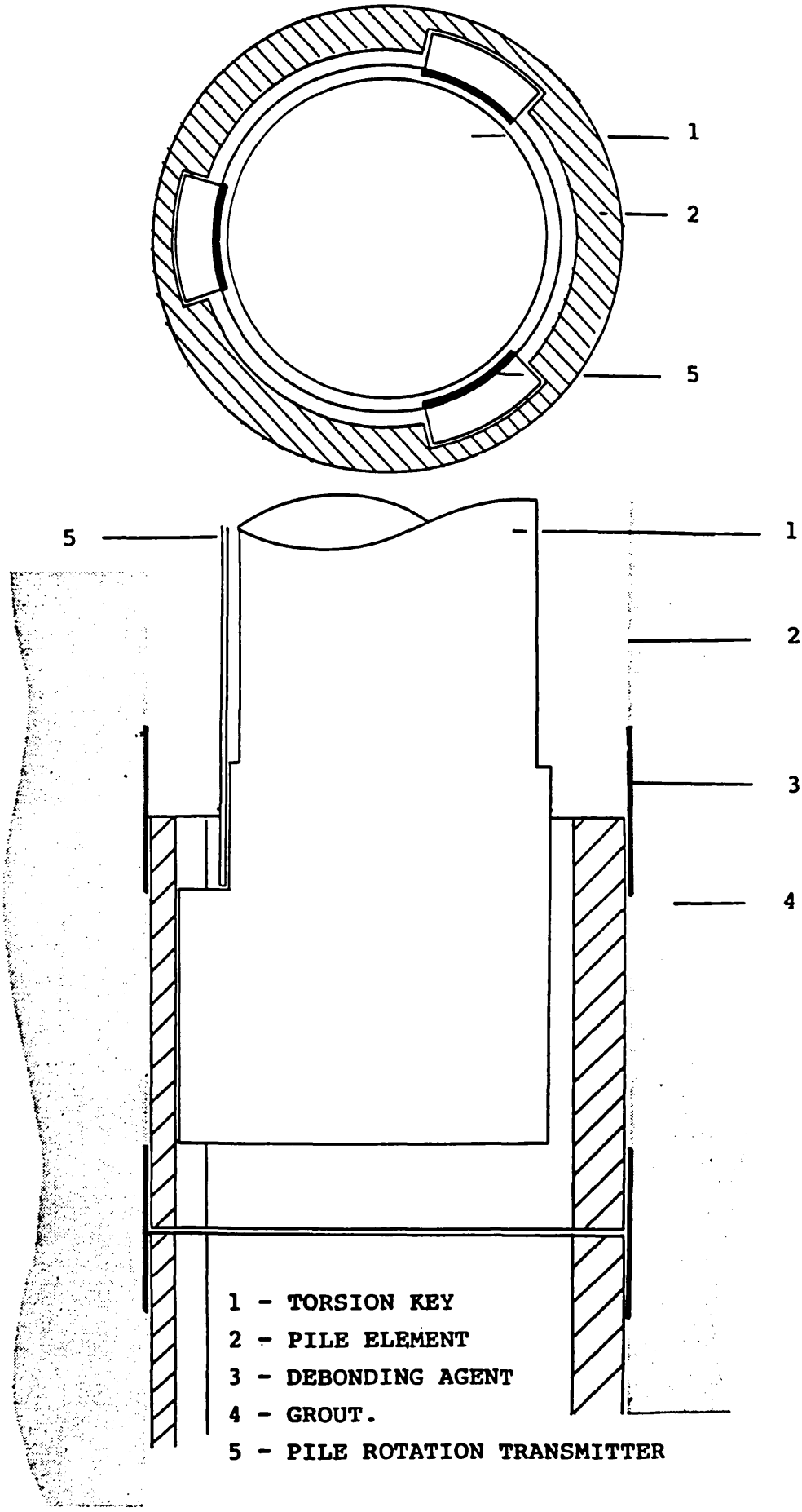


Figure 7.5 : ASSEMBLY OF THE PILE RING WITH THE TWISTING KEY FOR THE TORSION TEST

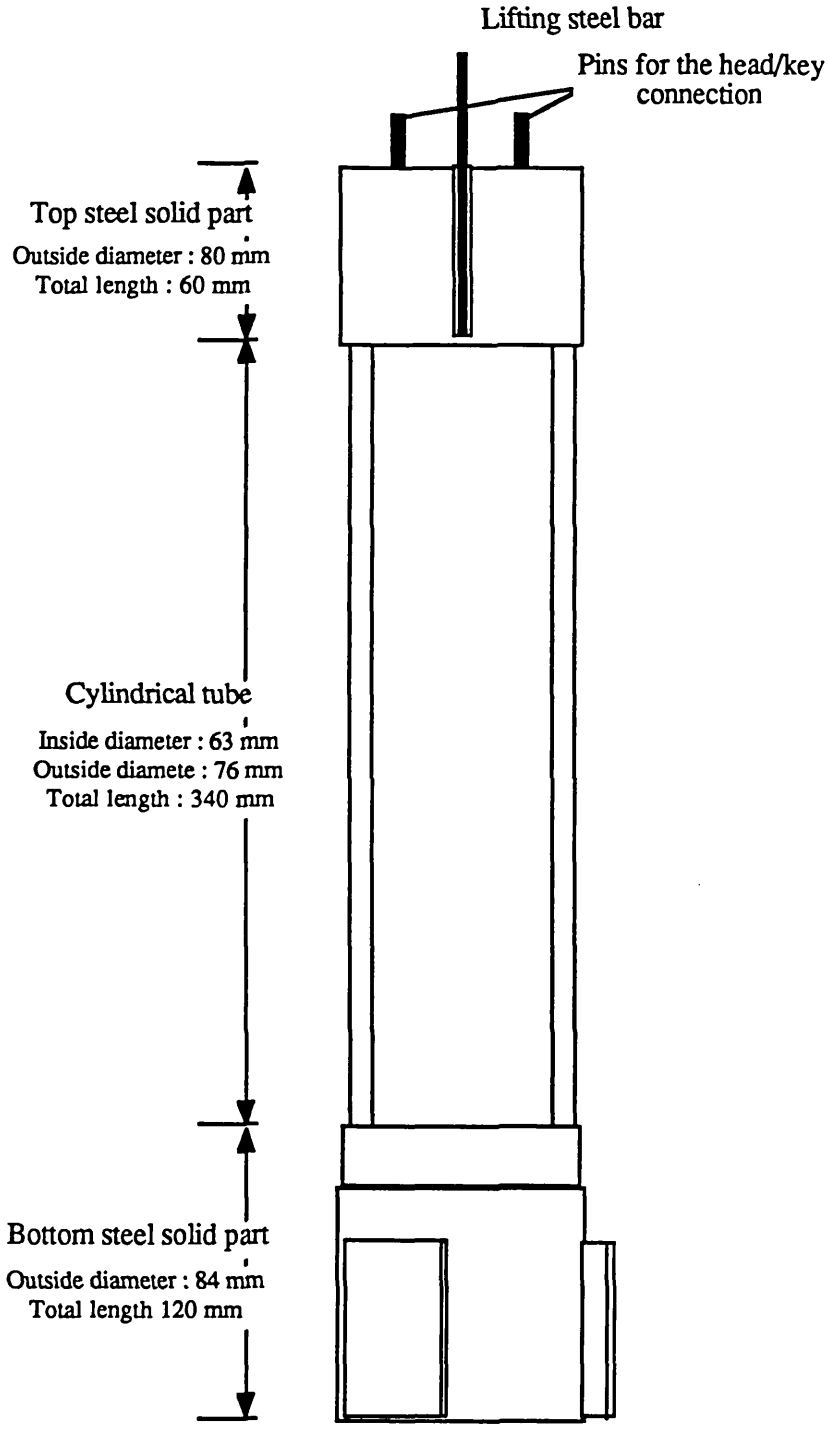


Figure 7.6a : DESCRIPTION OF THE TWISTING TOOL



Figure 7.6b : VIEWS OF THE MANUFACTURED TWISTING TOOL WITH THE CROSS-HEAD

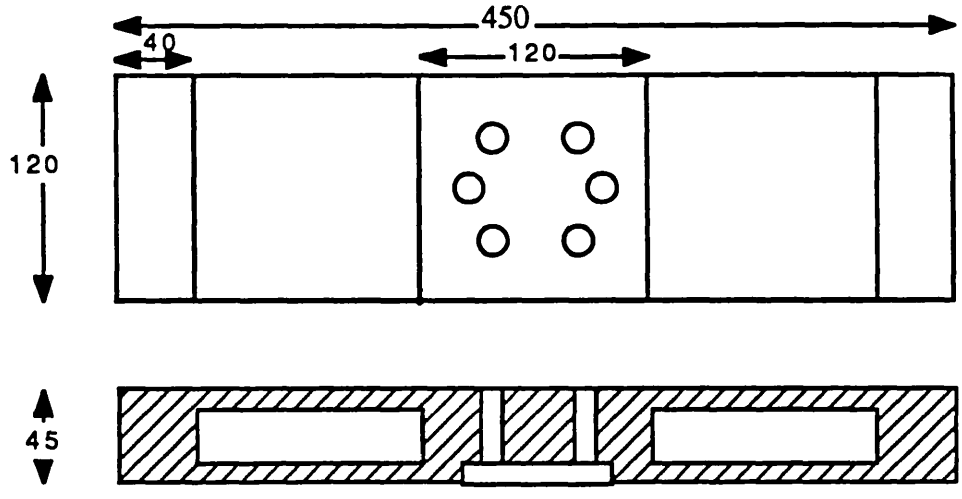
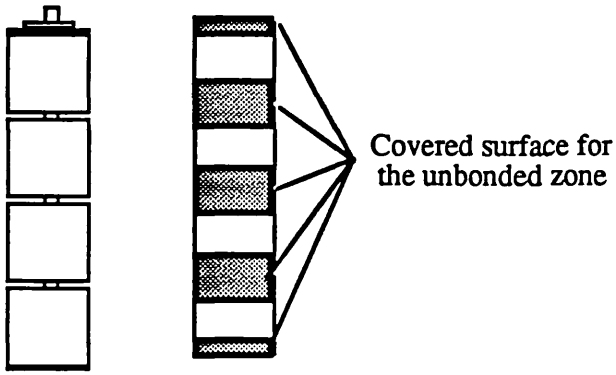
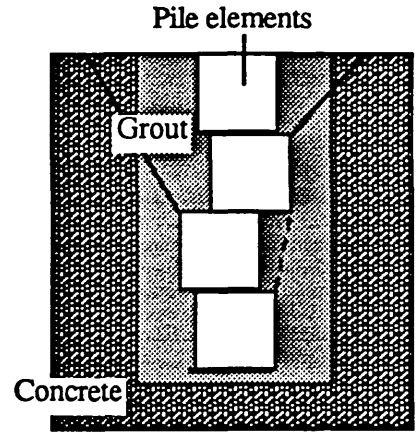


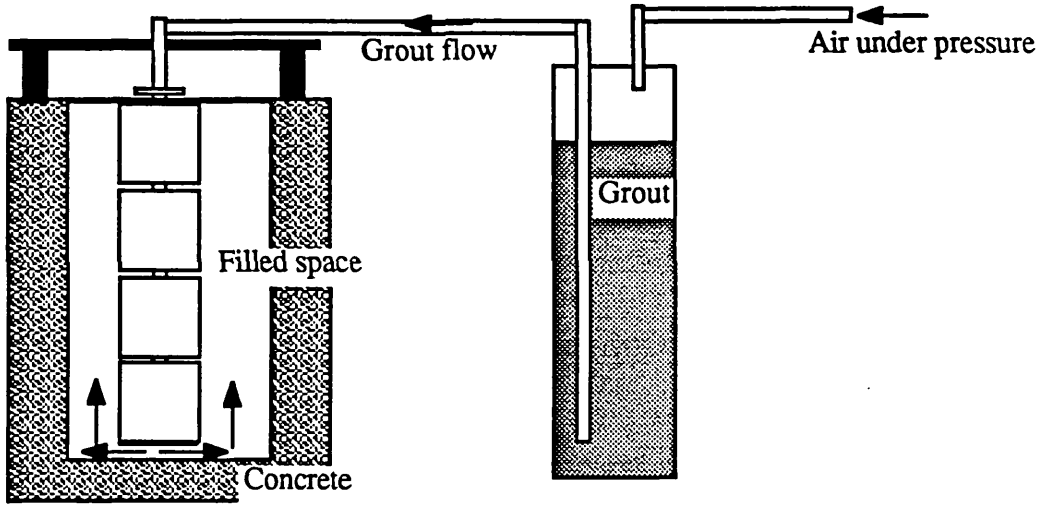
Figure 7.6c : DESCRIPTION OF THE TWISTING KEY CROSS-HEAD



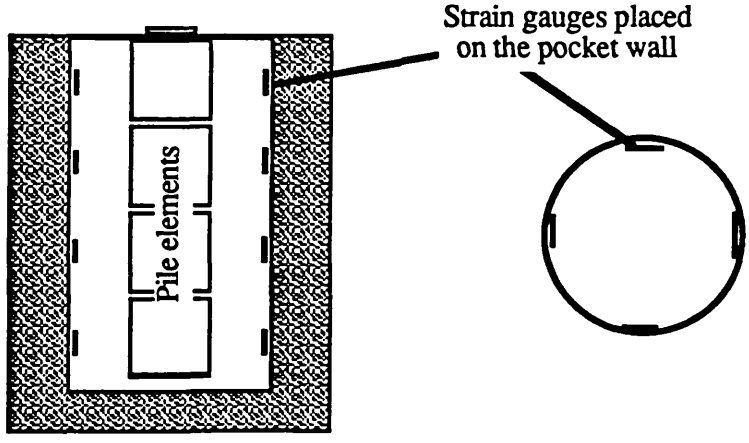
7.7a - Pile elements arrangement



7.7b - Over break of the pocket due to miss-alignment of the pile elements



7.7c - Casting operation of the pile element



7.7d - Concrete pocket instrumentation

Figures 7.7

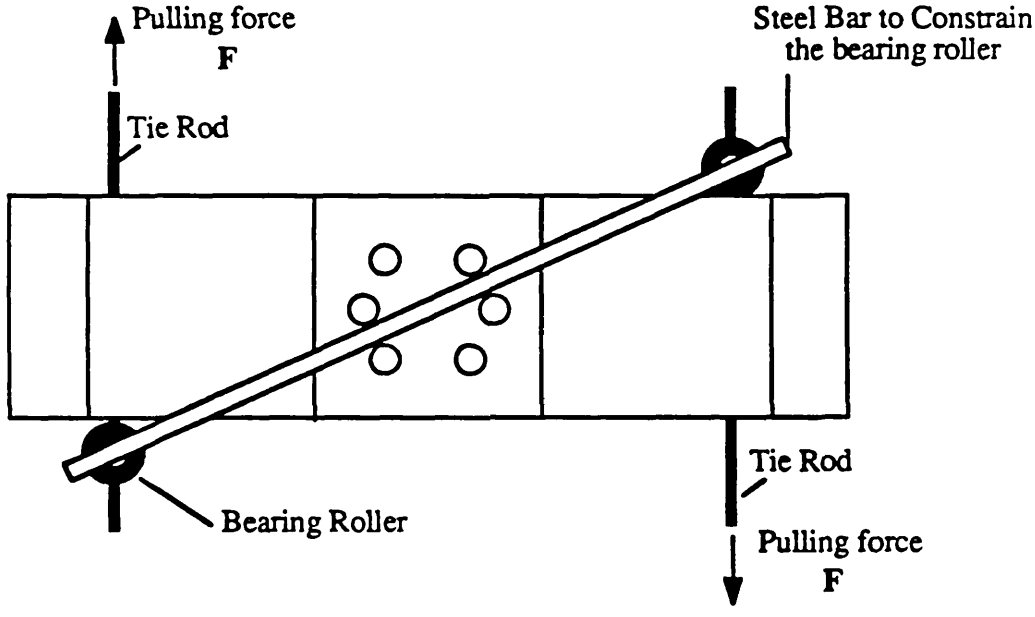


Figure 7.8 : CROSS-HEAD PULLING BAR CONNECTION

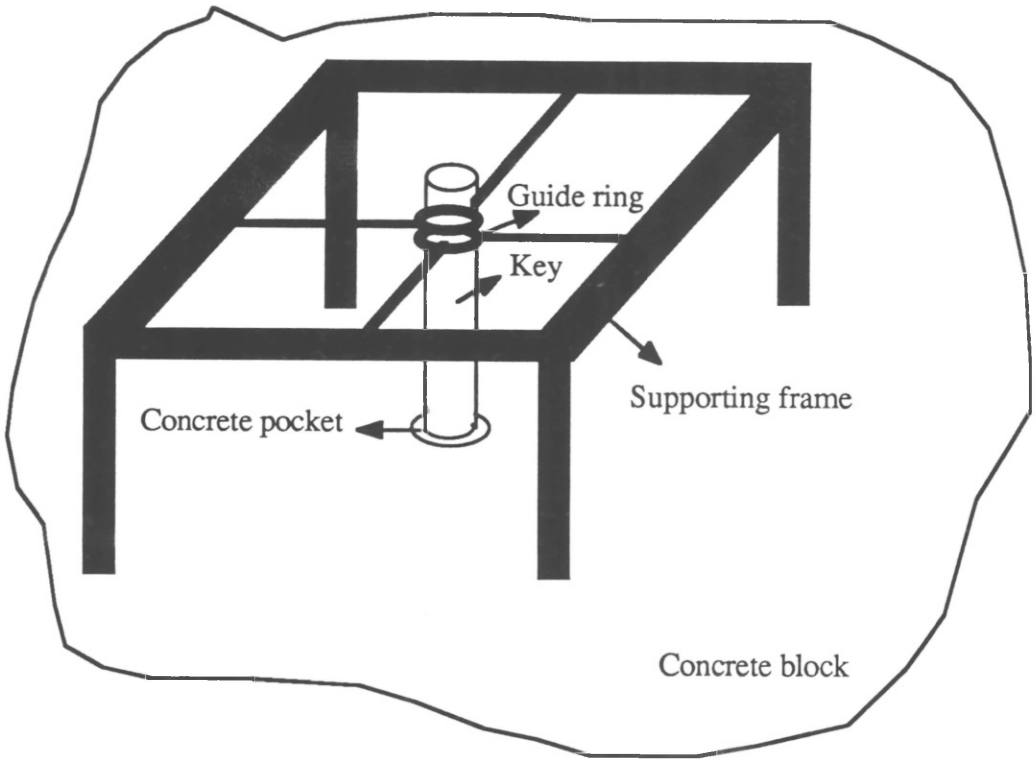


Figure 7.9 : STIFFENING ARRANGEMENT OF THE KEY

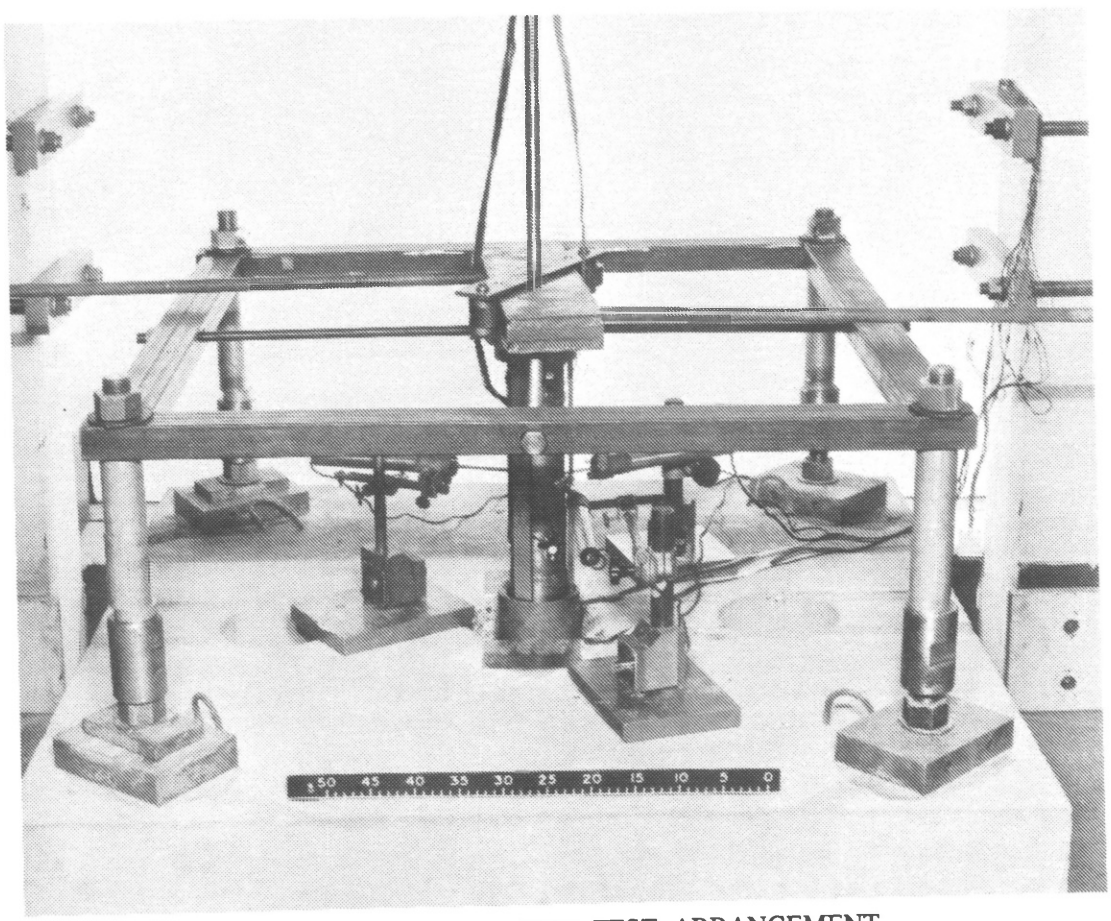


Figure 7.10 : TORSION TEST ARRANGEMENT

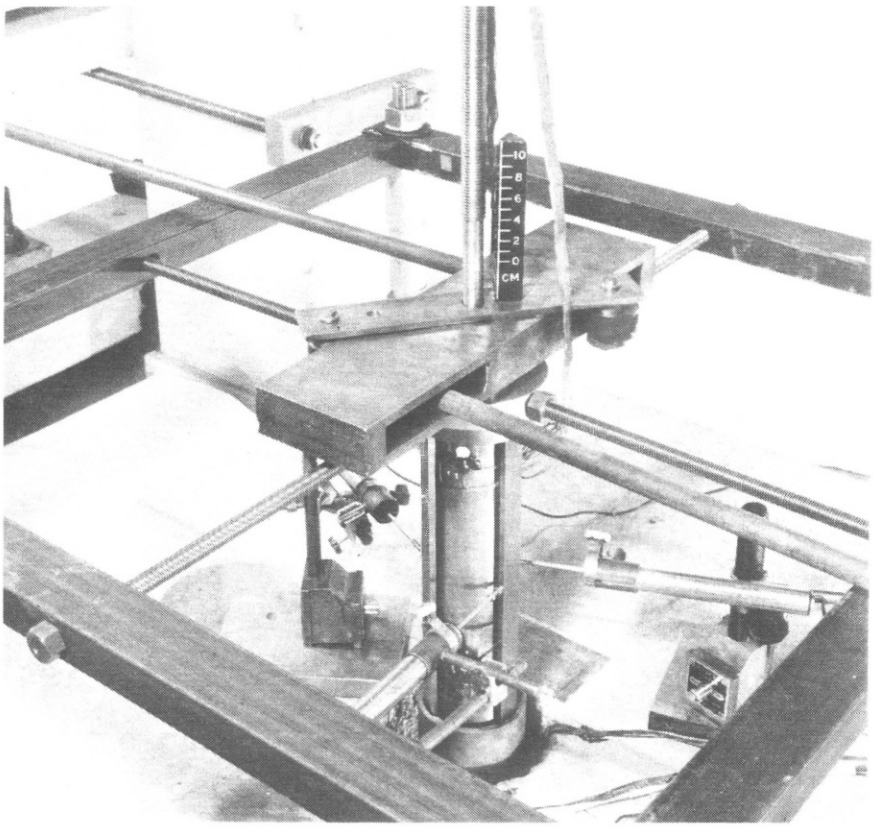


Figure 7.11a : VIEW OF THE TORSION TEST WITH THE **LVDT** FOR SLIP MEASUREMENT

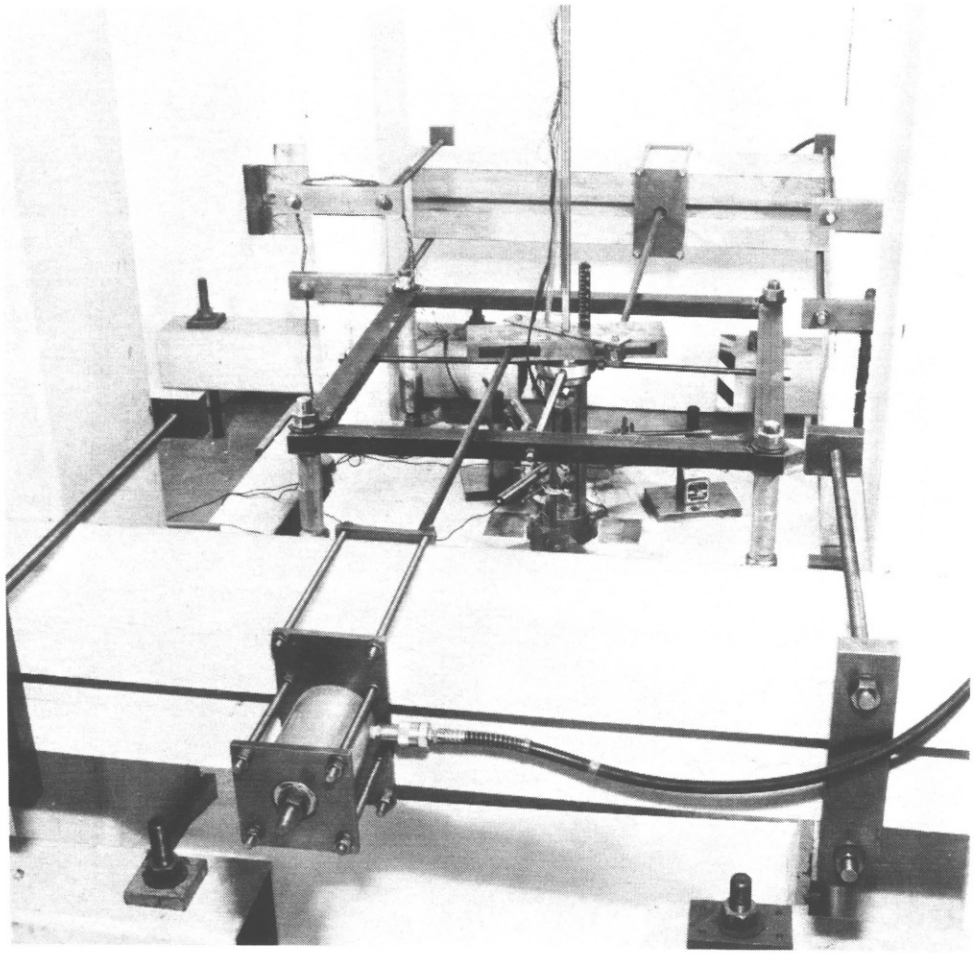


Figure 7.11b : VIEW OF THE TORSION TEST WITH THE HYDRAULIC EQUIPMENT DURING THE PRELIMINARY INVESTIGATION

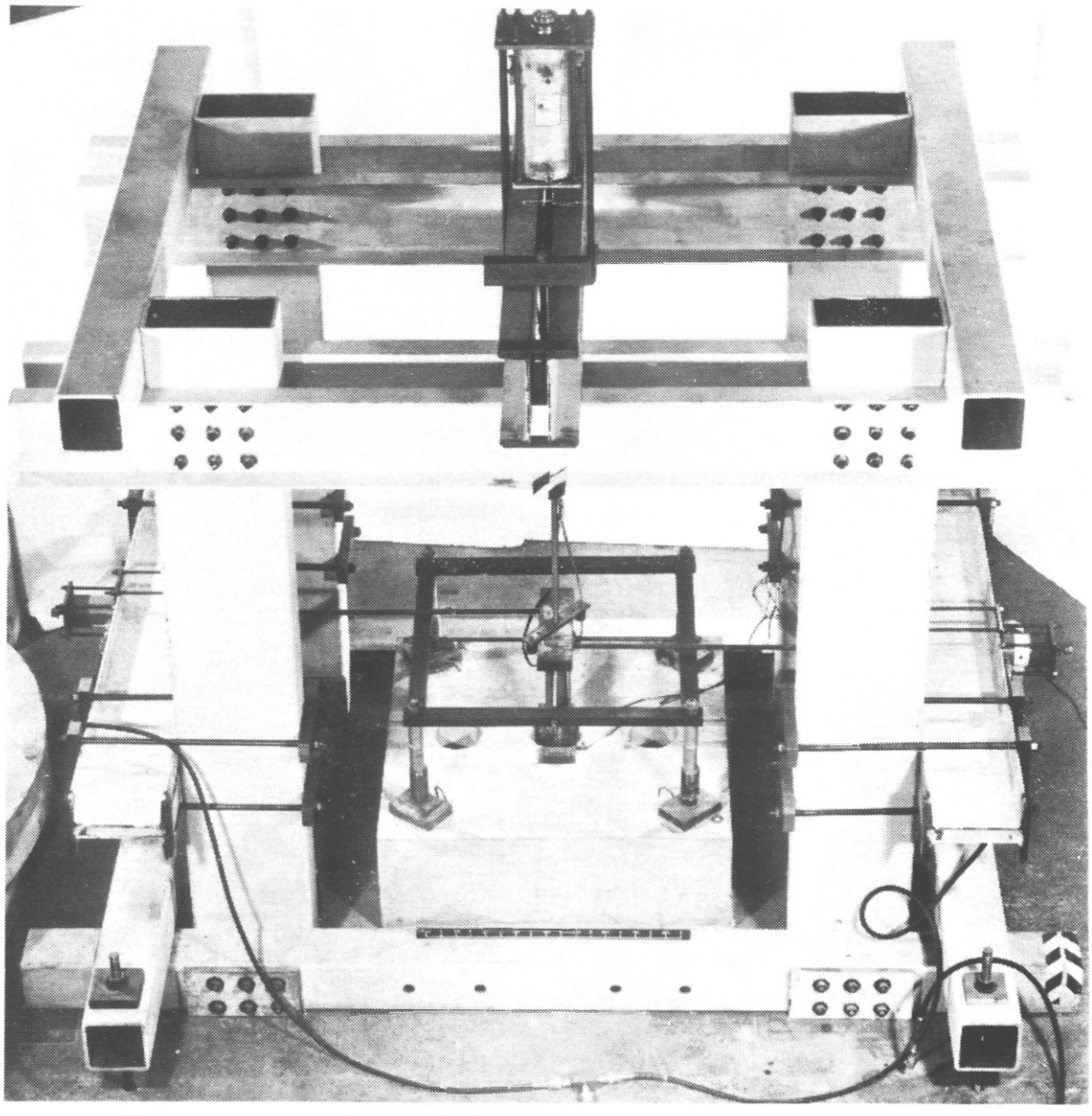


Figure 7.12 : VIEW OF THE RIG WITH THE CONCRETE BLOCK DURING THE PRELIMINARY INVESTIGATION

CHAPTER 8 : TORSION TEST RESULTS

8.1 INTRODUCTION

In this chapter, the results of the torsion tests, to quantify the bond and friction behaviour of the steel/grout interface, are presented and discussed.

The torsion test was carried out initially on three rings, using hydraulic equipment for the torque application. These tests were considered to be a part of the preliminary investigation aimed primarily at assessing the performance of the new test procedure. Each test was denoted as "P.T.T." (i.e. Preliminary Torsion Test), followed by the ring number (1,2,3). The first ring corresponds to the top ring of the pile elements.

During these tests, the interface was subjected to a complete cycle of slip displacement which was obtained by reversing the direction of the applied torque once a given rotation had been achieved. Negative shear stresses and negative shear slip increments were thus induced on the reversed portion of the cycle.

The main torsion test programme was carried out on a segmented pile having, four ring specimens. These tests were called "M.T.T." (i.e Main Torsion Test) followed by the ring number (1,2,3,4). In these tests the hydraulic loading system was replaced by mechanical screw jacks and electric motors in order to increase the stiffness of the loading system as described in chapter 7.

In the same way as in the preliminary test, reverse rotation cycles were again undertaken. In this case, the direction of the pile rotation was reversed three times.

During the first phase of torsional loading, very frequent measurements were made using all the instrumentation, in order to obtain the maximum information on the effects of bond failure.

Once the interface resistance had achieved an approximately constant value, the sense of the torque was reversed so that the pile element was then rotated in the opposite direction, back to its original position. The pile rotation was continued beyond this point, until the interface shear stress showed an increasing resistance.

At this stage, with the interface slip displacement showing a negative value, the torque was again reversed. Rotation of the pile was then continued until the slip displacement reached a large value of up to 50 mm, corresponding to a pile rotation of 50°.

Following these cycles, a third reverse rotation cycle was conducted in order to return the pile to its original location and so enable the pile ring element to be extracted.

The effect of cyclic shear stress was investigated during test M.T.T. 2. A series of unloading and reloading sequences were undertaken after different amounts of slip had occurred. On each occasion, the pile element rotation was stopped, and the shear stress cycled many times without generating additional slip movement. This operation was carried out during both the shear stress softening and frictional phases of the interface behaviour.

The histories of shear stress and slip paths followed during these tests are relevant to the use of piles in practice. There are a number of practical situations involving loading, unloading and reversed loading, or with repeated cycles of loading in the same direction. For example, under seismic loads, depending on the intensity of the shaking and the initial stress, the grouted pile may be either pulled out and pushed back, or merely loaded and unloaded without slip displacement occurring. Consequently both reversed shearing loads and reversed slip deformation are possible situations that can occur at the pile interface.

In all the experiments carried out, the slippage occurred at the steel pile surface/grout interface. This mode of failure requires the development of a zone of weakness along the contact surface, so that the deformation and slip are localized within a small band or even confined to the slip line on the perimeter of the steel pile element. From the test results, the interface behaviour was established in the following forms :

1- slip displacement vs average shear stress

2- slip displacement vs circumferential strain in the concrete pocket due to dilation effect

3- circumferential strain in the concrete pocket vs average shear stress

8.2 SLIP DISPLACEMENT - SHEAR STRESS

8.2.1 GENERAL BEHAVIOUR

The measurements of torque and rotation provide the relationship between the resisting average shear stress and the slip displacement in both the bond failure stage and the frictional sliding stage. This permits the determination of the peak bond resistance (i.e. bond strength) and the residual frictional resistance. Relationships giving the variation of shear stress with slip obtained from the torsion tests are presented in figures 8.1 for the preliminary investigation and in figures 8.2 for the main investigation. The numbers on the figures correspond to the order of the slip sequence undertaken during the tests.

The plots give the detailed sequences of the unloading and loading stress history as well as the reverse slip displacement cycles carried out on each pile specimen. Envelopes of the shear stress/slip relationship are also given to characterize the frictional behaviour of the interface. These envelopes provide an upper limit for the shear stress resistance for a given amount of slip.

From the envelope plots, the frictional behaviour following breakdown at the pile/grout interface can be seen as a stable hardening relationship. This can be explained by the development of a thin confined zone of damaged material which causes an increasing resistance to the pile rotation. Before this occurs, breakdown leads to softening from the peak shear stress achieved under small values of slip. Hardening could also be due to irregularity of the pile geometry. Any deviation of the pile perimeter from a true cylindrical shape could generate such behaviour. However the tested piles were prepared to a high accuracy, by turning the ring on a lathe and so should have had good circular symmetry.

When the shear stress direction was reversed, the direction of sliding was reversed on the surface that had been previously moving. This eventually caused a decrease of the interface resistance which, as can be seen from the figures, reached its minimum when the pile ring elements were rotated back to their initial position. A continued pile rotation in the same direction provides sliding between two surfaces that had not previously been matched so that an increase in the resistance is to be expected as new interlocks are broken down. These observations are very much a description of a frictional behaviour, and so can only be applied when a considerable amount of slip was

undertaken.

These observations bring attention to the fact that frictional behaviour is dependent on the history of loading. Celestino and Goodman (1979) have illustrated such behaviour for rock joints.

8.2.2 BOND FAILURE

Figure 8.3a shows the shear stress - slip relationship during the first stage of pile rotation. The softening behaviour that follows the attainment of peak shear stress is considered to be due to bond breakdown. The hardened cement paste develops a shear resistance to the pile rotation through an interlock between the cement grout and microscopic roughness on the surface of the pile. The observed bond break down is accompanied by a loss of shear resistance. The failure development can be formulated into three stages :

1 - linear increase of the shear stress - as an elastic behaviour- up to a maximum shear stress corresponding to the conventional bond strength.

2 - fracturing behaviour or loss of bond causing a sharp reduction in shear stress.

3 - a residual minimum shear stress which characterizes the frictional behaviour of the failed steel surface/grout interface. At a much larger value of slip, the shear resistance again increases due to dilatancy in the failure zone.

This behaviour is similar to that of concrete and cement paste matrices when subjected to tensile stresses.

The description of such fracturing behaviour was provided by Dougill (1976) using an extension of classical plasticity theory involving a fracture loading surface expressed in strain space. This fracture surface has the same role as the yield surface in the theory of hardening plasticity. This approach to fracturing behaviour has been further developed by Dougill (1985a, 1985b), and Dougill and Rida (1980), and extended to include both fracturing and plastic behaviour by Bazant and Kim (1979). The application of such a theory to the bonded interface behaviour could well prove useful, with slip displacement at the interface taking the place of plastic strain in the continuum theory.

The observed bond failure appears to be localized at the contact surface

between the steel and the grout. Such a failure mechanism is well known for concrete and cement paste. Experimental investigations on these materials, under tensile and compressive stress conditions indicate that failure is developed within a finite size zone. It is well established that the localized zone size is related to the grain size within the material under consideration. In the case of grout the size of such a region would be determined by the size of the cement particles and the asperities on the steel tube. In effect the failure zone can be regarded as being so thin as to approach a failure surface.

Analytical works, such as those reported by Zubelewicz and Bazant (1987) and Schreyer and Chen (1986), support these observations. A general description of the significance of the localization phenomenon is proved by Dougill (1987). It appears that localization is a characteristic phenomenon associated with fracturing behaviour. Heterogeneity and imperfections are the major causes of material failure localization in a nominally uniformly loaded specimen. In addition, failure may be localized by local variation in stress and strain. The effect of strain gradient can explain the mode of failure of the pile/grout interface. The difference of rigidity of the steel and the grout provides a large strain gradient which causes the failure along the interface, in addition to its physical nature as a line of weakness.

The assumption of the existence of a cohesive bond between the pile element and the grout is also supported by the examination of the extracted specimens. Visual observation of the tested pile showed traces of cement paste on the steel surface in the form of a very thin irregular layer. This can be explained by the development of adhesion of the grout to the steel surface.

8.2.3 ADHESION OF THE CEMENTITIOUS MATRIX TO OTHER MATERIALS

In an attempt to determine the nature of cement grout adhesion, Barnes et al (1970) used glass 'aggregates' set in cement paste to study the contact zone between aggregate and cement. They concluded that soon after coming into contact with the cement paste, the aggregate is covered by a thin layer of calcium hydroxide ($Ca(OH)_2$) on which the calcium-silicate-hydrates (C-S-H) later start to grow. At the same time, a porous zone (with a thickness of 10 - 40 μ) is formed between the dense cement matrix and the coating surface. Subsequently, this arrangement of layers is maintained regardless of the cement maturity.

Barnes et al work concerns bond with an ideal quartzite aggregate. Other work by Lian Hui-Zen (1982) has been carried out to the adhesion of cement on natural

aggregates (e.g. zeolite, carbonate). In these cases, chemical reactions were developed between the cement components and the aggregates. Water interchange between the two matrices was also observed.

An even more complicated picture emerges from the work of Kerzek and Vipulanandan (1985) on the adhesion of chemical grout to soil material. These workers classified the nature of bond as follows :

1- mechanical bond : an interlocking, frictional interaction due to the confinement of the two media.

2- reaction bond : developed by the formation of a new chemical product at the interface

3- exchange reaction bond : a reaction bond with multiple final products

4- oxide bond : an oxide coated surface created at the interface due to the presence of some trace of oxygen at the contact area

5- dissolution and wetting bond : originated by the development of physical forces, such as capillary forces

6- mixed bond : transition from one type of bond to another

These types of adhesion can be present separately or in combination in any particular case.

The situation that can emerge from the literature can be represented diagrammatically as shown in figure 8.3c. Irrespective of the details, it is evident that the surface layer is extremely thin and likely to depend on both the roughness of the steel and the morphology of the cementitious components.

8.2.4 BOND STRENGTH AND FRICTION RESISTANCE

British Standard (BS 8110) design specifications, for reinforced concrete structural elements, defines the bond strength between plain steel bar and concrete to be proportional to the square root of the concrete strength.

Billington et al (1978,1980), have established bond strength between steel pipe and cementitious grout in the same manner as BS 8110. Their experimental investigation was carried out on connection elements for offshore applications. The equation for developed bond strength takes account of the pile geometry as well as the pipe surface condition. A detailed description of their work is discussed in chapter 1 of

this thesis.

The American Petroleum Institute (API 1986) recommendations specify a design constant bond strength of 0.184 N/mm^2 for grouted plain pipe connection regardless of the grout strength and the pile geometry. Since this bond strength value included a safety factor of 6, and that according to Billington and Tebbett (1980), the ultimate bond strength is in the order of 1.105 N/mm^2. The safety factor given by the API (1986), when comparing results from previous reports is in the range of 2.5 to 33.6, with a mean value of 11.

In the present study, it has been found that the pile/grout interface is characterized by two strength parameters :

1 - Peak shear stress (bond strength)

2 - Residual shear stress (frictional resistance)

Figure 8.3b summarizes both interface strength characteristics as a function of the unconfined compressive strength of the grout. These results are compared with BS 8110, and the API (1986) recommended ultimate bond strengths.

From figure 8.3a, it is clear that the bond strength is developed with small interface deformation. During this stage, since the pile movement involves the grout matrix deformation, the interface resistance might well be related to the grout strength. When significant slippage has occurred, the interface resistance will be developed due to friction which is dependent principally on the surface condition. These observations are supported by the results given in table 8.1 and shown in figures 8.3a, and 8.3b. It can be seen that the frictional resistance is much less dependent on the grout strength than is the peak shear stress.

The pile surface condition (roughness) affects both bond strength and frictional resistance. During the test main programme, specimens M.T.T 1,2,3 were prepared from rings used in preliminary tests by sand blasting the surface for a second time. The test specimen of M.T.T. 4 was used for the first time. Consequently it had a different surface finish from the other ring specimens. For this reason, the interface resistances in the M.T.T 4 test were marginally larger than the ones given by the other tests, although the grout strength hardly varied. Accordingly, results for ring 4 are presented separately in figure 8.3b, without been considered in conjunction with the results from the other tests.

The effect of pile roughness needs more consideration than was possible in the present study. Surface roughness is defined by the surface profile. Tools such as the Taylor-Hobson device or macroscopic observations on the specimen steel surface can be used, although its application to a large surface might be impractical and very costly. It is not evident however whether such measurements do provide a useful description of roughness in the context of bond strength determination.

8.2.5 FRICTIONAL BEHAVIOUR FOR LARGE DISPLACEMENT

During the main torsion test programme, the shear stress was additionally recorded on an X-Y plotter. Part of the plotter outputs for each pile element (ring) are presented in figures 8.4. It is clear that the shear stress along the interface shows a fluctuating behaviour with slip displacement. Such behaviour has been also observed during pull-out tests on grouted piles by Cox and Reese (1976) as well as during the test PLT 1 carried out during the present investigation on the grouted pile behaviour.

These stress fluctuations are typical of stick - slip phenomena associated with frictional behaviour. The fluctuation can be explained by the failure of the grout along an irregular pile/grout surface. The presence of such irregularity might be due to the "bad fit" of the failed contact surface around the ring pile element and that of the grout matrix. The stress fluctuation can however be caused by the wear of such irregularities which happen when the pile element is subjected to a large slip displacement.

Once the rotation direction had been reversed, the stress fluctuation decreased and disappeared within a couple of millimeters of reversed slip displacement. It seems possible that the surfaces of both the pile ring and the grout had deteriorated in such a way that they became parallel, allowing a simple frictional contact between the pile ring and the grout. In this case slip displacement occurred without an increase of normal stress, as will be discussed later in this chapter. The assumptions underlying the explanation of stress fluctuation behaviour are shown diagrammatically in figure 8.5.

8.2.6 STRESS CYCLING

The shear stress path history applied to the ring 2 in the main torsion test series (specimen M.T.T 2) during cyclic loading including the bond failure, is presented in figure 8.6. The cyclic stresses were applied during the fracturing stage (stage A), and the frictional stage (stage B) of the interface behaviour. Both stages are illustrated in the

larger scale plot in figures 8.7.

The cycling effect can be characterized by successive reductions of the stiffness in each cycle during the fracturing stage of the bond behaviour, and by progressive slip during the residual frictional stage of the interface (stage B).

Stiffness degradation is a well established phenomenon for concrete materials. Descriptions of such behaviour, based on fracture mechanics are reported by Gylltoft (1983) for material under tensile loading. This approach to represent stress cycling behaviour, during the fracturing stage can be used to model the pile/grout interface under cycling loads.

A simplified representation of the interface behaviour is presented in figures 8.8, for both stage A and stage B. There is much in common between the interface behaviour and that of concrete material under cyclic load. Spooner and Dougill (1985a) reported that, for fracturing material like concrete, there are two types of dissipating energy related to the loading and unloading of fracturing material :

1- energy dissipation related to the damage due to the loading of the material.

2- energy related to repeated loading due to material damping effect.

Dougill (1985a) suggested that different criteria could be used to deal separately with the different energy components, providing more flexible approach to describe material behaviour

The fracture theory by itself presented by Dougill (1976) excluded consideration of permanent plastic deformation under monotonic load, and hysteresis response under cyclic load. Dougill's idealisation of the fracture requires that any unloading and re-loading sequence is carried out on the same path in stress (or strain) space, and with the same stiffness. In addition, complete stress unloading of the material (i.e. zero stress) at any stage of the loading process produces no permanent deformation (i.e. zero strain). However a combined approach of fracturing theory with additional terms taking account of the two forms of energy dissipation can be envisaged.

Bazant and Kim (1979) used plasticity with a form of fracture theory to introduce permanent plastic deformation for a fracturing - plastic material model. Additionally, they extended this approach (i.e. introducing an additional term of energy dissipation) with their endo-chronic material theory to model hysteresis behaviour such as

that observed for concrete. Similar results have been obtained using a combination of conventional plasticity and the theory of progressively fracturing solid by Rida (1981), as reported by Dougill (1985a). It is suggested that approaches of this kind will have a use in developing more detailed analytical models of interface behaviour.

It is interesting to note that once slip displacement (pile rotation) is resumed after an unloading and reloading cycle, the shear stress displays a "localized" peak stress. This may be caused by a "locking" phenomenon which happens once the shear stress is unloaded and the slip displacement is stopped. The localized peak apparently represents the additional effort required to overcome the material interlocking. Once the pile slip is continued the shear stress resumes the value associated with the slip before the stress unloading cycle.

8.3 DILATANCY

Despite the narrowness of the shear zone at the interface, behaviour is affected by material dilatancy so that shear is accompanied by the generation of direct stresses normal to the interface. These normal stresses result in a form of radial confinement, which might be due to the confinement of the pile specimen within a stiff surrounding, or even to a non uniform steel surface.

As was discussed in chapter 7, circumferential strain gauges were installed on the concrete pocket for every ring pile specimen. It was demonstrated that the outputs of these gauges reflect the existence of normal stresses along the slip interface. An expression for the radial normal stress as a function of the gauges outputs ε_{SG} has already been given in chapter 7. Development of circumferential strain and so normal stress was observed in all the tests undertaken.

It is important to note that the outputs of the four strain gauges placed at the same level corresponding to the same ring pile specimen were not uniform and their symmetry was not maintained. The change of the gauge outputs was similar, although they differed by a margin of as much as $\pm$ 40%, with respect of their average value, for large slippage values. Because of this, interpretation in terms of a value of normal stress, based on the expression in chapter 7, is uncertain. However, the relevance of these results lies in the qualitative assessment of the interaction between the different parameters involved during the bond failure and the frictional behaviour of the interface. The results are given in terms of the average value of the gauges outputs for each ring specimen.

8.3.1 SLIP - CIRCUMFERENTIAL STRAIN RELATIONSHIP

The average circumferential gauge outputs are plotted against the slip displacement in figures 8.9 for both P.T.T. and M.T.T. tests. The results, particularly from the main series, show an early development of the material dilatancy accompanied by the bond failure. The breakdown of the 'adhesion' or bond is combined with a loss of the lateral effect. This might be explained by a transition behaviour between two phases of the interface condition. Further pile slip results in a steady increase of the dilatancy phenomenon. The lateral strain values obtained during the preliminary investigation and the main investigation have a different order of magnitude, because during the main investigation the gauges were glued to a steel shim which caused a decrease in the gauges deformation and so the measured outputs. This underlines the earlier remarks that the results for the circumferential strain must be regarded as indicative values rather than a true quantitative value. In figures 8.9,the numbers on the graph, show the progression of the slip and circumferential strain observed during the tests.

Once the slip had been reversed, all results showed an instantaneous drop in radial effect to a residual value which is approximately maintained for a continued large slip. In the case of test M.T.T. 4, a slip displacement in the opposite direction relative to the initial position of the pile caused an increase of the dilatancy. For large pile slip displacement, the dilatancy effect shows a steady increase in all tests carried out. This effect would increase the frictional shear capacity of the interface and so would lead to stable hardening behaviour observed at large values of slip.

8.3.2 DILATANCY AND SHEAR STRESS

The circumferential strain developed for different values of shear stress is shown in figures 8.10. These results can be interpreted in terms of a yield surface, in shear stress - normal stress space if the circumferential strain is transformed to normal stresses, as described in chapter 7. For monotonic loading, as shown in figure 8.10b, the results, following initial behaviour controlled by bond breakdown, suggest a form of Coulomb - Mohr yield surface to describe the interface behaviour. This idealization has been adopted by a number of workers, for instance Desai (1981, 1984), Ghaboussi et al (1986) and, Zamen and Desai (1983). Here again, numbers are introduced in figures 8.10 to indicate the progression of the paths (shear stress - circumferential strain) observed during the tests.

During all the tests carried out, initial application of shear stress on the interface generated a significant dilatancy. During initial breakdown, there is a reduction of both shear stress and normal stress. Once frictional slippage occurs, the circumferential strain is quickly built up with a relatively small (or no) increase of the shear stress. Reverse slip causes a considerable reduction in the circumferential strain and associated dilatancy. For a large value of slip, both the shear stress and the circumferential strain showed a steady increase with slip.

One point of importance is that a significant normal stress is built in even after the shear stress is removed following unloading. This residual normal stress suggests the development of an interface zone where deteriorated material is locked and confined between the ring pile element and the surrounding grout matrix. This would fit the structure suggested in figure 8.3c.

8.3.3 GROUTED INTERFACE BEHAVIOUR MODELING

While the pile remains bonded to the grout, the interface behaviour is governed by the response of the grout to condition of shear stress. The failure criterion is directly related to that for the grout material. Dilatancy effects are important so that fracture or yield could be described using Mohr-Coulomb, Drucker-Prager or other similar yield condition in shear stress - normal stress space. However, expression of the yield function in terms of slip could be more convenient, especially if the theory derived for progressive fracturing solids was applicable and led to appropriate expression for the change of stiffness due to breakdown.

Once significant slip occurs, which means that there has been complete breakdown of adhesion bond, the yield characteristics of the interface change. The interaction between the resisting shear stress and the normal stress developed by dilation will be governed principally by the nature of the failed surface and the degree of the grout deterioration along the interface. This interaction can be idealized as a contact or frictional problem.

Recent analytical studies on contact problem modeling have been based on Coulomb's law. Fredriksson (1975) had used a Coulomb type criterion, with an associative slip hardening condition. Curnier (1984) developed a plasticity based friction theory where the Druker/Prager yield criterion was used. In this theory the plastic behaviour is formulated with a non associative relationship between the yield criterion

and slip to give an improved description of dilatancy.

The normal stress developed, once the bond has failed, has to be considered as dependent on the history of slippage. Consequently the origin of the interface yield surface under slip conditions moves from the origin of the (τ,σ_n) space, with changes in slip. Clearly the determination of normal stress effects and the development of residual stress should be investigated further in more detail.

8.4 SUMMARY

The idealized mechanism of bond breakdown at grouted interface has the same characteristics as that of an ideal fracturing material. The evolution of shear stress to a peak, and its sharp reduction to a residual frictional resistance, clearly observed in figure 8.3a, would be a suitable model of the interface shear/slip variation. The general paths of slip, shear stress, and lateral effect, observed during the tests, are summarized in figure 8.10.

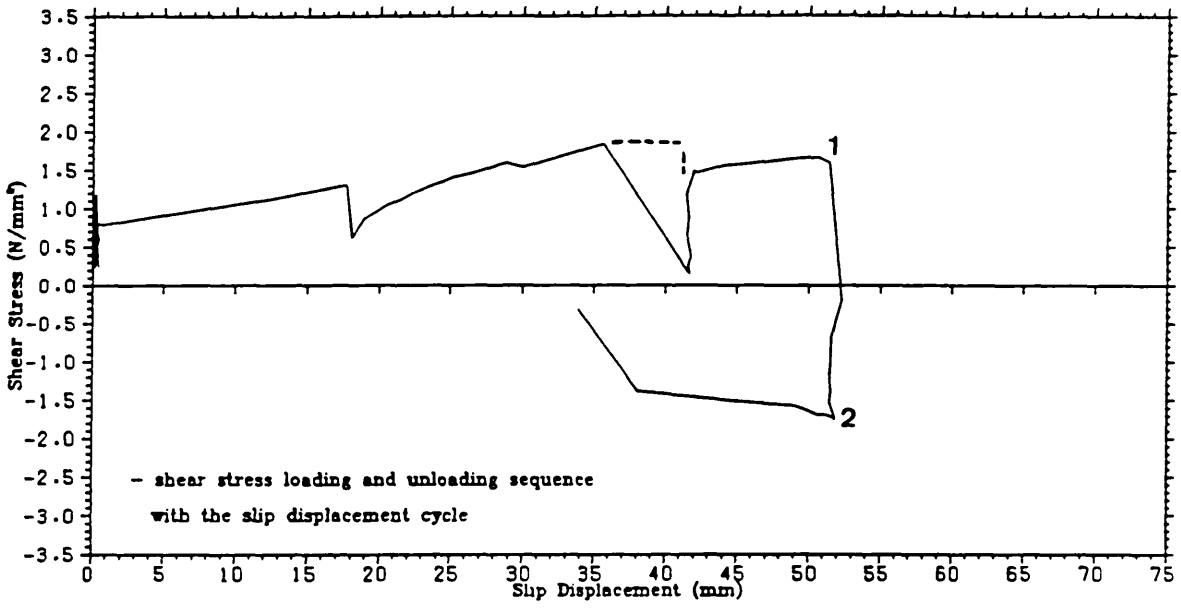
The strength criterion of the pile/ grout interaction requires more careful representation than those of common materials because two phases of material behaviour must be taken into account. Based on plasticity, the model presented here (figure 8.11), is deduced to fit test results obtained during this investigation. The fracturing behaviour can be regarded as a transition from the bonded state to the frictional state. In all tests carried out, this transition was stable, being accompanied by a progressive slip displacement.

The data provided are not sufficient to develop a comprehensive model. It is evident however that reliance on the observed peak value of bond stress as a measure of shear resistance is not satisfactory. The uncertainties can be hidden by using large load factors but these are really factors of ignorance of the true behaviour. A conservative approach might be to base design on a plastic analysis using the minimum residual shear stress. However, this could be uneconomic for long piles for which significantly large shear - slip displacement could be expected prior to failure. Here hardening due to dilatancy is likely to provide a substantial increase in failure load over that estimated using the lower bound, minimum shear stress, approach.

Table 8.1 : SUMMARY OF THE BOND STRENGTH AND FRICTIONAL RESISTANCE OBTAINED FROM THE TORSION TESTS

Torsion Test	Ring's Number	Grout's age (Days)	Bond strength N/mm^2	Residual frictional resistance (N/mm^2)	Grout compressive strength (N/mm^2)
P.T.T. 1	1	3	-	0.72	34
P.T.T. 2	2	7	-	0.65	42
P.T.T. 3	3	10	-	0.60	45
M.T.T. 1	1 *(Re-sand blasted)*	1	1.00	0.54	18
M.T.T. 2	2 *(Re-sand blasted)*	8	1.72	0.67	42
M.T.T. 3	3 *(Re-sand blasted)*	37	1.83	0.63	62
M.T.T. 4	4* *(Used for first time)*	45*	2.85*	1.13*	64

API (1986) recommeded design bond strength = 0.184 N/mm^2



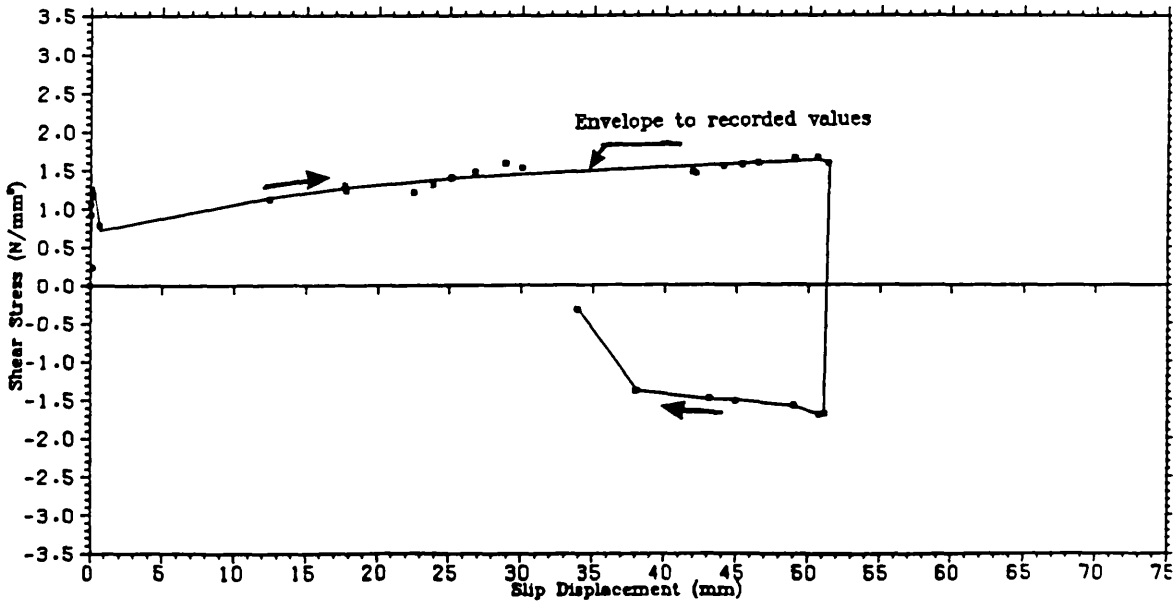
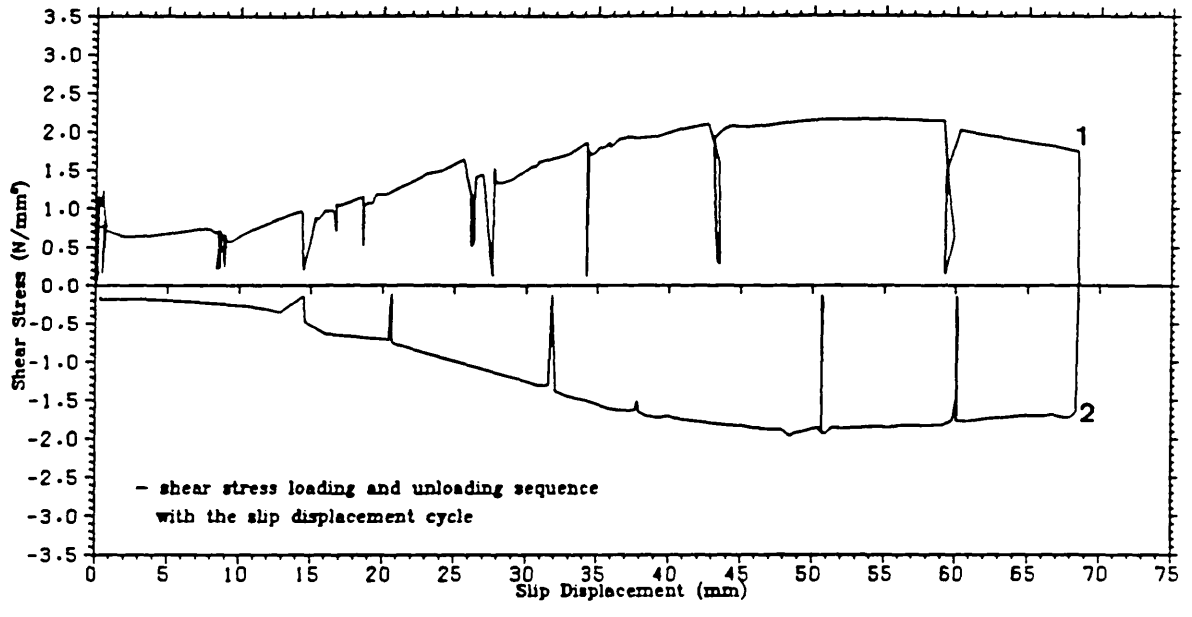


Figure 8.1a : SHEAR STRESS - SLIP (from Preliminary Test - Ring 1 -)



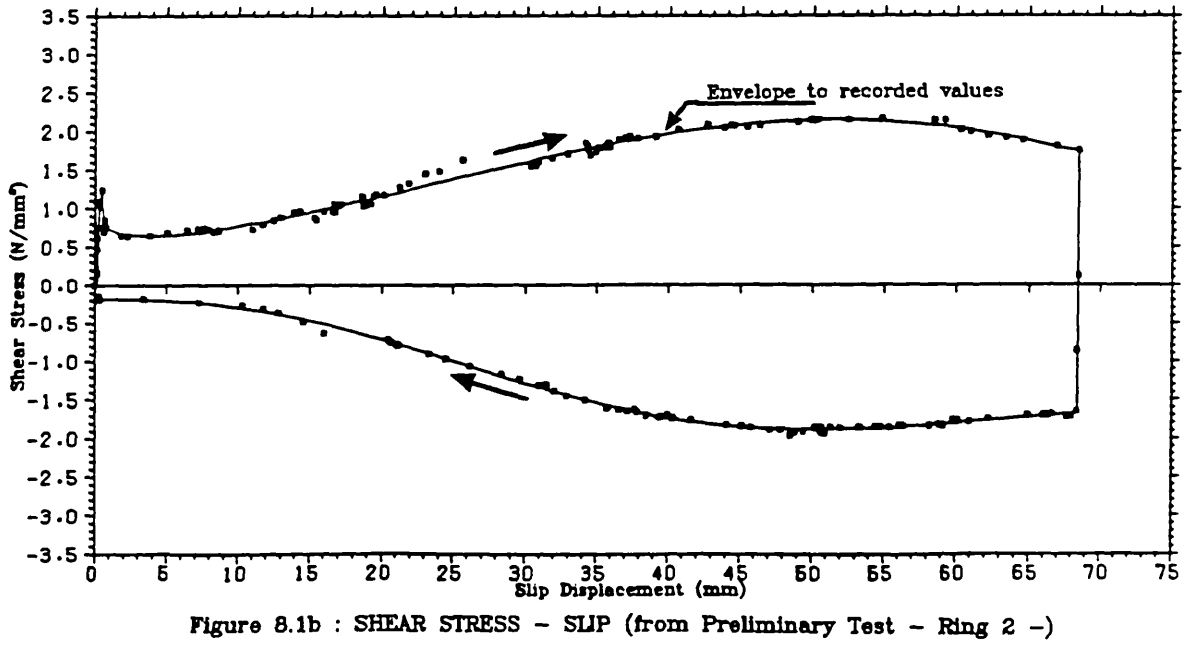
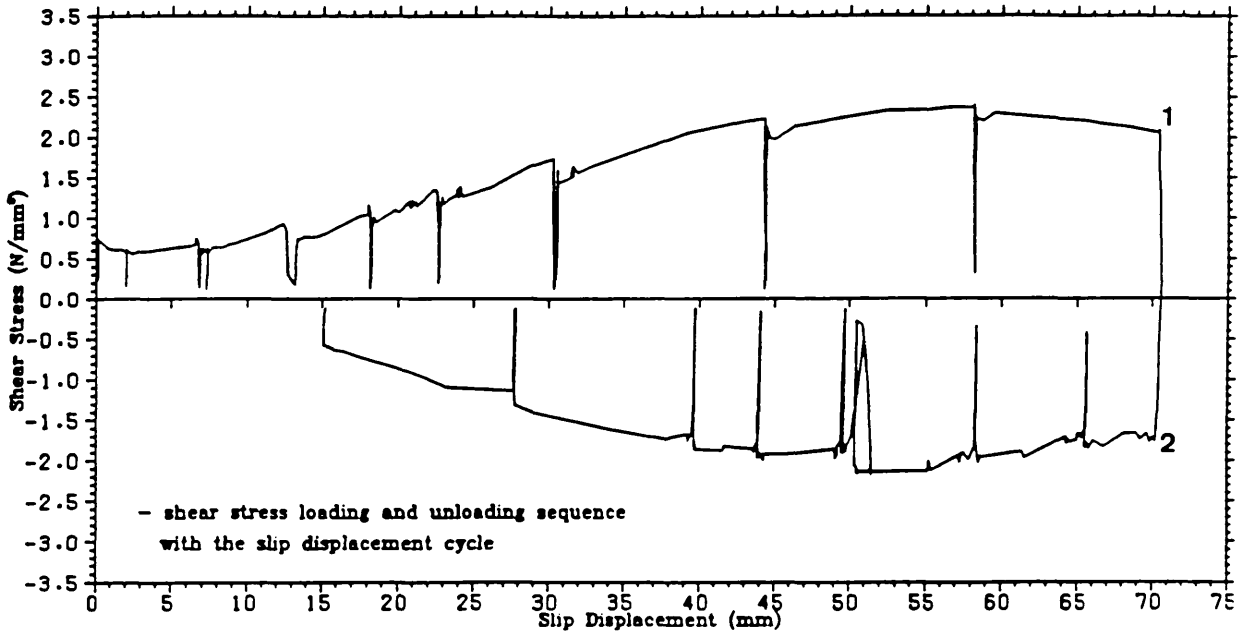


Figure 8.1b : SHEAR STRESS – SLIP (from Preliminary Test – Ring 2 –)



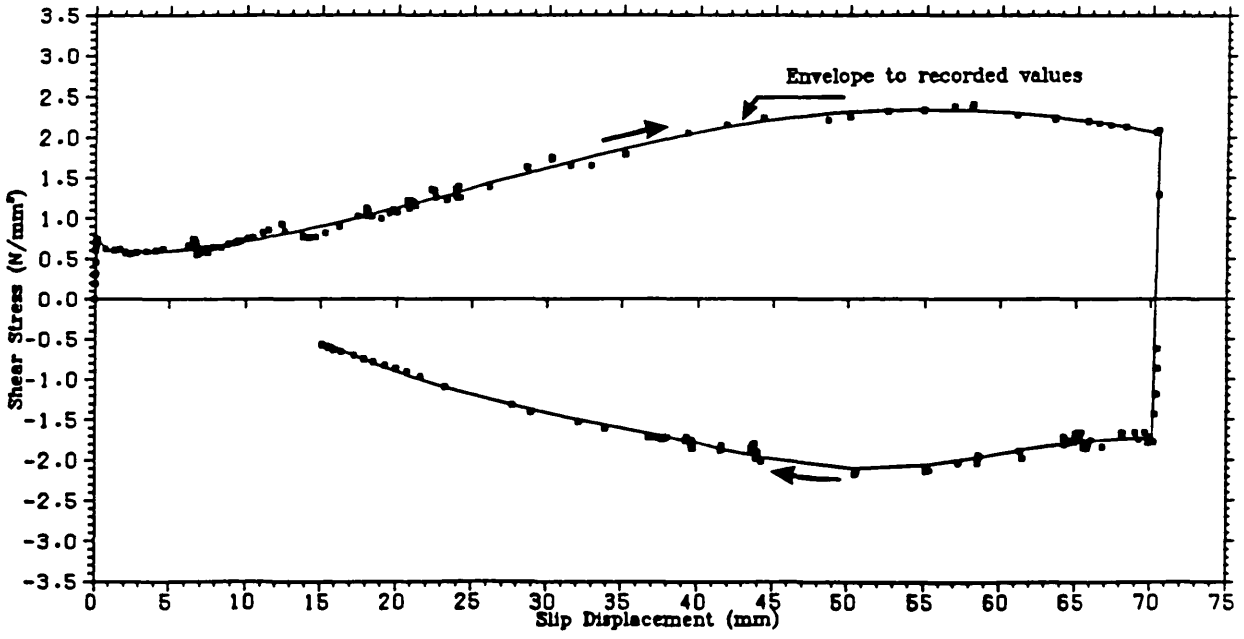
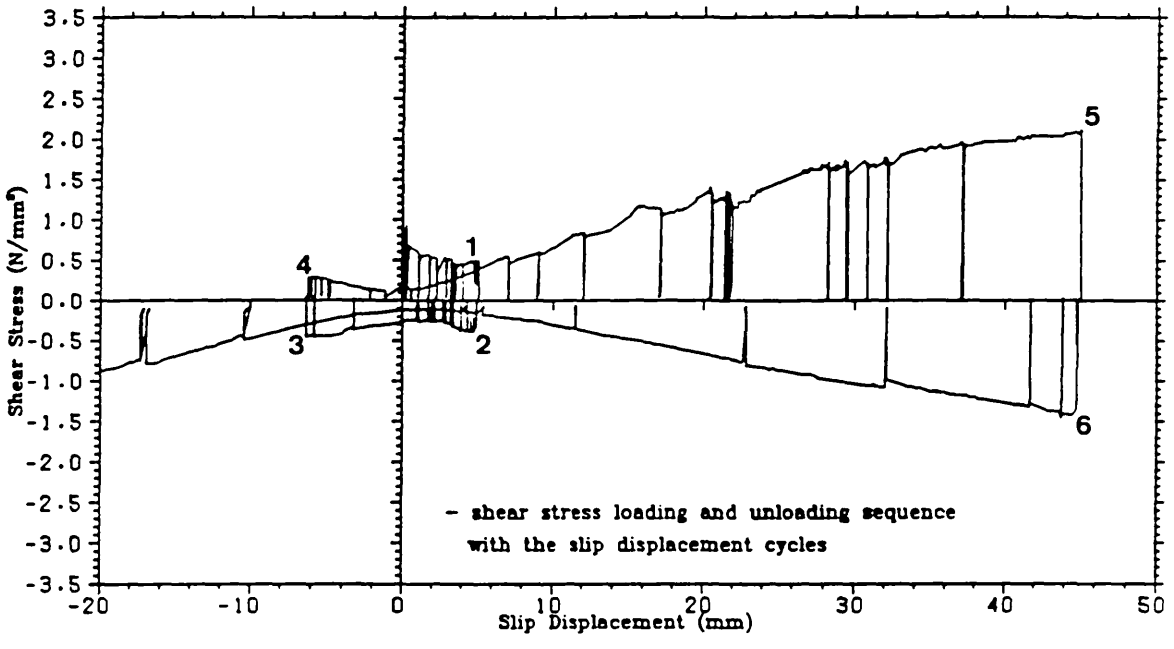


Figure 8.1c : SHEAR STRESS – SLIP (from Preliminary Test – Ring 3 –)



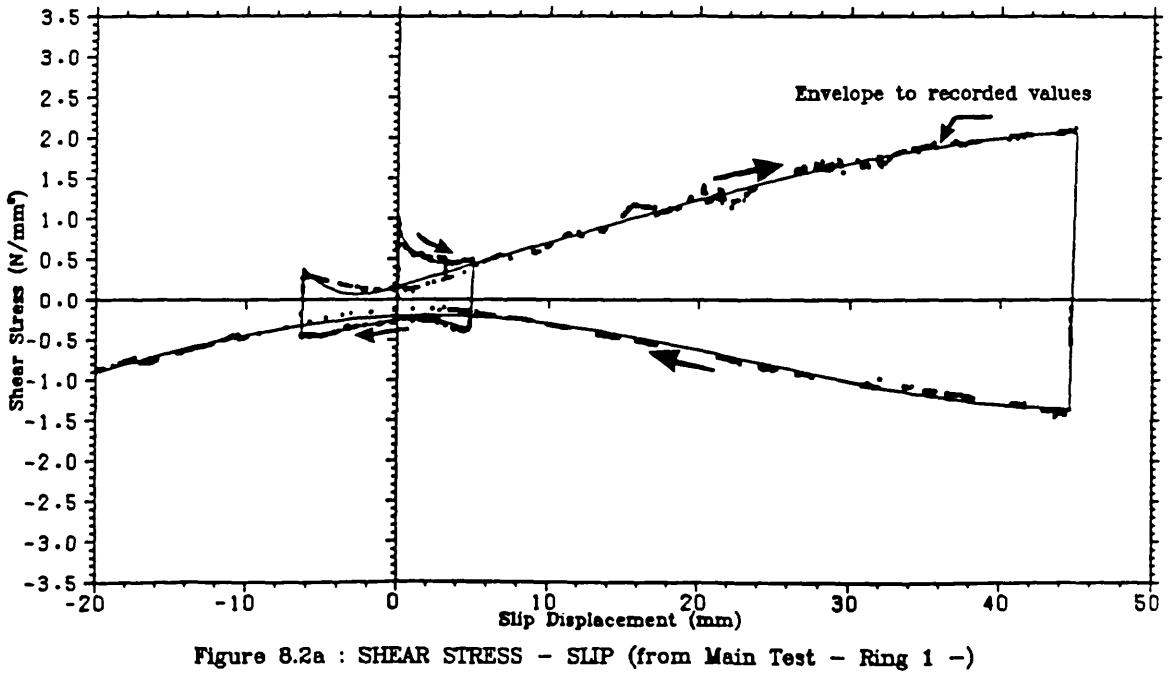
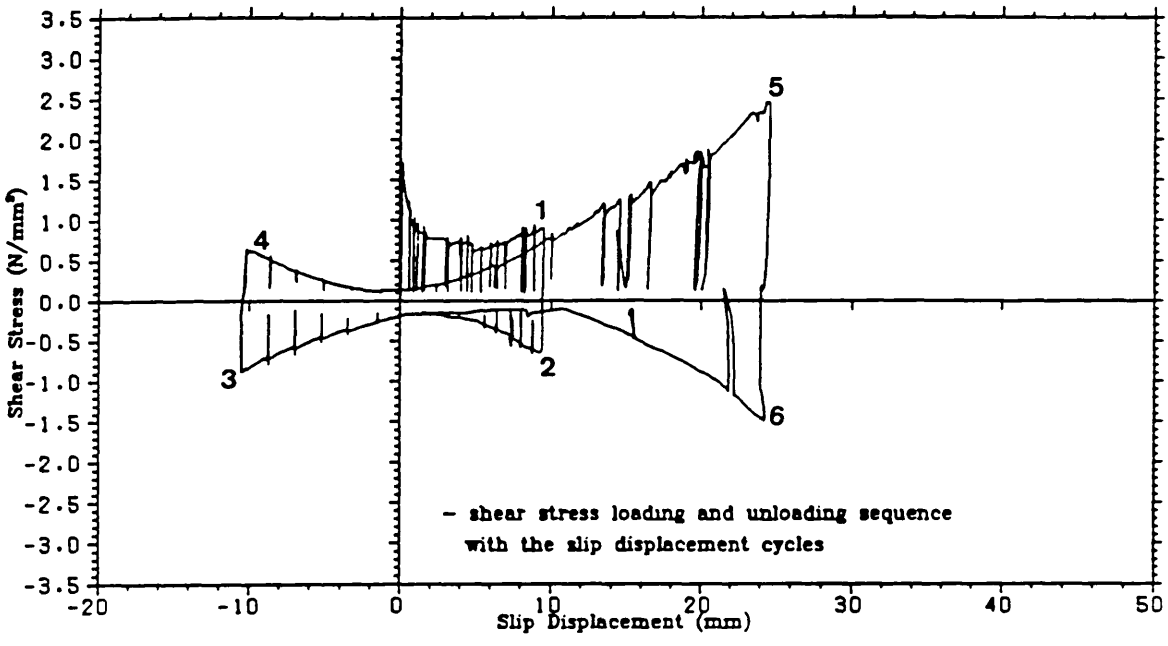


Figure 8.2a : SHEAR STRESS - SLIP (from Main Test - Ring 1 -)



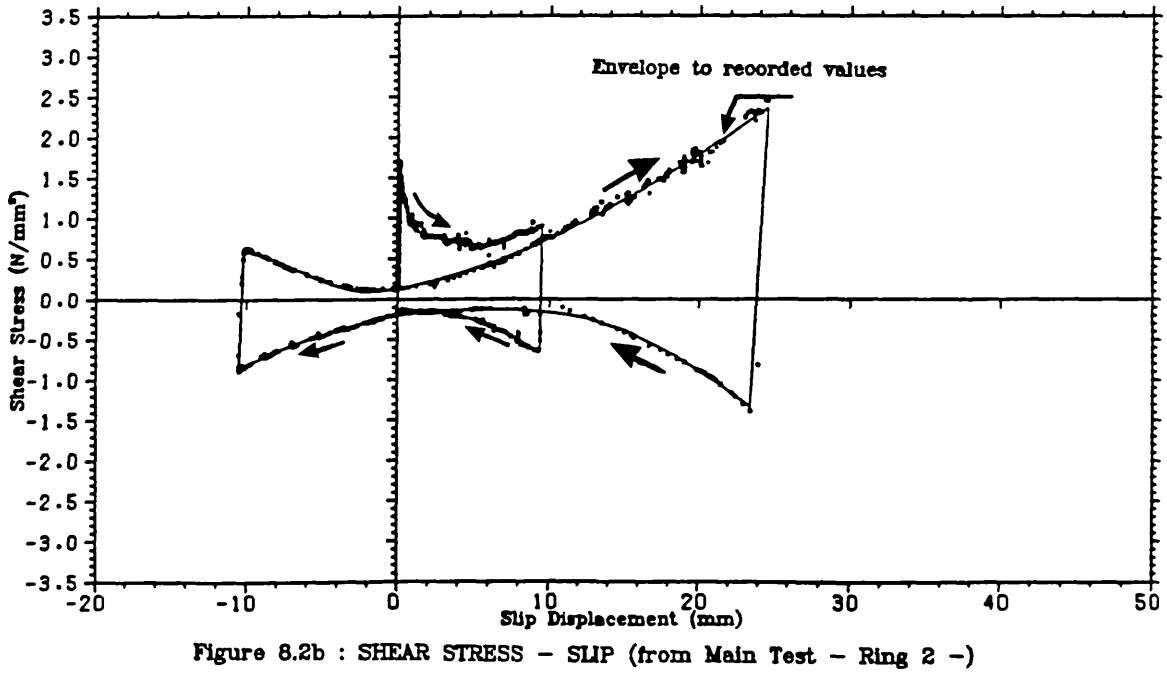
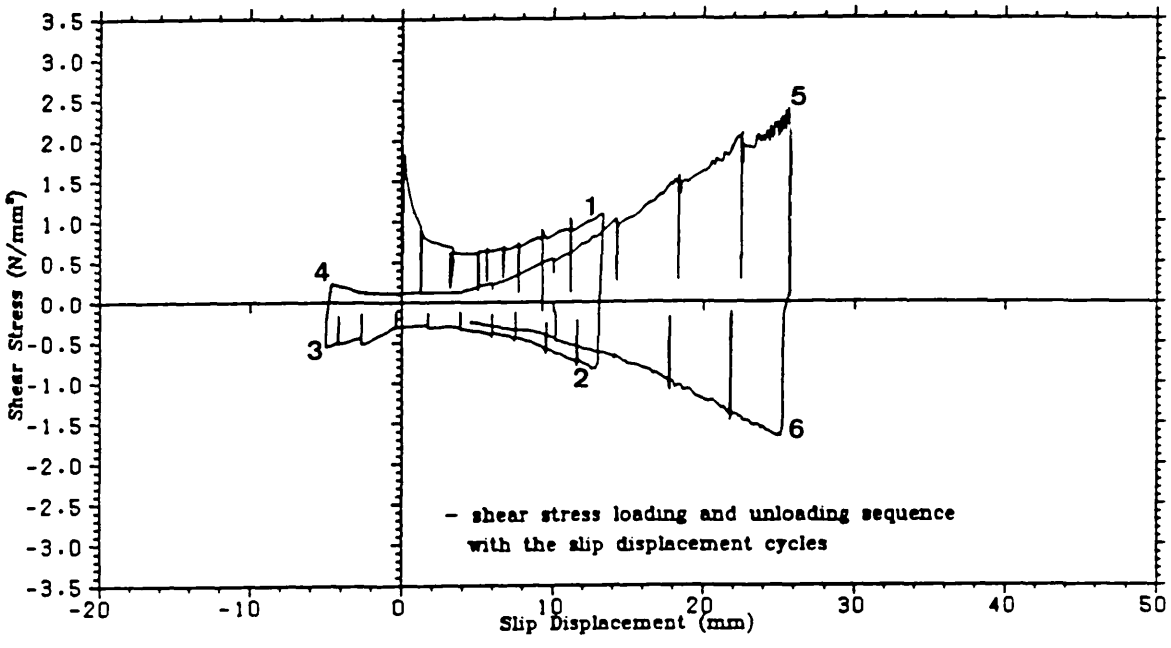


Figure 8.2b : SHEAR STRESS – SLIP (from Main Test – Ring 2 –)



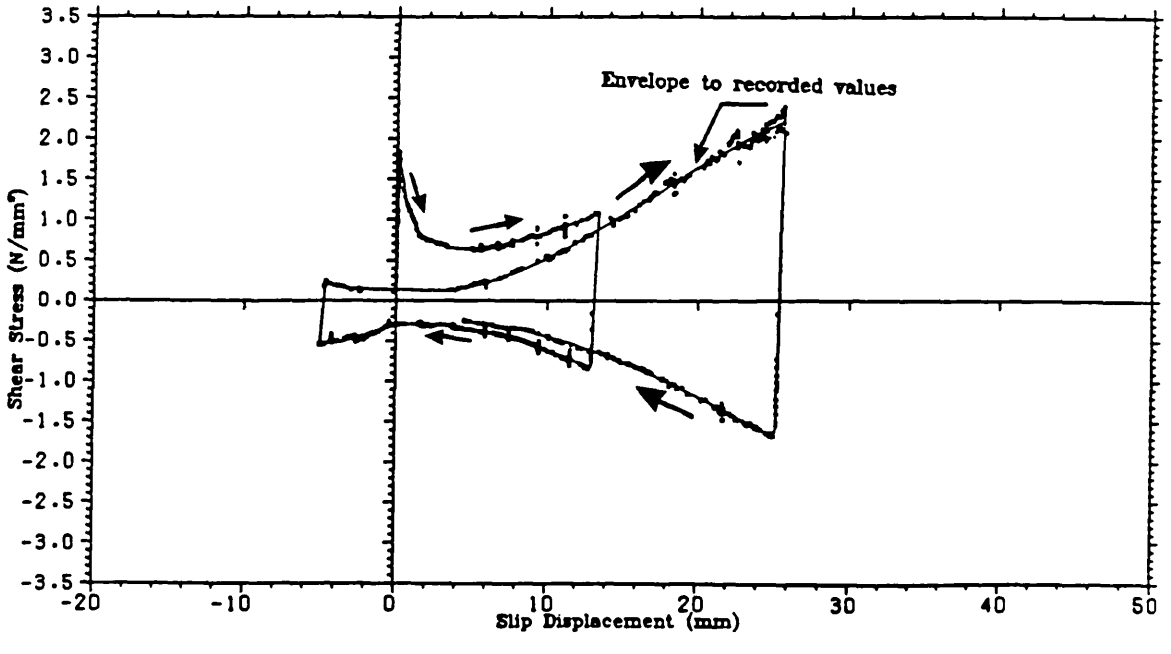
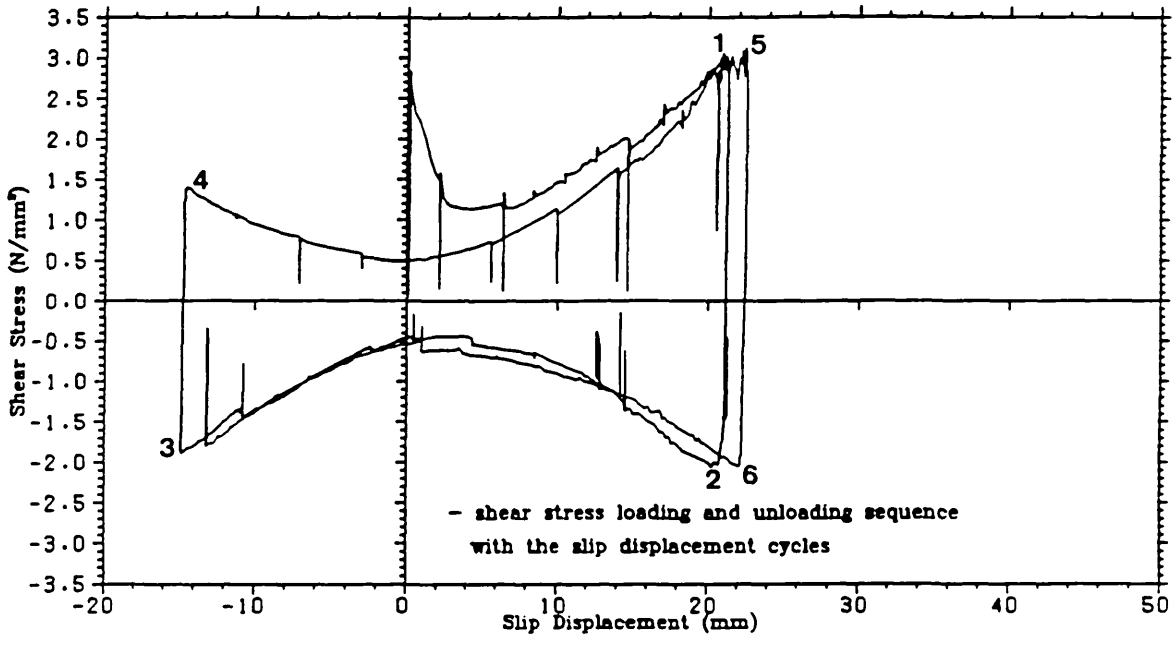


Figure 8.2c : SHEAR STRESS – SLIP (from Main Test – Ring 3 –)



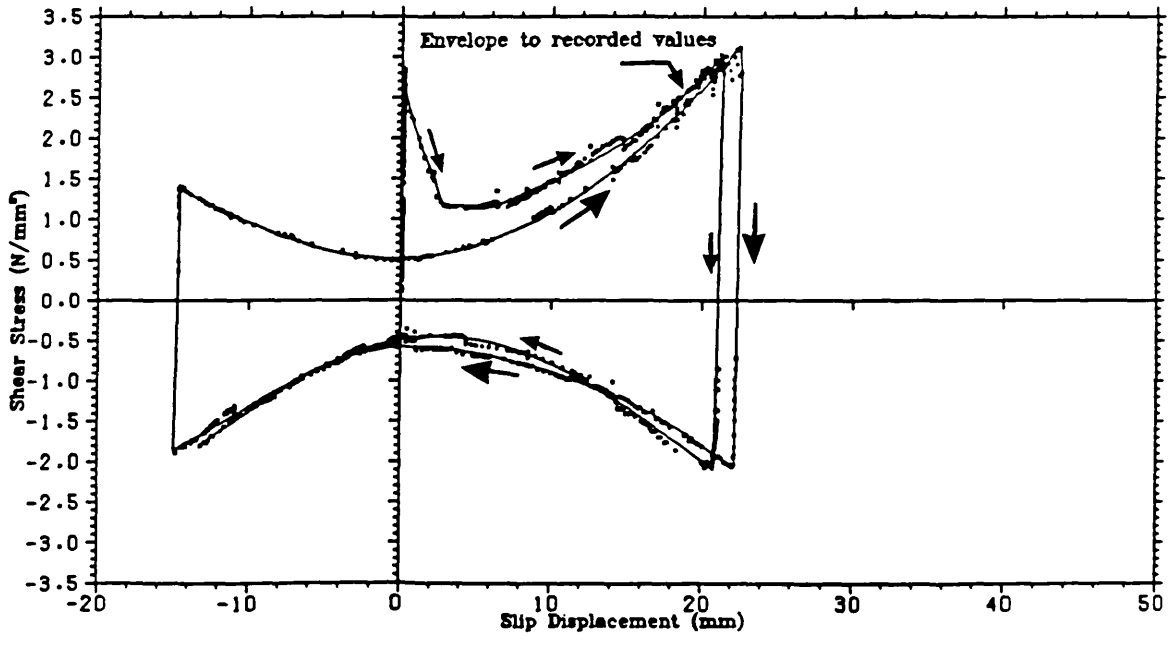


Figure 8.2d : SHEAR STRESS – SLIP (from Main Test – Ring 4 –)

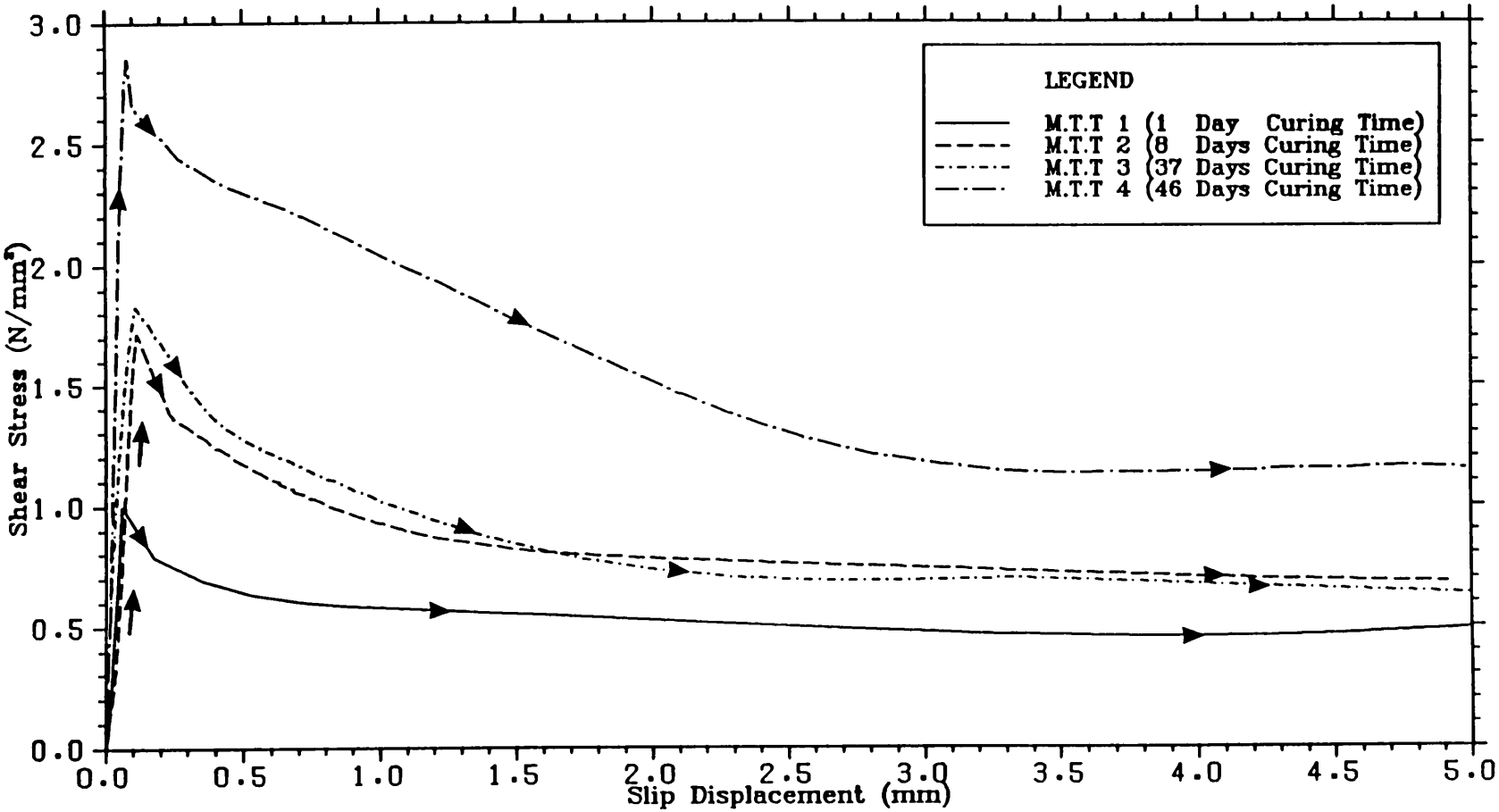


Figure 8.3a : SHEAR – SLIP RELATIONSHIP FOR INITIAL STAGE OF SLIP

(showing the effect of bond breakdown and development of frictional resistance)

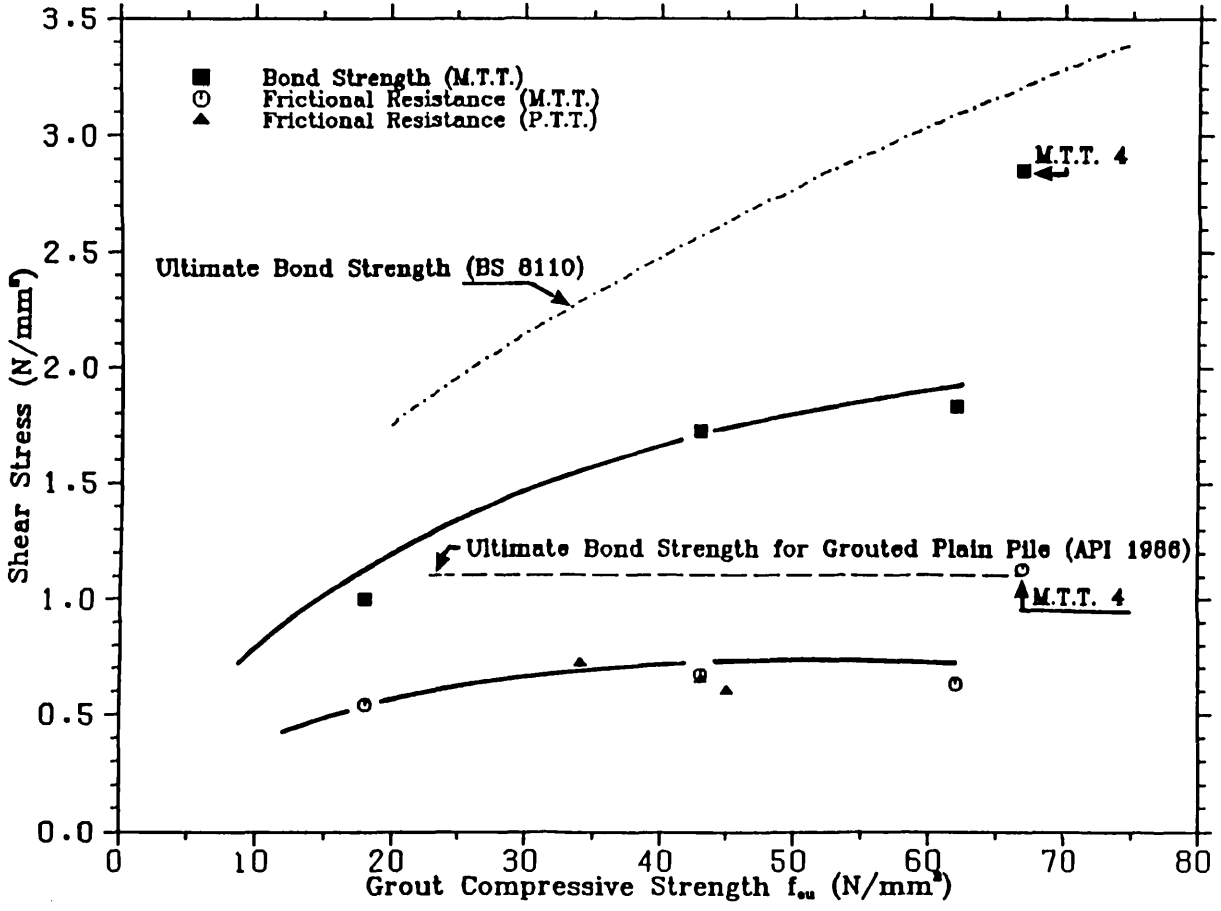


Figure 8.3b : BOND STRENGTH AND RESIDUAL FRICTIONAL RESISTANCE WITH GROUT STRENGTH

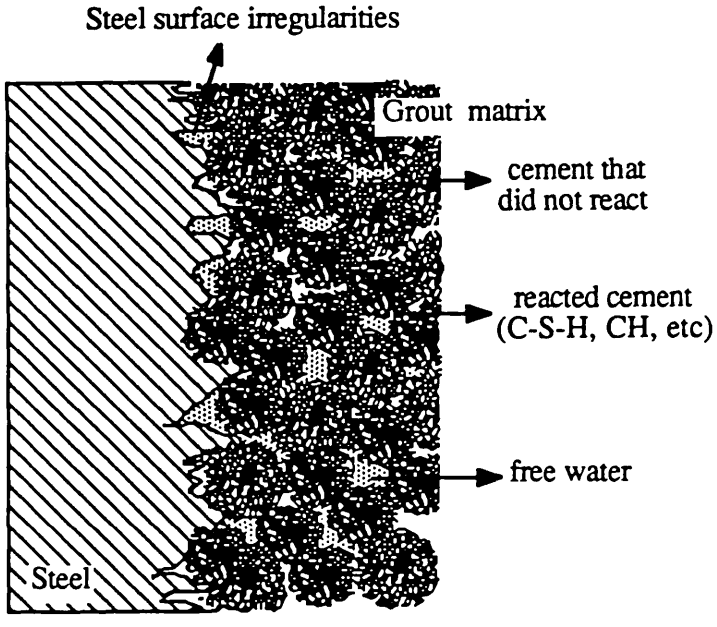


Figure 8.3c : **DESCRIPTION OF THE NATURE OF BOND BETWEEN STEEL SURFACE AND GROUT**

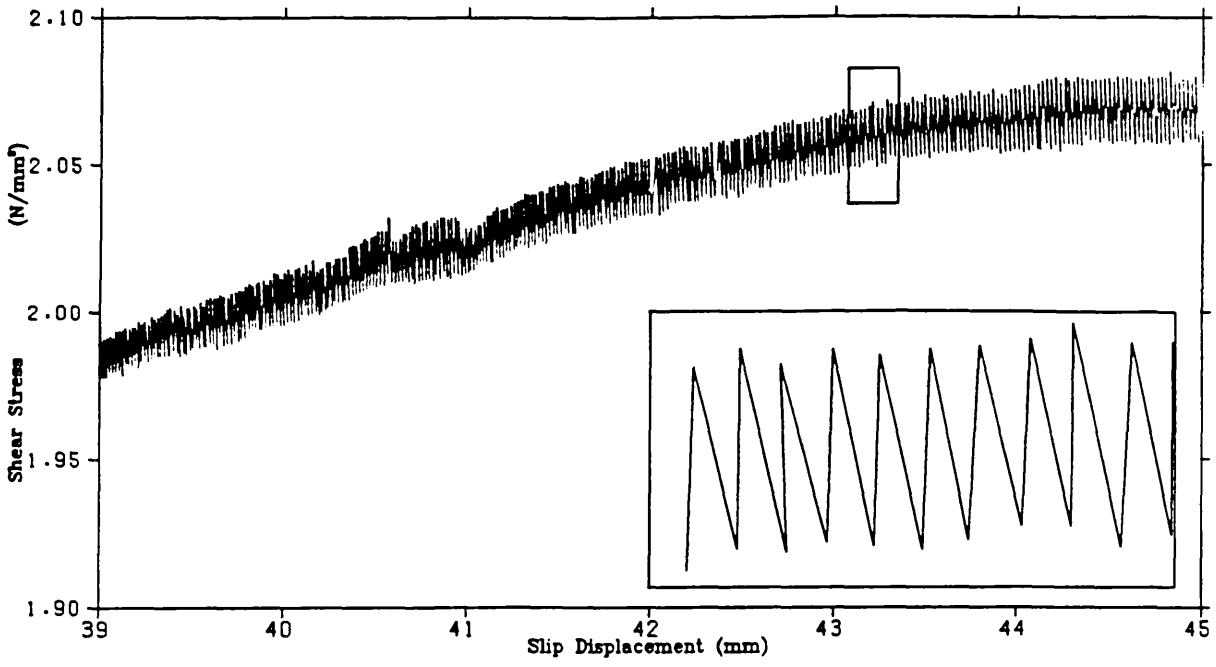


Figure 8.4a : SHEAR STRESS FLUCTUATION – SLIP (Main Test Series – Ring 1)

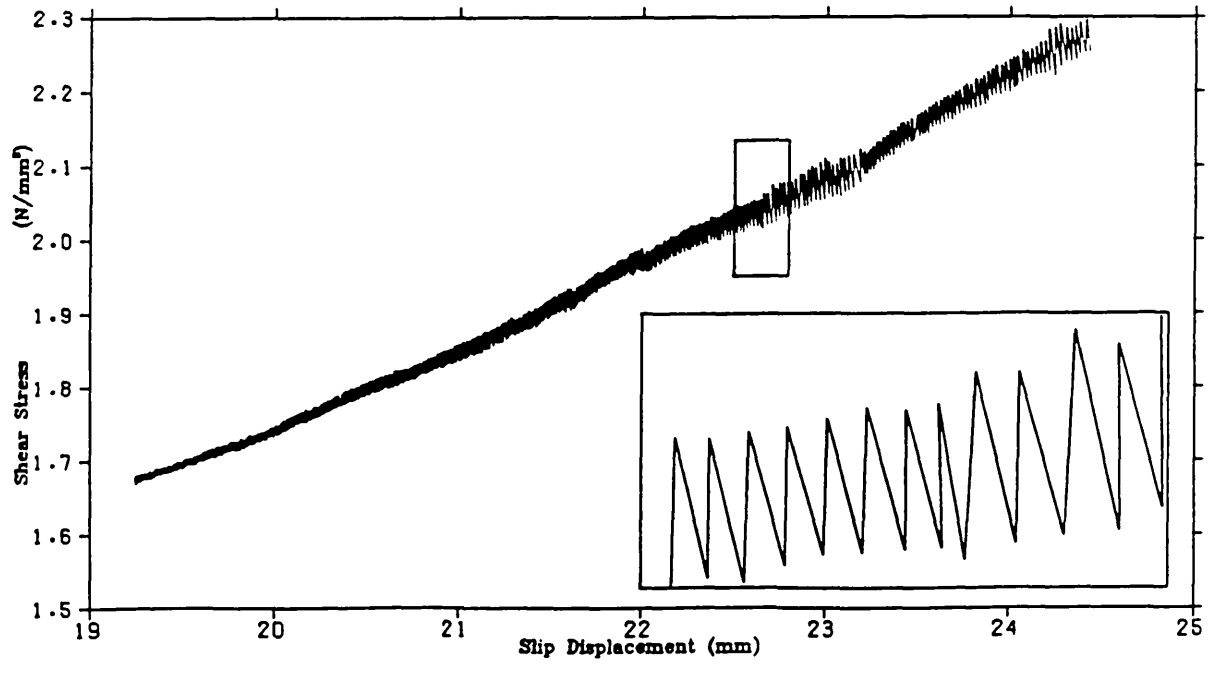


Figure 8.4b : SHEAR STRESS FLUCTUATION – SLIP (Main Test Series – Ring 2)

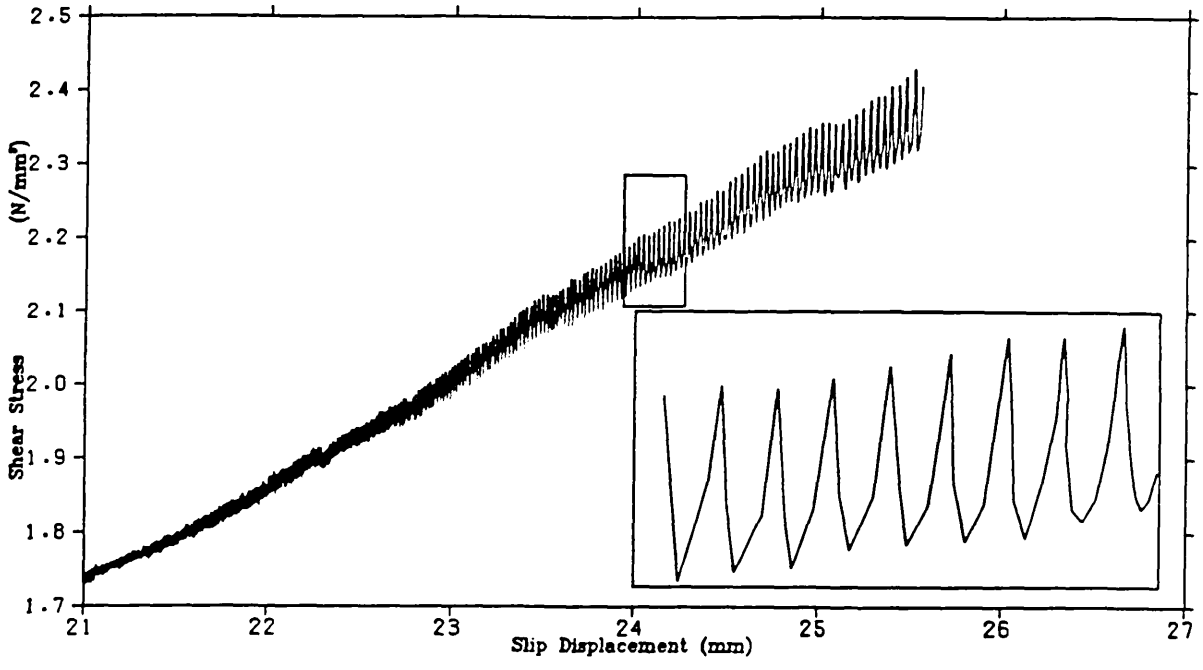


Figure 8.4c : SHEAR STRESS FLUCTUATION – SLIP (Main Test Series – Ring 3)

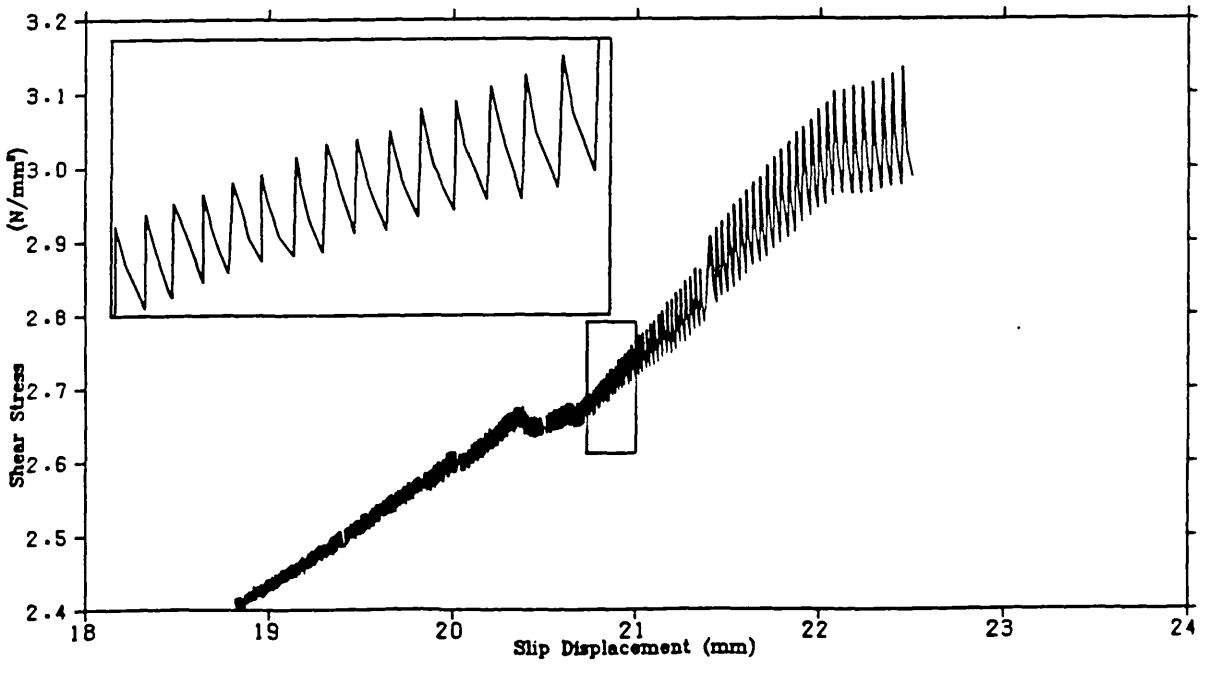
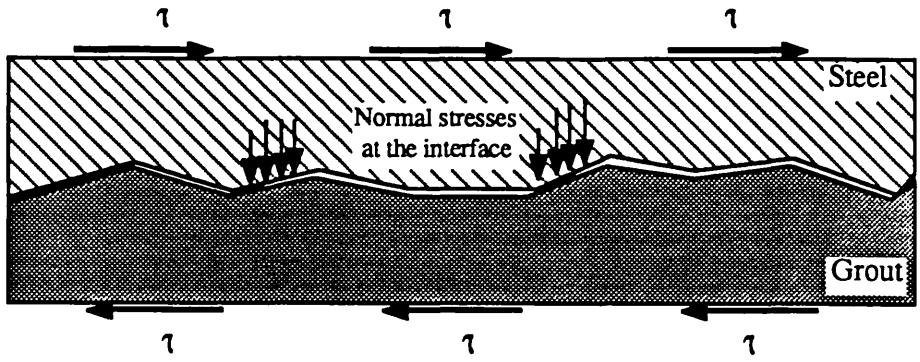
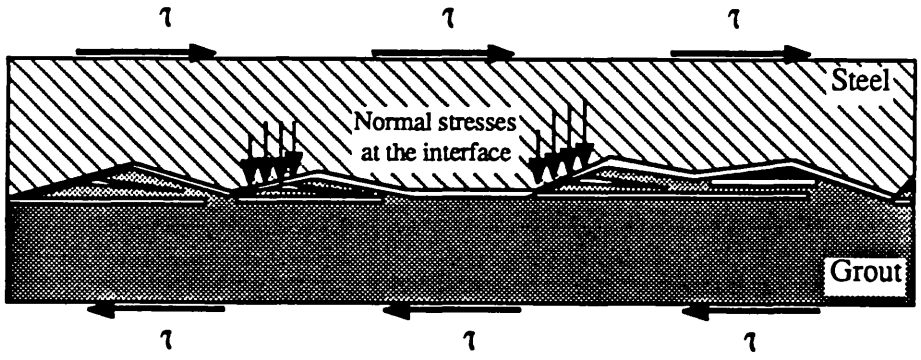


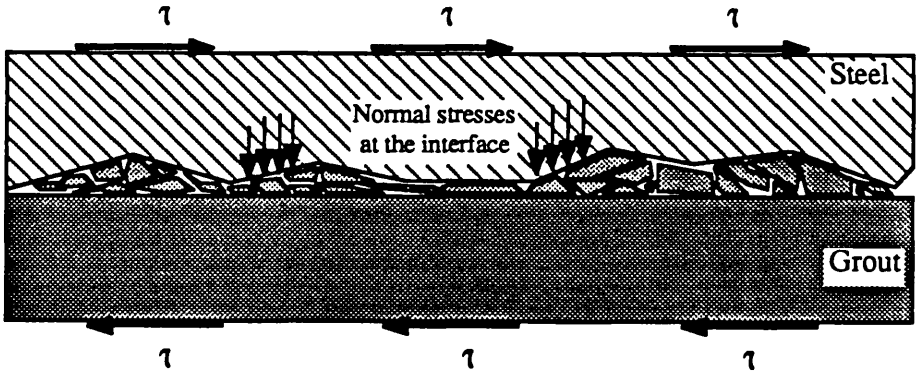
Figure 8.4d : SHEAR STRESS FLUCTUATION – SLIP (Main Test Series – Ring 4)



Step 1 : Bond break down at pile/grout interface and formation of slip surface



Step 2 : Grout damage at the pile/grout interface



Step 3 : Material degradation at the pile/grout interface due to large slip displacement

Figure 8.5 : **SURFACE CONDITIONING CAUSED BY LARGE SLIP DISPLACEMENT**

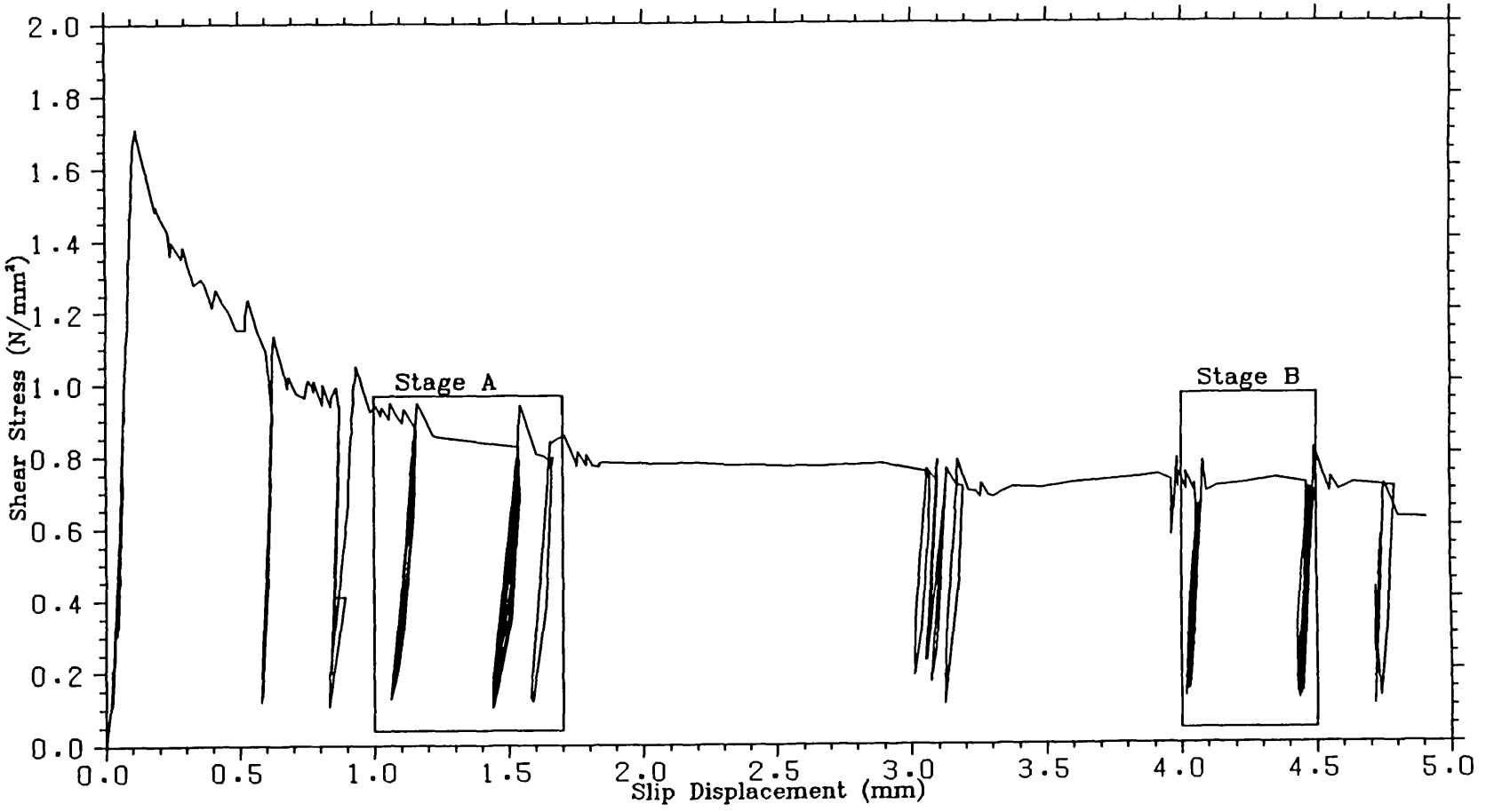


Figure 8.6 : EFFECT OF CYCLIC LOADING ON SHEAR STRESS – SLIP RESPONSE
(Main Test Series – Ring 2 –)

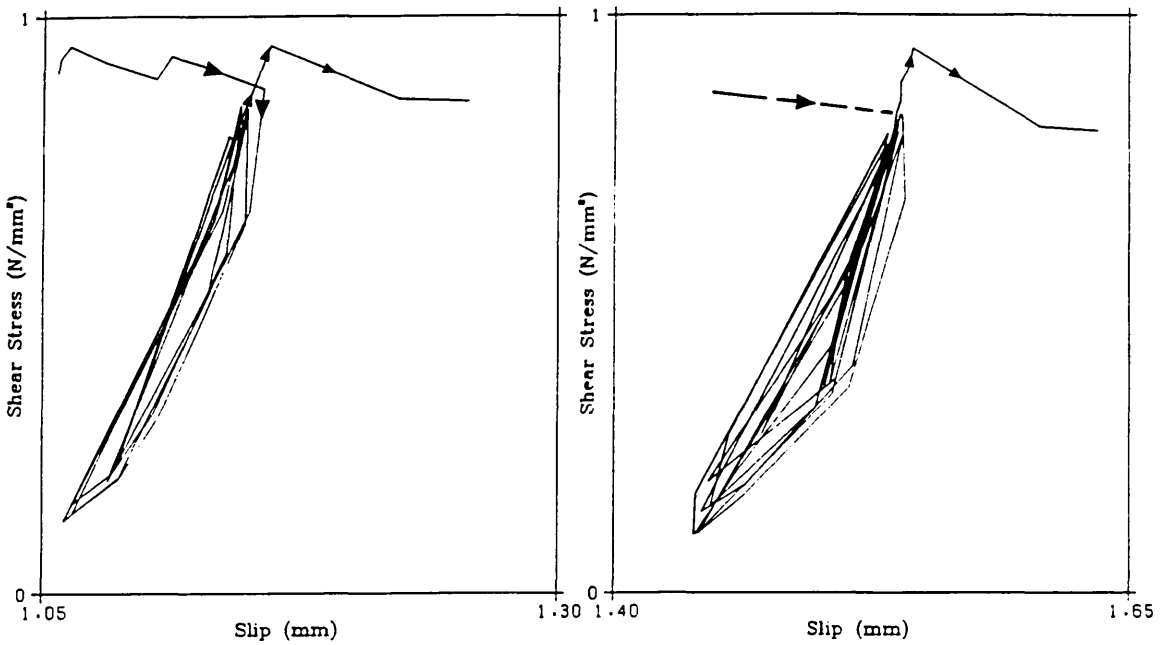


Figure 8.7a : SHEAR STRESS – SLIP CYCLING (Ring 2 – Stage A –)

(Stage A – Progressive breakdown / fracture)

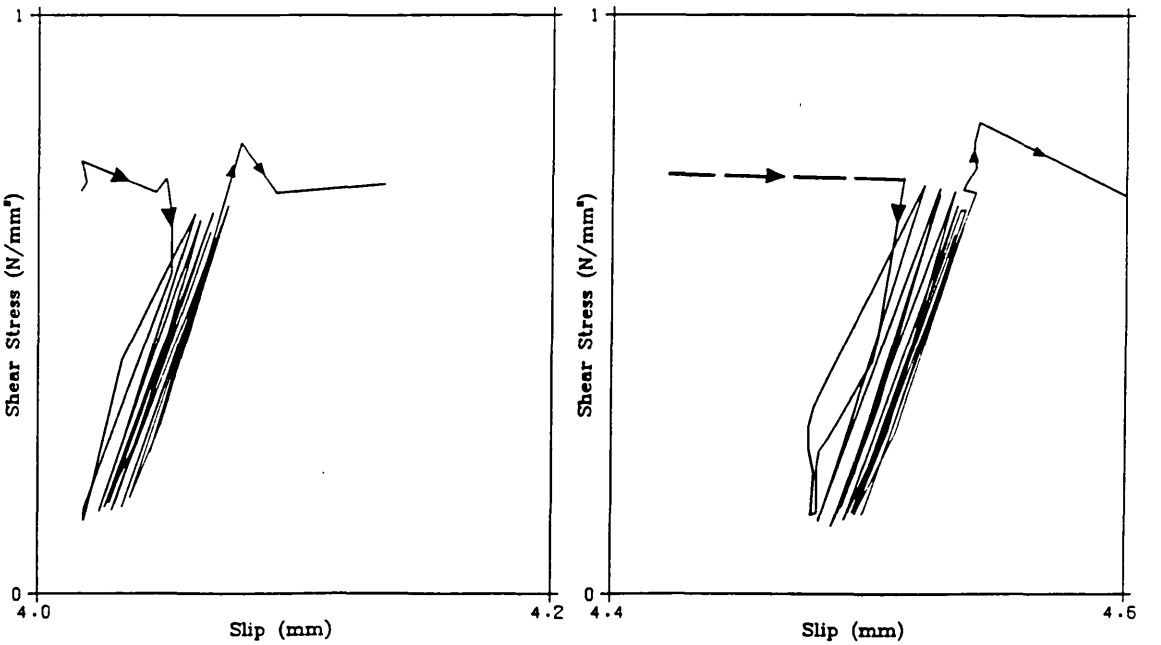


Figure 8.7b : SHEAR STRESS – SLIP CYCLING (Ring 2 – Stage B –)

(Stage B – Frictional behaviour)

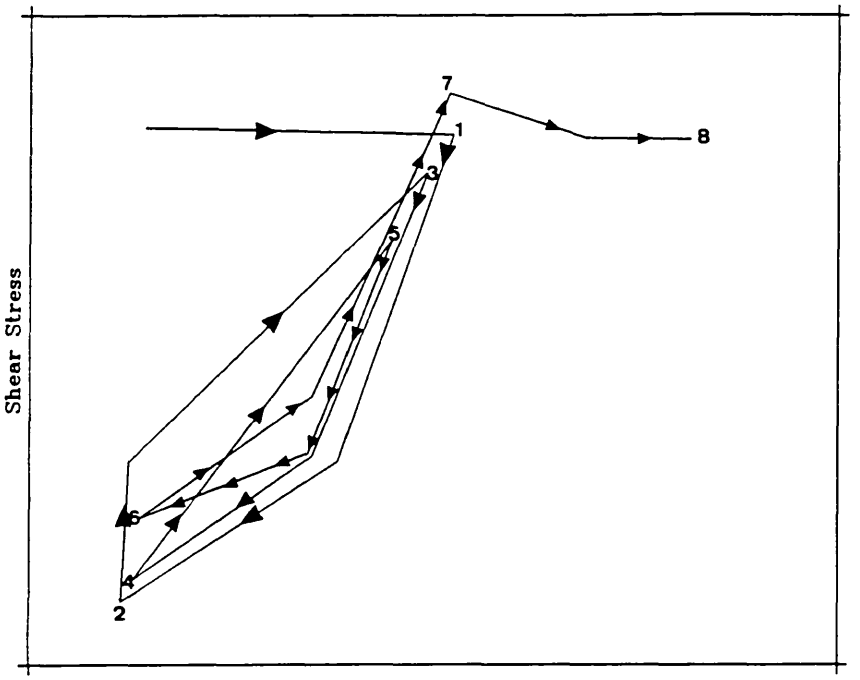


Figure 8.8a : SHEAR STRESS – SLIP CYCLING MODEL (Ring 2 – Stage A –)

(Stage A – Progressive breakdown / fracture)

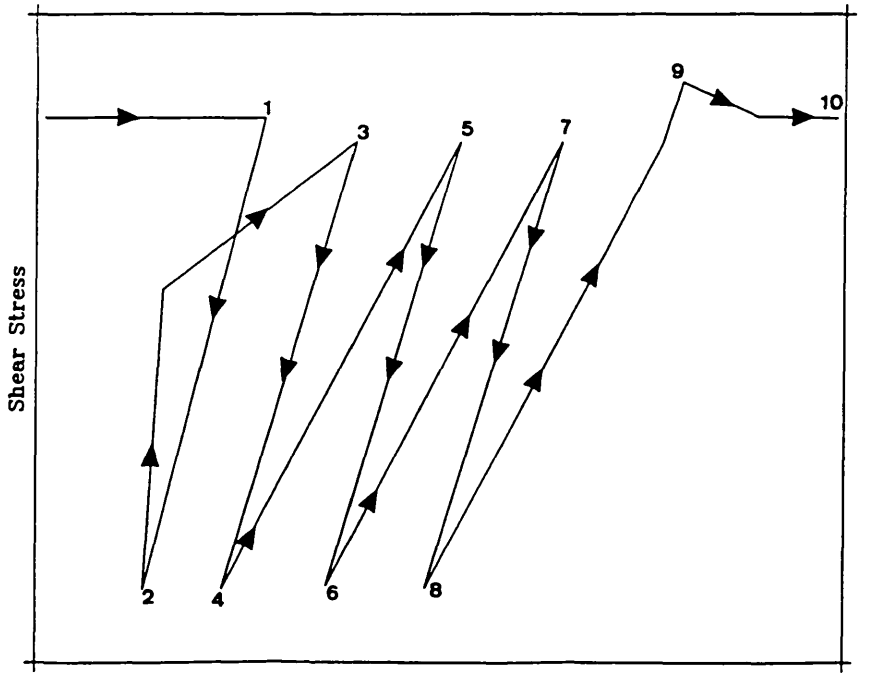


Figure 8.8b : SHEAR STRESS – SLIP CYCLING MODEL (Ring 2 – Stage B –)

(Stage B – Frictional behaviour)

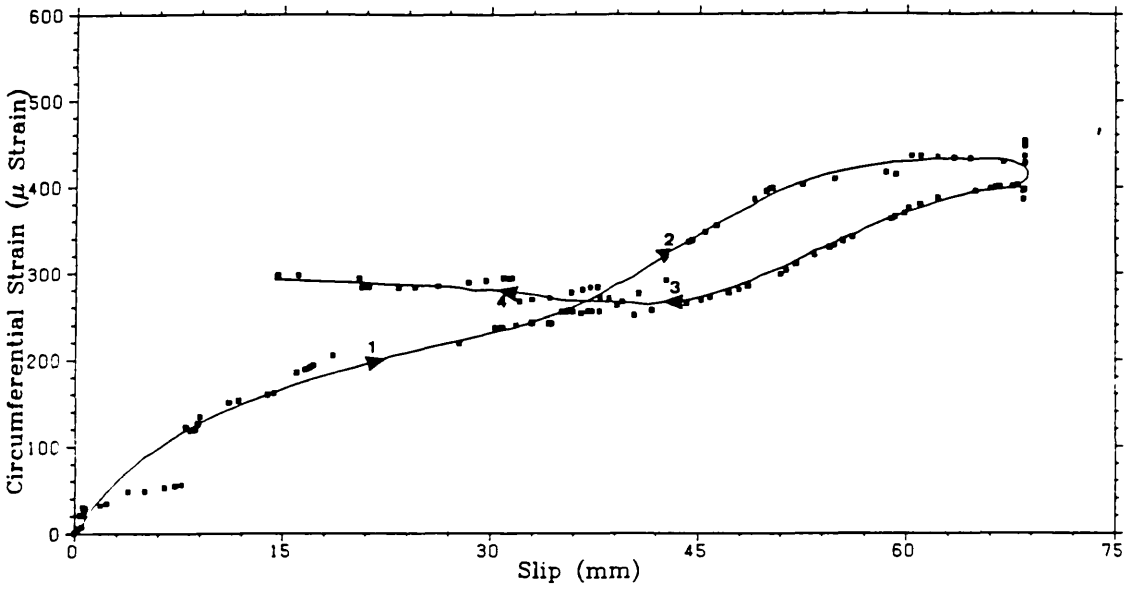


Figure 8.9a : EFFECT OF DILATION ACCOMPANYING SLIP (Test P.T.T. 2)

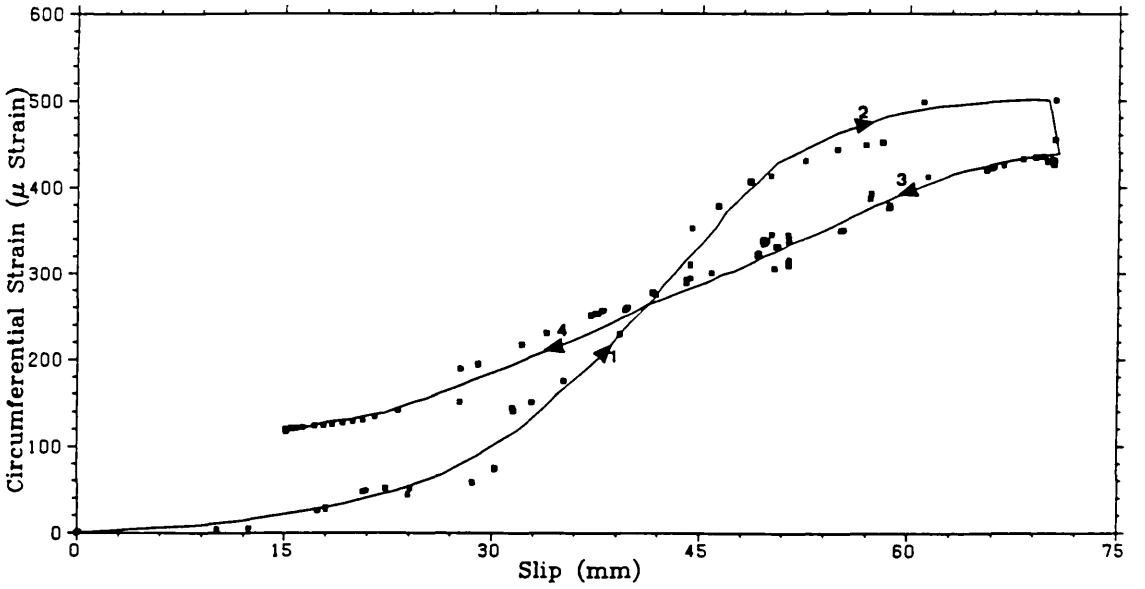


Figure 8.9b : EFFECT OF DILATION ACCOMPANYING SLIP (Test P.T.T. 3)

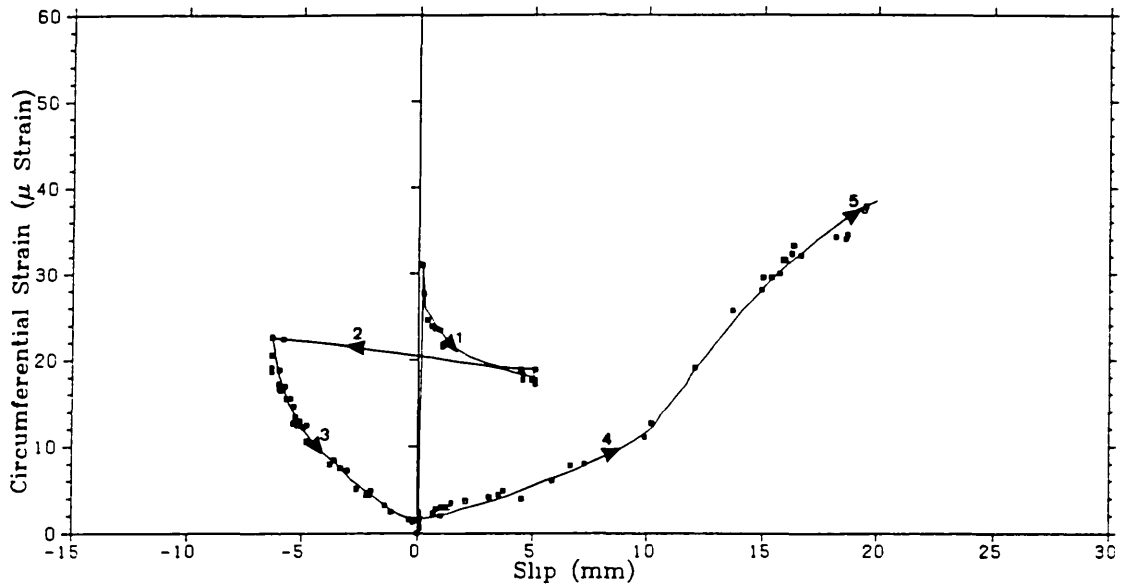


Figure 8.9c : EFFECT OF DILATION ACCOMPANYING SLIP (Test M.T.T. 1)

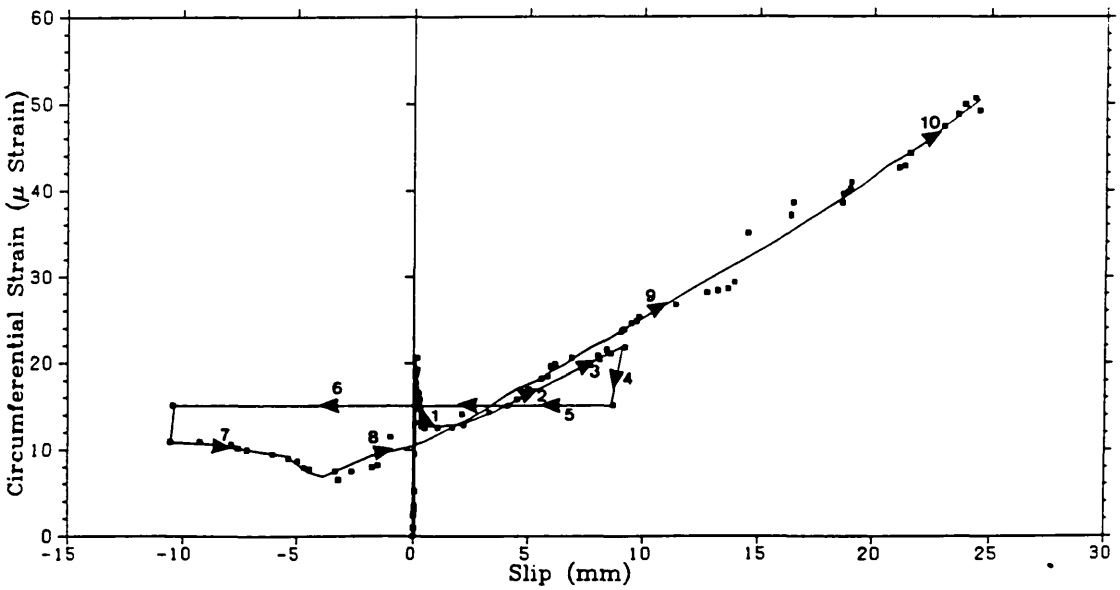


Figure 8.9d : EFFECT OF DILATION ACCOMPANYING SLIP (Test M.T.T. 2)

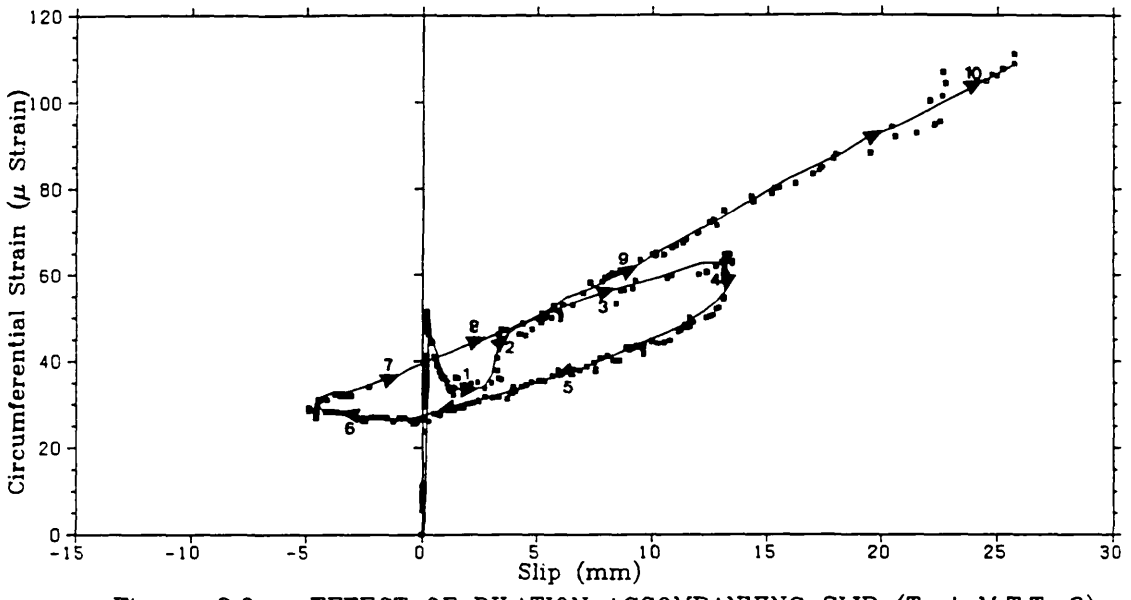


Figure 8.9e : EFFECT OF DILATION ACCOMPANYING SLIP (Test M.T.T. 3)

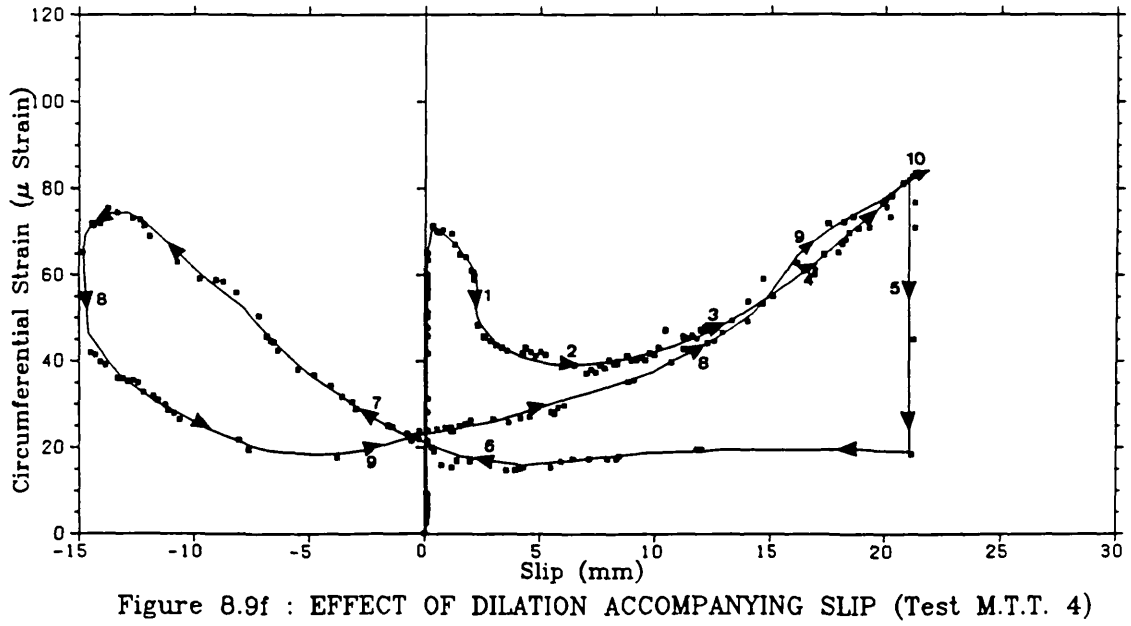


Figure 8.9f : EFFECT OF DILATION ACCOMPANYING SLIP (Test M.T.T. 4)

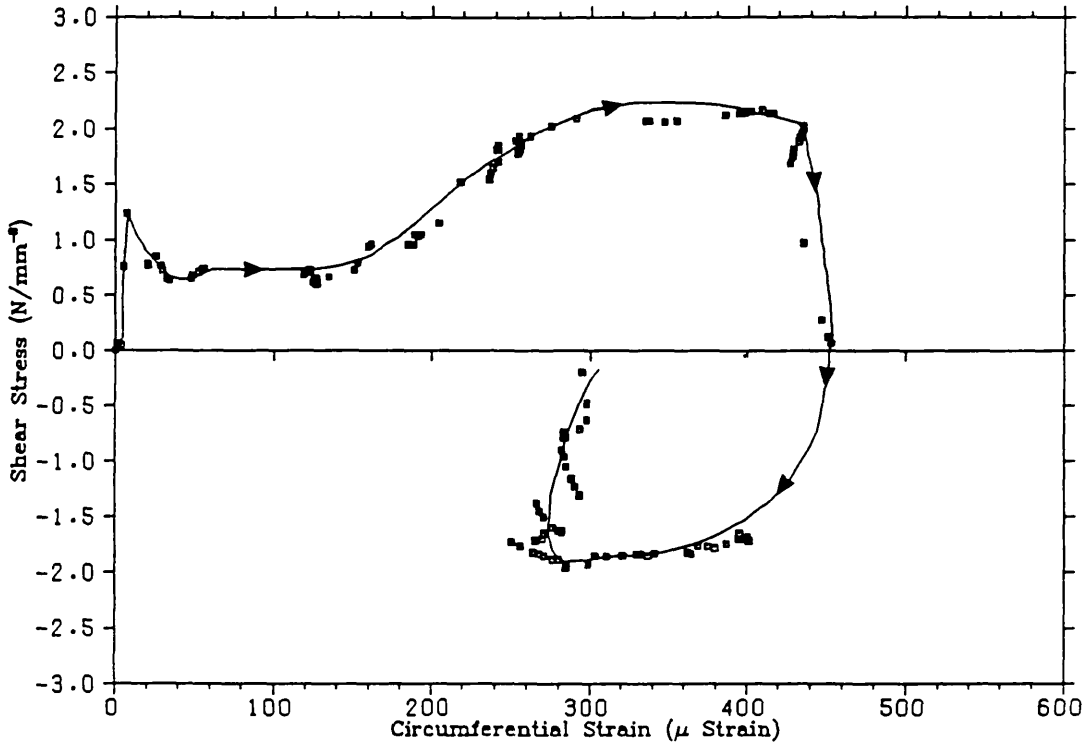


Figure 8.10a : SHEAR STRESS WITH EFFECT OF DILATION (Test P.T.T. 2)

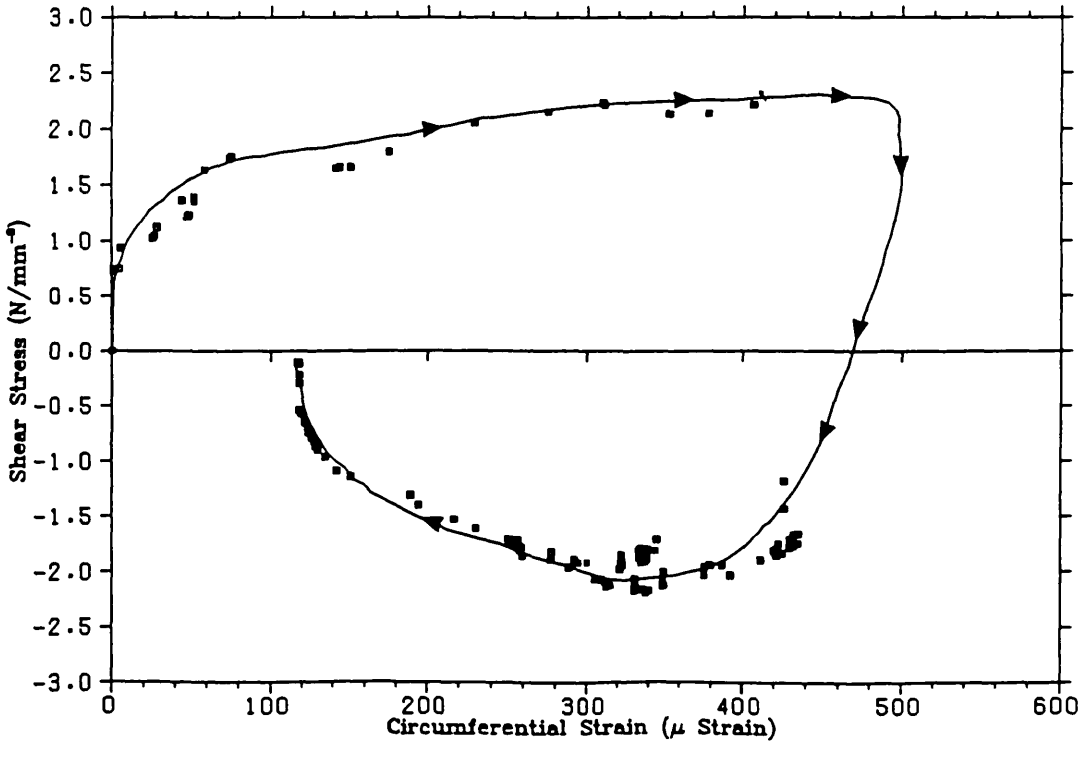


Figure 8.10b : SHEAR STRESS WITH EFFECT OF DILATION (Test P.T.T. 3)

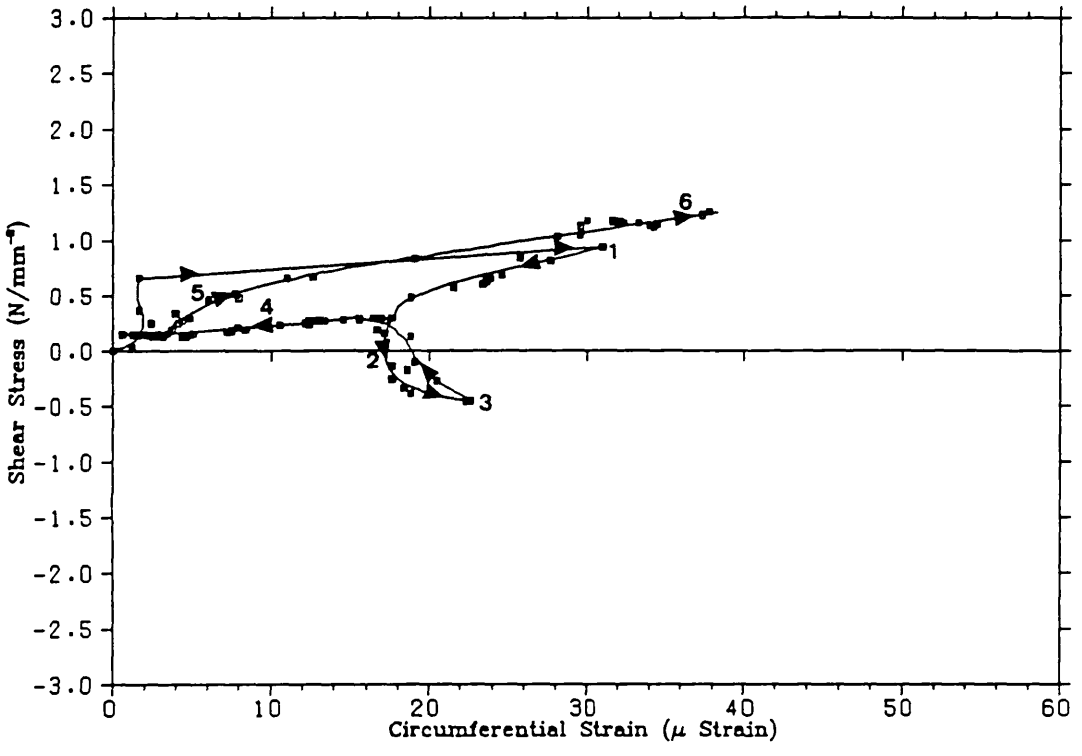


Figure 8.10c : SHEAR STRESS WITH EFFECT OF DILATION (Test M.T.T. 1)

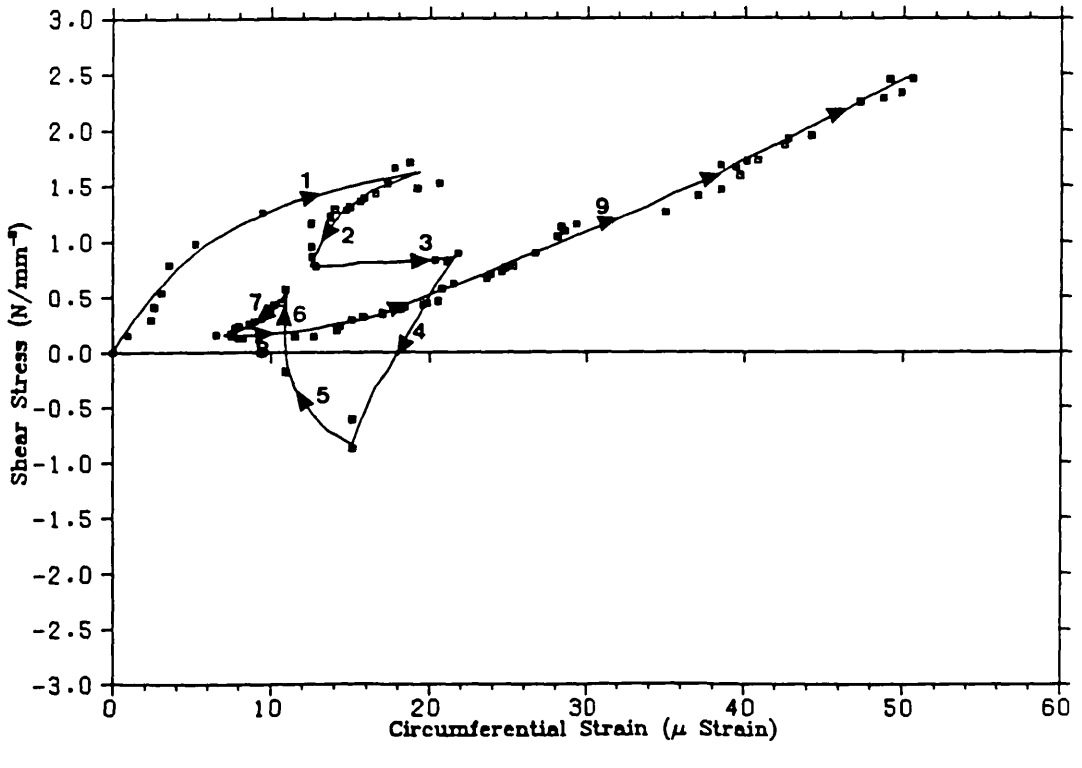


Figure 8.10d : SHEAR STRESS WITH EFFECT OF DILATION (Test M.T.T. 2)

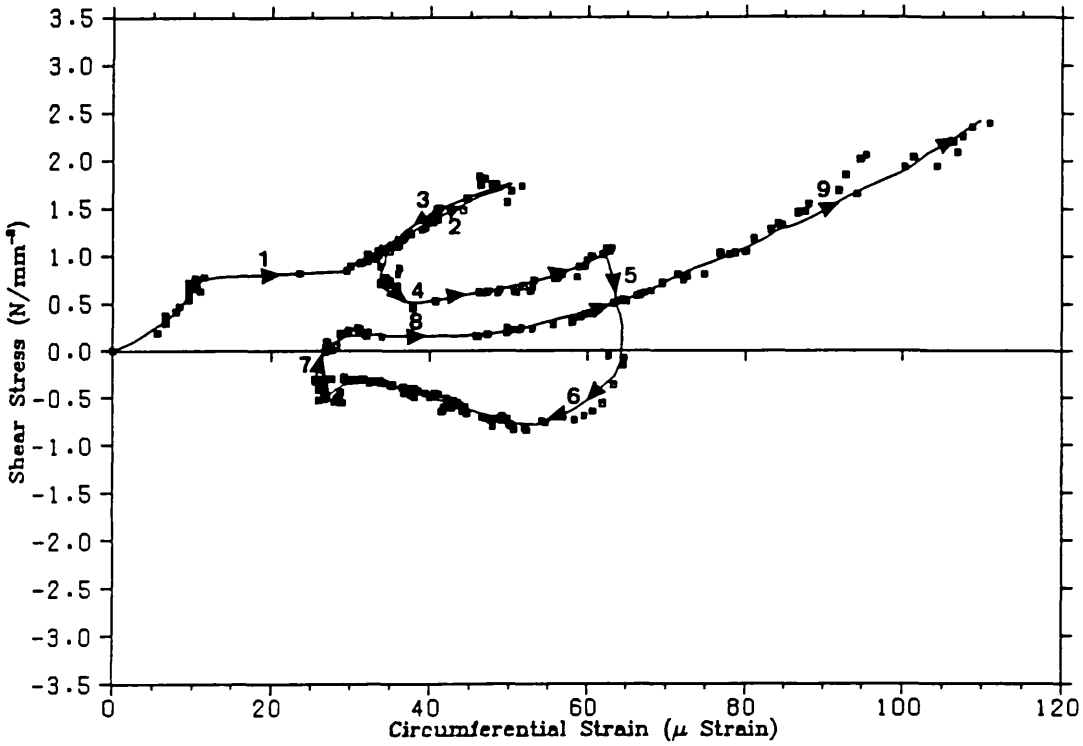


Figure 8.10e : SHEAR STRESS WITH EFFECT OF DILATION (Test M.T.T. 3)

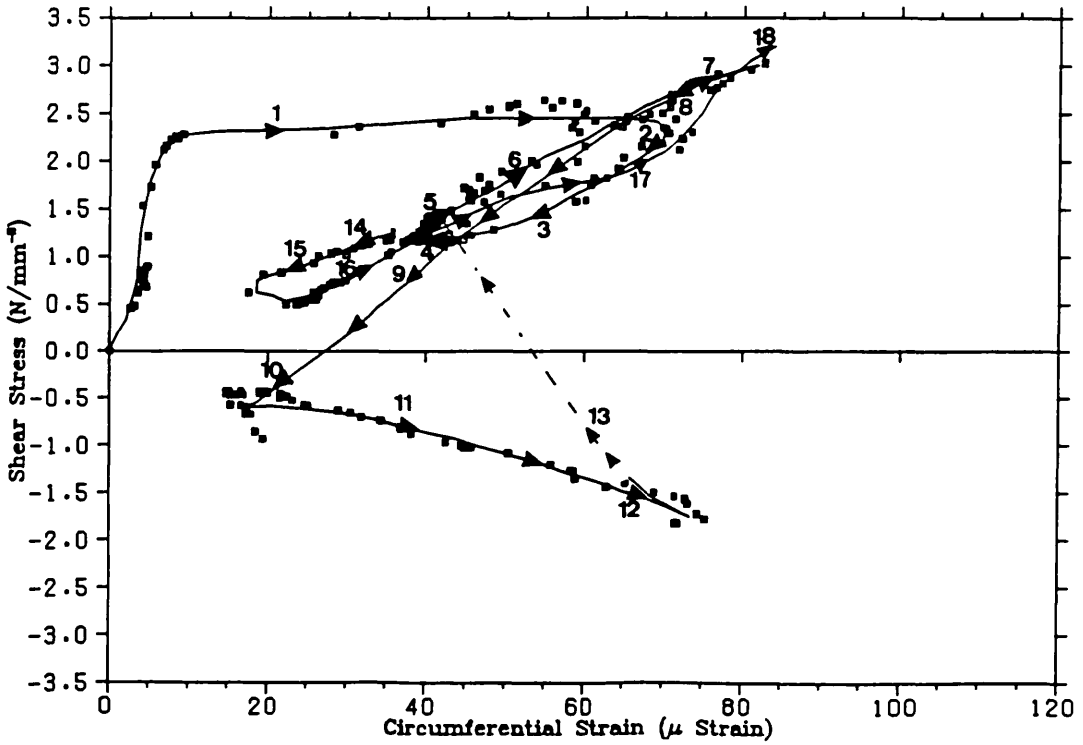


Figure 8.10f : SHEAR STRESS WITH EFFECT OF DILATION (Test M.T.T. 4)

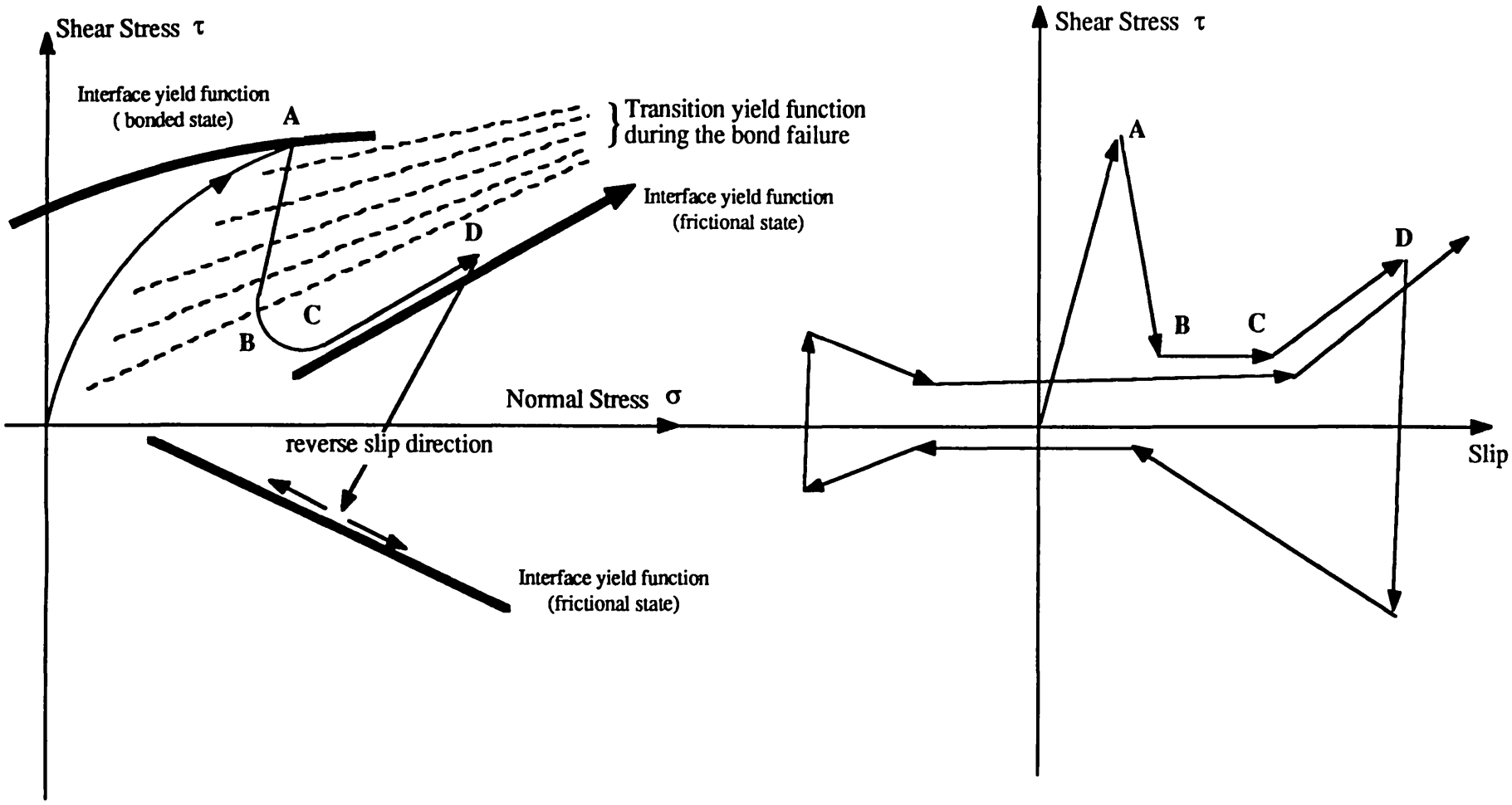


Figure 8.11 : **STEEL PILE SURFACE - CEMENTITIOUS GROUT INTERFACE MODEL**

CHAPTER 9 : CONCLUSIONS AND RECOMMENDATIONS

9.1 NUMERICAL STUDY

Results from a simple numerical model for the interaction between a pile and its interface with a stiff surrounding medium were presented in chapter 2. In this model, the behaviour of the interface was described by a shear stress/slip relationship involving elastic, softening and residual perfectly plastic behaviour. By including fracturing or softening behaviour at the interface in the model, the results showed, that there is a size effect on the behaviour of grouted piles. Pile geometry and interface characteristics control the pile resistance and behaviour. The influence of the latter variables need to be introduced during the design of grouted piles. In the model study, the size effect could be characterised by the non-dimensional quantity

$$\beta = \frac{P_p L_p^2}{A_p} \cdot \frac{D_{int}}{E_p},$$

but practical situations would need a more comprehensive treatment to include the effects of dilatancy and lateral restraint from the surrounding medium. The numerical studies have shown that increasing the length of the pile does not necessarily improve pile behaviour and that longer piles may fail in an unstable manner. At the other extreme, short stiff piles are likely to behave in a more stable manner.

The average shear stress along the pile at failure or maximum load, also varies with the pile length. For short stiff piles this average shear stress (or bond strength) corresponds to the peak stress experienced at the interface. With long piles and stable behaviour, the average stress tends to the residual shear strength (τ_{res}).

As yet, the model is very much simplified. More information on dilatancy and restraint effects would be required to extend the use of the model to practical situations involving axial loading. Extension to include the effects of lateral loading would require a different treatment as explained in chapter 2.

9.2 GROUT SELECTION

As a preliminary to the experimental investigation, tests were carried out to select a suitable grout mix. The mix chosen had little plastic shrinkage with practically no

bleeding. It was found that pulverized fuel ash (PFA) was very useful in improving the grout quality, particularly during the plastic stage of setting. Results of the tests on grout properties are provided in chapter 4.

Measurement of the properties of the selected grout were confined to its compressive strength, Young's modulus and Poisson's ratio. However, it is possible that knowledge of the properties of grout under multi-axial loads might be necessary in future work to establish the yield or failure criteria of the grout for use when analysing grouted piles under combined vertical and horizontal loads. This suggestion is supported by the observations presented in chapter 6 and 8, involving crushing in the grout adjacent to the pile and at the surface.

9.3 LOAD COMBINATIONS : VERTICAL AND HORIZONTAL LOADS

In chapter 6, a test series is described of grouted piles submitted to combinations of vertical and horizontal loads. The pile behaviour, under axial pull-out force, was shown to be similar to the local interface behaviour, with pile end displacement softening, due to a progressive failure along the pile embedded length. The application of lateral load, either prior to or simultaneously with the pile pull-out, considerably reduced the pile axial load capacity. Through - zero reverse lateral loading applied on the pile prior to its extraction caused breakdown and the failure of the bond at the interface between the pile and grout, leaving only the frictional resistance for the pile against any axial extraction. As a result, it was found that the pile strength tends to correspond to the residual resistance of the pile under axial tension load. This residual pile resistance is governed by the residual interface shear strength.

An interaction curve for the load capacity of a pile under vertical and horizontal loading was obtained from results of tests on grouted piles submitted to proportional loading with horizontal and vertical forces. The results focused attention on the need for consideration of lateral loading in the design of grouted piles, especially those with a short grouted length such as tested here. The design procedure for a grouted tension pile, should be based on the resistance of the pile under combined loads rather than studying the pile under each type of load independently.

The results of tests to determine the effect of load path dependency of the load capacity of grouted piles were not conclusive and further tests are needed to deduce final conclusions. Nevertheless, it seemed clear that the application of lateral load before the vertical force generated an additional stiffness to the pile end vertical displacement. This

could be caused by the development of normal stresses at the pile/grout interface. However, when the lateral load was applied after the vertical force, additional pile end vertical movement was observed, and the stiffness effect of the lateral load was not developed.

The effects of lateral load application on a grouted pile can be summarised as follows :

1 - a reduction of the axial load capacity under an extracting force

2 - a possible separation between the pile and the grout with the formation of a gap at the pile/grout interface.

3 - crushing of the grout and the surrounding media on the side restraining the pile against the lateral load, particularly for low V/H ratio.

4 - occasional tensile cracking of the grout near to the foundation surface due to bending of the pile and its associated grout. This is accompanied by separation between the grout and the surrounding media for a short depth below the surface of the foundation.

Cyclic tensile loading, produced increased pile displacement with each cycle of loading. This is an important factor that needs to be taken into account for piles under varying tension load, such as with tensioned floated offshore structures.

9.4 INTERFACE PROPERTIES

A torsion test was designed to investigate local behaviour at the pile/grout interface when subjected to shear stress. The test used short ring pile elements which were grouted in position inside a concrete block pocket and then rotated. The test was designed in this way to provide a short length of a pile subject to shear so that uniform conditions could be assumed.

In chapter 8 the results obtained from the torsion tests were presented. The local interface behaviour showed the effects of breakdown or fracture in the form of softening in the observed shear stress/slip relationship. With larger slips, the shear stress achieved a minimum value but with continuing shearing (several millimeters slip) hardening occurred due to dilatancy causing an increase in friction resistance. The effects

of dilatancy were observed indirectly by monitoring circumferential strains developed in the concrete surrounding the grouted pile. Results were not entirely satisfactory due to difficulties in interpreting the measured strain. However, the qualitative picture that emerged suggested that, during slip, the interface shear was determined by a failure envelope in shear stress/normal stress (Mohr) space and that this envelope (or yield surface) was affected by both progressive breakdown at small slips and dilatancy at large value of slip. The situation is complicated under stress cyclic loading when the interface exhibited a loss of stiffness during the fracturing stage. During the frictional stage, stress cycling caused an additional slip movement which is not recovered.

Dilatancy is important for the global stability of the pile. However, further tests would be needed to quantify such interaction between the pile and the surrounding media and to provide more detailed description for the interaction between the slip and stress variations.

Although the interface bond strength varies with the grout compressive strength, the frictional shear stress shows much less variation with grout strength. This might suggest that the frictional behaviour is more dependent on the steel surface roughness than the strength of the grout.

9.5 PRACTICAL APPLICATIONS

On the basis of the results obtained in this research programme, it appears essential to distinguish between the bond strength and the frictional resistance of the interface. Current design techniques depend on the use of measured bond strengths corresponding to the peak values obtained in pull out tests. The results obtained here suggest that the residual shear strength would be more relevant quantity to use when dealing with long piles. The use of residual strength could be combined with lower safety factors compared with the value of around six in current use.

9.6 FURTHER WORK

There is a broad frame-work needed to achieve a complete model of the interface behaviour to include softening, friction, stress cycling, reverse slip movement, and dilatancy phenomena. Such a study is likely to incorporate, fracture theory and plasticity, with an additional focus on energy dissipation terms for a general model of the interface.

The pile surface roughness proved to have critical effects on the interface resistance and behaviour. Establishment of an improved method of measuring the surface condition is regarded as an immediate need for future studies. Once such a method is established, a laboratory investigation could be planned to provide a correlation between the steel surface roughness and the interface characteristics, including the bond strength, the residual frictional resistance, slip softening rate, and the dilatancy phenomenon.

Different effects can be introduced to simulate the site conditions, such as the presence of drilling mud in the concrete pocket, before the grouting operation. Also variations in the surrounding stiffness can be adopted to study in more detail the interaction between the pile and its surroundings.

9.7 SUMMARY OF PRINCIPAL CONCLUSIONS

1 - The results of torsion tests confirmed that softening is a characteristic phenomenon associated with bond break-down at an interface.

2 - model studies showed that softening at the pile/grout interface leads to size effects on pile load capacity and global behaviour of the pile.

3 - with large values of slip, the interface behaviour showed stress hardening due to dilation generated in the grout in the vicinity of the pile/grout interface. This behaviour would lead to increased stability in the behaviour of piles during extension but only after significant slip had occurred.

4 - cyclic tensile loads produced increased end pile displacement with each cycle of loading.

5 - application of lateral loads simultaneously with an axial pull out force considerably reduces the pile capacity under the condition of test used in the experimental programme.

6 - For design, it is suggested that the residual or minimum shear strength obtained in bond tests is a more reliable parameter than the peak values currently used. There are indication that the residual strength is less affected by load history. More work is required to confirm this preliminary conclusion.

APPENDIX 1

A1.1 INTRODUCTION

This appendix is concerned with the solution of the system of equations developed for the numerical model presented in chapter 2. Based on the model description, the general differential equation, expressed in finite difference form, provides the following system of equations :

$$\begin{aligned} & u_1 = -U^{(1)} \quad \text{at the foundation surface} \\ & u_{n+1} = u_n \quad \text{at the end of the pile} \\ & u_{i-1} - 2u_i + u_{i+1} + k_p \, \delta X^2 \, \tau(u) = 0 \qquad (i = 2,3,4.....N) \end{aligned} \tag{A1.1}$$

with $$k_p = \frac{P_p}{A_p} \cdot L_p^2 \cdot \frac{1}{E_p} \quad \text{(pile stiffness factor)} \quad \text{and} \quad \delta X = \frac{1}{N}$$

by including the expression for the shear stress given by equation 2.1 (chapter 2), the system becomes :

$$\begin{aligned} (2-K_p^2)\, u_2 + u_3 &= U - S_2 \\ u_{i-1} - (2-K_p^i)\, u_i + u_{i+1} &= -S_i \\ u_{N-1} - (1 - K_p^N)\, u_N &= -S_N \end{aligned} \tag{A1.2}$$

where

$$K_p^i = -E_{int}\, k_p\, \delta X^2 \quad \text{and} \quad S_i = 0 \qquad \text{if } |u_i| \le u_{max}$$

$$K_p^i = D_{int}\, k_p\, \delta X^2 \quad \text{and} \quad S_i = -(E_{int} + D_{int})\, u_{max}\, k_p\, \delta X^2 \quad \text{if } u_{max} \le |u_i| \le u_{res}$$

$$K_p^i = 0 \quad \text{and} \quad S_i = \left[D_{int}\, u_{res} - (E_{int} + D_{int})\, u_{max} \right] k_p\, \delta X^2 \quad \text{if } u_{res} \le |u_i|$$

---

[1] The sign (-) is conventional since U is chosen to be an absolute value

This system can be expressed in matrix form i.e :

$$[A(U)][U]=[B(U)] \quad \text{which becomes} \quad [U]=[A(U)]^{-1}[B(U)] \quad \text{(A1.3)}$$

The system is nonlinear and the solution requires an iterative procedure. Additionally, for certain cases with long pile embedded length, the pile failure is developed in an unstable manner. In other words, once the maximum force has been reached, the full description of the pile behaviour requires a decrease of the pile tip displacement. Such behaviour can never be observed in practical cases. The numerical procedure will reflect this instability and can indicate an unstable mode of failure.

A1.2 NUMERICAL INSTABILITY AND EXISTENCE OF SOLUTION

Numerically,the occurrence of instability in the pile behaviour is accompanied by a change of the system matrix characteristics. At a certain stage of the loading process, the matrix becomes indefinite. At each iteration, the general equation at the node i can be written as :

$$(2 - K_p^i)\, u_i = (u_{i-1} - u_{i+1}) + S_i \qquad \text{(A1.4)}$$

for a specific iteration j, the slip displacement at the node i can be determined by the following equation, with u_i^j is the slip displacement at the node i, obtained from the iteration j :

$$(2 - K_p^{i,j-1})\, u_i^j = (u_{i-1}^{j-1} - u_{i+1}^{j-1}) + S_i^{j-1} \qquad \text{(A1.5)}$$

or

$$(2 - K_p^{i,j-1})\, u_i^j = G([u_m^{j-1}]) \qquad \text{with} \quad m \neq i$$

where $K_p^{i,j-1}$ parameters vary in each iteration, and $G([u_m^{j-1}])$ is a function of the slip displacement at all nodes (except m) obtained during the iteration j-1. From equations A1.5, it is possible to solve uniquely for u_i^j, which leads to updated values for $K_p^{i,j}$ and $G([u_m^j])$ ready for the next iteration. Figure A1.1 shows the algorithm of the procedure used to obtain the convergence of the iterations. However, because K_p^i varies according to the state of the pile interface (elastic, fracturing, and friction as in equations A1.2), a

situation can arise in which K_p^i alternates between two states on successive iteration and convergence does not occur. This has been observed to occur in cases where the term $(2-K_p^{i,j-1})$ and the left hand site of A1.5 is negative, so that for convergence to occur

$$(2 - K_p^i) > 0 \quad \text{or} \quad \frac{P_p}{A_p} . L_p^2 . \frac{D_{int}}{E_p} . \delta X^2 < 1 \qquad \text{(A 1.6)}$$

or more simply

$$\beta \, \delta X^2 < 1$$

Figures A1.2 illustrate these criteria for stability and uniqueness of the solution for a pile analysed with a prescribed displacement at its end.

Physically, this condition can be related to the energy dissipation of the pile when failure occurs. For a given load increment, the instability is generated when the accumulation of slip displacement energy released in the fractured zone is larger than the energy increase in other part of the pile model. It is important to note that the pile instability is a physical phenomenon and will be revealed in the analysis regardless of the pile subdivision size used. The increase of the number of nodes used in the analysis will only provide more detailed description of the pile behaviour, and might affect marginally the iteration and loading step when failure instability would be observed. Figure A1.3 shows the study case 2 output using small and large pile subdivision.

Consequently, a second subroutine has been prepared with a different boundary conditions, to overcome the lack of stability of the numerical analysis based an pile tip displacement. The idea is to impose the bottom pile end displacement to undertake a slip displacement value within the local slip softening range. In this way, the interface is caused to fail completely and progressively and the theoretical description of the pile behaviour will be completed. This subroutine is used only when the normal procedure can not provide a detailed description of the pile failure and end displacement softening.

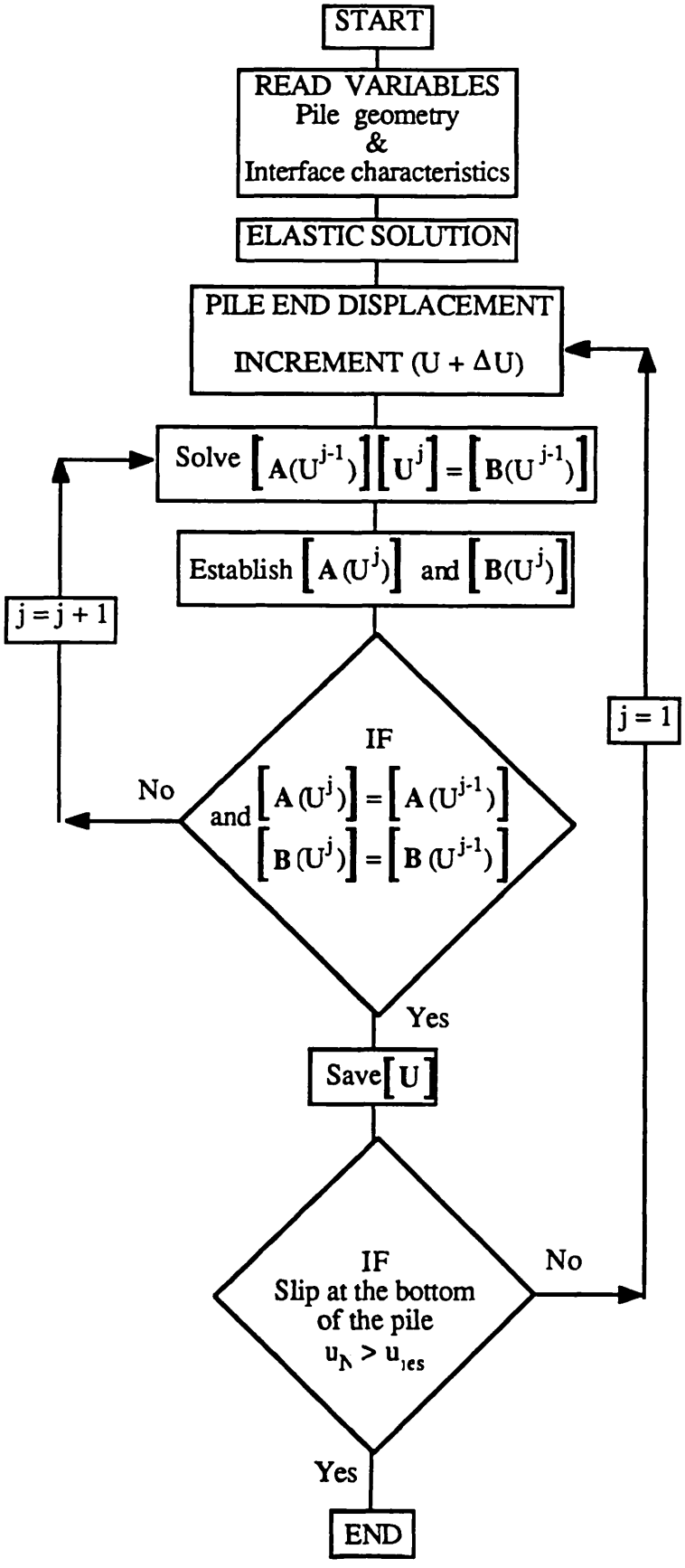


Figure A1.1 : ALGORITHM FOR SOLVING THE SYSTEM OF EQUATIONS OF THE NUMERICAL MODEL OF A GROUTED PILE

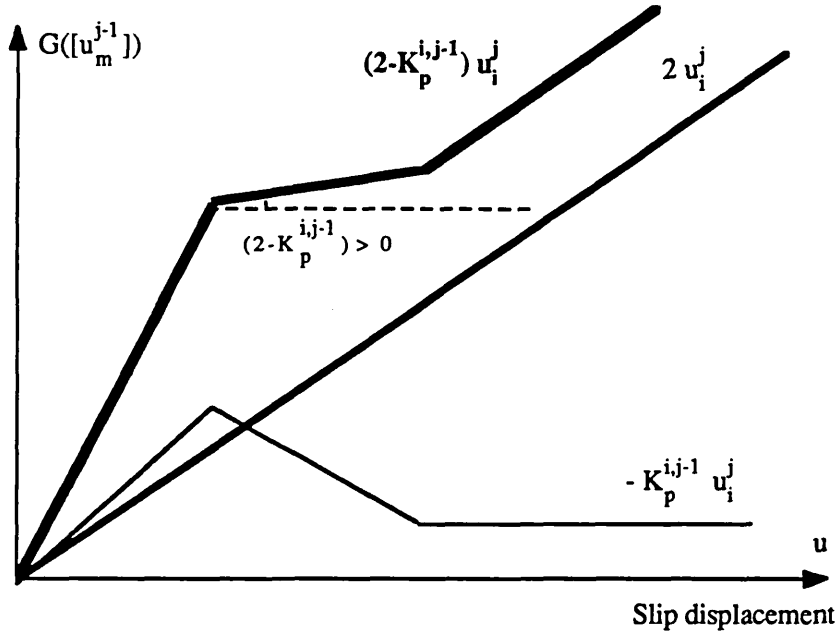


Figure A1.2a : CONVERGENT NUMERICAL SYSYTEM OF EQUATIIONS

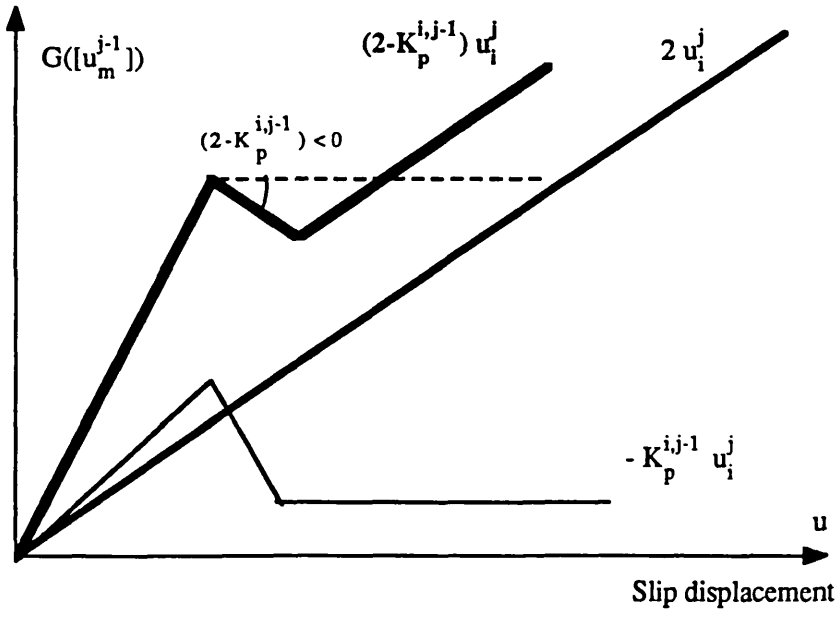


Figure A1.2b : NON CONVERGENCE OF THE NUMERICAL SYSYTEM OF EQUATIONS

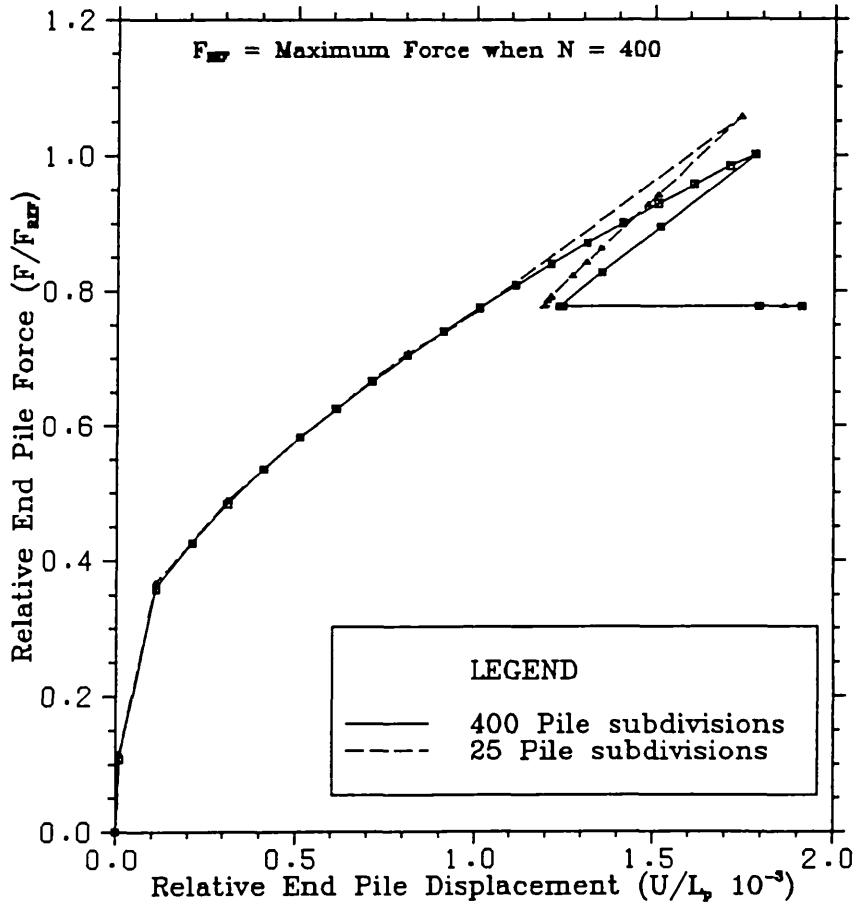


Figure A1.3 : PILE SUBDIVISIONS EFFECT ON THE OUTPUT OF THE PILE BEHAVIOUR

MAIN PROGRAM

```
      PROGRAM PROGC (INPUT,OUTPUT,TAPE5=INPUT,TAPE6=OUTPUT)
      COMMON /COMPR/ N,DX,UM,UR,DES,DEF,TAUM,TAUER,A0(400)
C
C UM : THE SLIP  FOR THE MAXIMUM STRESS TAUM
C UR : THE SLIP FOR THE RESIDUAL STRESS TAUER
C
   10 PRINT 40
C
C  SUBROUTINE CALL FOR PILE GEOMETRY AND INTERFACE
CHARACTERISTICS
C
      CALL GEOMAT (BETA)
      IF (N.GE.401) GO TO 10
      PRINT 30
      DES = -(ABS(TAUM/UM))*BETA
      DEF = (ABS((TAUM-TAUER)/(UM-UR)))*BETA
C
C INITIALIZING THE VARIABLES OF THE STIFFNESS MATIX
C
      DO 20 I = 1, N
        A0(I) = -2.0
   20 CONTINUE
      A0(N) = -1.
C
C SUBROUTINE CALL FOR THE PILE BEHAVIOUR DETERMINATION
C
      CALL SUBF (BETA)
      STOP
C
   30 FORMAT ('THE PROGRAM ANALYZES A PILE AXIALLY PULLED WHILE THE'/,
     *  'SLIP AT THE TOP IS INCREMENTALLY INCREASED.'////)
   40 FORMAT ('THE NUMBER OF PILE DIVISIONS SHOULD BE LESS THAN 400. '/,
     *'IF NOT, THE ARRAY DIMENSIONS MUST BE CHANGED IN THE MAIN PROGRAM'
     *  /,' AND SUBROUTINES.'////)
C
      END
```

DATA INPUT SUBROUTINES

```
      SUBROUTINE GEOMAT (BETA)
       COMMON /COMPR/ N,DX,UM,UR,DES,DEF,TAUM,TAUER,A0(400)
       REAL IPD
       REWIND (1)
      OPEN (UNIT=1,STATUS='OLD',FILE='DATAI')
C 1 - PILE  CHARACTERISTICS
       READ (1,*) OPD
       READ (1,*) IPD
       READ (1,*) TPL
       READ (1,*) N
       READ (1,*) EM
C 2 - INTERFACE  CHARACTERISTICS
       READ (1,*) TAUM
       READ (1,*) TAUER
       READ (1,*) UM
       READ (1,*) UR
      CLOSE (UNIT=1)
       PRINT 10000,OPD
       PRINT 10100,IPD
       PRINT 10200,TPL
       PRINT 10300,N
       PRINT 10400,EM
       PRMTER = 3.1416*OPD
      AREA = 3.1416*((OPD**2)-(IPD**2))/4
      DX = TPL/(N+1)
      BETA = ((DX**2)*PRMTER)/(EM*AREA)
       PRINT 10500
       PRINT 10600,PRMTER,AREA,BETA,DX
      TAUM = -ABS(TAUM)
      TAUER = -ABS(TAUER)
       PRINT 10700,TAUM
       PRINT 10800,TAUER
       PRINT 10900,UM
       PRINT 11000,UR
       RETURN
10000 FORMAT (' OUTER PILE DIAMETER  : ',F6.1,' MM ')
```

```
10100 FORMAT (' INNER PILE DIAMETER  : ',F6.1,' MM ')
10200 FORMAT (' PILE LENGTH          :',E12.6,' MM ',/)
10300 FORMAT (' NUMBER OF PILE ELEMENTS ( DIVISIONS ) : ',I6,//)
10400 FORMAT (' ELASTIC MODULUS ( PILE MATERIAL ) :',E12.6,' N/MM2',//)
10500 FORMAT (3X,'PERIMETER',7X,'AREA',10X,'BETA:T-MUL',7X,'DX')
10600 FORMAT (4(E12.5,3X),//)
10700 FORMAT (' MAXIMUM SHEAR STRESS  : ',F7.3,' N/MM2')
10800 FORMAT (' RESIDUAL SHEAR STRESS : ',F7.3,' N/MM2')
10900 FORMAT (' MAXIMUM SHEAR SLIP    : ',F7.4,' MM')
11000 FORMAT (' RESIDUAL SHEAR SLIP   : ',F7.4,' MM',//)
      END
```

SUBROUTINE FOR THE ELASTIC SOLUTION DETERMINATION

```
      SUBROUTINE SUBLS (ITEST)
       COMMON /COMPR/ N,DX,UM,UR,DES,DEF,TAUM,TAUER,A0(400)
      COMMON /COMLS/ A(400),B(400),C(400),RHS(400)
      INTEGER IN(400)
      REAL D(400)
      REAL LAMBDA
      ITEST = 1
      LAMBDA = 0.0
      TOL = 1.E-20
      IFAIL = 1
C SOLUTION OF THE SYSTEM OF EQUATIONS
C F01LEF IS IN THE NAG LIBRARY OF IMPERIAL COLLEGE COMPUTER CENTER
      CALL F01LEF (N,A,LAMBDA,B,C,TOL,D,IN,IFAIL)
      IF (IFAIL.EQ.0) GO TO 2000
      PRINT 20200,IFAIL
      GO TO 2020
 2000 IF (IN(N).EQ.0) GO TO 2010
      PRINT 20100,IN(N)
      ITEST = 0
      GO TO 2020
 2010 CONTINUE
      IFAIL = 1
C F04LEF IS IN THE NAG LIBRARY OF IMPERIAL COLLEGE COMPUTER CENTER
      CALL F04LEF (1,N,A,B,C,D,IN,RHS,TOL,IFAIL)
```

```
      IF (IFAIL.EQ.0) GO TO 2020
      PRINT 20000,IFAIL
 2020 RETURN
20000 FORMAT ('0F04LEF FAILS. IFAIL=',I3)
20100 FORMAT (' MATRIX IS SINGULAR OR NEARLY SINGULAR'/,
     *  ' DIAGONAL ELEMENT',I4,' IS SMALL')
20200 FORMAT ('0F01LEF FAILS. IFAIL=',I3)
      END
```

SUBROUTINES FOR THE SLIP INTERFACE ANALYSIS WITH PILE UNDER INCREMENTAL END SLIP DISPALCEMENT

```
      SUBROUTINE SUBF (BETA)
      COMMON /COMPR/ N,DX,UM,UR,DES,DEF,TAUM,TAUER,A0(400)
      COMMON /COMLS/ A(400),B(400),C(400),RHS(400)
      DIMENSION IPR(400),IP(400),UPG(402,40),DDISP(40)
      DIMENSION FORCE(40,3),XP(402),Y(402),SPG(402,40)
C INITIALIZING THE VARIABLES
      ES = DES/BETA
      EF = DEF/BETA
C SLIP DISPLACEMENT INCREMENT
      UINCR = (N+1)*DX/10000.
      K = 1
      M = 2
      DDISP(1) = UM
      ALFA = UM
      DALFA = UINCR
      MAXDAM = 0.
      RESDAM = 0.
C ELASTIC SOLUTION
      DO 3000 I = 1, N
        B(I) = 1.
        C(I) = 1.
        RHS(I) = 0.
        A(I) = A0(I)+DES
        IPR(I) = +1
        IP(I) = +1
 3000 CONTINUE
```

```
      RHS(1) = UM
      CALL SUBLS (ITEST)
      IF (ITEST.EQ.0) THEN
        GO TO 3200
      ENDIF
      UPG(1,1) = SIGN(UM,RHS(1))
      DO 3010 I = 1, N
        UPG(I+1,1) = RHS(I)
 3010 CONTINUE
      UPG(N+2,1) = UPG(N+1,1)
C SOLUTION WHILE SOME PART OF THE BOND IS FRACTURED
C
C SLIP INCREMENT ACCUMULATION
 3020 ALFA = ALFA+DALFA
C MATRICES FORMULATION
 3030 DO 3040 I = 1, N
        B(I) = 1.
        C(I) = 1.
        UMAX = SIGN(UM,RHS(I))
        URES = SIGN(UR,RHS(I))
        IF (ABS(RHS(I)).LE.UM) THEN
          A(I) = A0(I)+DES
          RHS(I) = 0.
        ELSEIF (ABS(RHS(I)).LE.UR) THEN
          A(I) = A0(I)+DEF
          RHS(I) = (DEF-DES)*UMAX
        ELSE
          A(I) = A0(I)
          RHS(I) = -DEF*URES+((DEF-DES)*UMAX)
        ENDIF
 3040 CONTINUE
      DDISP(M) = DALFA
      RHS(1) = ALFA+RHS(1)
      CALL SUBLS (ITEST)
      K = K+1
      IF (ITEST.EQ.0) THEN
        M = M-1
        GO TO 3200
      ENDIF
      IF (K.GT.(3*N)) THEN
```

```
      K = 0
      DO 3050 I = 1, N
        RHS(I) = UPG(I+1,MR)
3050   CONTINUE
      GO TO 3020
    ENDIF
C INDEX VECTOR DETERMINATION (IPR) AND CORRECTION OF THE INDEX
VECTOR (IP) FROM THE PREVIOUS ITERATION
    DO 3060 I = 1, N
      IF (ABS(RHS(I)).LE.UM) THEN
        IPR(I) = +1
      ELSEIF (ABS(RHS(I)).LE.UR) THEN
        IPR(I) = -1
      ELSE
        IPR(I) = 0.
      ENDIF
      IF (IP(I).NE.IPR(I)) THEN
        IP(I) = IPR(I)
        FAIL = 0.
        GO TO 3030
      ENDIF
3060 CONTINUE
    IF (FAIL.EQ.0.) THEN
      FAIL = 1.
      GO TO 3030
    ENDIF
    FAIL = 0.
    UPG(1,M) = SIGN(ALFA,RHS(1))
    DO 3070 I = 1, N
      UPG(I+1,M) = RHS(I)
3070 CONTINUE
    UPG(N+2,M) = UPG(N+1,M)
    M = M+1
    IF (MAXDAM) 3120 , 3080 , 3120
3080 IF (ABS(RHS(N)).GE.UM) THEN
      MB = M-1
C SYSTEM DOES NOT CONVERGE, SO THE CALL FOR THE SECOND
SUBROUTINE WHERE THE SLIP AT THE BOTTOM WOULD THE CONTROLLED
BOUNDARY CONDITION
      CALL SUBIU (BETA,UMAX,RHS,ITEST)
```

```
      IF (ITEST.EQ.0) THEN
        DO 3090 I = 1, N
          RHS(I) = UPG(I+1,MR)
          IP(I) = -1
3090      CONTINUE
        GO TO 3110
      ENDIF
      DALFA = DALFA/10
      ALFA = ABS(RHS(1))
      DO 3100 I = 1, N
        UPG(I,M) = RHS(I)
        RHS(I) = RHS(I+1)
        IP(I) = -1
3100  CONTINUE
      UPG(N+1,M) = RHS(N+1)
      UPG(N+2,M) = RHS(N+1)
      MR = M
3110  DDISP(M) = 999.*ITEST
      M = M+(1*ITEST)
      K = 0
      MAXDAM = 1.
      GO TO 3020
    ENDIF
3120 IF (RESDAM) 3190 , 3130 , 3190
3130 IF (ABS(RHS(N)).GE.UR) THEN
      ME = M-1
      UINS = URES/4
      BCOND = 0.
      DO 3140 I = 1, N
        IP(I) = 0
3140  CONTINUE
      DO 3180 J = 1, 4
        BCOND = BCOND+UINS
        CALL SUBIU (BETA,BCOND,RHS,ITEST)
        IF (ITEST.EQ.0) THEN
          DO 3150 I = 1, N
            RHS(I) = UPG(I+1,MR)
3150        CONTINUE
          GO TO 3170
        ENDIF
```

```
        ALFA = ABS(RHS(1))
        DO 3160 I = 1, N
          UPG(I,M) = RHS(I)
          RHS(I) = RHS(I+1)
3160      CONTINUE
        UPG(N+1,M) = RHS(N+1)
        UPG(N+2,M) = RHS(N+1)
3170      DDISP(M) = 999.*ITEST
        M = M+(1*ITEST)
3180    CONTINUE
      RESDAM = 1.
      K = 0
      GO TO 3020
    ENDIF
    MR = M-1
3190 IF (M.GE.39.OR.(ABS(RHS(N)).GE.UR.AND.ABS(UPG(N+1,M-2)).GE.UR))
   *   THEN
      M = M-1
      GO TO 3200
    ELSEIF (M.GT.20) THEN
      DALFA = 2*DALFA
    ENDIF
    K = 0
    GO TO 3020
C DATA ARRANGEMENT AND RESULTS OUTPUT
C FU : SLIP DISTRIBUTION FILE
C FS : SHEAR DISTRIBUTION FILE
C FF : PILE BEHAVIOUR (PILE END SLIP/PILE END FORCE
C
3200 OPEN (UNIT=7,STATUS='NEW',FILE='FU')
    OPEN (UNIT=8,STATUS='NEW',FILE='FS')
    OPEN (UNIT=9,STATUS='NEW',FILE='FF')
    N1 = N+2
    DO 3220 I1 = 1, 2
      DO 3210 I = 1, N1
        UPG(I,M+1) = UPG(I,MB)
        DO 3210 J = MB, M
          UPG(I,J) = UPG(I,J+1)
3210    CONTINUE
      MB = ME
```

```
3220 CONTINUE
C DATA ARRANGEMENT
   ID = 2
   ARR = UPG(N1,1)
3230 IR = ID
   DO 3250 J = IR, M
    IF (ABS(UPG(N1,J)).LT.ABS(ARR)) THEN
      DO 3240 I = 1, N1
        Y(I) = UPG(I,J)
        UPG(I,J) = UPG(I,J-1)
        UPG(I,J-1) = Y(I)
3240    CONTINUE
      ARR = UPG(N1,J-2)
      ID = J-1
      GO TO 3230
    ENDIF
    ARR = UPG(N1,J)
3250 CONTINUE
   JB = 2
3260 DO 3280 J = JB, M-2
    IF (DDISP(J).EQ.999.AND.DDISP(J+1).NE.999.) THEN
      JB = J
      DDISP(J) = DDISP(J+1)
      DO 3270 KA = J, M-1
        DO 3270 I = 1, N1
          UPG(I,KA) = UPG(I,KA+1)
3270    CONTINUE
    ENDIF
3280 CONTINUE
   IF (JB.LT.M-2) THEN
    JB = JB+1
    GO TO 3260
   ENDIF
   M = M-1
   XP(1) = 0.
C PILE END FORCE AND SHEAR STRESS COMPUTATION
   FORCE(1,1) = 0.
   FORCE(1,2) = 0.
   FORCE(1,3) = 0.
   PL = (N+1)*DX
```

```
      DO 3290 J = 1, M
        DO 3290 I = 1, N1
          IF (ABS(UPG(I,J)).LE.UM) THEN
            SPG(I,J) = ABS(ES*UPG(I,J)/TAUM)
          ELSEIF (ABS(UPG(I,J)).LE.UR) THEN
            UMAX = SIGN(UM,UPG(I,J))
            SPG(I,J) = ABS((EF*UPG(I,J)+(ES-EF)*UMAX)/TAUM)
          ELSE
           SPG(I,J) = ABS((-SIGN(ABS(TAUER),UPG(I,J)))/TAUM)
          ENDIF
          UPG(I,J) = 1000*ABS(UPG(I,J)/PL)
 3290 CONTINUE
      DO 3300 I = 2, N1
        XP(I) = XP(I-1)+DX
 3300 CONTINUE
      FMAX = 0
      DO 3320 J = 1, M
        DO 3310 I = 1, N1
          Y(I) = SPG(I,J)
 3310   CONTINUE
        IFAIL = 0
C D01GAF IS IN THE NAG LIBRARY OF IMPERIAL COLLEGE COMPUTER CENTER
        CALL D01GAF (XP,Y,N1,ANS,ER,IFAIL)
        FORCE(J+1,1) = UPG(1,J)
        FORCE(J+1,2) = 351.8583*ANS/1000.
        FORCE(J+1,3) = ANS
        FMAX = MAX(FMAX,FORCE(J+1,2))
 3320 CONTINUE
      FMAX1 = -TAUM*FMAX
      WRITE (9,30300) FMAX1
      DO 3330 J = 1, M+1
        FORCE(J,2) = FORCE(J,2)/FMAX
        WRITE (9,30300) FORCE(J,1),FORCE(J,2),FORCE(J,3)
 3330 CONTINUE
C WRITING THE DATA FILE OUTPUT
      MB = 1
      M1 = INT(M/10)
      IF (M1.EQ.0) THEN
        GO TO 3360
      ENDIF
```

```
      DO 3350 IM = 1, M1
        MB = 10*(IM-1)+1
        ME = 10*IM
        WRITE (7,30000) MB,ME
        WRITE (8,30000) MB,ME
        DO 3340 I = 1, N1
          WRITE (7,30100) XP(I),(UPG(I,J),J=MB,ME)
          WRITE (8,30100) XP(I),(SPG(I,J),J=MB,ME)
 3340   CONTINUE
        WRITE (7,30200) (DDISP(J),J=MB,ME)
 3350 CONTINUE
      MB = ME+1
 3360 MB = MAX(MB,M1+1)
      WRITE (7,30000) MB,M
      WRITE (8,30000) MB,M
      DO 3370 I = 1, N+2
        WRITE (7,30100) XP(I),(UPG(I,J),J=MB,M)
        WRITE (8,30100) XP(I),(SPG(I,J),J=MB,M)
 3370 CONTINUE
      WRITE (7,30200) (DDISP(J),J=MB,M)
      CLOSE (UNIT=7)
      CLOSE (UNIT=8)
      CLOSE (UNIT=9)
      RETURN
30000 FORMAT (10X,' DISPLACEMENT INCREMENT NO FROM ',I5,'  TO ',I5)
30100 FORMAT (11(1X,E10.4))
30200 FORMAT ('  DDISP.   ',10(1X,E10.4))
30300 FORMAT (3(1X,E15.6))
      END
```

SPECIAL SUBROUTINE FOR UNSTABLE PILE BEHAVIOUR

```
      SUBROUTINE SUBIU (BETA,BCOND,RHS,ITEST)
      COMMON /COMPR/ N,DX,UM,UR,DES,DEF,TAUM,TAUER,A0(400)
C LOCAL  ARRAYS
      INTEGER IN(401),IS(401),ISR(401)
      REAL A(3,401),AL(1,401),RHS(401)
      INTEGER I,IFAIL,IV,J,N
```

```
      ITEST = 1
      FAIL = 0.
      KSUB = 0
C RESOLUTION OF THE LINEAR EQUATIONS
      DO 4000 I = 1, N
        L = N+2-I
        RHS(L) = RHS(L-1)
 4000 CONTINUE
      DO 4010 J = 1, N+1
        IS(J) = -1
        ISR(J) = -1
        DO 4010 I = 1, 3
          A(I,J) = 0.
 4010 CONTINUE
 4020 KSUB = KSUB+1
      IF (KSUB.GE.2*N) THEN
        ITEST = 0
        GO TO 4050
      ENDIF
      DO 4030 I = 1, N
        A(1,I) = +1.
        A(3,I) = +1.
        UMAX = SIGN(UM,RHS(I+1))
        IF (ABS(RHS(I+1)).LE.UR) THEN
          A(2,I) = A0(I)+DEF
          RHS(I) = (DEF-DES)*UMAX
        ELSE
          A(2,I) = A0(I)
          URES = SIGN(UR,RHS(I))
          RHS(I) = ((DEF-DES)*UMAX)-DEF*URES
        ENDIF
 4030 CONTINUE
      A(1,N+1) = +1.
      RHS(N+1) = BCOND
      IFAIL = 1
C F01LBF IS IN THE NAG LIBRARY OF IMPERIAL COLLEGE COMPUTER CENTER
      CALL F01LBF (N+1,0,2,A,3,AL,1,IN,IV,IFAIL)
      IF (IFAIL.NE.0) THEN
        WRITE (6,40000) IFAIL,IV
        GO TO 4050
```

```
      ENDIF
      IFAIL = 1
C F04LDF IS IN THE NAG LIBRARY OF IMPERIAL COLLEGE COMPUTER CENTER
       CALL F04LDF (N+1,0,2,1,A,3,AL,1,IN,RHS,N+1,IFAIL)
      IF (IFAIL.NE.0) THEN
        WRITE (6,40100) IFAIL,IV
        GO TO 4050
      ENDIF
      DO 4040 I = 1, N
        IF (ABS(RHS(I+1)).LE.UR) THEN
          ISR(I) = -1
        ELSE
          ISR(I) = 0
        ENDIF
        IF (IS(I).NE.ISR(I)) THEN
          IS(I) = ISR(I)
          FAIL = 0.
          GO TO 4020
        ENDIF
 4040 CONTINUE
      IF (FAIL.EQ.0) THEN
        FAIL = 1.
        GO TO 4020
      ENDIF
 4050 RETURN
40000 FORMAT (' ERROR IN F01LBF IFAIL = ',I2,' IV = ',I4)
40100 FORMAT (' ERROR IN F04LBF IFAIL = ',I2,' IV = ',I4)
      END
```

DATA FILE INPUT FOR THE PROGRAM MODEL FOR THE TWO CASE STUDIED DURING THIS INVETIGATION

DATA INPUT FOR STUDY CASE 1

112./ OUTER PILE DIAMETER
90./ INNER PILE DIAMETER
600./ PILE LENGTH
119/ NUMBER OF PILE ELEMENTS (DIVISIONS)
210000./ ELASTIC MODULUS OF THE PILE MATERIAL
3.5/ MAXIMUM INTERFACE SHEAR STRESS
0.80/ RESIDUAL INTERFACE SHEAR STRESS
0.06/ MAXIMUM SHEAR SLIP
0.50/ RESIDUAL SHEAR SLIP

DATA INPUT FOR STUDY CASE 2

112./ OUTER PILE DIAMETER
90./ INNER PILE DIAMETER
6000./ PILE LENGTH
299/ NUMBER OF PILE ELEMENTS (DIVISIONS)
210000./ ELASTIC MODULUS OF THE PILE MATERIAL
3.5/ MAXIMUM SHEAR STRESS
0.80/ RESIDUAL SHEAR STRESS
0.06/ MAXIMUM SHEAR SLIP
0.50/ RESIDUAL SHEAR SLIP

DATA FILE OUTPUT FOR THE PILE TIP DISPLACEMENT-TIP FORCE (FOR THE STUDY CASE 1)

MAXIMUM PILE RESISTING FORCE (KN) = .616550E+03

PILE TIP SLIP DISP. (U/L)	REALTIVE RESISTING FORCE (F/F_{max})	AVERAGE SHEAR STRESS
.000000E+00	.000000E+00	.000000E+00
.100000E+00	.376538E+00	.314188E+00
.200000E+00	.639628E+00	.533714E+00
.300000E+00	.801315E+00	.668628E+00
.400000E+00	.914078E+00	.762719E+00
.500000E+00	.987540E+00	.824016E+00
.557557E+00	.100000E+01	.834413E+00
.577557E+00	.959437E+00	.800567E+00
.587557E+00	.939155E+00	.783644E+00
.597557E+00	.918874E+00	.766721E+00
.600000E+00	.913920E+00	.762587E+00
.607557E+00	.898592E+00	.749798E+00
.613747E+00	.886039E+00	.739323E+00
.617557E+00	.878311E+00	.732874E+00
.627557E+00	.858029E+00	.715951E+00
.637557E+00	.837748E+00	.699028E+00
.647557E+00	.817466E+00	.682105E+00
.657557E+00	.797185E+00	.665182E+00
.667557E+00	.776903E+00	.648259E+00
.677557E+00	.756622E+00	.631335E+00
.687557E+00	.736340E+00	.614412E+00
.707557E+00	.695777E+00	.580566E+00
.721804E+00	.666883E+00	.556456E+00
.747557E+00	.614651E+00	.512873E+00
.827557E+00	.452399E+00	.377488E+00
.829861E+00	.447727E+00	.373590E+00
.947585E+00	.273931E+00	.228571E+00
.987557E+00	.273931E+00	.228571E+00
.110758E+01	.273931E+00	.228571E+00

DATA FILE OUTPUT FOR THE PILE TIP DISPLACEMENT-TIP FORCE (FOR THE STUDY CASE 2)

MAXIMUM PILE RESISTING FORCE (KN) = .217727E+04

PILE TIP SLIP DISP. (U/L)	REALTIVE RESISTING FORCE (F/F_{max})	AVERAGE SHEAR STRESS
.000000E+00	.000000E+00	.000000E+00
.100000E-01	.106936E+00	.315102E-01
.110000E+00	.358198E+00	.105548E+00
.210000E+00	.424877E+00	.125195E+00
.310000E+00	.482453E+00	.142161E+00
.410000E+00	.533839E+00	.157302E+00
.510000E+00	.580703E+00	.171111E+00
.610000E+00	.624045E+00	.183882E+00
.710000E+00	.664559E+00	.195821E+00
.810000E+00	.702747E+00	.207073E+00
.910000E+00	.738973E+00	.217748E+00
.101000E+01	.773518E+00	.227927E+00
.111000E+01	.806564E+00	.237664E+00
.121000E+01	.838328E+00	.247024E+00
.131000E+01	.868924E+00	.256039E+00
.141000E+01	.898519E+00	.264760E+00
.151000E+01	.927224E+00	.273218E+00
.161000E+01	.955234E+00	.281472E+00
.171000E+01	.982816E+00	.289599E+00
.177929E+01	.100000E+01	.294662E+00
.151465E+01	.892689E+00	.263042E+00
.135047E+01	.825877E+00	.243355E+00
.123161E+01	.775706E+00	.228571E+00
.124161E+01	.775706E+00	.228571E+00
.181000E+01	.775706E+00	.228571E+00
.183929E+01	.775706E+00	.228571E+00

DATA FILE INPUT (EXAMPLE)

112./ OUTER PILE DIAMETER
90./ INNER PILE DIAMETER
600./ PILE LENGTH
29/ NUMBER OF PILE ELEMENTS (DIVISIONS)
210000./ ELASTIC MODULUS OF THE PILE MATERIAL
3.5/ MAXIMUM INTERFACE SHEAR STRESS
0.80/ RESIDUAL INTERFACE SHEAR STRESS
0.06/ MAXIMUM SHEAR SLIP
0.50/ RESIDUAL SHEAR SLIP

THE VISUAL DISPLAY UNIT (VDU) OUTPUT (EXAMPLE)

THE NUMBER OF PILE DIVISIONS SHOULD BE LESS THAN 400. IF NOT, THE ARRAY DIMENSIONS MUST BE CHANGED IN THE MAIN PROGRAM AND SUBROUTINES.

OUTER PILE DIAMETER : 112.0 MM
INNER PILE DIAMETER : 90.0 MM
PILE LENGTH : .600000E+03 MM

NUMBER OF PILE ELEMENTS (DIVISIONS) : 29

ELASTIC MODULUS (PILE MATERIAL) : .210000E+06 N/MM2

PERIMETER	AREA	BETA:T-MUL	DX
.35186E+03	.34903E+04	.19202E-03	.20000E+02

MAXIMUM SHEAR STRESS : -3.500 N/MM2
RESIDUAL SHEAR STRESS : -.800 N/MM2
MAXIMUM SHEAR SLIP : .0600 MM
RESIDUAL SHEAR SLIP : .5000 MM

THE PROGRAM ANALYZES A PILE AXIALLY PULLED WHILE THE SLIP AT THE TOP IS INCREMENTALLY INCREASED.

SLIP DISPLACEMENT DISTRIBUTION (U/L_p) 10-3: INCREMENT No FROM 1 TO 10

DEPTH (X/L_p)	INCRE. 1	INCRE 2	INCRE. 3	INCRE. 4	INCRE. 5	INCRE. 6	INCRE. 7	INCRE. 8	INCRE. 9	INCRE. 10
.0000E+00	.1000E+00	.2000E+00	.3000E+00	.4000E+00	.5000E+00	.5471E+00	.5671E+00	.5771E+00	.5871E+00	.5971E+00
.3333E-01	.9000E-01	.1826E+00	.2780E+00	.3749E+00	.4728E+00	.5197E+00	.5408E+00	.5514E+00	.5619E+00	.5724E+00
.6667E-01	.8101E-01	.1662E+00	.2570E+00	.3505E+00	.4464E+00	.4930E+00	.5151E+00	.5262E+00	.5373E+00	.5483E+00
.1000E+00	.7293E-01	.1509E+00	.2369E+00	.3270E+00	.4206E+00	.4669E+00	.4901E+00	.5016E+00	.5132E+00	.5248E+00
.1333E+00	.6567E-01	.1366E+00	.2177E+00	.3043E+00	.3956E+00	.4415E+00	.4656E+00	.4777E+00	.4898E+00	.5019E+00
.1667E+00	.5914E-01	.1234E+00	.1995E+00	.2826E+00	.3713E+00	.4168E+00	.4419E+00	.4545E+00	.4671E+00	.4797E+00
.2000E+00	.5327E-01	.1113E+00	.1823E+00	.2617E+00	.3479E+00	.3928E+00	.4189E+00	.4320E+00	.4451E+00	.4581E+00
.2333E+00	.4800E-01	.1003E+00	.1662E+00	.2417E+00	.3253E+00	.3696E+00	.3967E+00	.4102E+00	.4237E+00	.4373E+00
.2667E+00	.4327E-01	.9038E-01	.1511E+00	.2227E+00	.3035E+00	.3473E+00	.3752E+00	.3892E+00	.4031E+00	.4171E+00
.3000E+00	.3902E-01	.8151E-01	.1370E+00	.2047E+00	.2826E+00	.3257E+00	.3545E+00	.3689E+00	.3833E+00	.3977E+00
.3333E+00	.3521E-01	.7355E-01	.1240E+00	.1877E+00	.2626E+00	.3050E+00	.3347E+00	.3495E+00	.3643E+00	.3791E+00
.3667E+00	.3180E-01	.6642E-01	.1122E+00	.1717E+00	.2436E+00	.2852E+00	.3156E+00	.3308E+00	.3460E+00	.3612E+00
.4000E+00	.2874E-01	.6002E-01	.1014E+00	.1567E+00	.2255E+00	.2663E+00	.2975E+00	.3131E+00	.3286E+00	.3442E+00
.4333E+00	.2600E-01	.5431E-01	.9172E-01	.1428E+00	.2084E+00	.2483E+00	.2802E+00	.2961E+00	.3121E+00	.3280E+00
.4667E+00	.2355E-01	.4919E-01	.8309E-01	.1299E+00	.1922E+00	.2313E+00	.2638E+00	.2801E+00	.2964E+00	.3127E+00
.5000E+00	.2137E-01	.4463E-01	.7539E-01	.1182E+00	.1771E+00	.2152E+00	.2484E+00	.2650E+00	.2816E+00	.2982E+00
.5333E+00	.1942E-01	.4057E-01	.6853E-01	.1075E+00	.1630E+00	.2001E+00	.2339E+00	.2508E+00	.2677E+00	.2846E+00
.5667E+00	.1770E-01	.3697E-01	.6244E-01	.9796E-01	.1500E+00	.1861E+00	.2204E+00	.2376E+00	.2547E+00	.2719E+00
.6000E+00	.1617E-01	.3378E-01	.5705E-01	.8950E-01	.1380E+00	.1730E+00	.2078E+00	.2253E+00	.2427E+00	.2601E+00
.6333E+00	.1482E-01	.3096E-01	.5230E-01	.8205E-01	.1271E+00	.1610E+00	.1963E+00	.2140E+00	.2316E+00	.2493E+00
.6667E+00	.1364E-01	.2850E-01	.4813E-01	.7552E-01	.1172E+00	.1500E+00	.1857E+00	.2036E+00	.2215E+00	.2394E+00
.7000E+00	.1262E-01	.2635E-01	.4451E-01	.6983E-01	.1085E+00	.1400E+00	.1762E+00	.1943E+00	.2124E+00	.2305E+00
.7333E+00	.1173E-01	.2450E-01	.4138E-01	.6492E-01	.1009E+00	.1312E+00	.1677E+00	.1860E+00	.2042E+00	.2225E+00
.7667E+00	.1097E-01	.2292E-01	.3872E-01	.6074E-01	.9439E-01	.1234E+00	.1603E+00	.1787E+00	.1971E+00	.2155E+00
.8000E+00	.1034E-01	.2160E-01	.3649E-01	.5724E-01	.8896E-01	.1168E+00	.1538E+00	.1724E+00	.1909E+00	.2095E+00
.8333E+00	.9825E-02	.2052E-01	.3466E-01	.5438E-01	.8451E-01	.1112E+00	.1485E+00	.1672E+00	.1858E+00	.2045E+00
.8667E+00	.9419E-02	.1967E-01	.3323E-01	.5213E-01	.8102E-01	.1067E+00	.1442E+00	.1630E+00	.1817E+00	.2004E+00
.9000E+00	.9118E-02	.1905E-01	.3217E-01	.5047E-01	.7843E-01	.1034E+00	.1410E+00	.1598E+00	.1786E+00	.1974E+00
.9333E+00	.8919E-02	.1863E-01	.3147E-01	.4937E-01	.7672E-01	.1011E+00	.1388E+00	.1577E+00	.1765E+00	.1954E+00
.9667E+00	.8821E-02	.1842E-01	.3112E-01	.4882E-01	.7587E-01	.1000E+00	.1378E+00	.1566E+00	.1755E+00	.1944E+00
.1000E+01	.8821E-02	.1842E-01	.3112E-01	.4882E-01	.7587E-01	.1000E+00	.1378E+00	.1566E+00	.1755E+00	.1944E+00
S/INCREMENT	.6000E-01	.6000E-01	.6000E-01	.6000E-01	.6000E-01	.6000E-01	.6000E-02	.6000E-02	.6000E-02	.6000E-02

SLIP DISPLACEMENT DISTRIBUTION (U/L_p)10-3 : INCREMENT No FROM 11 TO 20

DEPTH (X/L_p)	INCRE. 11	INCRE. 12	INCRE. 13	INCRE. 14	INCRE. 15	INCRE. 16	INCRE. 17	INCRE. 18	INCRE. 19	INCRE. 20
.0000E+00	.6000E+00	.6045E+00	.6071E+00	.6171E+00	.6271E+00	.6371E+00	.6471E+00	.6571E+00	.6671E+00	.6771E+00
.3333E-01	.5755E+00	.5802E+00	.5830E+00	.5935E+00	.6041E+00	.6146E+00	.6252E+00	.6357E+00	.6462E+00	.6568E+00
.6667E-01	.5515E+00	.5565E+00	.5594E+00	.5705E+00	.5816E+00	.5926E+00	.6037E+00	.6148E+00	.6259E+00	.6369E+00
.1000E+00	.5282E+00	.5334E+00	.5364E+00	.5480E+00	.5596E+00	.5712E+00	.5828E+00	.5944E+00	.6060E+00	.6176E+00
.1333E+00	.5054E+00	.5109E+00	.5140E+00	.5261E+00	.5382E+00	.5503E+00	.5624E+00	.5745E+00	.5866E+00	.5987E+00
.1667E+00	.4833E+00	.4890E+00	.4923E+00	.5049E+00	.5175E+00	.5301E+00	.5426E+00	.5552E+00	.5678E+00	.5804E+00
.2000E+00	.4619E+00	.4678E+00	.4712E+00	.4843E+00	.4973E+00	.5104E+00	.5235E+00	.5365E+00	.5496E+00	.5626E+00
.2333E+00	.4412E+00	.4472E+00	.4508E+00	.4643E+00	.4778E+00	.4914E+00	.5049E+00	.5184E+00	.5319E+00	.5455E+00
.2667E+00	.4212E+00	.4274E+00	.4311E+00	.4450E+00	.4590E+00	.4730E+00	.4870E+00	.5009E+00	.5149E+00	.5289E+00
.3000E+00	.4019E+00	.4083E+00	.4121E+00	.4265E+00	.4409E+00	.4553E+00	.4697E+00	.4841E+00	.4985E+00	.5129E+00
.3333E+00	.3834E+00	.3900E+00	.3939E+00	.4087E+00	.4235E+00	.4383E+00	.4531E+00	.4679E+00	.4827E+00	.4975E+00
.3667E+00	.3656E+00	.3725E+00	.3764E+00	.3916E+00	.4068E+00	.4220E+00	.4372E+00	.4524E+00	.4676E+00	.4828E+00
.4000E+00	.3487E+00	.3557E+00	.3598E+00	.3754E+00	.3909E+00	.4065E+00	.4221E+00	.4377E+00	.4532E+00	.4688E+00
.4333E+00	.3326E+00	.3398E+00	.3439E+00	.3599E+00	.3758E+00	.3917E+00	.4077E+00	.4236E+00	.4395E+00	.4555E+00
.4667E+00	.3174E+00	.3247E+00	.3289E+00	.3452E+00	.3615E+00	.3777E+00	.3940E+00	.4103E+00	.4266E+00	.4428E+00
.5000E+00	.3030E+00	.3104E+00	.3148E+00	.3314E+00	.3480E+00	.3645E+00	.3811E+00	.3977E+00	.4143E+00	.4309E+00
.5333E+00	.2895E+00	.2971E+00	.3015E+00	.3184E+00	.3353E+00	.3522E+00	.3690E+00	.3859E+00	.4028E+00	.4197E+00
.5667E+00	.2769E+00	.2846E+00	.2891E+00	.3062E+00	.3234E+00	.3406E+00	.3578E+00	.3749E+00	.3921E+00	.4093E+00
.6000E+00	.2652E+00	.2730E+00	.2776E+00	.2950E+00	.3124E+00	.3299E+00	.3473E+00	.3647E+00	.3821E+00	.3996E+00
.6333E+00	.2544E+00	.2623E+00	.2670E+00	.2846E+00	.3023E+00	.3200E+00	.3376E+00	.3553E+00	.3730E+00	.3907E+00
.6667E+00	.2446E+00	.2526E+00	.2573E+00	.2752E+00	.2931E+00	.3110E+00	.3288E+00	.3467E+00	.3646E+00	.3825E+00
.7000E+00	.2357E+00	.2438E+00	.2486E+00	.2666E+00	.2847E+00	.3028E+00	.3209E+00	.3390E+00	.3571E+00	.3751E+00
.7333E+00	.2278E+00	.2360E+00	.2408E+00	.2590E+00	.2773E+00	.2955E+00	.3138E+00	.3321E+00	.3503E+00	.3686E+00
.7667E+00	.2208E+00	.2291E+00	.2339E+00	.2523E+00	.2707E+00	.2892E+00	.3076E+00	.3260E+00	.3444E+00	.3628E+00
.8000E+00	.2149E+00	.2232E+00	.2280E+00	.2466E+00	.2651E+00	.2837E+00	.3022E+00	.3208E+00	.3393E+00	.3579E+00
.8333E+00	.2099E+00	.2182E+00	.2231E+00	.2418E+00	.2604E+00	.2791E+00	.2978E+00	.3164E+00	.3351E+00	.3537E+00
.8667E+00	.2059E+00	.2143E+00	.2192E+00	.2379E+00	.2567E+00	.2754E+00	.2942E+00	.3129E+00	.3317E+00	.3504E+00
.9000E+00	.2029E+00	.2113E+00	.2162E+00	.2350E+00	.2539E+00	.2727E+00	.2915E+00	.3103E+00	.3291E+00	.3479E+00
.9333E+00	.2009E+00	.2093E+00	.2143E+00	.2331E+00	.2520E+00	.2708E+00	.2897E+00	.3086E+00	.3274E+00	.3463E+00
.9667E+00	.1999E+00	.2083E+00	.2133E+00	.2322E+00	.2510E+00	.2699E+00	.2888E+00	.3077E+00	.3266E+00	.3454E+00
.1000E+01	.1999E+00	.2083E+00	.2133E+00	.2322E+00	.2510E+00	.2699E+00	.2888E+00	.3077E+00	.3266E+00	.3454E+00
S/INCREMENT	.6000E-02	.6000E-02	.6000E-02	.6000E-02	.6000E-02	.6000E-02	.6000E-02	.6000E-02	.6000E-02	.6000E-02

APPENDIX 2

A2.1 TEST STABILITY

Fracture is a prime cause of material instability. It is reflected by the decrease of a material's ability to maintain a given level of applied load. For this kind of material, the relationship, the force - displacement relationship for a test specimen is characterised by a decreasing branch, when increasing displacement is accompanied by a reduction in applied force.

Considerable care is needed in devising test procedures for such material. The load variation, in the decreasing part of the curve, must be controlled. In fact, success in determining the behaviour of a fracturing material depends largely on the stiffness of the test arrangement and the size of specimen (Petersson (1981)).

A2.2 TEST EQUIPMENTS

The use of simple hydraulic equipments, actuator and oil pressure pump, in generating forces are normally not sufficient to control the failure of a fracturing material.

During the preliminary torsion test, the equipment used was not stiff enough so that the drop in shear stress due to fracture at the interface could be not recorded. The use of a screw jack, which provided controlled displacement rather than force, provided a considerable increase in the tests equipment stiffness.

A2.3 SCHEME OF TESTED MATERIAL AND TEST EQUIPMENTS

In the torsion test presented in chapter 7, the system included elements with different stiffness as shown in figure A2.1 i.e.

1 - steel rig and beams on which the actuator was supported together with a steel rod linking the actuator with the twisting tool head. These can be represented with an elastic spring with a stiffness k_{rig}
2 - twisting tool (head and key) assumed to behave as an elastic spring with a stiffness k_{tool}
3 - pile/grout interface, the behaviour of which had to be determined.

The elastic stiffness and slip fracturing stiffness (negative) are represented by k_e, k_f respectively.

4- grout and concrete material around the pile ring with a stiffness k_{surr}.

The energy necessary to generate a movement (slip) at the pile/grout interface can be expressed as :

$$W_f = \int_o^{\delta} \tau_{interface}(\delta)\, d\delta \qquad \text{(A2.1)}$$

At the same time, the rig, the beams, the actuator, the pulling bar between the actuator and the head twisting tool, the twisting tool and the material around the pile ring form a system with a stored energy equivalent to

$$W_{sys} = \frac{[\tau(\delta)]^2}{2\, k_{sys}} \qquad \text{(A2.2)}$$

k_{sys} is the stiffness of the equivalent system which is shown in figure A2.1. This means that k_{sys} can be expressed by :

$$k_{sys} = \frac{k_{rig} \cdot k_{tool} \cdot k_{surr}}{k_{rig} \cdot k_{tool} + k_{rig} \cdot k_{surr} + k_{tool} \cdot k_{surr}} \qquad \text{(A2.3)}$$

If energy needs to be supplied when the slip at the pile/grout interface increases from δ to $\delta+d\delta$, the fracture will be stable. This leads to a condition for stability i.e.

$$\frac{\partial}{\partial\delta}(W_f + W_{sys}) = \tau_{interface} + \frac{\tau_{interface}}{k_{sys}} \cdot \frac{\delta\tau_{interface}}{\partial\delta} > 0 \qquad \text{(A2.4)}$$

or on putting $\dfrac{\partial\tau_{interface}}{\partial\delta} = k_f$

the condition for test stability becomes

$$k_{sys} > - k_f \qquad \text{(A2.5)}$$

By replacing the hydraulic equipments with a screw jack, k_{sys} was increased. As shown in chapter 8, this allowed a description of the fracturing behaviour of the pile/grout interface, to be obtained. The increase of k_{sys} was obtained from the additional stiffness in the jack as well as from the rod since the latter's diameter was also increased.

Other parameters could also affect the stability of the test :

1 - the grout and matrix stiffness which depends of the grout age, the thickness on the grout ring, the diameter of the grout at the pile/grout and grout/concrete interfaces.

2 - the stiffness of the twisting tool and its head.

3 - the stiffness of the rod which increased during the main test

4 - the stiffness of the rig.

These parameters were not changed in modifying the loading system.

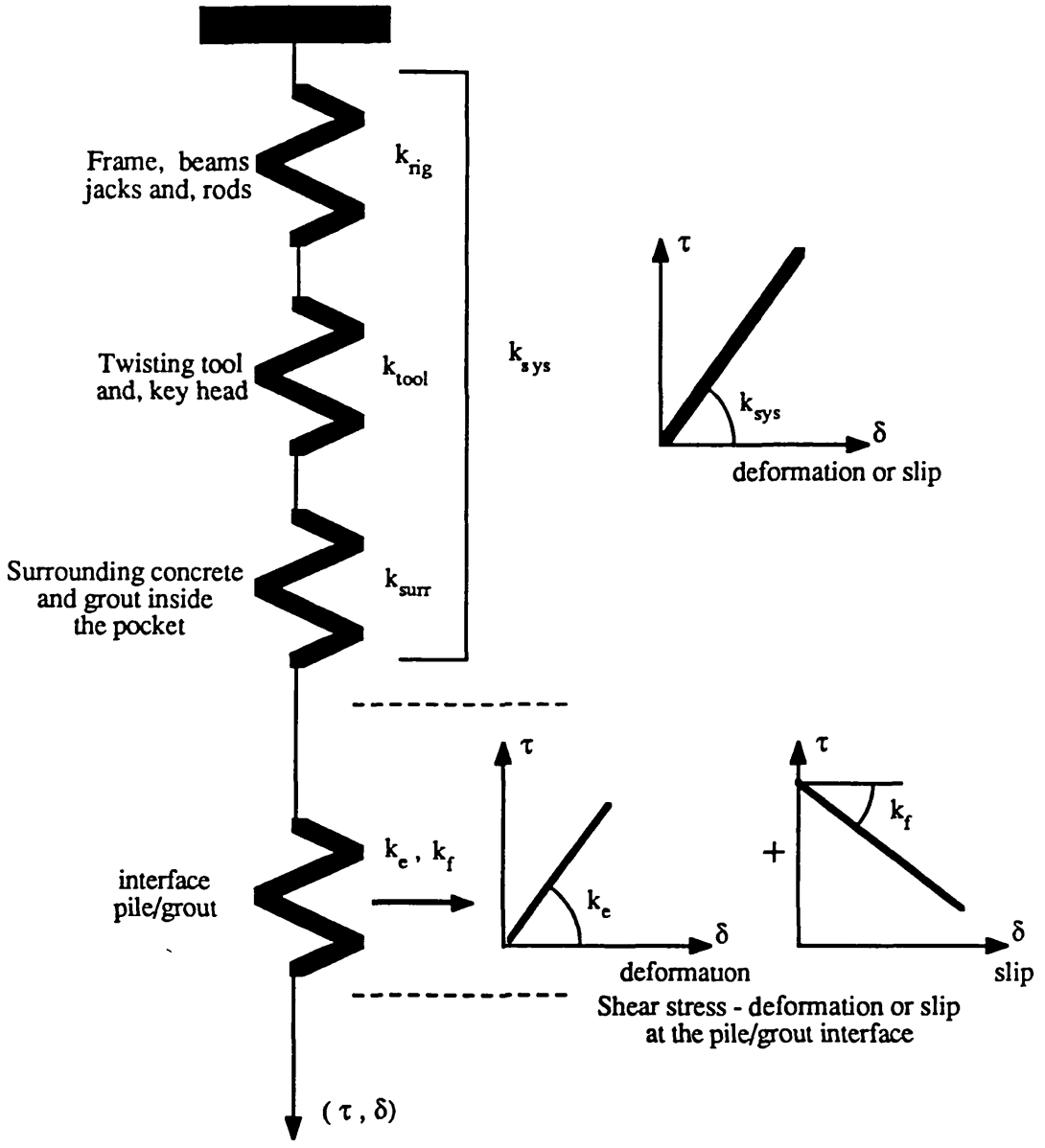


Figure A2.1 : MATERIAL AND TEST EQUIPMENT REPRESENTATION

REFERENCES

(The following papers have been specifically referred to in the text.)

Abbs, D.F; and Needhman, A.D. [1985]
"*Grouted Piles in Week Carbonate Rock*"
17th Annual Offshore Technology. Conf. Proc.. Houston, Texas, May 6-9 1985, Paper OTC 4852.

A.P.I., American Petroleum Institute [1979]
"*Commentary on Grouted Pile to Structure Connections* ".
Recommended Practice For Planning, Designing, and Constructing Fixed Offshore Platforms. Specification API [RP2A]; 10th Edition March 1979 .

A.P.I., American Petroleum Institute [1982]
"*Commentary on Grouted Pile to Structure Connections* ".
Recommended Practice For Planning, Designing, and Constructing Fixed Offshore Platforms. Specification API [RP2A]; 13th Edition January 1982.

A.P.I., American Petroleum Institute [1986]
"*Commentary on Grouted Pile to Structure Connections* ".
A.P.I Recommended Practice for planning, Designing and Constructing Fixed Offshore Platforms. Specification API [RP2A]; 16th Edition April 1986.

A.S.T.M., American Society for Testing and Materials.
"*Designation C 827-75T : Tentative Test Method For Early Volume Change Of Cementitious Mixtures.*"
Am. Soc. Test. Mater. Part 14-1977.

A.S.T.M., American Society for Testing and Materials
"*ANSI./ASTM. C305-65 (Reapproved 1975) : Standard Method For Mechanical Mixing of Hydraulic Cement Paste And Mortars Of Plastic Consistency.*"
Am. Soc. Test. Mater. Part 13-1977.

Barnes, B.D.; Diamond, S.; and Dolch, W. L. [1978]
"*The Contact Zone between Portland Cement and Glass 'Aggregate' Surface*".
Cem. Conc. Res. Vol. 8, pp. 233-244 1978.

Bazant, Z.P.; and Kim Sang-Sik [1979]
"Plastic Fracturing Theory for Concrete"
J. Eng. Mech. Div. Am. Soc. Civ. Eng. Vol. 105, EM3, June 1979.

Bazant, Z.P.; Belytschko, T.B.; and Chang, T. [1984]
"Continuum theory for strain softening"
J. Eng. Mech. Div. Am. Soc. Civ. Eng. Vol. 110 No 12, December 1984.

Bea, R.G.; Dover, A.R.; and Amdibert J.M.E.[1982]
"Pile Foundation Design Considerations For Deeper Water Fixed Structures."
Behaviour of Off-Shore Structures. 3rd Conf. Proc. Vol.1, pp 125-136. Edited by Chryssostomos Chryssostomidis and Jerome J. Conner

Billington, C. J.; and Lewis, G. H. G. [1978]
"The Strength of Large Diameter Grouted Connection ".
10th Annual Offshore Technology Conf. Proc. Houston Texas. May 8 11 1978. Paper OTC 3083.

Billington, C. J.; and Tebbett, I. E. [1980]
"The Basis for New Design Formulae for Grouted Jacket to Pile Connections".
12th Annual Offshore Technology Conf. Proc. Houston Texas. May 5 8 1980. Paper OTC 3788.

Brandt, A. M. [1982]
"On the Calculation of fracture Energy in S.F.R.C. Elements Subjected to Bending ".
Bond in Concrete .Edited by P. BARTOS. APPLIED SCIENCES PUBLISHERS [1982].

BS 4232:1967 Gr 4 [1967]
"Specification for Surface Finish of Blast-cleaned Steel for Painting"
British Standard Institution

BS 1881 Part 121 [1983]
"Method for Determination Static Modulus of Elasticity in Compression"
British Standard Institution.

BS 1881 Part 117 [1983]
"*Method for Determination of Tensile Splitting Strength*"
British Standard Institution.

BS 8110 Part 1 [1985]
"*Structural Use of concrete*"
British Standard Institution

BS 1881 Part 206 [1986]
"*Recommendation for Determination of Strain in Concrete*"
British Standard Institution.

BS 4887 Part 1 [1986]
"*Specification for Air-Entraining (Plasticizing) Admixtures*"
British Standard Institution.

Burge, T.A [1982]
"*Densified Cement Matrix Improves Bond With Reinforcing Steel.*"
Bond in Concrete .Edited by P. BARTOS. APPLIED SCIENCES PUBLISHERS [1982]..

Carette, G.; Malhotra, V.M. [1983]
"*Early-Age Strength Development Of Concrete Incorporating Fly Ash And Condensed Silica Fume.*"
Fly Ash, Silica 1 Fume, Slag & Other Mineral Material In Concrete . Edited by Malhotre, V.M.. Vol. II ,Paper SP 79-41, pp 765 784. AMERICAN CONCRETE INSTITUTE PUBLICATION SP-79

Carles-Gribergues; A.; Grandet, J.; and Ollivier J.P [1982]
"*Contact Zone Between Cement Paste and Aggregate* "
Bond in Concrete .Edited by P. BARTOS. APPLIED SCIENCES PUBLISHERS [1982].

Casey, J.; and Naghdi, P.M. [1984]
"*Strain Hardening Response of Elastic-Plastic Materials*"
Mechanics of Engineering Materials. Edited by Desai, C.S.. [J. Wiley & Sons Ltd. 1984.]

Celestino, T.B.; and Goodman, R.Z. [1979]
"Path Dependency in Rough Joint in Bi-Directional Shearing"
Proc. 4th Congr. Int. Soc. Rock Mech. Montreux. Switzerland. Vol. 1, Sept 1979.

Chen, Z.; and Schreyer H. L. [1987]
"Simulation of Soil-Concrete Interfaces with Nonlinear Constitutive Models ".
J. Eng. Mech. Div. Am. Soc. Civ. Eng., Vol. 113, EM11, November. 1987.

Coleman, B.D.; and Hodgdon, M.L. [1985]
"On shear Bands in Ductile Materials"
Arch. Rational Mech. Anal., Vol. 85, pp 219-247.

Cox, W. R.; and Reese L. C. [1976]
"Pull Out Tests of Grouted Piles in Stiff Clay "
8th Annual Offshore Technology Conf. Proc. Houston Texas. May 1976. Paper OTC 2473.

Curnier, A. [1984]
"A Theory of Friction"
Int. J. Solids Structures. Vol. 20, No 7, pp 637-647, 1984.

Desai, C.S. [1981]
"Behaviour of interfaces Between structural and Geologic Media."
A State of the art paper. Proc. Int. Conf. on recent Advances in Geotech. Earthquake Eng., and Soil Dynamics. St Louis Mo. Vol. 2, pp 619-638.

Desai, C.S. [1984]
"Modelling and Implementation of constitutive Behaviour of Interfaces"
Int. Symp. on Dynamic Soil-Structure Interaction, pp 103-111 Minneaplis 1984.

Department of Energy [1977]
"Offshore Installations : Guidance on Design and Construction"
London, 1977

Department of Energy (Offshore Energy Technology Board) [1982]
"Report on the Working Party on the Strength of Grouted Pile/Sleeve Connections for Offshore Structure"
OTP 11. Offshore Research Development. CIRIA publication [1982]

Dougill, J.W. [1976]
"On Stable Progressively Fracture Solids"
Zeitschrif fuer Angewandte Mathematik und Physik (ZAMP). Vol. 27, No. 4, 1976, pp 423-437

Dougill, J.W.; and Rida, M.A.M [1980]
"Further Consideration of Progressively Fracturing Solids"
J. Eng. Mech. Div. Am. Soc. Civ. Eng. Vol. 106, EM5 October, 1980.

Dougill, J.W. [1983]
"Path Dependence and a General Theory for Progressively Fracturing Solid"
Proc. R. Soc. Lond. A 390, pp 341-351, 1983.

Dougill, J.W. [1985a]
"Constitutive Relations for Concrete and Rock : an Application and Extensions of Elasticity Theory"
IUTAM William Prager Symposium (1983 : Evanston) Ed. Bazant, Z.P. .Mechanics of Geomaterial Wiley 1985, pp 21-46.

Dougill, J.W. [1985b]
"Structural and Continuum Aspects of Fracture in Brittle Matrix Composites"
Paper presented at Euromech 204 colloquium on Structure and crack propagation in brittle matrix composite materials. Warsaw. November 12-15 1985.

Dougill, J.W. [1987]
"Physical and Mechanical Aspects of Failure in Concrete and Concrete Structures".
Paper presented at the 5th Int. Conf. Struct. Mech. in Reactor Technology SMIRT 9- August 1987.

FEB Product Data Sheet A9 [1985]
"FebAdmix : Mortar Plasticiser"

Federation International de la Precontrainte [1977]
"*Recommendations for the Design and Construction of Concrete Sea Structures*"
3rd edition, Cement & Concrete Association, Slough, July 1977.

Fragio, A.G; Santiago, J.L.; and Sutton, V.J.R [1985]
"*Load Tests on Grouted Piles in Rocks*"
17th Annual Offshore Technology Conf. Proc. Houston. Texas. May 6-9 1985. Paper OTC 4851.

Fredriksson, B. [1976]
"*Finite Element Solution of Surface Nonlinearities in Structural Mechanics with Special Emphasis on Contact and Fracture Mechanics Problems*"
Computer & Structures. Vol. 6, pp 281-290, 1976.

Ghaboussi, J.; Wilson, E.L.; Isenberg, J [1983]
"*Finite Element for Rock Joints and Interfaces*"
J. Soil. Mech. Found. Div. Am. Soc. Civ. Eng. Vol. 99,. SM10 , October 1973.

Grutzeck, M.W.; Atkinson, S., and Roy, D.M. [1983]
"*Mechanism Of Hydration Of Condensed Silica Fume In Calcium Hydroxide Solutions*"
Fly Ash, Silica Fume, Slag & Other Mineral Material In Concrete . Edited by Malhotre, V.M.. Vol. II ,Paper SP 79-33, pp 643 664. AMERICAN CONCRETE INSTITUTE PUBLICATION SP-79

Gylltof, K. [1983]
"*Fracture Mechanics Models for Fatigue in Concrete Structures*"
Doctoral thesis 1983 : 261, presented at Lulea university of technology, division of structural engineering.

Hewlett, P.C. [1980]
"*Physico-Chemical Mechanisms of Admixtures*"
Lecture Note on the CGLI Advanced Concrete Technology Course, 6 May 1980. Cement and Concrete Association Training Centre. TDH 5401.

Jefferis, S.A [1988]
"Application of Bleed and Settlement Theory to Problem of Offshore Grouting"
Grout & Grouting for Construction and Repair of Offshore Structure. A summary report, OTH88.289. Offshore Technology report. Department of Energy (UK), pp 72 -99.

Jiang, D., H.; Andonian, A. T.; and Shah S. P. [1982]
"A New Type of Bond Test Specimen ".
Bond in Concrete .Edited by P. BARTOS. APPLIED SCIENCES PUBLISHERS [1982].

Kay, S.; Kolk, H.J.; and van Hooydonk, W.R. [1983]
"Site Specific Design of Laterally Loaded Piles"
Proc. Conf. Geotech Practice in Offshore Engineering. Edited by Stephen G.Wright.

Kraft, L.M.Jr.; and Lyons, C.G.[1974]
"State of the Art Ultimate Axial Capacity Of Grouted Piles."
6th annual Offshore Technology Conf. Proc. Houston Tex. May 6-8 1974.

Krizek, R. J., and Vipulanandan,C. [1985]
"Evaluation of Adhesion in Chemically Grouted Geomaterials ".
Geotech. Test. J., GTJODJ, Vol. 8, N°. 4, Dec. 1985, pp 184-190.

Lian Hui Zhen [1982]
"Morphology of Interface between Zeolites Aggregates and Cement Paste"
Bond in Concrete .Edited by P. BARTOS. APPLIED SCIENCES PUBLISHERS [1982].

Long, J.E. [1976]
"Experience in Prestressing and Grouting Concrete Offshore Structures"
Design and Construction of Offshore Structures. INSTITUTION OF CIVIL ENGINEERS PUBLICATION. London 1976.

Loset, O. [1981]
"Grouted Connection in Steel Platforms : Testing and Designing ".
Offshore Structures : The use of Physical Model in their Design. Edited by Armer G. St.; and Garas, F. K. .

Mehta, P.K. [1983]
"Pozzolanic and Cementitious By-products as Mineral Admixture for Concrete; A Critical Review"
Fly Ash, Silica Fume, Slag & Other Mineral Material In Concrete . Edited by Malhotre,V.M.. Vol. I ,Paper SP 79-1, pp 1 34. AMERICAN CONCRETE INSTITUTE PUBLICATION SP-79

Meland, I. [1983]
"Influence Of Condensed Silica Fume And Fly Ash On The Heat Evolution In Cement Paste."
Fly Ash, Silica Fume, Slag & Other Mineral Material In Concrete . Edited by Malhotre,V.M.. Vol. II ,Paper SP 79-34, pp 665 676. AMERICAN CONCRETE INSTITUTE PUBLICATION SP-79

Morrison J.K.; Surendra P.S; and Yeou-Shang J. [1988]
"Analysis of Fibre Debonding and Pull-out in Composites"
J. Eng. Mech. Div. Am. Soc. Civ. Eng. Vol. 114, EM 2, February 1988.

Muspid, J.M.; Gudmestad, O.T; and Alm-Paulsen, A. [1982]
"Alternative Deep Water Concepts for Northern Sea Extreme Conditions"
Behaviour of Offshore Structures. Proc. 3th Int. Conf.. Vol. 1, pp 18-49. Edited by Chryssostomidis, C. and Conner J.J..

Neville, A.M. [1983]
"Properties of concrete"
Third Edition. (1983). LONGMAN SCIENTIFIC & TECHNICAL PUBLICATION

Petersson, P.E. [1981]
"Crack growth and development of fracture zone in plain concrete and similar materials"
Report TUBM 1006. Lund Institute of Technology, Sweeden

Regourd, M.; Mortureux, B.; Hornain, H.[1983]
"Use Of Condensed Silica Fume As Filler In Blended Cements"
Fly Ash, Silica Fume, Slag & Other Mineral Material In Concrete . Edited by Malhotre, V.M.. Vol. II ,Paper SP 79-46, pp 847 866. AMERICAN CONCRETE INSTITUTE PUBLICATION SP-79

Rida, H.A.M [1981]
"*The Use of Linear Loading Functions in Progressive Fracture, Plasticity, and Combined Behaviour*"
Ph.D. Thesis. University of London (1981)

Sakamoto, N.; and Iwasaki, N. [1982]
" *Influence of Sodium Chloride on the Concrete/Steel and Galvanised Steel Bond*"
Bond in Concrete .Edited by P. BARTOS. APPLIED SCIENCES PUBLISHERS [1982].

Sellevold, E.S.; Radjy, F.F.[1983]
"*Condensed Silica Fume (Micro-silica) In Concrete: Water Demand and Strength development*"
Fly Ash, Silica Fume, Slag & Other Mineral Material In Concrete . Edited by Malhotre, V.M.. Vol. II ,Paper SP 79-35, pp 667 694. AMERICAN CONCRETE INSTITUTE PUBLICATION SP-79

Spooner D.C.; and Dougill,J.W. [1975]
"*A Quantitative Assessment of Damage Sustained in Concrete during Compression Loading*"
Mag. Concr. Res. Vol. 27, N^0 92, pp 151-160, September 1975

StJohn, H.D.; Randolph M.F.; McAnoy R.P.; Gallagher, K.A. [1983]
"*Design of Piles for Tethered Platforms*"
Developments in the Design and Construction of Offshore Structures. Institution of Civil Engineers. 23-24 March 1983.

Stroeven, P.; and De Wind, G.[1982]
"*Structural and Mechanical Aspects of Debonding of a Steel Bar from a Cementitious Matrix*".
Bond in Concrete .Edited by P. BARTOS. APPLIED SCIENCES PUBLISHERS [1982].

Tassios, T. P.; and Koroneos E. G. [1979]
"*Preliminary Results of Local Bond-Slip Relationships by Means of Moire Methods* ".
C. E. B., Bulletin d'Information N°. 132. Structural Concrete under Seismic Actions. Rome. Vol. 2, Mai 1979.

Tebbett, I.E.; Williams, J.R.; and Sands T.B.(non dated report)
"*Design and Installation of Piled Foundations for Sea Bed Structures.*"
Wimpey Offshore Engineers and Constructors Limited.

Theodor A.B. [1982]
"*Densified Cement Matrix Improves Bond with Reinforcing Steel*"
Bond in Concrete .Edited by P. BARTOS. APPLIED SCIENCES PUBLISHERS [1982].

Timoshenko, S. P.; Goodier, J. N.
"*Theory of elasticity*"
Third Edition. Mc Graw-Hill Book Company

Wimpey Laboratories Limited [1977]
"*Lafarge Aluminous Cement Co Ltd : Effect of Cyclic Loading on Bond Strength*"
Report ST18/77, May 1977.

Wimpey Laboratories Limited [1979]
"*Department of Energy. Review of Offshore Grout Strengths*"
Report ST55/79, October 1979.

Wimpey Laboratories Limited [1984].
"*Joint Industry Project. Grouted Pile/Sleeve Connections : Length, Longitudinal Stiffening and Size Effects Study*".
Report N° WOL 55/84B. Final Issue, [December 1984].

Woodward, J. C. [1982]
"*Cement Grouts in Offshore Steel Structures* ".
Proc. Conf. Grouting in Geotechnical Engineering. New Orleans, Lousiana, February. 10-12, 1982. Edited by Baker, W. H. [1982].

Yoshimi, Y and Kishida, T.[1981].
"*A Ring Torsion Apparatus for Evaluating Friction between Soil and Metal surfaces* ".
Geotech. Test. J., GTJODJ, Vol. 4, N° 4, December 1981, pp 145-152.

Zaman, Z.Z.; and Desai, C.S. [1983]
"Model for Sliding and Separation at Interfaces under Static and Cyclic Loading"
Proc. Int. Conf. Constitutive Laws for Engineering Materials, Theory and Application, pp 384-390. Edited by Desai, C.S., and Gallagher R.H. (1983).

Zubelewicz, A.; and Bazant, Z.P. [1987]
"Interface Element Modeling of Fracture in Aggregate Composites"
J. Eng. Mech. Div. Am. Soc. Civ. Eng. Vol. 113 No. EM11, November, 1987.

BIBLIOGRAPHY

(The following papers have been used for background reading and may be of interest to others working in the field.)

Arnaud, M.; Bourabrab, M. and Lorrain. M. [1982]
"On The Reversibility Properties of the Bond in Concrete "
Bond in Concrete .Edited by P. BARTOS. APPLIED SCIENCES PUBLISHERS [1982].

- Bennett, E. W. and Snounou, I. G. [1982]
"Bond Slip Characteristics of Plain Reinforcing Bars Under Varying Stress ".
Bond in Concrete .Edited by P. BARTOS. APPLIED SCIENCES PUBLISHERS [1982].

Chandhuri, K.P.R.; and Symons, M.V. [1983]
"Uplift Resistance of Model Single Piles"
Proc. Conf. Geotech. Practice in Offshore Engineering. Edited by Stephen G.Wright..

Clausen, C.J.F; And, P.M.; and Almend, I.B.[1982]
"Analysis Of The Pile Foundation System For a north Sea Drilling Platform".
Behaviour of Off-Shore Structures.Proc. 3rd Conf. Vol. 1. Edited By Chryssostomidis, C. and Conner, J. J. .

Cleary, M.P.; Dong Jian Lian [1983]
"Analysis of Deformation and Failure in Geological Materials"
Proc. Int. Conf. on Constitutive Laws for Engineering Materials : Theory & Application. Tucson, Arizona, January 10 - 14, 1983. Edited by Desai. and Gallagher, pp 341 - 348.

Cornell, C.A. ; Rackwitz, R.; Guenard, Y. and Bea, M. [1984]
"Reliability Evaluation of Tension Leg Platforms ".
Proc. 4th Conf. Probabilistic Mech. and Struct. Reliability. Edited by Wen, Y. K.

Dawson, P.,Long, J.E., Somerville, G.; and Thorpe, W. [1978].
"Grouting of Tall Vertical Prestressed Ducts"
J. Concr. Soc., Current Practice Sheet Nº 37. Vol. 12. May 1978.

Dawson, P.,Long, J.E., Somerville, G.; and Thorpe, W.[1979].
"Grouting in Prestressing"
J. Concr. Soc., Current Practice Sheet Nº 44. Vol. 13. September 1979.

De. Conte, S.; and De Boor C
"Elementary Numerical Analysis : An algorithmic Approach"
Mc Graw Hill. 3th printing 1983. INTERNATIONAL STUDENT EDITION

Desai, C.S.; Nagaraj, B.K. [1988]
"Modeling for Cyclic Normal and Shear Behaviour of Interfaces"
J. Eng. Mech. Div. Am. Soc. Civ. Eng.. Vol. 114, MD 7, July 1988.

Desai, C.S.; Sirwardane [1984]
"Constitutive Law for Engineering Material with Emphasis on Geotechnical Materials"
Englewoods Cliffs, Practice Hall 1984.

Gambarova, P.G.; Karakoc G [1982]
"Shear Confinement Interaction at the Bar to Concrete Interface."
Bond in Concrete .Edited by P. BARTOS. APPLIED SCIENCES PUBLISHERS [1982].

Hawkins, N.E.; Lin, I.J.; and Jeang F.L.[1982]
"Local Bond Strength For Cyclic Reversed Loading".
Bond in Concrete .Edited by P. BARTOS. APPLIED SCIENCES PUBLISHERS [1982].

Heuse, F.E. [1979]
"Dilatant Effects of Rock Joints"
Proc. 4th Congr. Int. Soc. Rock Mech.. Montreux, Switzerland. Vol.1 pp 169 - 175.

Heuse, F.E.; Barbour T. [1982]
"New Models for Rock Joints and Interfaces"
J. Geotech. Div. Am. Soc. Civ. Eng.. Vol 108, GT 5, May 1982.

Karasan, D.H; and Karahl, N.W. [1984]
"New API Equation for grouted Pile-to-Structure Connections"
16th annual Offshore Technology Conf. Proc. Houston Tex. Paper OTC 4715.

Lagoni, P. [1982]
"Skin Friction on Piles".
Behaviour of Offshore Structures. Proc. 3rd Conf. Vol. 1. Edited By Chryssostomidis, C. and Conner, J. J. .

Lian Hui Zhen [1982]
"*Morphology of Interface Between Zeolites Aggregate and Cement Paste*".
Bond in Concrete .Edited by P. BARTOS. APPLIED SCIENCES PUBLISHERS [1982].

Littlejohn, G.S. [1983]
"*Design of Cement Based Grout*"
Proc. Conf. in Grouting in Geotechenical Engineering. Edited by Baker, W.H.. AMERICAN SOCIETY OF CIVIL ENGINEERS PUBLICATION (1983).

Monteiro, P.J.M; and Andrade, W.P. [1987]
"*Analysis of the Rock-Cement Paste Bond using probabilistic Treatment of Brittle Strength*"
Cem. Conc. Res. Vol. 17, pp 919-926, 1987.

Monteiro, P. J. M. and Mehta, P. K. [1986]
"*Interaction between Carbonate Rock and Cement Paste* "
Cem. Conc. Res. Vol. 16, pp 127-134, 1986.

Muki, R. and Sternberg, E. [1970].
"*Elastostatic Load Transfer to a Half-Space from a Partially Embedded Axially Loaded Rod* ".
Int. J. Solids Structures, 1970. Vol. 6. Pergamon Press.

Natau, O.; Leichnitz, W. and Balthasar, K. [1979]
"*Construction of a Computer Controlled Direct Shear Testing Machine for Investigations on Rock Discontinuities* ".
Proc. 4th Congr. Int. Society Rock Mech..Vol. 3, pp 241 -243. Montreux 1979

Oden, J.T.; Pires, E.B. [1983]
"*Numerical Analysis of certain Contact Problems in Elasticity with Non-classical Friction Laws*"
Computers & Structures. Vol. 16, N°. 1-4, pp 481 - 485.

Pleasha, M.E. [1987]
"*Constitutive Models for Rock Discontinuities with Dilatancy and Surface Degradation*"
Int. J. Num. Anal. Methods Geomech.. Vol 11 345 - 362.

Rajapakse, R. K. N. D. and Selvadurai, A. P. S. [1985].
"Torsional Stiffness of Non-Uniform and Hollow Rigid Piers Embedded in Isotropic Elastic Media ".
Int. J. Num. Anal. Meth. in Geomech.. Vol. 9, 525 539 [1985]

Rehm, G. ; Diem, P. and Zimbelmann, R. [1977]
"Technishe Moglichkeiten zur Erhohung der Zugfestigkeit von Beton".
Schritenreihe des DAfStb, Heft 283, Berlin 1977.

Robins P. J. and Standish I.G. [1982]
"Effect of Lateral Pressure on Bond of Reinforcing Concrete ".
Bond in Concrete .Edited by P. BARTOS. APPLIED SCIENCES PUBLISHERS [1982].

Schreyer H.L.; and Chen, Z [1986]
"One-Dimensional Softening with Localization"
J. Applied Mechanics. Vol. 53, December 1986.

Smith, T.D [1987]
"Pile Horizontal Soil Modulus Values".
J. Eng Geotch.Div. Am. Soc. Civ. Eng. Vol 119. GT 9. September 1987.

Su, W.; and Fragaszy, R.J. [1988]
"Uplift Testing of Model Anchors"
J. Eng Geotch.Div. Am. Soc. Civ. Eng.. Vol. 114, GT. 9, September 1988.

Torstenfelt, Bo [1983]
"Contact Problems with Friction in General Purpose Finite Element Computer Programs"
Computers & Structures. Vol. 16, N°. 1-4, pp 486 - 493.

Triantafyllidis, N.; and Anifantis [1986]
"A Gradient Approach to Localisation of Deformation. Hyperelastic Material"
J. Elasticity. Vol. 16. pp 225-237.

Van Loenen, J.H. [1975]
"*Guide to Good Practice : Grouting of vertical Ducts*".
Complementary Report for FIP Commission on Practical Construction at the 1974 New York Congress. Edited by Kavyrchine, M..

Xiurum Ge [1981]
"*Non-linear Analysis of a Joint Element and its Application in Rock Engineering.*
Int. J. Num. Anal. Methods Geomech.. Vol 5, pp 229 - 245.

Xiurum Ge [1982]
"*Some considerations about the Constitutive Relations of Joints in Rocks*"
Int. Symp. Num. Models in Geomech.. Zurich. pp 227 - 233.

Xiurum Ge [1983]
"*The Constitutive Relations of Joints in Considerations of the Shear Dilatancy and the Hardening Properties*"
Proc. Int. Conf. on Constitutive Laws for Engineering Materials : Theory & Application. Tucson, Arizona, January 10 - 14, 1983. Edited by Desai. and Gallagher, pp 369 - 382.

Zaman, M.M.; Desai, C.S. [1983]
"*Models for Sliding and Separation at Interfaces under Static and Cyclic Loading*"
Proc. Int. Conf. on Constitutive Laws for Engineering Materials : Theory & Application. Tucson, Arizona, January 10 - 14, 1983. Edited by Desai. and Gallagher, pp 383 - 389.

BIBLIOGRAPHY (ADDENDUM)

Carroll, B.C. [1987]
"*Behaviour of Prestressed Grout Bond Joints*"
Ph.D thesis. Imperial College, University of London, January 1987.

Chilvers, J.A. [1984]
"*Analysis of the Structural Behaviour of Grouted Pile/Sleeve Connection for Offshore Structures*"
Ph.D Thesis, The City University, 1984.

Dowling, P.J.; Elnashai A.S. and; Carroll, B.C. [1983]
"*A new Pressurised Grouted Connection for Steel Tubulars*"
J. Constructional Steel Res., Vol. 3, No. 3, 1983.

Elnashai, A.S.; and Dowling, P.J. [1982]
"*Nonlinear Modeling of plain Concrete*"
Marine Technology Report No. SS-40, London Centre for Marine Technology, Imperial College.

Elnashai, A.S.; and Dowling, P.J. [1983]
"*Bond Strength of Grouted connections*"
Report : Marine Technology, Imperial College, 1983.

Elnashai, A.S. [1984]
"*Non Linear Analysis of Composite Tubular Joints*"
Ph.D thesis. Imperial College, University of London July 1984.

Elnashai, A.S.; and Dowling, P.J. [1984]
"*Nonlinear Analysis of Composite Structures*"
Festschrift Roik, Mitteilung 84-3, Ruhr-Universitat Bochum 1984, pp. 412-425.

Elnashai, A.S.; Carroll, B.C.; and Dowling, P.J. [1985]
"*A prestressed High Strength Grouted Joint for Offshore Construction*"
17th Annual Offshore Technology Conf. Proc. Houston Texas. May 1985, pp 457-467.
Paper OTC 4892.

Elnashai, A.S.; Carroll, B.C.; Dowling, P.J.; and Billington, C.J. [1986]
"Full Scale testing and analysis of grouted pile/platform connections"
18th Annual Offshore Technology Conf. Proc. Houston Texas. May 1986, pp 301-311. Paper OTC 5325.

Elnashai, A.S.; and Dowling, P.J. [1986]
"Composite steel/concrete connections: Analytical Studies and a design equation"
report : Engineering Seismology and Earthquake Report No ESEE 6/86, Imperial College, 1986.

Elnashai, A.S.; Carroll, B.C.; and Dowling, P.J. [1987]
"Experimental and Analytical Investigations of the Integrity of pile/platform composite connections"
Integrity of Offshore Structure Conf., Glasgow, 28-29 September 1987.

Elnashai, A.S.; and Dowling, P.J. [1987]
"Assessment of Design Recommendations for Composite Connections in Offshore Construction"
Engineering Foundation Conference on Composite Construction. Henniker, New Hampshire, June 1987.

Elnashai, A.S.; and Dowling, P.J. [1988]
"Failure Mechanisms of Weld-Beaded Composite pile/Sleeve Connections"
Behaviour of Offshore Structures Conference (Boss '88'), Trondheim, 21-25 June 1988.

Elnashai, A.S.; and Dowling, P.J. [1989]
"Composite Connections for the repair and Strengthening of Offshore Installations"
3rd Arab Conference of Structural Engineering, Al-Ain, United Arab Emirates, March 1989.

Elnashai, A.S.; and Dowling, P.J. [1989]
"Behaviour of Composite Tubular Connections Part I : Analytical Modelling. Part II : Parametric Studies and Design Equation"
To be submitted to the Institution of Civil Engineers, Proceeding, March 1989.